UNIVERSITEIT VAN PRETORIA
UNIVERSITY OF PRETORIA
YUNIBESITHI YA PRETORIA

Modified Layered Double Hydroxides as PVC Heat Stabilisers

MD Royeppen

UNIVERSITEIT VAN PRETORIA
UNIVERSITY OF PRETORIA
YUNIBESITHI YA PRETORIA

Modified Layered Double Hydroxides as PVC Heat Stabilisers

MD Royeppen

Submitted in partial fulfilment of part of the requirements for the degree of Master of Engineering in the Faculty of Engineering, the Built Environment and Information Technology, University of Pretoria, Pretoria

2016

Modified Layered Double Hydroxides as PVC Heat Stabilisers

MD Royeppen

Supervisor: Dr FJWJ Labuschagné

Department: Chemical Engineering

Degree: MEng (Chemical Engineering)

Synopsis

Hydrotalcite (HTC) was intercalated with different aromatic carboxylic acids *via* two synthesis methods: reconstruction and co-precipitation. The reconstruction method involves the rehydration of the products of LDH calcination. The co-precipitation method involves the addition of a base to solutions containing a mixture of the M^{II} and M^{III} ions found in the metallic layers of an LDH.

The intercalated compounds were then compounded with flexible grade PVC to see if these compounds had any effect on the heat stability of the PVC.

Complete intercalation of these stabilisers did not occur; however layered double hydroxides did form for almost every synthesis. The organic acids that were to be intercalated were also present in every synthesised stabiliser.

Neat hydrotalcite was the best overall stabiliser with an early stability time of 32.40 min and a final or long term stability time of 106.51 min.

The best modified layered double hydroxide (LDH) in terms of early stability was 4-hydroxybenzoic acid + HTC synthesised with the reconstruction method. This stabiliser had an early stability time of 25.40 min.

The best performing modified stabiliser in terms of late stability was salicylic acid + HTC synthesised with the co-precipitation method. This stabiliser had a late stability time of 71.32 min.

The highly activating nature of the hydroxyl substituent group should make hydrotalcites intercalated with hydroxybenzoic acids good free radical scavengers.

The substituent group positions that give the best PVC heat stability are the ortho and para positions.

The pKa 2 value for an organic acid may be used as a selection parameter for intercalation into hydrotalcite. If a high pKa 2 value organic acid is intercalated into hydrotalcite, the resulting compound will have good PVC heat stabilisation properties.

KEYWORDS: LDH, PVC, Heat stability, Intercalation

Acknowledgments

I would like to thank the following people and organisations:

- The National Research Foundation for financial assistance during my two years of post-graduate study.
- My supervisor, Dr Johan Labuschagne.
- Ansie Wiid and Monique Schmidt for help with the stabiliser synthesis.
- Isbé van der Westhuizen for help with TGA.
- Emmanuel Adu-Awuku for help with the FTIR and co-precipitation Rheomix runs.
- My parents and brother for their love and support during the writing of this thesis.

Contents

Synopsis ii

List of tables viii

List of figures ix

1. Introduction 1

2. Literature 4

2.1 PVC synthesis and properties 4

2.2 Thermal degradation of PVC 5

2.2.1 Mechanisms of primary thermal degradation 6

2.2.2 Thermal oxidative degradation of PVC 11

2.2.3 Mechanisms of secondary PVC degradation 13

2.2.4 Consequences of thermal degradation 14

2.3.1 Background 15

2.3.2 Mechanisms of heat stabilisation 16

2.4 Layered double hydroxides 21

2.4.1 Background 21

2.4.2 Structure 23

2.4.3 LDH synthesis 26

2.4.4 Use of LDH as a PVC heat stabiliser 30

2.4.5 Aromatic carboxylic acids as potential intercalants 32

2.5 Thermal degradation testing methods 33

2.5.1 Hydrogen chloride evolution tests 33

2.5.2 Static testing 34

2.5.3 Dynamic testing 35

3. Experimental 37

3.1 LDH synthesis 37

3.1.1 Apparatus 37
3.1.2 Materials list 37
3.1.3 Planning 38
3.1.4 Reconstruction method for hydrotalcite intercalation 39
3.1.6 Co-precipitation method 39
3.2 Material characterisation 40
3.2.1 Particle size analysis (PSA) 40
3.2.2 X-ray diffraction (XRD) 40
3.2.3 Fourier transform infra-red spectroscopy (FTIR) 40
3.3 Heat stability testing 40
3.3.1 Apparatus 40
3.3.2 Materials list 41
3.3.3 Planning 41
3.3.4 Method 42
4. Results and discussion 44
4.1 Characterisation 44
4.1.1 X-ray diffraction 44
4.1.2 Thermogravimetric analysis 50
4.1.3 Fourier transform infrared spectroscopy 58
4.1.4 Particle size analysis 67
4.2 Heat stability results 70
4.2.1 Co-precipitation synthesis vs reconstruction synthesis 70
4.2.2 The effect of substituent group type 75
4.2.3 The effect of substituent group position 82
4.2.4 The effect of substituent group length 84
5. Conclusions and recommendations 86
6. References 88

Appendix A: XRD results 92
A.1 Reconstruction method synthesis 92
A.2 Co-precipitation method synthesis 97
Appendix B – FTIR results 102
B.1 Reconstruction method synthesis 102
B.2 - Co-precipitation method synthesis 107
Appendix C: Particle size distributions 112
C.1 - Reconstruction method synthesis 112
C.2 – Co-precipitation method synthesis 117
Appendix D – Torque curves 122
D.1 Reconstruction method synthesis 122
D.2 – Co-precipitation method synthesis 136
D.3 – Neat hydrotalcite torque curves 141

List of tables

Table 3.1: PVC dry blend recipe 41
Table 4.1.1: XRD results summary for reconstruction method samples. 48
Table 4.1.2: Theoretical and actual organic mass loss percentages for the reconstruction synthesised stabilisers. 54
Table 4.1.3: Theoretical and actual organic mass loss percentages for the co-precipitation synthesised stabilisers. 57
Table 4.1.4: Infrared absorption frequencies found in the analysed samples 58
Table 4.1.5: FTIR result summary for reconstruction synthesised stabilisers 64
Table 4.1.6: FTIR result summary for co-precipitation synthesised stabilisers 66
Table 4.1.7: Reconstruction stabiliser average particle sizes 69
Table 4.1.8: Co-precipitation average particle sizes 69
Table 4.2.1: Substituent rankings of the aromatic acids intercalated into hydrotalcite. 81

List of figures

Figure 2.1: Reaction scheme showing degradation of structural irregularities in PVC (Bacalogulu & Fisch, 2000: 429). 8
Figure 2.2: Reaction scheme showing the chain reaction model of thermal degradation (Bacalogulu & Fisch, 2000: 430). 8
Figure 2.3: Reaction scheme showing clarification of the intermediate products and their arrangements (Bacalogulu & Fisch, 2000: 433). 9
Figure 2.4: Reaction scheme showing the effects of HCl or a metal chloride on the degradation of PVC (Bacalogulu & Fisch, 2000: 433). 10
Figure 2.5: Reaction scheme showing the formation of chloroalkanes (Bacalogulu & Fisch, 2000: 434). 10
Figure 2.6: Reaction scheme showing thermal oxidative degradation of PVC (Bacalogulu & Fisch, 2000: 435). 12
Figure 2.7: Reaction scheme depicting the Diels-Alder condensation of cisoid trans-trans dienes with other polyenes (Bacalogulu & Fisch, 2000: 436). 14
Figure 2.8: Stabilisation mechanisms of organotin stabilisers (Wypych, 2008: 271). 17
Figure 2.9: Mixed metal stabiliser reaction scheme (Wypych, 2008: 271)..... 18
Figure 2.10: Mixed metal stabiliser reaction schemes showing both primary and secondary stabilisation mechanisms (Bacalogulu & Fisch, 2000: 440). 19
Figure 2.12: Secondary stabilisation mechanism of PVC by phosphite compounds (Wypych, 2008: 271). 20
Figure 2.13: Secondary stabilisation mechanism of epoxidised stabilisers (Wypych, 2008: 272). 21
Figure 2.14: LDH structure and composition (Bergaya *et al* 2006: 1022). 23
Figure 2.15: Equilibrium structure of hydrotalcite from an NPT molecular dynamics simulation (Cygan, Liang & Kalinichev, 2004). 24
Figure 2.16: Crystal structure of dehydrated Friedel's salt, hydrocalumite with chloride anions in the interlayer (Vielle *et al* 2003). 25
Figure 2.17: Schematic of stabilisation mechanism provided by hydrotalcite to PVC. 31
Figure 2.18: Torque curve showing heat stability parameters (American Society for Testing and Materials, 2002). 35

Figure 3.1: Chemical structures of the organic acids used for intercalation (ChemSketch 14.01, 2016). ……...38

Figure 4.1.1: XRD pattern for neat hydrotalicte. 45
Figure 4.1.3: XRD pattern for thiosalicylic acid + HTC (reconstruction method)..... 46
Figure 4.1.4: XRD pattern for 3-hydroxybenzoic acid + HTC (reconstruction method). 46
Figure 4.1.6: XRD pattern for thiosalicylic acid + HTC (co-precipitation method)..... 49
Figure 4.1.7: TGA curves for reconstruction stabilisers intercalated with ortho and para mercaptobenzoic acids. 50
Figure 4.1.8: TGA curves for reconstruction stabilisers intercalated with ortho, meta and para hydroxybenzoic acids. 51
Figure 4.1.9: TGA curves for reconstruction stabilisers intercalated with ortho, meta and para aminobenzoic acids..... 51
Figure 4.1.10: TGA curves for reconstruction stabilisers intercalated with 4-ethylthiobenzoic acid and benzoic acid. 52
Figure 4.1.11: TGA curves for co-precipitation stabilisers intercalated with ortho and para mercaptobenzoic acids. 55
Figure 4.1.12: TGA curves for co-precipitation stabilisers intercalated with ortho, meta and para hydroxybenzoic acids. 55
Figure 4.1.13: TGA curves for co-precipitation stabilisers intercalated with ortho, meta and para aminobenzoic acids..... 56
Figure 4.1.14: TGA curves for co-precipitation stabilisers intercalated with 4-ethylthiobenzoic acid and benzoic acid. 56
Figure 4.1.17: FTIR spectra for 4-Aminobenzoic acid + HTC (reconstruction)..... 61
Figure 4.1.18: FTIR spectra for benzoic acid + HTC (reconstruction) 62
Figure 4.1.19: Average particle size distribution for anthranilic acid intercalated into hydrotalcite using the reconstruction method. 67
Figure 4.1.20: Average particle size distribution for 3-aminobenzoic acid intercalated into hydrotalcite using the reconstruction method. 68
Figure 4.2.1: Comparison of the effect of synthesis method on early stability. 70
Figure 4.2.2: Reconstruction stabiliser early heat stability as a function of organic loading mass percentage 72

Figure 4.2.3: Co-precipitation stabiliser early heat stability as a function of organic loading mass percentage 73
..... 74
Figure 4.2.4: Comparison of the effect of synthesis method on late stability. 74
Figure 4.2.5: Comparison of the effect of substituent group type for ortho position reconstruction stabilisers. 75
Figure 4.2.6: Comparison of the effect of substituent group type for ortho position co-precipitation stabilisers. 76
Figure 4.2.7: Comparison of the effect of substituent group type for meta position reconstruction stabilisers. 77
Figure 4.2.8: Comparison of the effect of substituent group type for meta position co-precipitation stabilisers. 78
Figure 4.2.9: Comparison of the effect of substituent group type for para position reconstruction stabilisers. 79
Figure 4.2.10: Comparison of the effect of substituent group type for para position co-precipitation stabilisers. 80
Figure 4.2.11: Early and late stability of amino and hydroxyl stabilisers (reconstruction) comparing the effect of substituent group position. 82
Figure 4.2.12: Early and late stability of amino and hydroxyl stabilisers (co-precipitation) comparing the effect of substituent group position. 83
Figure 4.2.13: The effect of substituent group length on PVC heat stability for reconstruction synthesised stabilisers. 84
Figure 4.2.14: The effect of substituent group length on PVC heat stability for co-precipitation synthesised stabilisers. 85
Figure A.1.1: XRD pattern for benzoic acid + HTC. 92
Figure A.1.2: XRD pattern for anthranilic acid + HTC. 92
Figure A.1.3: XRD pattern for 3-aminobenzoic acid + HTC. 93
Figure A.1.4: XRD pattern for 4-aminobenzoic acid + HTC. 93
Figure A.1.5: XRD pattern for salicylic acid + HTC. 94
Figure A.1.6: XRD pattern for 3-hydroxybenzoic acid + HTC 94
Figure A.1.7: XRD pattern for 4-hydroxybenzoic acid + HTC 95
Figure A.1.8: XRD pattern for 4-ethylthiobenzoic acid + HTC 95
Figure A.1.9: XRD pattern for thiosalicylic acid + HTC 96
Figure A.1.10: XRD pattern for 4-mercaptobenzoic acid + HTC 96

Figure A.2.1: XRD pattern for benzoic acid + HTC. 97
Figure A.2.2: XRD pattern for anthranilic acid + HTC. 97
Figure A.2.3: XRD pattern for 3-aminobenzoic acid + HTC. 98
Figure A.2.4: XRD pattern for 4-aminobenzoic acid + HTC. 98
Figure A.2.5: XRD pattern for salicylic acid + HTC. 99
Figure A.2.6: XRD pattern for 3-hydroxybenzoic acid + HTC 99
Figure A.2.7: XRD pattern for 4-hydroxybenzoic acid + HTC 100
Figure A.2.8: XRD pattern for 4-ethylthiobenzoic acid + HTC 100
Figure A.2.9: XRD pattern for thiosalicylic acid + HTC 101
Figure A.2.10: XRD pattern for 4-mercaptobenzoic acid + HTC 101
Figure B.1.1: FTIR spectra for benzoic acid + HTC. 102
Figure B.1.2: FTIR spectra for anthranilic acid + HTC. 102
Figure B.1.3: FTIR spectra for 3-aminobenzoic acid + HTC. 103
Figure B.1.4: FTIR spectra for 4-aminobenzoic acid + HTC. 103
Figure B.1.5: FTIR spectra for salicylic acid + HTC. 104
Figure B.1.6: FTIR spectra for 3-hydroxybenzoic acid + HTC. 104
Figure B.1.7: FTIR spectra for 4-hydroxybenzoic acid + HTC. 105
Figure B.1.8: FTIR spectra for 4-ethylthiobenzoic acid + HTC. 105
Figure B.1.9: FTIR spectra for thiosalicylic acid + HTC. 106
Figure B.1.10: FTIR spectra for 4-mercaptobenzoic acid + HTC 106
Figure B.2.1: FTIR spectra for benzoic acid + HTC. 107
Figure B.2.2: FTIR spectra for anthranilic acid + HTC. 107
Figure B.2.3: FTIR spectra for 3-aminobenzoic acid + HTC. 108
Figure B.2.4: FTIR spectra for 4-aminobenzoic acid + HTC. 108
Figure B.2.5: FTIR spectra for salicylic acid + HTC. 109
Figure B.2.6: FTIR spectra for 3-hydroxybenzoic acid + HTC. 109
Figure B.2.7: FTIR spectra for 4-hydroxybenzoic acid + HTC. 110
Figure B.2.8: FTIR spectra for 4-ethylthiobenzoic acid + HTC. 110
Figure B.2.9: FTIR spectra for thiosalicylic acid + HTC. 111
Figure B.2.10: FTIR spectra for 4-mercaptobenzoic acid + HTC 111
Figure C.1.1: Particle size distribution for benzoic acid + HTC. 112
Figure C.1.2: Particle size distribution for anthranilic acid + HTC. 112
Figure C.1.3: Particle size distribution for 3-aminobenzoic acid + HTC. 113
Figure C.1.4: Particle size distribution for 4-aminobenzoic acid + HTC. 113

Figure C.1.5: Particle size distribution for salicylic acid + HTC. 114
Figure C.1.6: Particle size distribution for 3-hydroxybenzoic acid + HTC. 114
Figure C.1.7: Particle size distribution for 4-hydroxybenzoic acid + HTC. 115
Figure C.1.8: Particle size distribution for 4-ethylthiobenzoic acid + HTC. 115
Figure C.1.9: Particle size distribution for thiosalicylic acid + HTC. 116
Figure C.1.10: Particle size distribution for 4-mercaptobenzoic acid + HTC. 116
Figure C.2.1: Particle size distribution for benzoic acid + HTC. 117
Figure C.2.2: Particle size distribution for anthranilic acid + HTC. 117
Figure C.2.3: Particle size distribution for 3-aminobenzoic acid + HTC. 118
Figure C.2.4: Particle size distribution for 4-aminobenzoic acid + HTC. 118
Figure C.2.5: Particle size distribution for salicylic acid + HTC. 119
Figure C.2.6: Particle size distribution for 3-hydroxybenzoic acid + HTC. 119
Figure C.2.7: Particle size distribution for 4-hydroxybenzoic acid + HTC. 120
Figure C.2.8: Particle size distribution for 4-ethylthiobenzoic acid + HTC. 120
Figure C.2.9: Particle size distribution for thiosalicylic acid + HTC. 121
Figure C.2.10: Particle size distribution for 4-mercaptobenzoic acid + HTC. 121
Figure D.1.1: Torque curve for benzoic acid + HTC run 1. 122
Figure D.1.2: Torque curve for benzoic acid + HTC run 2. 122
Figure D.1.3: Torque curve for benzoic acid + HTC run 3. 123
Figure D.1.4: Torque curve for anthranilic acid + HTC run 1. 123
Figure D.1.5: Torque curve for anthranilic acid + HTC run 2. 124
Figure D.1.6: Torque curve for anthranilic acid + HTC run 3. 124
Figure D.1.7: Torque curve for 3-aminobenzoic acid + HTC run 1. 125
Figure D.1.8: Torque curve for 3-aminobenzoic acid + HTC run 2. 125
Figure D.1.9: Torque curve for 3-aminobenzoic acid + HTC run 3. 126
Figure D.1.10: Torque curve for 4-aminobenzoic acid + HTC run 1. 126
Figure D.1.11: Torque curve for 4-aminobenzoic acid + HTC run 2. 127
Figure D.1.12: Torque curve for 4-aminobenzoic acid + HTC run 3. 127
Figure D.1.13: Torque curve for salicylic acid + HTC run 1. 128
Figure D.1.14: Torque curve for salicylic acid + HTC run 2. 128
Figure D.1.15: Torque curve for salicylic acid + HTC run 3. 129
Figure D.1.16: Torque curve for 3-hydroxybenzoic acid + HTC run 1. 129
Figure D.1.17: Torque curve for 3-hydroxybenzoic acid + HTC run 2. 130
Figure D.1.18: Torque curve for 3-hydroxybenzoic acid + HTC run 3. 130

Figure D.1.19: Torque curve for 4-hydroxybenzoic acid + HTC run 1. 131
Figure D.1.20: Torque curve for 4-hydroxybenzoic acid + HTC run 2. 131
Figure D.1.21: Torque curve for 4-hydroxybenzoic acid + HTC run 3. 132
Figure D.1.22: Torque curve for 4-ethylthiobenzoic acid + HTC run 1. 132
Figure D.1.23: Torque curve for 4-ethylthiobenzoic acid + HTC run 2. 133
Figure D.1.24: Torque curve for 4-ethylthiobenzoic acid + HTC run 3. 133
Figure D.1.25: Torque curve for thiosalicylic acid + HTC run 1. 134
Figure D.1.26: Torque curve for thiosalicylic acid + HTC run 2. 134
Figure D.1.27: Torque curve for thiosalicylic acid + HTC run 3. 135
Figure D.1.28: Torque curve for 4-mercaptobenzoic acid + HTC. 135
Figure D.2.1: Torque curve for benzoic acid + HTC. 136
Figure D.2.2: Torque curve for anthranilic acid + HTC. 136
Figure D.2.3: Torque curve for 3-aminobenzoic acid + HTC. 137
Figure D.2.4: Torque curve for 4-aminobenzoic acid + HTC. 137
Figure D.2.5: Torque curve for salicylic acid + HTC. 138
Figure D.2.6: Torque curve for 3-hydroxybenzoic acid + HTC. 138
Figure D.2.7: Torque curve for 4-hydroxybenzoic acid + HTC. 139
Figure D.2.8: Torque curve for 4-ethylthiobenzoic acid + HTC..... 139
Figure D.2.9: Torque curve for thiosalicylic acid + HTC. 140
Figure D.2.10: Torque curve for 4-mercaptobenzoic acid + HTC. 140
Figure D.3.1: Torque curve for HTC run 1. 141
Figure D.3.2: Torque curve for HTC run 2. 141
Figure D.3.3: Torque curve for HTC run 3. 142

1. Introduction

Poly(vinyl chloride) (PVC) is currently a widely used material. Rigid PVC is used as a material of construction for pipes, window frames and gutters. Softer, plasticised PVC may also be used to make clothing and electrical cable insulation.

The market for PVC additives is also large (Markarian, 2007). Thermal stabilisers and lubricants are required during the processing of PVC. Lubricants are necessary for easier processing and for preventing the PVC from adhering to the processing equipment. Depending on the desired end use, other additives such as plasticisers, fillers, impact modifiers, antioxidants and UV stabilisers are also added to PVC compounds. The versatility of PVC should not be underestimated. By changing the formulation of the PVC compound, the material may be hard and rigid or soft and flexible. PVC may be clear or opaque. It may act as an insulator or anti-static. These properties may be imparted or enhanced by the addition of certain additives.

PVC is highly susceptible to thermal degradation at its processing temperatures. Stabilisers must be added to increase the thermal stability of PVC and to mitigate the effects of the degradation. In the past heavy metal stabilisers (those based on lead and cadmium) were used to good effect to stabilise PVC. These stabilisers are currently being phased out owing to health concerns. Organotin stabilisers and mixed metal stabilisers are popular at present; however, organotin stabilisers are quite expensive. The current group of zinc and calcium based mixed metal stabilisers are not as effective as their cadmium and lead based counterparts (Gökçel, Balköse and Köktürk, 1998). These calcium-zinc stabilisers need to be used in conjunction with other stabilisers in order to perform effectively.

Hydrotalcite (HTC), a naturally occurring layered double hydroxide (LDH), has been shown to enhance the thermal stability of PVC to good effect. These LDHs may be modified by replacing the interstitial anion between the layers with certain organic species. It is anticipated that by performing this intercalation, a co-stabiliser may be synthesised that could impart good short and long term heat stability to PVC during processing.

There are various reasons for intercalating molecules into the LDH structure. Rossi *et al* (2005) states that the UV absorber, ferulic acid, may be intercalated into hydrotalcite to prevent induced environmental degradation of the acid.

Markland, Williams and O'Hare (2011) intercalated various flavouring compounds into different layered double hydroxides to improve the flavour retention of the compounds. They also determined that their flavourants were released over a gradual time period at a constant rate.

Kohno *et al* (2009) stated that natural dyes while superior to their synthetic counterparts are unstable. However, they proved that by intercalating these dyes into hydrotalcite, the stability of these dyes can be significantly improved.

Blooming and plate out are two factors of significance that must be taken into consideration when processing polymers. Blooming is defined as the deposit of partially compatible, non-volatile compounds such as oligomers, additives and degradation products by migration from the polymeric matrix to the surface during use (Jan & Bart, 2006: 139). Plate out is caused by additives volatilising during processing and condensing on the take-up equipment or dies (Giles, Mount & Wagner, 2007: 203). It is imperative for PVC not to have its heat stabilisers leaving the polymer matrix prematurely. This can also reduce the smell of foul smelling stabilisers like short chain thio- and mercapto based stabilisers. Therefore, intercalation of these stabilisers into layered double hydroxides may prove useful.

The purpose of this investigation is to see whether intercalating the LDH with different aromatic carboxylic acids will have an effect on the thermal stability of PVC. It is also of interest to see which properties of the organic compounds impart optimal stability, these properties being: substituent group type, substituent group length and substituent group position on the aromatic chain.

Samples of intercalated hydrotalcite were compounded with a flexible-grade PVC dry blend in a Haake® Polylab Rheomix torque rheometer. This testing gave an indication of the dynamic heat stability of the polymer. The torque curves produced by the Rheomix software were then analysed.

X-Ray Diffraction (XRD), Thermogravimetric Analysis (TGA), Fourier Transform Infrared Spectroscopy (FTIR) and, Particle Size Analysis (PSA) were performed on the synthesised stabilisers as means of characterisation. XRD determined whether or not intercalation occurred. TGA determined the mass percentage of the organic acid present in the stabiliser. FTIR results were used to confirm the presence of organic acids in the stabiliser. PSA determined the particle size distributions for the stabilisers.

2. Literature

2.1 PVC synthesis and properties

PVC is made from the polymerisation of the vinyl chloride monomer (VCM). VCM is made from natural gas and oil, which are cracked to form ethylene (Wilkes *et al*, 2005: 1). The ethylene then reacts with chlorine produced from the electrolysis of sodium chloride to form ethylene dichloride, which is finally cracked to form VCM. According to Wilkes *et al* (2005: 1), the chlorine content of PVC is 57 %. This implies that the production of PVC is less dependent on the use of fossil fuels than other polymers. Other thermoplastics, being largely comprised of hydrocarbons, are more dependent on fossil fuels for their synthesis. This makes PVC a unique polymer in terms of its raw materials source.

VCM has low reactivity but its radical is highly reactive. Due to this fact PVC is manufactured by radical polymerisation. This is a process where a chemical initiator is used to produce free radicals which then react with the monomer forming a second radical. This second radical propagates and forms long polymer chains by reacting with the rest of the monomer. Termination of these chains then occurs, thus ending the polymerisation process (Wypych, 2008: 26).

There are four methods of production for PVC, including bulk, emulsion, solution and suspension polymerisation (Wypych, 2008: 30). Suspension polymerisation is the most commonly used method and accounts for 80 % of the world's production of PVC.

Another unique property of PVC, imparted to it by its chlorine content, is its natural flame retardance. In other words, there is less fuel to burn due to the fact that more than half of the content of PVC is chlorine. The chlorine also provides condensed and gas phase combustion resistance by acting as a radical scavenger. The chloride ion attaches itself to a hydrogen ion, forming HCl thus reducing the available fuel for combustion (Wilkes *et al*, 2005: 13).

From a commercial standpoint, PVC is important. In 2000, 26 million metric tonnes of PVC was used worldwide, second only to the polyolefins (Wilkes *et al*, 2005: 14).

The growth of the PVC industry can be attributed to the development of thermal stabilisers thus making the processing of PVC viable. PVC is also recyclable. According to Wilkes *et al* (2005: 11), 135 000 tons of PVC are annually diverted from landfills and reused in second-generation products.

2.2 Thermal degradation of PVC

When PVC is processed at elevated temperatures it is degraded by dehydrochlorination, chain scission and crosslinking of macromolecules (Bacalogulu & Fisch, 2000: 427). The evolution of hydrogen chloride from the polymer chain causes discolouration of the resin as well as other changes to the physical and chemical makeup of the polymer. The discolouration results from the formation of polyene sequences. These sequences subsequently crosslink the polymer chain and form benzene or alkylated benzenes. The degradation process is autocatalytic in nature due to the fact that the evolved hydrogen chloride increases the degradation rate (Wypych, 2008: 89).

Wilkes *et al* (2005: 98) state that if the perfect PVC molecule could be manufactured it would be totally linear with all the VCM units linked in a head to tail fashion. The molecule would contain no branches, no unsaturation, no unusual terminal groups and no catalyst or emulsifier residues. This perfect PVC would be stable up to approximately 300 °C. Real PVC however contains numerous structural defects in the form of long and short chain branches, terminal and internal unsaturation, unusual end groups and both initiator and emulsifier residues. Structural defects may also arise from the polymerisation process.

Chloride groups that are present in some of the defect structures are unstable and therefore termed labile. Labile chlorides have a great effect on the heat stability of PVC. Their presence causes degradation at temperatures as low as 100 °C and causes rapid degradation in the processing temperature range of 170 °C to 220 °C (Wilkes *et al*, 2005: 98).

Other factors that increase the degradation rate are the presence of oxygen and chloride salts (metal chlorides). These chloride salts are usually present due to the reaction of thermal stabilisers with HCl. If the chloride salt is a strong Lewis acid, it will have a higher degradative effect on the PVC. These salts catalyse the

dehydrochlorination of PVC (Wypych, 2008: 82). Not all chloride salts catalyse the dehydrochlorination process. For instance, calcium chloride has no effect on the degradation of PVC. This is due to the fact that calcium chloride is not a Lewis acid. Other chloride salts that are thought not to influence the degradation rate are salts of potassium, barium, strontium, magnesium and lead.

Zinc chlorides formed by the reaction of zinc stabilisers with PVC during dehydrochlorination, act as catalysts for the dehydrochlorination process. It is also thought that as the concentration of these stabilisers increases, so to, do the degradative effects (Wypych, 2008: 83). Chlorides of aluminium, antimony, iron, germanium, silicon, boron, gallium and cadmium also accelerate the degradation process (Bacalogulu & Fisch, 2000: 430).

It is important to know these facts as these materials are used in additives to impart desirable properties to PVC. Additive antagonism can play a role in the entire system, therefore additive mixtures should be optimised in order to achieve a balance between desirable properties and the degradation they may cause to the system. Tin stabilisers can potentially form four different chlorine containing compounds. Each of these compounds has a varying degree of Lewis acidity. According to Wypych (2008: 86), tin stabilisers react with HCl according to the following reaction:

R_2SnY_2 HCl R_2SnClY HCl R_2SnCl_2 HCl RSn Cl_3 HCl S nCl_4

$SnCl_4$ and $RSnCl_3$ form strong Lewis acids and are therefore detrimental to the thermal stability of PVC. The character of the R group also plays a role in the Lewis acidity of the chloride salt. The R_2SnCl_2 groups should theoretically have a lower stability when compared to the $RSnCl_3$ groups. However, they are able to form different stabilising complexes which help to reduce the catalytic activity of the tin products when reacting with HCl.

2.2.1 Mechanisms of primary thermal degradation

There are two steps to the thermal degradation process of PVC. Primary degradation involves the zipper chain dehydrochlorination of the PVC molecules. The structural irregularities described in the previous section increase the degradation rate (Bacalogulu & Fisch, 2000: 428).

The dehydrochlorination results in the discolouration of the PVC due to the formation of conjugated polyene sequences

Figure 2.1 taken from Bacalogulu & Fisch (2000: 429) illustrates the degradation of structural irregularities such as allylic chlorides, tertiary chlorides and cis-keto allylic chlorides. The dehydrochlorination of regular monomer units is also shown.

The cis-keto allylic structures are not normally present in commercial PVC but can be generated by thermal oxidative processes. Once the irregularities have been degraded, the process continues degrading the normal monomer units. Not all allylic chloride species contribute to the degradation process. It has been found that some of these species do indeed become stable under degradation conditions.

Figure 2.2 taken from Bacalogulu & Fisch (2000: 430) illustrates the chain reaction model of PVC thermal degradation.

The first elimination reaction from either a monomer residue from the chain ($-CH_2-CHCl-$) or a structural irregularity such as a tertiary chlorine atom ($-CH_2CCl<$) forms an active intermediate (I_1) or a stable monoalkene (Bacalogulu & Fisch, 2000: 431). I_1 partitions itself to form a second intermediate I_2 and a stable sequence of two double bonds. I_2 proceeds to react in the same manner as I_1 thus promoting the formation of more double bond sequences.

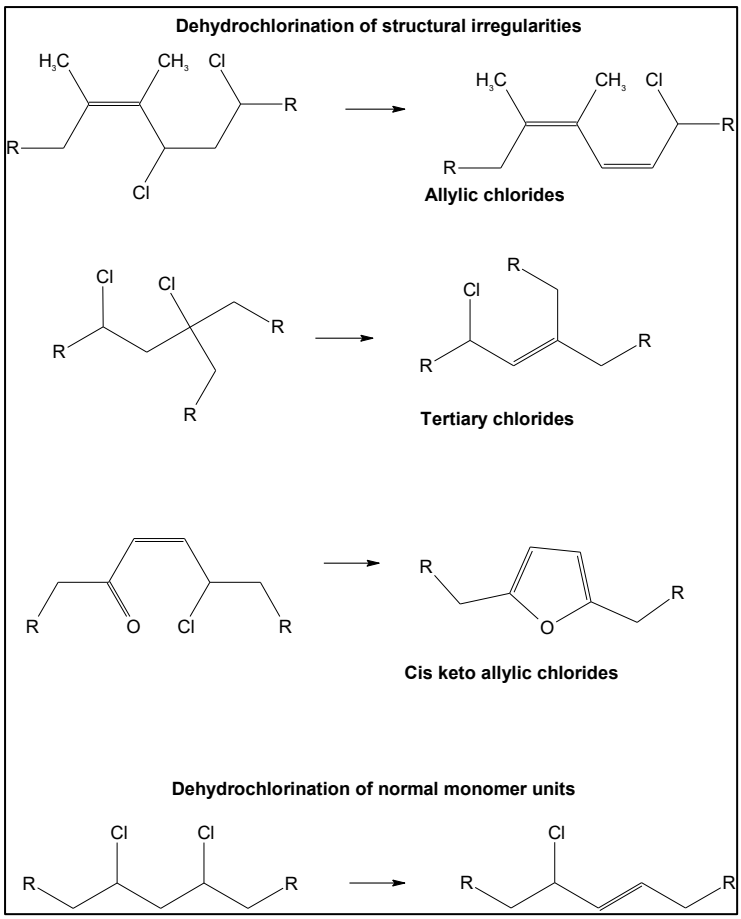

Figure 2.1: Reaction scheme showing degradation of structural irregularities in PVC (Bacalogulu & Fisch, 2000: 429).

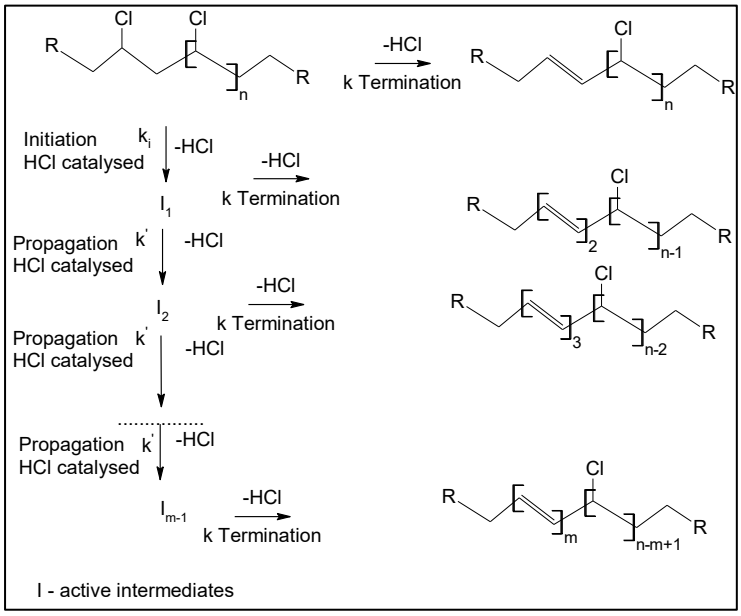

Figure 2.2: Reaction scheme showing the chain reaction model of thermal degradation (Bacalogulu & Fisch, 2000: 430).

The reaction scheme in figure 2.2 does not take into account the catalytic presence of chloride salts that may be present from reacted stabiliser molecules nor does it clarify the actual form of the intermediate molecules. The reaction schemes in figures 2.3, 2.4 and 2.5 rectify these problems. The following three figures are taken from Bacalogulu & Fisch (2000: 433-434).

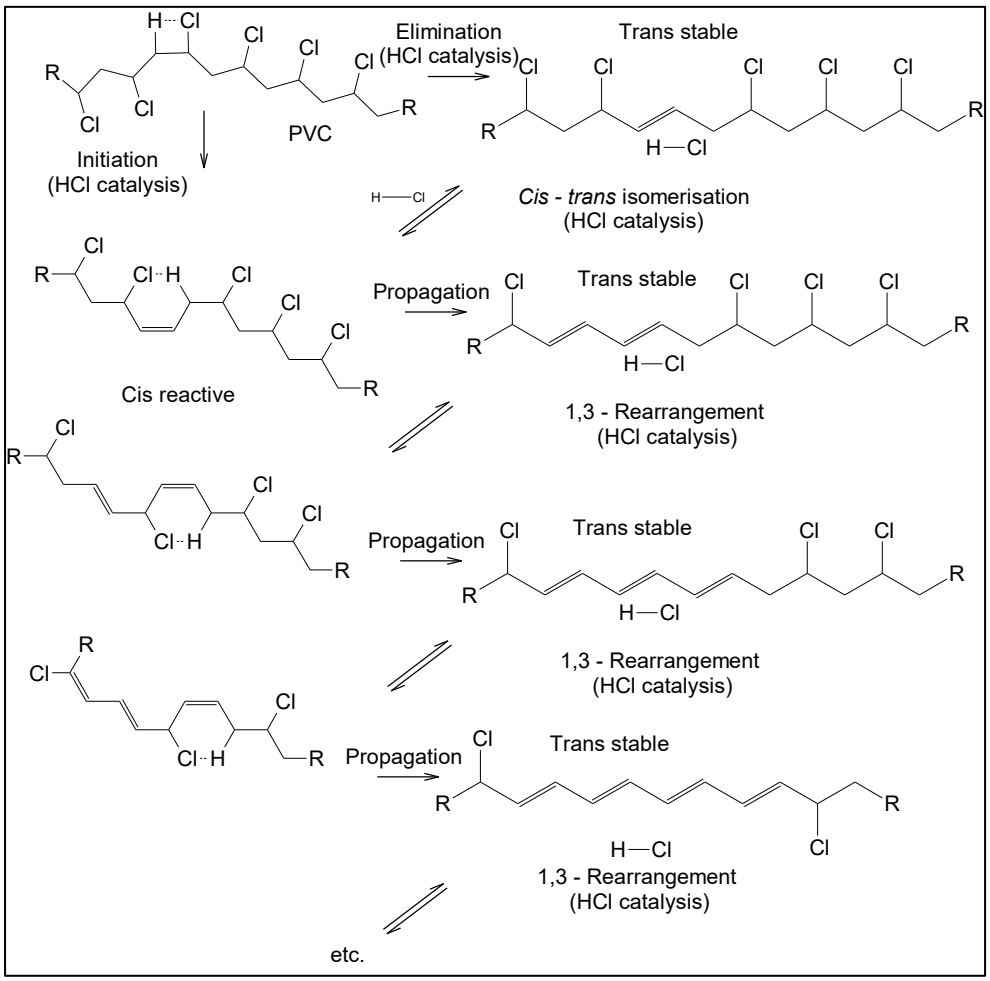

Figure 2.3: Reaction scheme showing clarification of the intermediate products and their arrangements (Bacalogulu & Fisch, 2000: 433).

The first step is a slow formation of a double bond at a random point on the polymer chain *via* a 1-2-unimolecular elimination of HCl through a four-centre transition state or a six-centre transition state in the presence of HCl or a metal chloride, in this case $ZnCl_2$, shown in figure 2.4 below.

The second and third steps of the processes involve the chain elimination at any point on the polymer chain regardless of the initiation site. In the second step, the HCl molecule is eliminated from a cis γ-alkyl-allyl chlorine through a six-centre transition state forming a conjugated diene or polyene. The third step involves a HCl-catalysed 1,3 chlorine rearrangement forming a new cis γ-alkyl-allyl chlorine from the conjugated polyene.

The second and third steps may continue as long as HCl is present in the system. Any Lewis acids in the system take on a similar role to HCl. Figure 2.5 shown below shows the formation of chloroalkanes from both HCl and metal chlorides (Lewis acids).

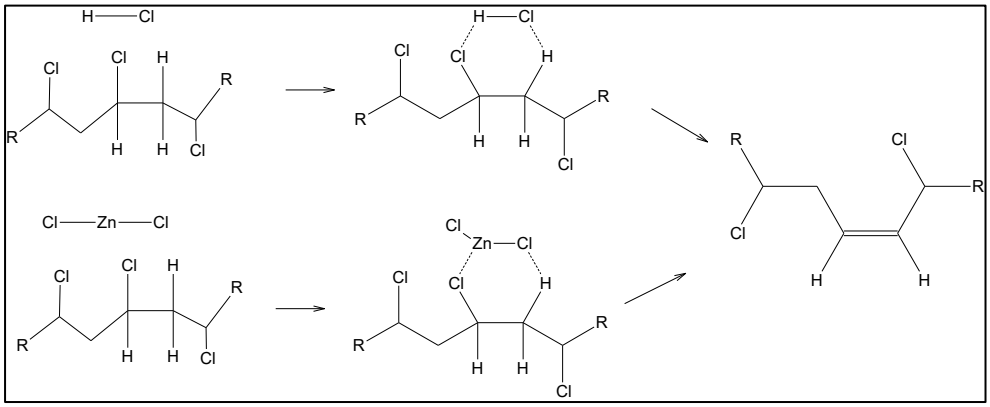

Figure 2.4: Reaction scheme showing the effects of HCl or a metal chloride on the degradation of PVC (Bacalogulu & Fisch, 2000: 433).

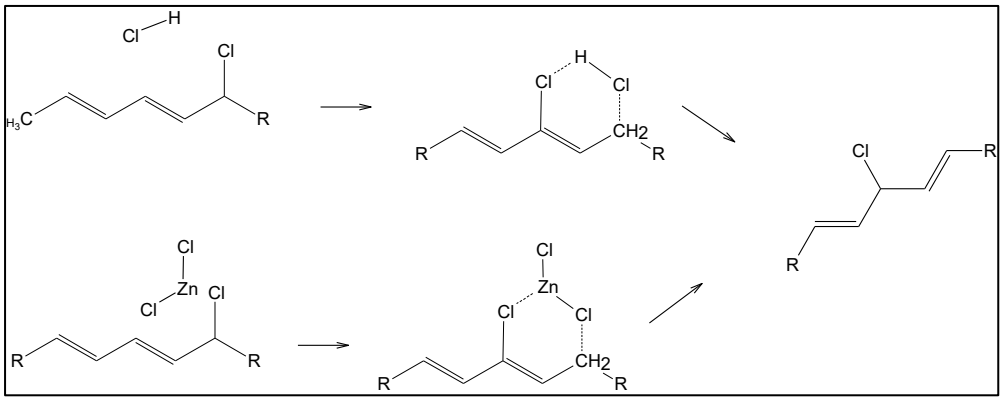

Figure 2.5: Reaction scheme showing the formation of chloroalkanes (Bacalogulu & Fisch, 2000: 434).

These chloroalkanes also act in a similar way to HCl and the Lewis acids in terms of PVC degradation.

2.2.2 Thermal oxidative degradation of PVC

In the previous section the mechanisms involving the thermal degradation of PVC takes place in the absence of oxygen. However, during processing, in addition to the thermal dehydrochlorination process, PVC is subject to thermo-oxidative degradation resulting from oxygen. Mechanical stress from processing may also cause chain scission (Bacalogulu & Fisch, 2000: 435).

The main feature of this type of degradation is the dehydrochlorination; however the presence of oxygen accelerates the dehydrochlorination process. This results in shorter polyene sequences due to the sequences reacting with oxygen.

Figure 2.6 depicts the dehydrochlorination process in the presence of oxygen.

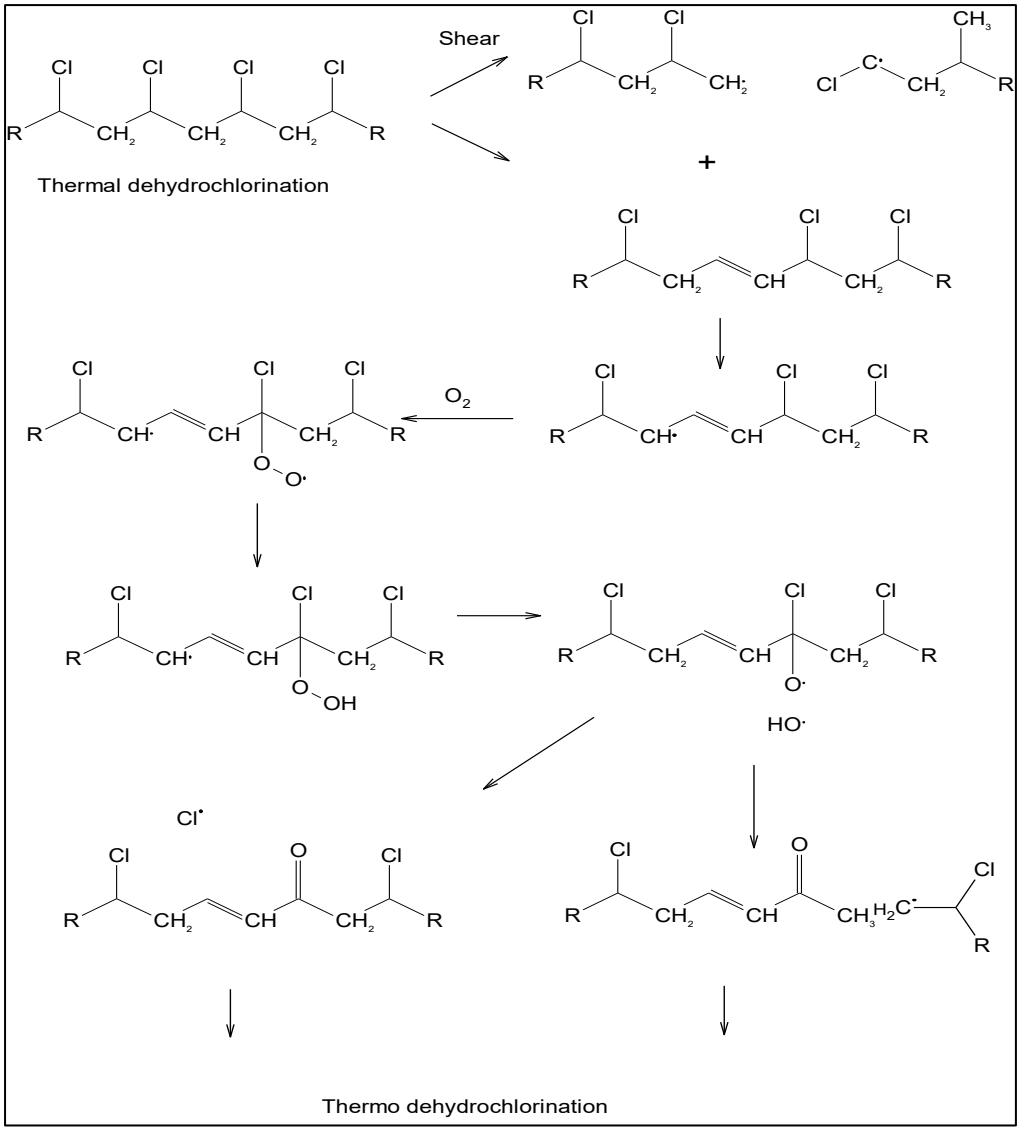

Figure 2.6: Reaction scheme showing thermal oxidative degradation of PVC (Bacalogulu & Fisch, 2000: 435).

It can be seen from the reaction scheme that shear forces caused by processing may cause chain scission of the polymer which generates radicals.

Thermally-initiated HCl loss is followed by radical oxidation of polyenes to form peroxy radicals and hydroperoxides. The hydroperoxides decompose to generate alkoxy and hydroxyl radicals that accelerate the oxidation process and form ketones and acid chlorides.

2.2.3 Mechanisms of secondary PVC degradation

Secondary degradation involves the highly reactive polyene sequences crosslinking and the subsequent cleaving of the polymer chain. This leads to the formation of benzene and condensed or alkylated benzenes. The chain scission and crosslinking results in a loss of physical properties of the polymer (Wilkes *et al*, 2005: 100).

During PVC degradation, polyene sequences increase linearly with HCl evolution. At higher HCl concentrations the polyene concentration levels off. This plateau value is lower when degradation temperatures and oxygen pressures are higher. When the plateau is reached, no long polyenes are formed from the double bond sequences (Bacalogulu & Fisch, 2000: 436).

In the absence of oxygen, a measurable increase in molecular weight occurs. An increase in the melt viscosity also occurs. It can therefore be observed that crosslinking of the polymer is occurring. This crosslinking is catalysed by HCl. The mechanism outlining the crosslinking process is shown below. The figure is taken from Bacalogulu & Fisch (2000: 436).

The Diels-Alder reaction is the most important crosslinking reaction. Benzene is formed in very small amounts by an intramolecular process.

At higher temperatures, substituted benzenes and condensed aromatic hydrocarbons are formed by radical scission of Diels-Alder condensation products and radical cyclisation of polyenes (McNeill, Memetea & Cole, 1995).

In the presence of oxygen, the same reactions take place but are more complex. Oxidative scission of the chain predominates and the molecular weight of the polymer decreases.

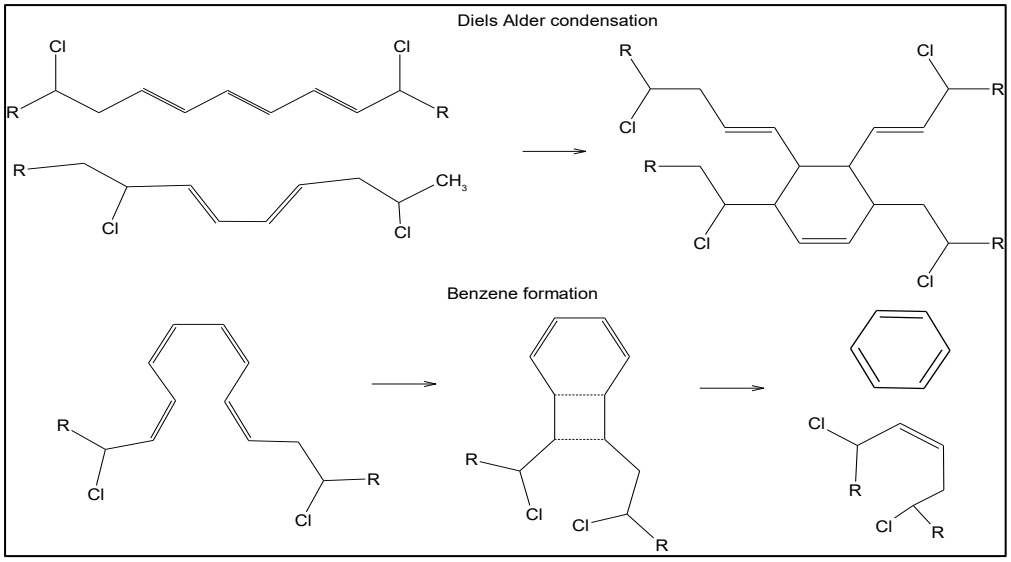

Figure 2.7: Reaction scheme depicting the Diels-Alder condensation of cisoid trans-trans dienes with other polyenes (Bacalogulu & Fisch, 2000: 436).

Due to the fact that the yellowing of PVC precedes the loss of any physical and mechanical properties of PVC, stabilisation efforts are focussed on preserving the initial colour of PVC both during processing and end use (Wilkes *et al*, 2005: 100).

2.2.4 Consequences of thermal degradation

Many of the consequences that occur as a result of PVC thermal degradation are influenced by the degradation temperature. The composition of the volatile components evolved from PVC is dependent on the degradation temperature (Wypych, 2008: 119). Between 160 °C and 180 °C HCl is the only evolved component. At 200 °C the composition of the evolved volatiles shifts towards being more organic in nature. The main organic component formed is benzene. At higher temperatures more HCl is emitted due to HCl catalysed dehydrochlorination. In addition to this, aromatic hydrocarbons, aliphatic hydrocarbons, chlorinated aliphatics and chlorinated aromatics are formed. Products of oxidation are formed in polymer and transferred to tar.

As the polymerisation temperature increases, the relative weight loss due to dehydrochlorination increases (Wypych, 2008: 120). This fact is consistent with the aforementioned thermal degradation mechanisms.

Char and ash are both able to form during the thermal degradation of PVC. Char usually forms either during pyrolysis or during a fire involving PVC.

Ash formation depends on the inorganic load of the polymer. The char formation is dependent on the temperature of the process. As this temperature increases so too does the char formation (Wypych, 2008: 121).

The colour change of PVC during thermal degradation is an important factor to consider. This colour change can be used as a measure of the degree of degradation. The colour changes very rapidly at the start of the degradation process and then levels off. The changes are from white to yellow to red to black (Wypych, 2008: 122). Black is an indication of complete degradation.

2.3 Heat stabilisation of PVC

2.3.1 Background

According to Wilkes *et al* (2005: 101) a general stabiliser is a substance which removes labile chloride groups, prevents oxidation, absorbs HCl and terminates the growth of polyene sequences all without generating any chloride salts which are Lewis acids that accelerate degradation. These stabilisers must be highly reactive materials that function rapidly at low concentrations without adversely affecting processing or aesthetics of the PVC.

Wilkes *et al* (2005: 101) go on to say that an ideal stabiliser provides good early colour, clarity, long-term stability, light stability, weatherability and processability. It should be perfectly compatible with the polymer, permanent, efficient, resistant to plate-out, stain resistant, non-volatile, colourless, odourless, tasteless, non-toxic and inexpensive. While no perfect stabiliser exists, groups of stabilisers may be combined to provide as many of the above qualities as possible. The efficiency of the stabiliser used is a function of its concentration in the system. Formulations should be optimised in order to extract the maximum possible performance from the stabiliser. Stabilisers present in incorrect concentrations may prove to be antagonistic to the system.

There are two ways in which heat stabilisers mitigate the effects of the thermal degradation of PVC. The stabiliser may react with the allylic chloride intermediate in the zipper degradation chain (Bacalogulu & Fisch, 2000: 437). This process should be faster than the chain propagation itself requiring a very active nucleophile.

The reactivity of the nucleophile should not be so high as to react with the secondary chlorine of the PVC chain. To be effective, the stabiliser must be associated by complex formation with polymer chlorine atoms. This implies the stabiliser should have Lewis acid character. These stabilisers prevent the formation of polyenes longer than four to five double bonds and maintain very good early colour in the polymer. These stabilisers are known as primary stabilisers (Bacalogulu & Fisch, 2000: 437).

Another way to stop thermal degradation is by scavenging the HCl evolved during the degradation process. The stabiliser should scavenge the HCl with high effectiveness to avoid its catalytic effect in chain initiation that starts another zipper dehydrochlorination chain. This stabiliser cannot prevent the formation of polyene sequences therefore early colour is not maintained. These stabilisers do provide good long term stabilisation. They are referred to as secondary stabilisers (Bacalogulu & Fisch, 2000: 437).

To maintain good early colour and to provide good long term stabilisation these stabilisers should be combined. As mentioned before, some stabilisers are capable of forming Lewis acids which accelerate the degradation process. In order to avoid this, the secondary stabilisers need to scavenge enough HCl to prevent the HCl reacting with the primary stabilisers which will result in the formation of Lewis acids. Another possibility is to include compounds called co-stabilisers in the system. Co-stabilisers form relatively stable complexes with the chloro derivatives of primary stabilisers and suppress their degradative effect. They are a combination of primary and secondary stabilisers (Bacalogulu & Fisch, 2000: 438).

2.3.2 Mechanisms of heat stabilisation

2.3.2.1 Organotin stabilisers

Figure 2.8 is taken from Wypych (2008: 271) and depicts the stabilisation mechanisms of different types of organotin stabilisers.

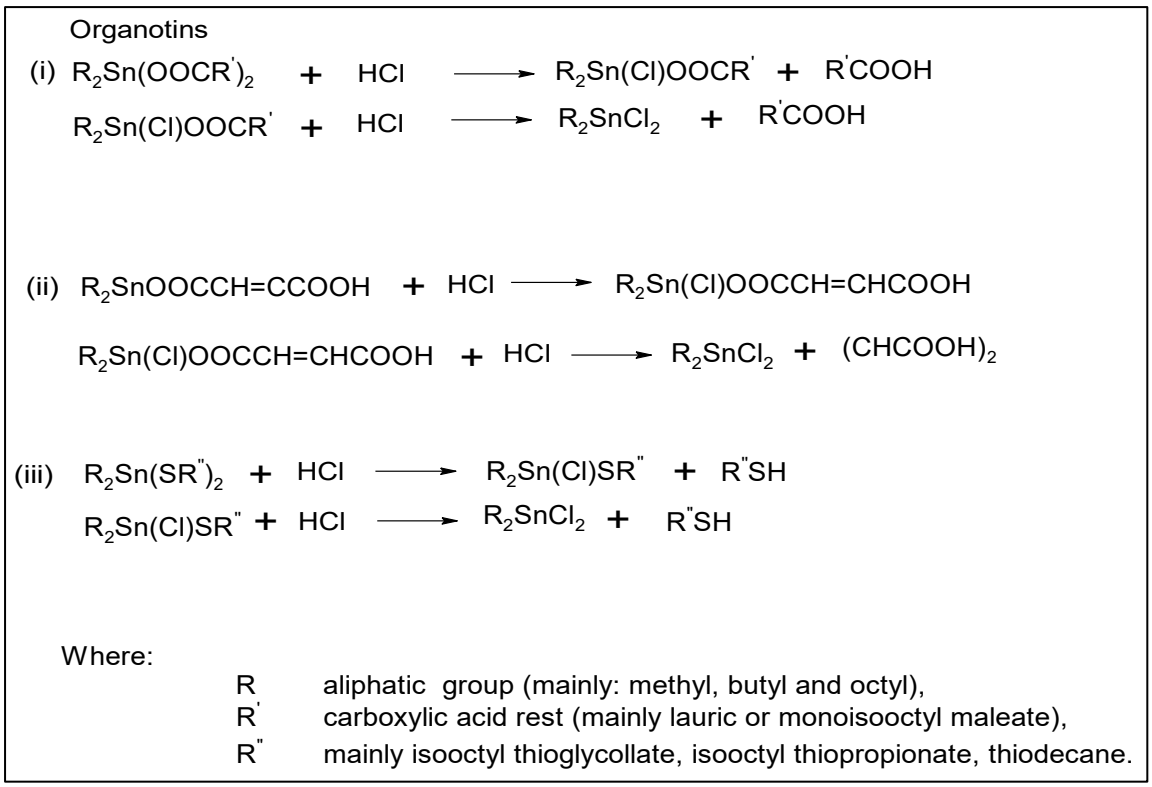

Figure 2.8: Stabilisation mechanisms of organotin stabilisers (Wypych, 2008: 271).

All of the above compounds react with HCl to form corresponding tin chlorides. However according to Bacalogulu & Fisch (2000: 438), the stabilisation effect does not correspond with the amount of HCl reacted nor with the rate of this reaction. Although it may be seen that the above stabilisers act as secondary stabilisers by scavenging HCl, this is not the main mechanism of their action. For example, alkyltin thioglycolates incorporate some of their thioglycolate groups into the polymer chain. Some of the thioglycolates are also exchanged with chlorine atoms from the allylic chloride groups on the polymer. The main stabilisation method of these compounds is that of a primary stabiliser. Organotin compounds are highly efficient PVC stabilisers.

They are highly compatible with the PVC matrix. One should be aware of the formation of the $RSnCl_3$ and $SnCl_4$ Lewis acids that will have a negative impact on the stabilisation process (Arkis & Balköse, 2005). The stability of the SnC bonds should be monitored as further reaction with HCl will result in the formation of the Lewis acids mentioned above.

Organotin compounds exhibit very good thermal stability as their decomposition temperature is much higher than the temperatures of PVC processing (Wypych, 2008: 324). It is interesting to note that the sulphur groups present in these organotin compounds play a valuable role in the primary stabilisation of PVC. These sulphur groups react with the PVC chain, substituting themselves for the allylic chloride groups (Wypych, 2008: 334). The sulphur containing organotins may react with isolated double bonds whereas non-sulphur containing compounds may not.

2.3.2.2 Mixed metal stabilisers

Figure 2.9 is taken from Wypych (2008: 271). It depicts the reactions involved with the metal soap stabilisation of PVC.

Metal soaps:

$$M(OOCR)_2 + HCl \longrightarrow ClMOOCR + RCOOH$$

$$ClMOOCR + HCl \longrightarrow MCl_2 + RCOOH$$

Figure 2.9: Mixed metal stabiliser reaction scheme (Wypych, 2008: 271).

Strongly basic carboxylates that contain metals such as K, Ca, Mg or Ba, which have little or no Lewis acidity act as HCl scavengers (Bacalogulu & Fisch, 2000: 439). Metals such as Zn or Cd which are stronger Lewis acids scavenge HCl and also substitute the carboxylate for the allylic chlorine atoms. Figure 2.9 shows the HCl scavenging mechanism

Figure 2.10 taken from Bacalogulu & Fisch (2000: 440) shows the primary stabilisation mechanism i.e. the reaction with the labile chlorine atoms on the polymer chain.

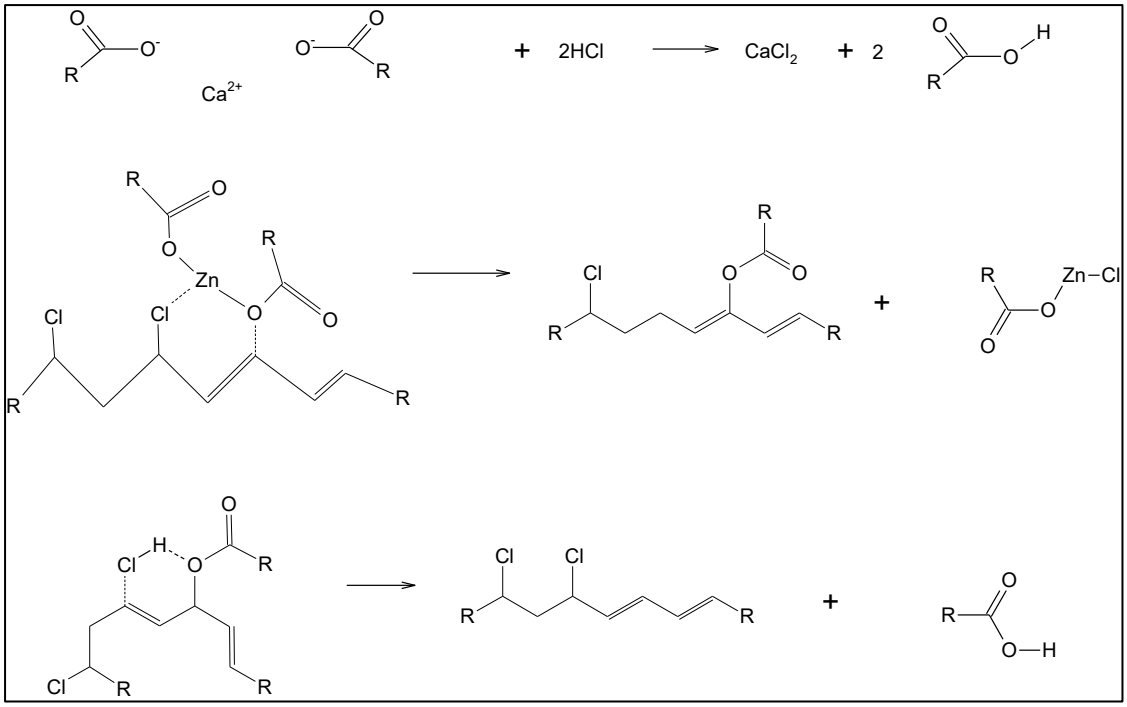

Figure 2.10: Mixed metal stabiliser reaction schemes showing both primary and secondary stabilisation mechanisms (Bacalogulu & Fisch, 2000: 440).

Once the concentration of metal carboxylates (metal soaps) is decreased, the ester group introduced into the polymer chain can be eliminated by reaction with HCl or by thermal degradation at higher temperatures. It has been found that there is a synergistic effect when using Zn or Cd carboxylates with Ba or Ca carboxylates. This is attributed to reactions between Zn or Cd chlorides and Ba or Ca carboxylates removing the catalytic effects of Zn or Cd chlorides in PVC degradation.

Figure 2.11 taken from Bacalogulu & Fisch (2000: 440) displays the synergism shown between Ca and Zn compounds.

The zinc stearate formed is more active in allylic chlorine substitution. Wypych (2008: 295) states that the following metals are used in combination with zinc carboxylates: Ba, Ca, Mg and K.

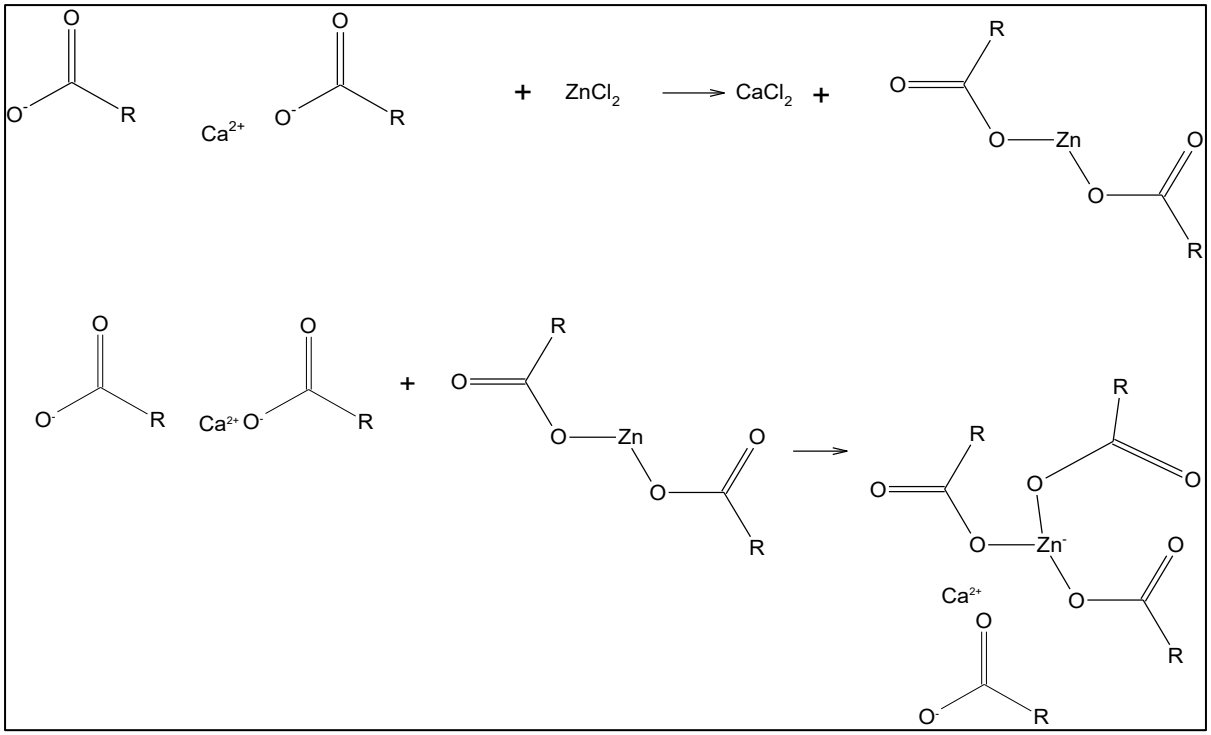

Figure 2.11: Ca and Zn co-stabilisers at work (Wypych, 2008: 295).

2.3.2.3 Alkyl phosphite stabilisers

Figure 2.12, taken from Wypych (2008: 271) shows the stabilisation mechanism of PVC by phosphite compounds.

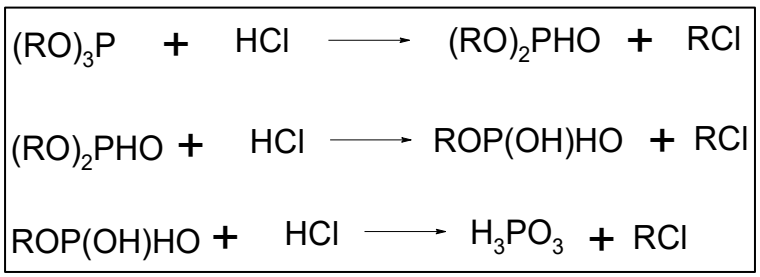

Figure 2.12: Secondary stabilisation mechanism of PVC by phosphite compounds (Wypych, 2008: 271).

Bacalogulu & Fisch (2000: 441) state that dialkyl phophites have no effect on PVC degradation. Trialkyl phosphites scavenge HCl and form dialkyl phosphites. They also react with allylic chlorides, but this process takes on a secondary role. In the presence of zinc di(dialkyl phosphites), formed from zinc salts and trialkyl phosphites as stabilisation proceeds, allylic substitution is considerably increased and becomes the dominant process in PVC stabilisation.

Thus in order to achieve effective long and short term stability, phosphite stabilisers should be used with zinc based stabilisers.

Phosphite stabilisers are also known to decompose peroxides and improve the transparency of PVC (Wypych, 2008: 342).

2.3.2.4 Epoxidised fatty acid ester stabilisers

Figure 2.13 taken from Wypych (2008: 272) shows the secondary stabilisation mechanism provided by epoxidised compounds to PVC.

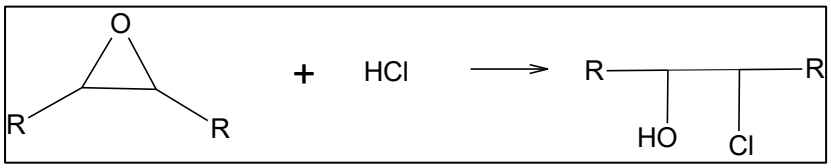

Figure 2.13: Secondary stabilisation mechanism of epoxidised stabilisers (Wypych, 2008: 272).

These stabilisers act as HCl scavengers; however Bacalogulu & Fisch (2000: 442) report that they can be effective primary stabilisers in the catalytic presence of Zn and Cd salts.

2.4 Layered double hydroxides

2.4.1 Background

Bergaya, Theng & Lagaly (2006: 1021) describe layered double hydroxides (LDHs) as being materials of a layered structure with a wide chemical composition (due to the variable isomorphous substitution of metallic cations). These materials have variable layer charge density, ion-exchange properties and a reactive interlayer space. These materials also swell in water. These properties make LDHs, clay-like materials. They are referred to as anionic clays due to their anion-exchange properties.

Hydrotalcite is the most representative mineral of the group hence LDHs are referred to as hydrotalcite-like compounds (Bergaya, Theng & Lagaly, 2006: 1021). Hydrotalcite has a structure similar to that of brucite ($Mg(OH)_2$) in which some of the Mg^{2+} ions in the metallic layer of the material are replaced by Al^{3+} ions.

Carbonate anions are found in the interlayer space of the material in order to maintain charge neutrality. The chemical formula of hydrotalcite is as follows: $Mg_{0.75}Al_{0.25}(OH)_2(CO_3)_{0.5}{\cdot}0.5H_2O$.

A general formula for the other LDHs, based on a combination of divalent and trivalent metal cations can be written as $[M^{II}_{1-x}M^{III}_x(OH)_2][X^{q-}_{x/q}{\cdot}nH_2O]$. $[M^{II}_{1-x}M^{III}_x(OH)_2]$ represents the composition of the metallic layer while $[X^{q-}_{x/q}{\cdot}nH_2O]$ represents the interlayer composition. Figure 2.14, taken from Bergaya *et al* (2006: 1022) depicts the LDH structure as well as the different elements that could possibly make up the composition of different synthetic and natural clays.

Hydrotalcite and the calcium containing hydrocalumite can be found naturally. However natural stocks of both materials are very limited (Bergaya *et al*, 2006: 1023). Synthetic LDHs may be produced in a wide variety of M^{2+}/M^{3+} combinations (Bergaya *et al*, 2006: 1024). LDHs are not limited to binary combinations of metal cations. Ternary, quaternary and multicomponent LDHs can also be synthesised (Bergaya *et al*, 2006: 1024). The ratio of M^{2+}/M^{3+} ions may vary depending on the synthesis conditions and the initial reagent concentrations. The interlayer may also be intercalated with many different types of anions. These anions include: halides, non-metal oxoanions, oxometallate anions, anionic complexes of transition metals, volatile organic anions and anionic polymers (Bergaya *et al*, 2006: 1026).

LDHs can act as catalysts, traps for anionic pollutants, antacids and delivery systems for pharmaceuticals (Auerbach, Carrado & Dutta, 2004: 374). The main commercial contribution though is to the polymer additive industry as PVC stabilisers, fillers and flame retardants. LDHs can also be used as a pigment stabiliser for plastics (Laguna *et al,* 2007).

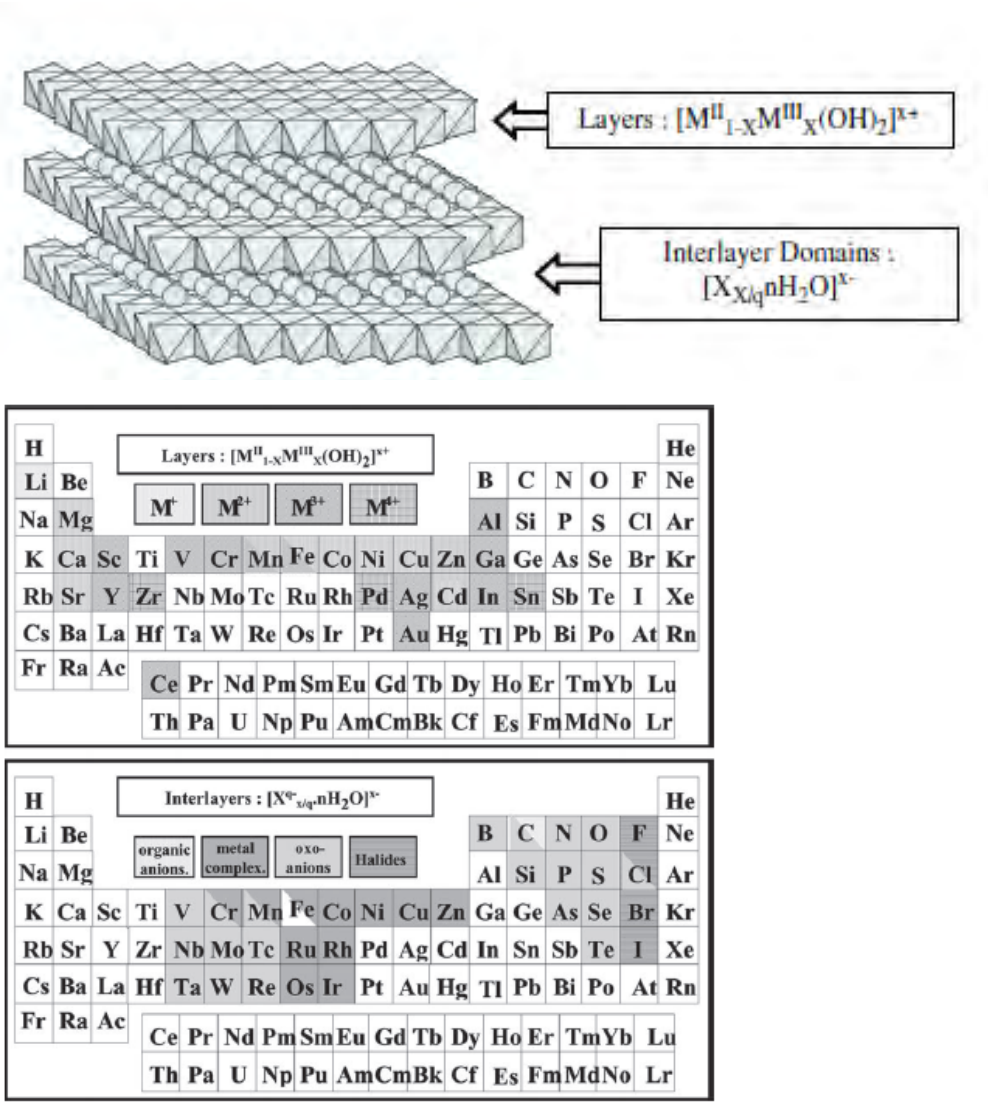

Figure 2.14: LDH structure and composition (Bergaya *et al* 2006: 1022).

2.4.2 Structure

The structure of hydrotalcite is that of cationic layers of Mg^{2+} and Al^{3+} ions with interstitial carbonate anions between the layers. Figure 2.15 below taken from Cygan, Liang & Kalinichev (2004) depicts the structure of hydrotalcite.

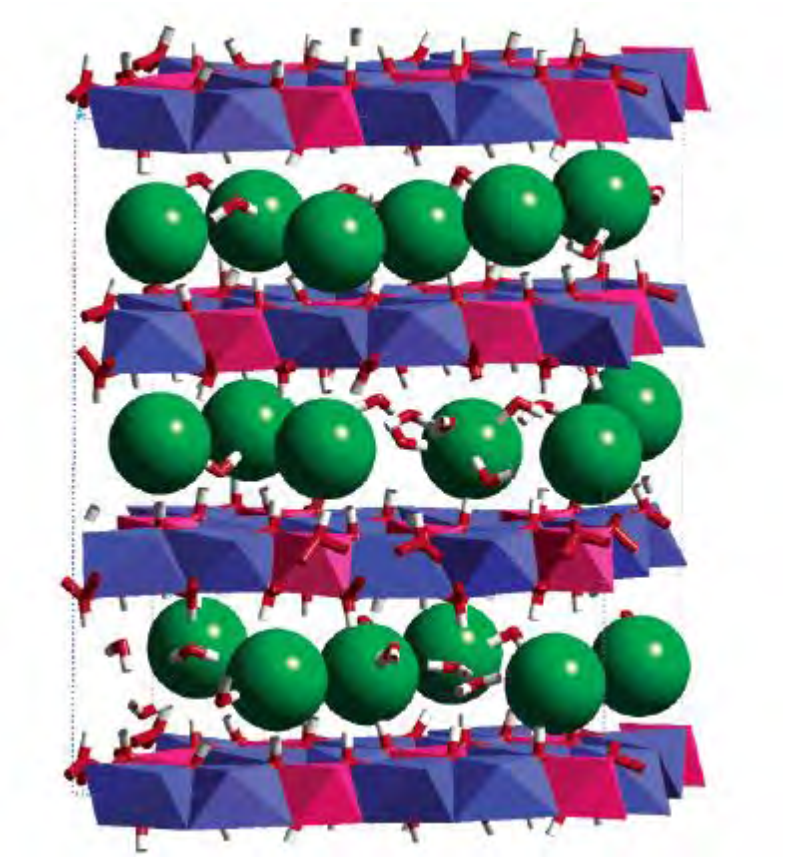

Figure 2.15: Equilibrium structure of hydrotalcite from an NPT molecular dynamics simulation (Cygan, Liang & Kalinichev, 2004).

The blue polyhedra represent magnesium and the pink polyhedra represent aluminium. The green spheres represent the interlayer anions (in this case chloride anions). The bent cylinders represent the water molecules.

Hydrocalumite is made up of cationic layers of Ca^{2+} and Al^{3+}ions with interstitial carbonate anions. Figure 2.16 taken from Vielle *et al* (2003) shows a structural representation of hydrocalumite.

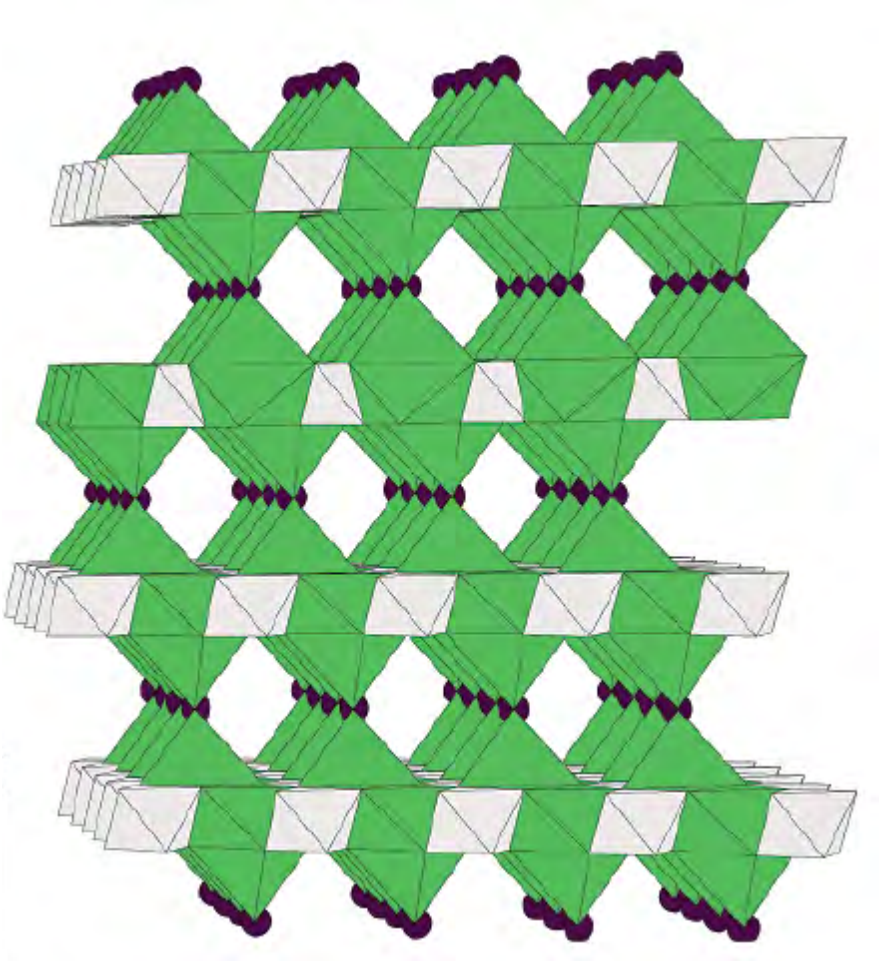

Figure 2.16: Crystal structure of dehydrated Friedel's salt, hydrocalumite with chloride anions in the interlayer (Vielle *et al* 2003).

The green and white polyhedral structures represent the metallic layers with the purple spheres representing the interstitial anions.

It can be seen from the structures that the shape of the metallic layer for hydrotalcite is different to that of hydrocalumite. The hydrotalcite has "straight" metallic layers compared to the more angled layers of hydrocalumite. This is due to the large difference in ion radii of the metal ions. The shape of the layers may have an effect on the intercalation of species between the layers.

2.4.3 LDH synthesis

LDHs are simple and inexpensive to synthesise (Bergaya *et al*, 2006: 1027). There are many methods available to prepare materials with specific physical and chemical properties for a variety of applications. Synthesis methods will be outlined in the sections that follow.

2.4.3.1 Co-precipitation

LDHs are readily prepared by the addition of a base to solutions containing a mixture of M^{II} and M^{III} ions. This method is known as the variable-pH co-precipitation method. Initially, M^{III} hydroxides and hydrous oxides are formed with further addition of base resulting in a co-precipitation or conversion into LDH. In order to obtain LDHs with high chemical homogeneity, co-precipitation at constant pH is recommended. This allows for the preparation of a great number of LDHs with carbonate, chloride and nitrate anions as precursors for subsequent reactions. A constant pH is obtained by simultaneous addition of a base solution (NaOH, KOH or NH_4OH) and a mixed metal salt solution. (Bergaya *et al*, 2006: 1027)

Bergaya *et al* (2006: 1028) report that materials prepared by the co-precipitation method have a high crystallinity (after aging), small particle size, high specific surface area and high average pore diameter. The co-precipitation method can be limited by competitive reactions such as the precipitation of metal salts as is the case of oxoanions with high metal ion affinity.

2.4.3.2 The urea method

The urea method involves performing the co-precipitation method with urea as the titrated base. During normal co-precipitation, supersaturation of the precipitating agent (OH^-) is reached rapidly and maintained throughout the reaction. (Bergaya *et al*, 2006: 1028)

This leads to continuous nucleation of mixed hydroxides as well as the growing and aggregation of the particles. Urea is used to separate the nucleation step from the particle growth thus preventing the particle aggregation. Urea is a very weak base and is highly soluble in water. Bergaya *et al* (2006: 1028) report that the hydrolysis of urea proceeds in two steps:

i. The formation of ammonium cyanate as the rate-determining step;

ii. The fast hydrolysis of cyanate into ammonium carbonate.

This hydrolysis rate can be controlled by temperature. The hydrotalcite formed by this method consists of large well crystallised platelets. The reaction temperature as well as the concentrations of the reactants controls the particle size.

2.4.3.3 Induced hydrolysis

This method of synthesis involves contacted dropwise addition of oxides such as ZnO, NiO and CuO. These oxides are added to acidic solutions of trivalent metal salts such as $AlCl_3$ or $CrCl_3$ and dissolved while an LDH is precipitated provided the pH is buffered by the oxide and/or hydroxide suspension (Bergaya *et al*, 2006: 1029).

This synthesis has been used to prepare [Zn-Cr-Cl] LDH, [Zn-Cr-NO_3] LDH, [Zn-Al-Cl] LDH and [Zn-Al-NO_3] LDH. Induced hydrolysis is not limited to reactions between di- and trivalent cations but can involve divalent-divalent, divalent-tetravalent and trivalent-trivalent species (Bergaya *et al*, 2006: 1029).

2.4.3.4 Reconstruction

The reconstruction method involves the hydration of calcined LDHs. It is possible to perform this type of synthesis due to the structural memory effect and can be used as a general preparation method of LDHs (Bergaya *et al*, 2006: 1029).

The original LDH is calcined at temperatures between 400 °C and 500 °C driving off the volatile interstitial anion leaving the original LDH as a mixture of oxides. The following reaction depicts the calcination of the LDH. It is assumed that the LDH in question is hydrotalcite:

$$Mg_4Al_2(OH)_{12}(CO_3)\cdot 3H_2O \rightleftharpoons 4MgO\cdot Al_2O_3 + CO_2 + 9H_2O$$

The calcined LDH is then rehydrated in an aqueous solution containing the anion to be intercalated into the LDH. The structural recovery of the LDH is determined by the calcination conditions i.e. the temperature, rate and duration.

The following chemical reaction is used to depict this rehydration step. The reaction assumes the use of hydrotalcite as the LDH to be reconstructed:

$$4MgO{:}Al_2O_3 + 2A^- + 6H_2O \longrightarrow Mg_4Al_2(OH)_{12}(A_2){\cdot}xH_2O$$

The A^- in the equation represents the monovalent acid anion to be intercalated into the LDH. The *x* represents the amount crystal water in the final product which is dependent on each reaction. The reconstruction method does have its limitations. It has been found that repeated calcination/hydration cycles with hydrotalcite decrease the content of the interlayer carbonate anions increasing the extraction of Al^{3+} from the brucite layers. The reconstruction method cannot be used for all M^{II}-M^{III} combinations (Bergaya *et al*, 2006: 1030).

The reconstruction method is suitable for the preparation of LDHs with large organic anions such as dyes (Bergaya *et al*, 2006: 1030).

2.4.3.5 Sol-gel technique

LDHs may be prepared by sol-gel processes. The samples produced by this technique are less crystalline than those produced by co-precipitation. They do however have a marked increase in surface area (Bergaya *et al*, 2006: 1030).

The sol-gel method is cost effective and produces LDHs of a high purity. The homogeneity and structural properties of the final product are controlled at the synthesis level by varying the composition of the precursor materials, temperature, ageing time and the removal or addition of reactant species (Othman, 2009).

During sol-gel processing, the desired metal precursors are hydrolysed in water, an aqueous solution or a liquid-organic solvent at ambient conditions to produce a polymeric or particulate sol. Acid or base is then added to the sol mixture during hydrolysis to facilitate peptisation of the solution so as to obtain highly dispersed metals in the solution (Bergaya *et al*, 2006: 1030).

2.4.3.6 Hydrothermal, microwave and ultrasound treatments

Different methods are used post-synthesis to alter or control the structural and textural properties of the LDH. Microwaves are used during synthesis to accelerate both the growing and ageing steps. Short microwave irradiation results in a well-crystallised material compared to normal co-precipitation methods. The surface area

and porosity of the material also increases with the increasing duration of microwave exposure (Bergaya *et al*, 2006: 1031).

Ultrasound irradiation can also be used to improve the crystallinity of the phases. Hydrothermal treatment can be used to the same effect (Bergaya *et al*, 2006: 1031).

Hydrothermal treatment also increases the anion-exchange rate of low-affinity ions such as alkyl carboxylates (Bergaya *et al*, 2006: 1031).

2.4.3.7 Anion exchange reactions (acid attack)

Anionic-exchange reactions are used to intercalate anionic species into the interlayer spaces of LDHs (Auerbach *et al*, 2004: 194). Ion exchange reactions are difficult for LDHs due to their high selectivity of carbonate anions and their large anion exchange capacity. The order of preference of anion selectivity is as follows (Auerbach *et al,* 2004:380):

NO_3^- < Br^- < Cl^- < F^- < OH^- < MoO_4^{2-} < SO_4^{2-} < CrO_4^{2-} < $HAsO_4^{2-}$ < HPO_4^{2-} < Naphthol Yellow^{2-} < CO_3^{2-}.

The order above is determined by the charge, the charge density and hydrogen bonding.

2.4.3.8 Synthesis of organo-LDH

Organo-LDHs are LDHs that have been intercalated with organic anions. These intercalations take place through direct precipitation as well as anion-exchange reactions. Urea hydrolysis may also be used to prepare these LDHs (Bergaya *et al*, 2006: 1035).

The reconstruction method involving the calcination of hydrotalcite is also a successful organo-LDH synthesis method (Bergaya *et al*, 2006: 1036).

2.4.3.9 Precursor intercalation method

According to Schmidt (2013), there exists a novel method that synthesises intercalated LDH from its precursor materials. This method produces no effluent and is less energy intensive than the reconstruction method of synthesis. An intercalated hydrocalumite would be synthesised using the following two reaction steps:

Step 1: $4CaO + 2Al(OH)_3 + H_2O \longrightarrow Ca_3Al_2(OH)_{12} + Ca(OH)_2$

Step 2: $Ca_3Al_2(OH)_{12} + Ca(OH)_2 + 2A^- + H_2O \longrightarrow Ca_4Al_2A_2(OH)\cdot 5H_2O$

Calcium oxide, aluminium hydroxide and water react to form katoite ($Ca_3Al_2(OH)_{12}$) and portlandite ($Ca(OH)_2$). The katoite and portlandite may then be reacted in a water-acid solution to form an intercalated LDH.

The largest hazard of this synthesis method is the presence of air. If the katoite and portlandite species are hydrated in the presence of air, carbon dioxide will intercalate between the layers as carbonate. This interstitial carbonate is extremely stable and thus very difficult to replace.

Due to the small amount of carbon dioxide in the air, the system need not be purged of air entirely. During the intercalation process, the system must simply be closed to prevent carbonate formation.

2.4.4 Use of LDH as a PVC heat stabiliser

Hydrotalcites are able to stabilise PVC during the thermal degradation process by acting as HCl scavengers (Gupta, Agarwal & Banerjee, 2009). Since they act as secondary stabilisers they are only able to promote the long term stability of PVC. The short term stability is only promoted to an extent by hydrotalcite.

The stabilisation mechanism provided by hydrotalcite is one of anion exchange between the interstitial carbonate anion and the chloride anion belonging to HCl (Gupta *et al*, 2009). This restricts the amount of HCl available to act as a catalyst during the dehydrochlorination process.

It is also thought that due to its high surface area, hydrotalcite acts as an acid absorber. Gupta *et al* (2009) report that the binding of anions is able to take place on the surface as well as the interlayer of hydrotalcite. The carbonate anion is difficult to displace from the interlayer due to its small size and divalent nature.

The HCl scavenging process is only possible once the HCl is converted to chloride anions. Thus the chloride anions are able to displace the interstitial carbonate anion. HCl gas is still adsorbed to the surface of the hydrotalcite. The adsorbed HCl eventually reacts with the layers causing them to be lost and resulting in the formation of metal chlorides (Lin *et al*, 2006).

Modifying both the structure as well as the interlayer composition of hydrotalcite is of interest in order to see if these modifications will provide good thermal stability for PVC. Lin *et al* (2006) investigated the stabilisation effects of an intercalated LDH as well as a LDH with modified layers compared with the stabilisation effects of hydrotalcite. They used MgZnAl-CO_3-LDH as the modified layer LDH and MgZnAl-maleate-LDH as the intercalated LDH.

They proved that the addition of the modified layer LDH leads to enhancements of both the long term and short term stability of the PVC. The intercalated LDH showed good enhancement of the short term stability. This is due to the intercalated maleate anion reacting with the polyene sequences formed during the dehydrochlorination process thus inhibiting the autocatalytic degradation of PVC. Maleate is able to react with the polyenes as it has a conjugated double bond.

The following figure depicts the stabilisation mechanism provided to PVC by hydrotalcite-like substances.

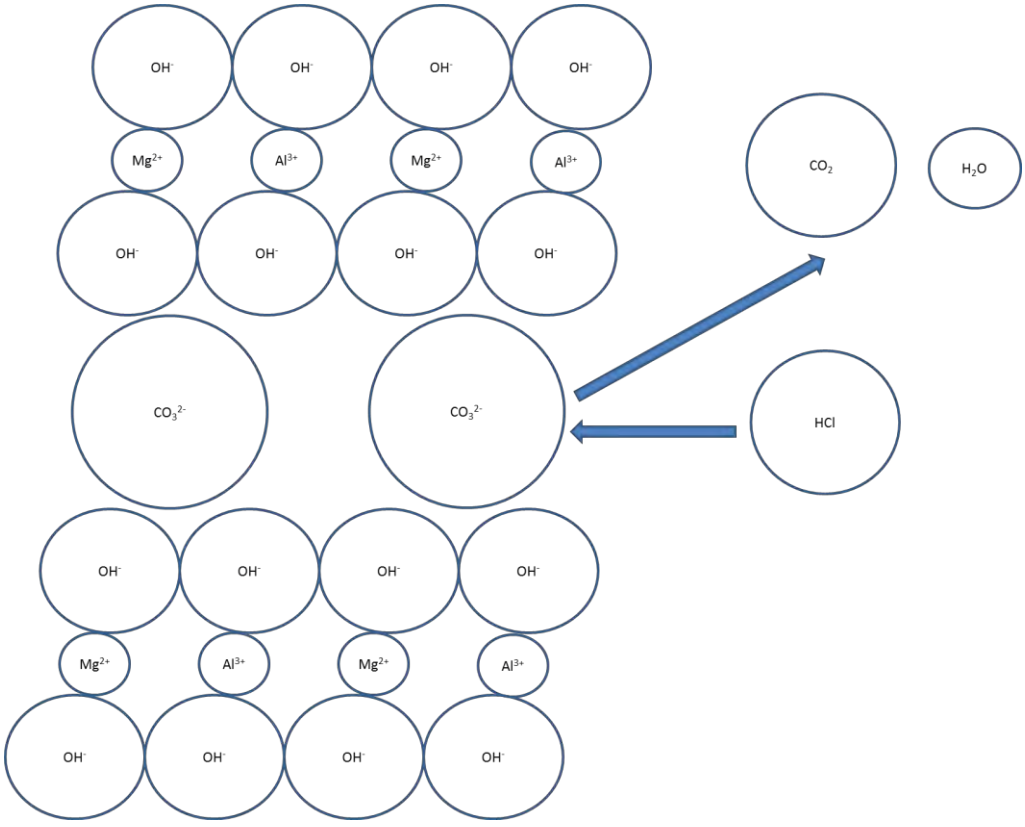

Figure 2.17: Schematic of stabilisation mechanism provided by hydrotalcite to PVC.

It can be seen from Figure 2.17 that the hydrochloric acid molecule produced in the degradation process replaces the interstitial carbonate anion. The carbonate anion then becomes CO_2 and H_2O. The stabilisation mechanism for intercalated LDHs is the same, the exception being the interstitial anion is the intercalated organic substance. The organic anion, once displaced by the chloride, proceeds to react with the polymer chain thus mitigating the effects of secondary degradation process.

2.4.5 Aromatic carboxylic acids as potential intercalants

It should be noted that all of the intercalated molecules featured in this investigation are substituted aromatic carboxylic acids. These aromatics contain an electron withdrawing group in the form of the carboxylic acid functional group and an electron donating group in the form of the substituted branches on the aromatic molecule.

Electron withdrawing groups remove electron density from a pi system making the system more electrophilic, that is the system is attracted to electrons (Bruice, 2014: 929). This factor explains why the aromatic carboxylic acid species are able to be intercalated within the LDH structure through anionic exchange reactions.

Electron donating groups donate electron density to a conjugated pi system *via* resonance or inductive electron withdrawal (Bruice, 2014: 930). This leads to the pi system becoming more nucleophilic; that is the intercalated molecule donates electrons to the system. This explains why intercalated molecules of the aromatic carboxylic acid type are able to stabilise free radicals on a degrading PVC chain.

Electron donating groups and electron withdrawing groups have different levels of activating ability and deactivating ability respectively: strong, moderate and weak. Strongly and moderately deactivating groups direct electrophilic attack to the meta position of the aromatic chain (Bruice, 2014: 931). Weakly deactivating groups are ortho and para directing. Strongly activating groups favour electrophilic substitution about the ortho and para positions on the aromatic chain. The carboxylic acid group on the aromatic chain is the only moderately deactivating group featured in this investigation. The amino and hydroxyl groups on the aromatic chain are strongly activating groups.

The mercapto group present on some of the intercalated molecules is also an activating group (Acton, 2013: 322). The substituents in order of most activating for this investigation are (Bruice, 2014: 932):

$$-NH_2 > -OH > -SH$$

Electron withdrawal decreases reactivity toward electrophilic aromatic substitution and increases acidity whereas electron donation increases reactivity toward electrophilic aromatic substitution and decreases acidity (Bruice, 2014: 939). The pKa value for a particular compound may be used as a measure of its reactivity.

2.5 Thermal degradation testing methods

2.5.1 Hydrogen chloride evolution tests

2.5.1.1 Congo red test

The Congo red test may be done in accordance with the ISO 182-1 standard (International Standards Office, 1990a). The principle behind this test is the measurement of HCl evolution from PVC at predetermined degradation temperature. Congo red indicator paper is held above the PVC sample while the degradation takes place. A colour change of the paper from red to blue is observed. The time required for the colour to change is the stability time.

The specification describes the test procedure and sample preparation for the different types of PVC i.e. PVC plastisols, PVC pellets, PVC films and sheets, PVC coatings and insulation or sheathing of cables and conductors. The predetermined degradation temperature should be 200 °C for unplasticised samples and cable insulation samples. A temperature of 180 °C should be used for plasticised samples.

2.5.1.2 pH testing method

The pH testing method may be done in accordance with the ISO 182-2 standard (International Standards Office, 1990b). The principle behind the test is the measurement of HCl evolution by measuring the pH change of a 0.1 mol/l sodium chloride solution which is used to absorb the evolved HCl. This test is performed in a gas stream.

The reagents and apparatus used are outlined in the standard. Two types of dehydrochlorination cells are available: a reusable cell and a disposable cell. The

dimensions for both of these cells are given in the standard. Preparation methods for the types of samples mentioned in the previous section are also given. The same testing temperatures are used as for the Congo red test.

2.5.1.3 Conductiometric method

The conductometric method may be done in accordance with the ISO 182-3 standard (International Standards Office, 1993). The principle behind this test is to measure the amount of HCl evolved during the thermal dehydrochlorination process. The HCl is absorbed into a given amount of demineralised water. The amount of HCl evolved is determined in relation to the recorded change in conductivity of the water.

The reagents and apparatus are outlined in the standard. The dehydrochlorination cells used in the previous test may also be used for this standard. Samples must be prepared according to the standard depending on the type of PVC to be tested

2.5.2 Static testing

The standard practice for the oven heat stability of PVC is laid out in ASTM D 2115-04 (American Society for Testing and Materials, 2002). This test measures the degree of discolouration of a PVC sample and correlates this measurement to thermal degradation that has taken place. In order for good comparative testing to occur, the thickness of each sample must be the same.

This test is good for the comparative testing of different stabilisers and is not intended to measure the absolute thermal stability. Molecular degradation phenomena such as chain scission or crosslinking may not be identifiable.

The PVC samples are made by compounding PVC dry blend on a two-roll mill to form sheets. The samples are then placed in a forced-air type oven. The samples degrade in the oven at a fixed temperature. Samples are removed at regular intervals over an exposure range to discolouration i.e. the sample that has been left in the oven for the longest time should be black.

The composition of the compound, test temperature and exposure times should be reported. The relative heat stabilities are based on time of exposure and degree of discolouration as compared to a standard sample or control.

2.5.3 Dynamic testing

The standard practice for fusion of PVC compounds using a torque rheometer is laid out in ASTM D 2538-02 (American Society for Testing and Materials, 2004). When PVC compounds are mixed under appropriate conditions of heat and shear a fused mass is produced. This mass has certain melt characteristics which can be defined with a torque rheometer operating at a fixed temperature and shear.

These melt characteristics can give an indication of the heat stability of the compound as well as other properties such as the colour stability, fusion torque, fusion time, melt torque and melt viscosity.

The PVC sample is usually a dry blend that is compounded in the rheometer. The procedure for thermal stability testing involves loading the rheometer with a pre-weighed amount of sample and then running the rheometer while the torque curve is plotted. The torque curve readout will give an indication of when the PVC has degraded and thus, when to stop the test. The Figure 2.18 taken from the standard shows a sample torque rheometer curve, with time elapsed plotted on the x axis and torque measured plotted on the y axis.

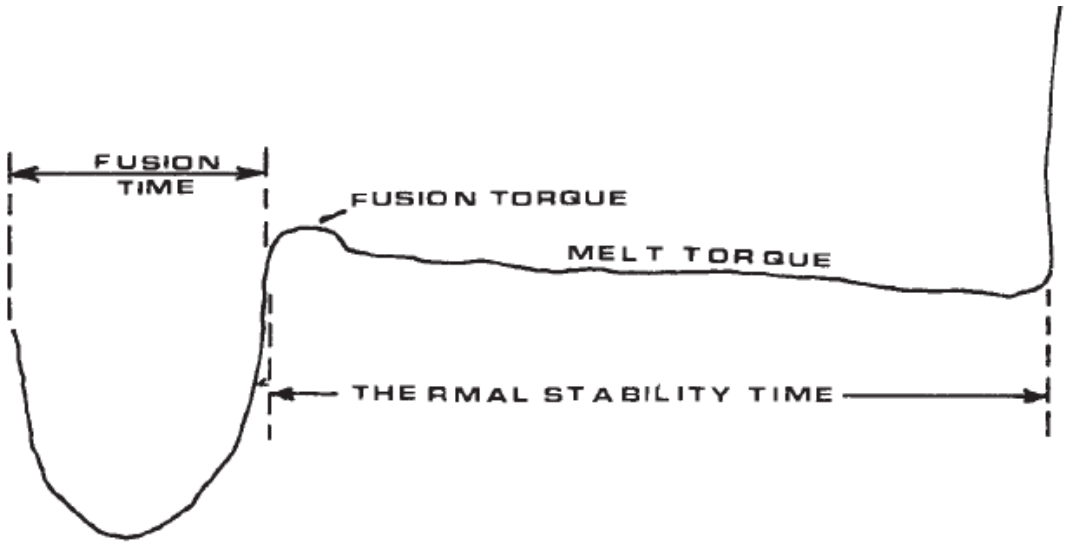

Figure 2.18: Torque curve showing heat stability parameters (American Society for Testing and Materials, 2002).

The long plateau gives an indication of the thermal stability time and is a good measure of the early colour provided to the PVC by the heat stabiliser. This thermal stability time is known as the early stability. The area where the torque reaches a maximum after the thermal stability time is an indication of the long term stability provided to the PVC by the stabiliser. This thermal stability time is known as the late stability.

The following information should be reported after the test: the compound heat stability, the temperature of the test, rotor revolutions per minute and the sample size used.

3. Experimental

3.1 LDH synthesis

3.1.1 Apparatus

A Carbolite CWF 1100 oven was used to calcine the hydrotalcite for the reconstruction method. Erlenmeyer flasks were used as reaction vessels for the reconstruction method. Beakers were used as reaction vessels for the co-precipitation method. A burette was used during the co-precipitation method to add reactants to the beaker in a dropwise fashion. Agimatic-N magnetic stirrers were used for all three synthesis methods. A vacuum filtration setup consisting of a Buchner funnel and a Neuberger d-79912 vacuum pump were used to filter the samples after the reaction period. An Ecotherm Labotec oven was then used to drive off the remaining water from the filter cake. The dry filter cakes were ground using a Phillips HR2021 blender. A four decimal Radwag mass balance was used to weigh all chemicals, samples and additives.

3.1.2 Materials list

The hydrotalcite used in the reconstruction method was synthesised at the University of Pretoria. The raw materials used in the co-precipitation method were procured from ACE Chemicals. These raw materials being: magnesium chloride, aluminium chloride and sodium hydroxide.

The following organic acids (from Sigma-Aldrich) were intercalated into hydrotalcite:

- 4-Ethylsulfanylbenzoic acid (4-Ethylthiobenzoic acid)
- Benzoic acid
- 2-Sulfanylbenzoic acid (Thiosalicylic acid)
- 4-Sulfanylbenzoic acid (4-Mercaptobenzoic acid)
- 2-Hydroxybenzoic acid (Salicylic acid)
- 3-Hydroxybenzoic acid
- 4-Hydroxybenzoic acid
- 2-Aminobenzoic acid (Anthranilic acid)
- 3-Aminobenzoic acid
- 4-Aminobenzoic acid

The structures for these organic acids may be found in figure 3.1 below. These structures were generated using ChemSketch :

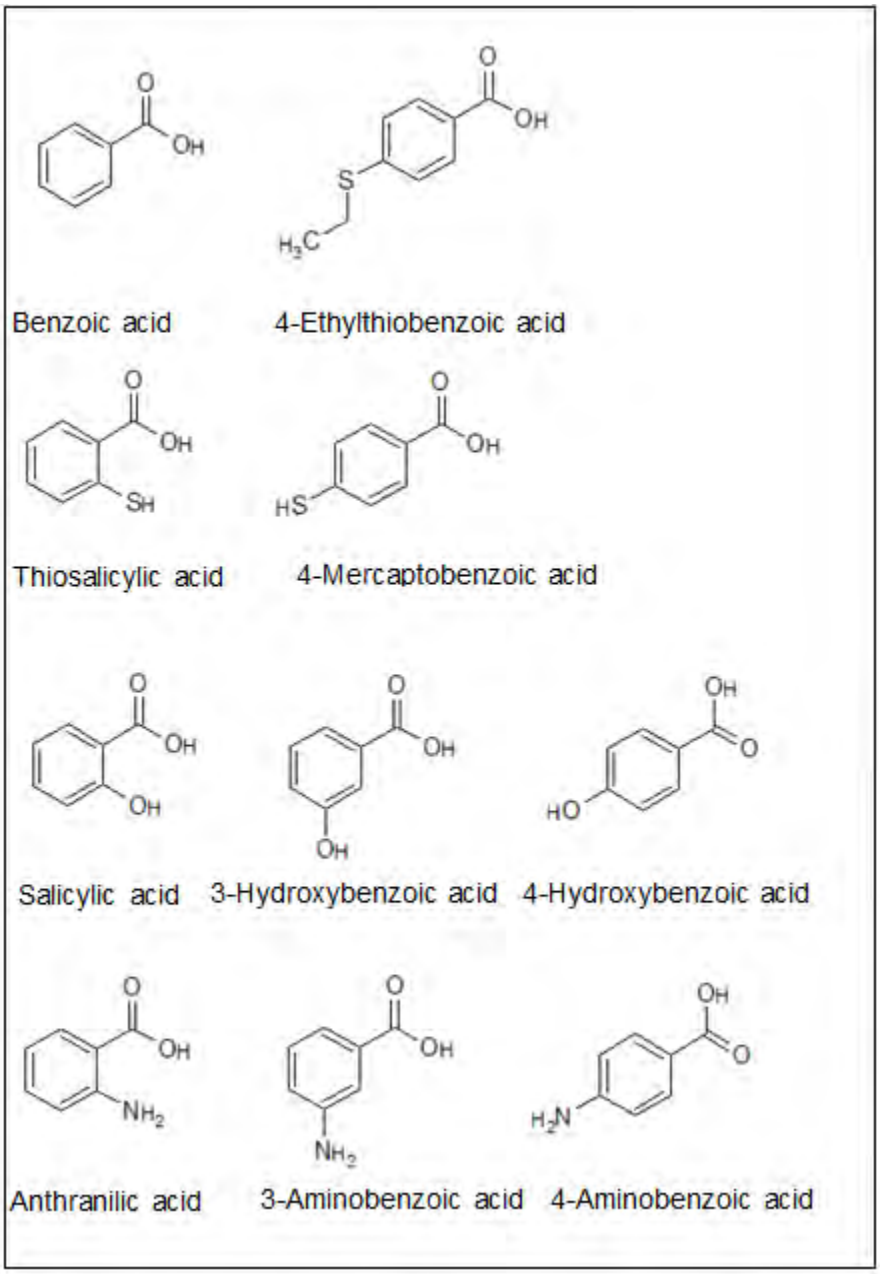

Figure 3.1: Chemical structures of the organic acids used for intercalation (ChemSketch 14.01, 2016).

3.1.3 Planning

Two methods of synthesis were used to create each intercalated LDH: the reconstruction method and co-precipitation method. This was done in order to see which synthesis method produced the better performing LDH in terms of PVC heat stability.

3.1.4 Reconstruction method for hydrotalcite intercalation

The hydrotalcite used for the synthesis was calcined for five hours at a temperature of 450 °C. After calcination, the calcined hydrotalcite was placed in a desiccator to cool. The desiccator contained a desiccant to prevent hydrolysis of the hydrotalcite.

Distilled water was boiled in order to decarbonate the water. The boiled distilled water was added to the Erlenmeyer flask. Stoichiometric amounts of the calcined hydrotalcite and the organic acid to be intercalated were then added to the distilled water. The mixture was covered and left to stir at ambient conditions for a period of three days. After this time, the sample was filtered using the vacuum filtration setup. The filter cake was then placed in the Ecotherm Labotec oven at 80 °C and left to dry overnight. The dry filter cake was ground into finer particles and stored in sealed plastic sample bags.

3.1.6 Co-precipitation method

The following method was adapted from Manzi-Nshuti *et al* (2009). It uses the following chemical reaction as a basis for the synthesis:

$$4M^{II}Cl_2 + 2M^{III}Cl_3 + NaOH + 2A^- \longrightarrow Mg_4Al_2(OH)_{12}A_2^{-}\cdot 5H_2O$$

Distilled water was boiled in order to decarbonate the water. The stoichiometric amounts of the organic acid and sodium hydroxide were added to a beaker of decarbonated distilled water. This beaker was then placed on a magnetic stirrer. Enough water was used to suspend these particles.

Both the divalent and trivalent metal salt chlorides were dissolved in the same beaker of decarbonated distilled water. The metal salt chloride solution was added dropwise to the organic acid intercalant and sodium hydroxide solution using a burette. Extra sodium hydroxide pellets were added to the beaker in order to maintain the pH of the mixture at around 10. The slurry was covered and left to react for two days at 60 °C. The slurry was then filtered using the vacuum filtration setup. The filter cake was washed with distilled water and ethanol and left to dry overnight at 80 °C. The dry filter cake was ground into finer particles and stored in sealed sample bags.

3.2 Material characterisation

3.2.1 Particle size analysis (PSA)

The particle size distributions of the synthesised LDH samples were determined with a Malvern Mastersizer Hydrosizer 3000. The stirrer speed of the Mastersizer was set to 1500 rpm. The ultrasound was enabled in order to break up particle agglomerates that formed during the measurements and was kept at a level of 100 % for the duration of the run. The Mastersizer performed five repeat runs on the same sample and then calculated an average particle size distribution based on these runs.

3.2.2 X-ray diffraction (XRD)

X-ray diffraction analysis of the synthesised LDH samples was performed on a PANalytical X-pert Pro powder diffractometer fitted with an X'celerator detector using Fe filtered Co K_α radiation (0.17901 nm). The instrument featured variable divergence and receiving slits. The X'Pert High Score Plus software was used for phase identification.

3.2.3 Fourier transform infra-red spectroscopy (FTIR)

FTIR spectra of the LDH samples were recorded on a Perkin Elmer 100 Spectrophotometer. Powder samples were pressed onto the Zn/Se plate of a MIRacle ATR attachment. The spectra were obtained over the range 500 cm^{-1} to 4000 cm^{-1} and represent the average of 32 scans at a resolution of 2 cm^{-1}.

3.2.4 Thermogravimetric analysis (TGA)

TGA was performed on the LDH samples using a Perkin Elmer TGA 4000. The TGA was done in air, from 25 °C to 900 °C at a heating rate of 10 °C/min.

3.3 Heat stability testing

3.3.1 Apparatus

A Haake Polylab OS Rheomix torque rheometer was used test the dynamic stability of the PVC samples. A computer was used to record the data output of the Rheomix in the form of a torque curve.

3.3.2 Materials list

PVC samples were taken from an in-house dry blend. The recipe of the dry blend is shown in table 3.1 below. Neat hydrotalcite synthesised at the University of Pretoria was used as a control for the experiment (the same material used for the reconstruction synthesis). The intercalated stabilisers synthesised using the methods mentioned in section 3.1 were the focus of the heat stability experiment.

Table 3.1: PVC dry blend recipe

Component	Composition (PHR)
Sasol PVC Resin S7106	100
iDwala Kulucote 2 $CaCO_3$	50
Isegen DINP (Plasticiser)	50
Faci Zinc Stearate	0.6
Faci Calcium Stearate	0.3
Solvay (Rhodia) Rhodiastab 50	0.4

3.3.3 Planning

The independent variable selected for the investigation was the additive selected to be compounded with the PVC inside the Rheomix. The measured variable was the torque output of the Rheomix rollers. This torque output gives an indication of the degradation of the PVC sample inside the Rheomix.

There were two specific values of interest on the torque curves of the various samples. These values were the length of the plateau on the curve in time units and the time at which the maximum degradation torque occurs. The length of the plateau gives an indication of the short term stability provided to the polymer by the additive.

The time at which the maximum degradation torque occurs is an indication of the long term stability. The time of at which the maximum degradation torque occurs gives an indication of the final loss of mechanical properties of the PVC (Jahrling, 2009).

While an overall comparison may be drawn to the short term and long term stability provided by the various LDHs, it is also of interest to draw comparisons between the various aromatic substituents of the intercalated compounds.

For instance, by looking at the stabilisation results of 4-ethylthiobenzoic acid and 4-mercaptobenzoic acid, it may be determined if the length of the substituent group of the intercalated compound plays any sort of role in affording additional heat stability to the polymer.

The following properties were analysed:

- The position of the substituent group on the benzene ring
- The presence of a mercapto, hydroxyl or amino substituent group
- Whether the additives perform better if they were synthesised with the reconstruction method or the co-precipitation method.

3.3.4 Method

The Rheomix tests were done in accordance with ASTM D 2538-02 (American Society for Testing and Materials, 2002). 72 g of the PVC dry blend was weighed off and 0.36 g of a specific stabiliser was added to the PVC in a beaker. This amount of stabiliser was chosen for all samples and is approximately 0.5 PHR.

Once the sample had been prepared it was placed into the Rheomix at a temperature of 200 °C and at a rotor speed of 50 rpm. The sample was then allowed to degrade while a torque curve was plotted by the Polylab OS software on the computer.

The Rheomix was stopped once the maximum torque value was. The degraded sample was removed, the Rheomix thoroughly cleaned and the next prepared sample was loaded. Three runs of each sample were done for most of the samples synthesised *via* the reconstruction method in order to generate results with a satisfactory statistical average.

Due to time constraints, only one run for each co-precipitation stabilisers and the sample intercalated with 4-mercaptobenzoic acid *via* the reconstruction method, was performed.

The torque curves of the samples were then analysed using methods laid out in ASTM standard as well as by Jahrling (2009) for the company, Thermo Scientific.

4. Results and discussion

4.1 Characterisation

4.1.1 X-ray diffraction

XRD was done on the all synthesised intercalated LDH stabilisers in order to determine whether intercalation had occurred.

The primary peak on an XRD pattern of a LDH is the most intense peak on the pattern. A shifted peak pattern is obtained in two situations: through intercalation of another anion in the interlayer or through substitution of the cations in the layers (Schmidt, 2013). This peak shift, in terms of anion intercalation, is related to an increase in the d-spacing (the space between two parallel planes). This increase in d-spacing causes the primary peak to shift to the left. A decrease in d-spacing will cause the peak to shift to the right. (Schmidt, 2013)

By looking at the primary peak for neat hydrotalcite and by comparing it to the primary peak for an intercalated compound, it may be determined if the compound has indeed undergone intercalation.

From the XRD patterns of the analysed stabilisers, it was determined that none of the organic acid used as a reagent for intercalation were found to be present (due to an absence of their unique fingerprint pattern in the sample patterns). This implies that three things may have occurred to the organic acid:

- The acid intercalated into hydrotalcite
- The acid was adsorbed onto the outer surface of hydrotalcite (or reacted to form salts of the Mg and Al)
- The acid washed out of the system during the filtration step of the synthesis process.

Since no direct washing of the filter cake occurred and since the organic acids are only slightly soluble in water, the organic acids were unlikely to have washed out. TGA and FTIR analysis will help to confirm this.

4.1.1.1 Reconstruction synthesis XRD results

Figure 4.1.1 below shows the XRD pattern for neat hydrotalcite.

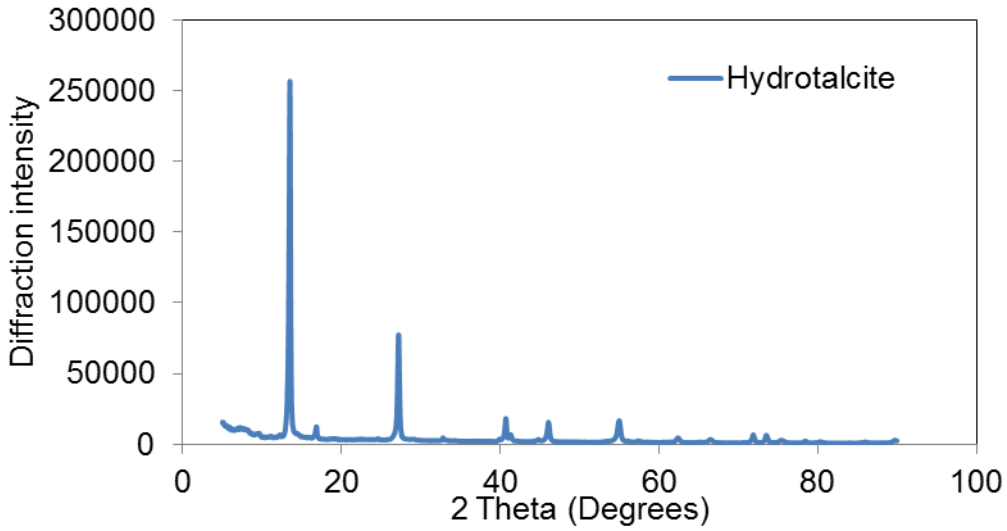

Figure 4.1.1: XRD pattern for neat hydrotalicte.

The primary peak at a 2θ value of 13.5°should be noted. This value will give an indication of whether successful intercalations occurred for the other samples. Figure 4.1.2 below shows the XRD pattern for calcined hydrotalcite

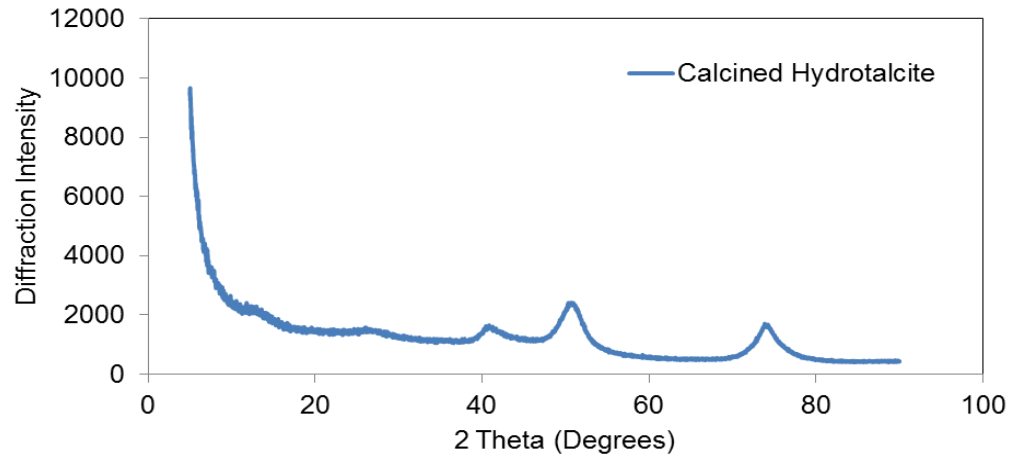

Figure 4.1.2 XRD pattern for calcined hydrotalcite

The amorphous peaks at 42, 55 and 76° indicate the presence of the mixed metal oxide calcination products.

If these peaks are present on the XRD patterns for the intercalated LDH, it is indicated that the rehydration of the mixed metal oxides was incomplete.

Figure 4.1.3 below shows an XRD pattern for a successfully intercalated sample. A successful intercalation is indicated by a very noticeable shift of the primary peak position to the left.

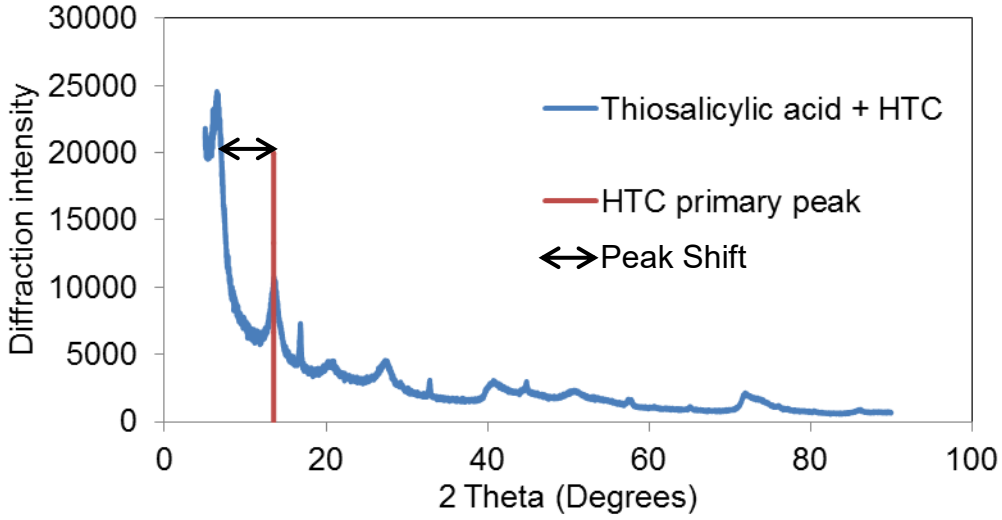

Figure 4.1.3: XRD pattern for thiosalicylic acid + HTC (reconstruction method).

The following figure shows an XRD pattern for a sample with an unsuccessful intercalation.

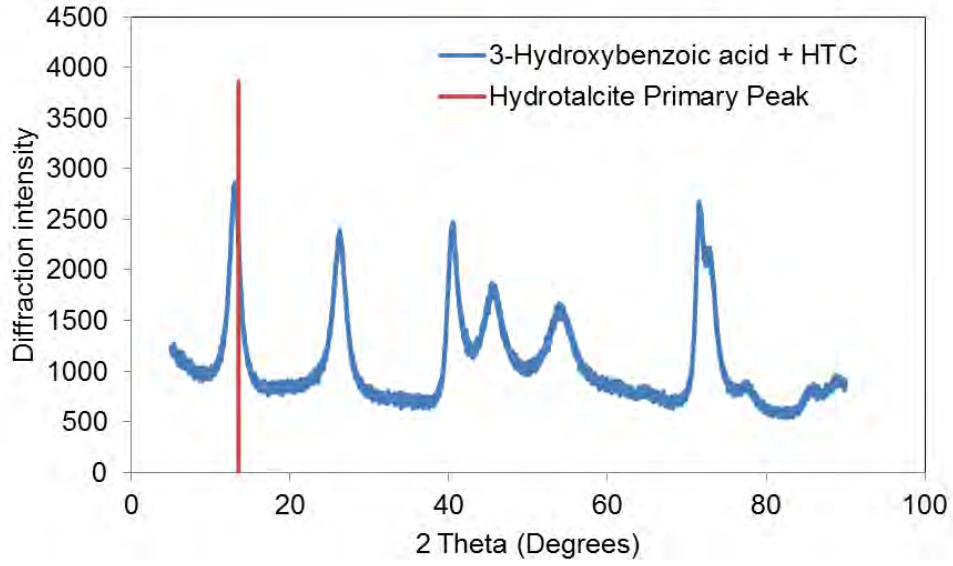

Figure 4.1.4: XRD pattern for 3-hydroxybenzoic acid + HTC (reconstruction method).

From Figure 4.1.4 it can be seen that no peak shift occurs which means the organic acid failed to intercalate within the hydrotalcite layers. None of the organic acid reagent is present either as indicated by the XRD pattern.

This implies that the acid either washed out during the synthesis process, which is unlikely due to the very low solubility of the acid in water, or the acid adsorbed onto the LDH surface. The acid may have also formed a salt as a product with the LDH.

Figure 4.1.5 below shows an XRD pattern for a synthesis product that did not seem to form a LDH. In the previous figures, the hydrotalcite primary peak lined up with the primary peak of the stabiliser (and the sample shows a subsequent repeat pattern) which indicated the presence of hydrotalcite in the system. Figure 4.1.5 does not display a primary peak at the location of the hydrotalcite primary peak (nor repeat pattern). In actual fact many of the peaks on this XRD were unidentified, save for an aluminium oxide hydroxide peak located at a 2θ value of around 17°.

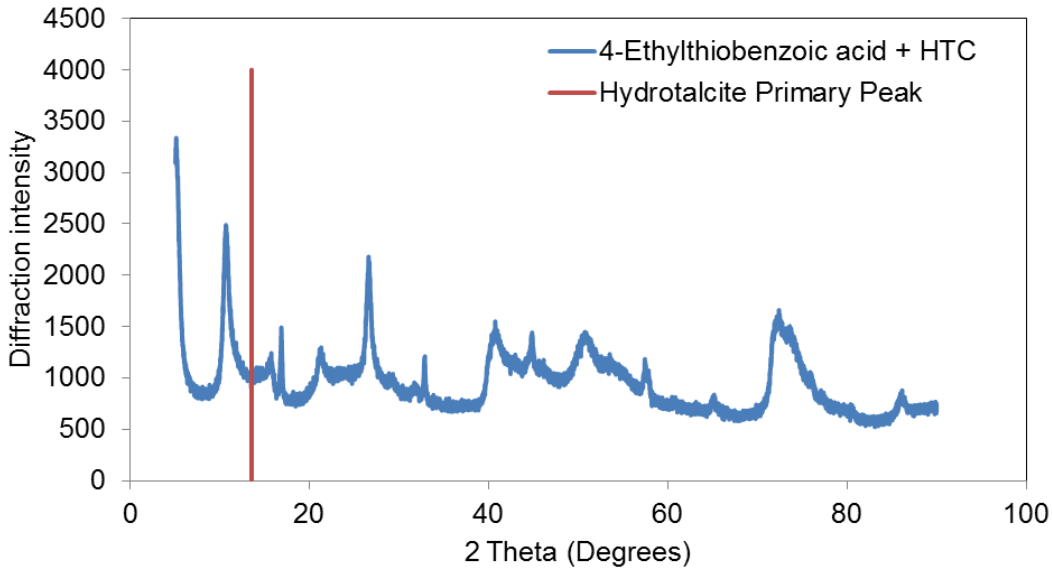

Figure 4.1.5: XRD pattern for 4-ethylthiobenzoic acid + HTC (reconstruction method).

The presence of this compound indicates an incomplete rehydration of the calcination products of the hydrotalcite.

Table 4.1.1 below summarises the XRD results for the reconstruction method samples.

Table 4.1.1: XRD results summary for reconstruction method samples.

Sample	LDH formed	Organic acid intercalated
Benzoic acid + HTC	Yes	No
Anthranilic acid + HTC	Yes	No
3-Aminobenzoic acid + HTC	Yes	No
4-Aminobenzoic acid + HTC	Yes	Yes
Salicylic acid + HTC	Yes	No
3-Hydroxybenzoic acid + HTC	Yes	No
4-Hydroxybenzoic acid + HTC	Yes	No
Thiosalicylic acid + HTC	Yes	Yes
4-Mercaptobenzoic acid + HTC	Yes	No
4-Ethylthiobenzoic acid + HTC	No	No

All the XRD patterns for the reconstruction method samples may be found in Appendix A.

4.1.1.2 Co-precipitation synthesis XRD results

For the samples synthesised using the co-precipitation method, it would appear that none of the organic acids intercalated within the LDH. However, for every sample, a layered double hydroxide did form. It is also worth noting that none of the organic acid reagent was found to be present, thus implying surface adsorption may have taken place.

Figure 4.1.6 shows and XRD pattern for a co-precipitation synthesised sample.

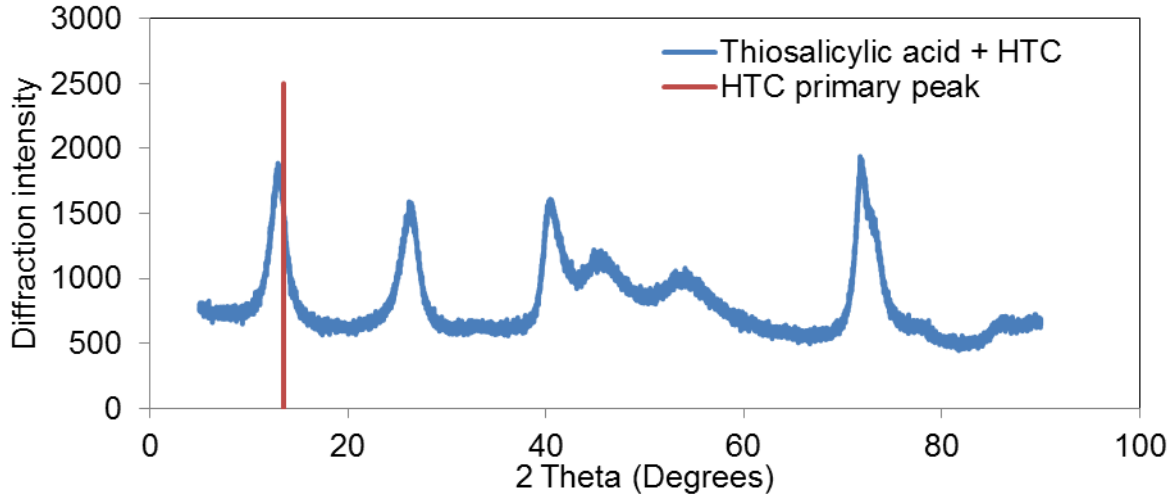

Figure 4.1.6: XRD pattern for thiosalicylic acid + HTC (co-precipitation method).

The lack of a peak shift should be taken to indicate that intercalation has not occurred. The XRD patterns for the other co-precipitation samples display a very similar pattern to the Figure 4.1.5. There is no evidence of a peak shift occurring in any of these patterns either. These patterns may be found in Appendix A.

4.1.2 Thermogravimetric analysis

4.1.2.1 Reconstruction method stabilisers TGA

The following figures depict TGA graphs for the reconstruction synthesised stabilisers. The hydrotalcite mass loss curve is posted on all the TGA graphs for comparison. Figures 4.1.7 to 4.1.9 are grouped according to substituent group composition whereas figure 4.1.10 displays curves for the remainder of the samples.

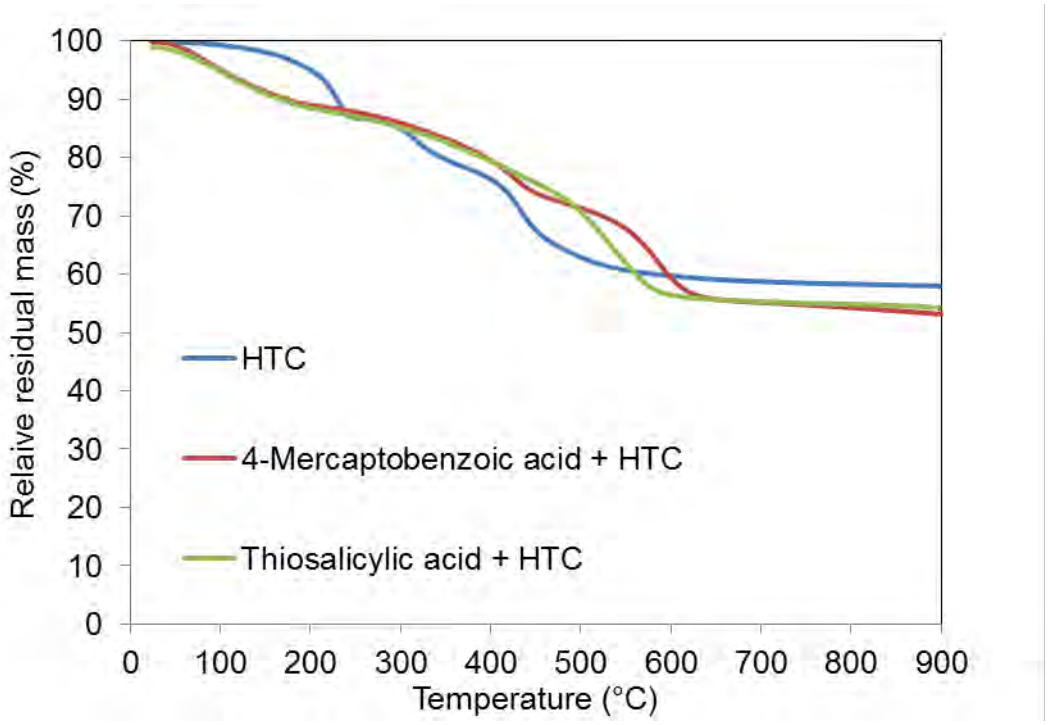

Figure 4.1.7: TGA curves for reconstruction stabilisers intercalated with ortho and para mercaptobenzoic acids.

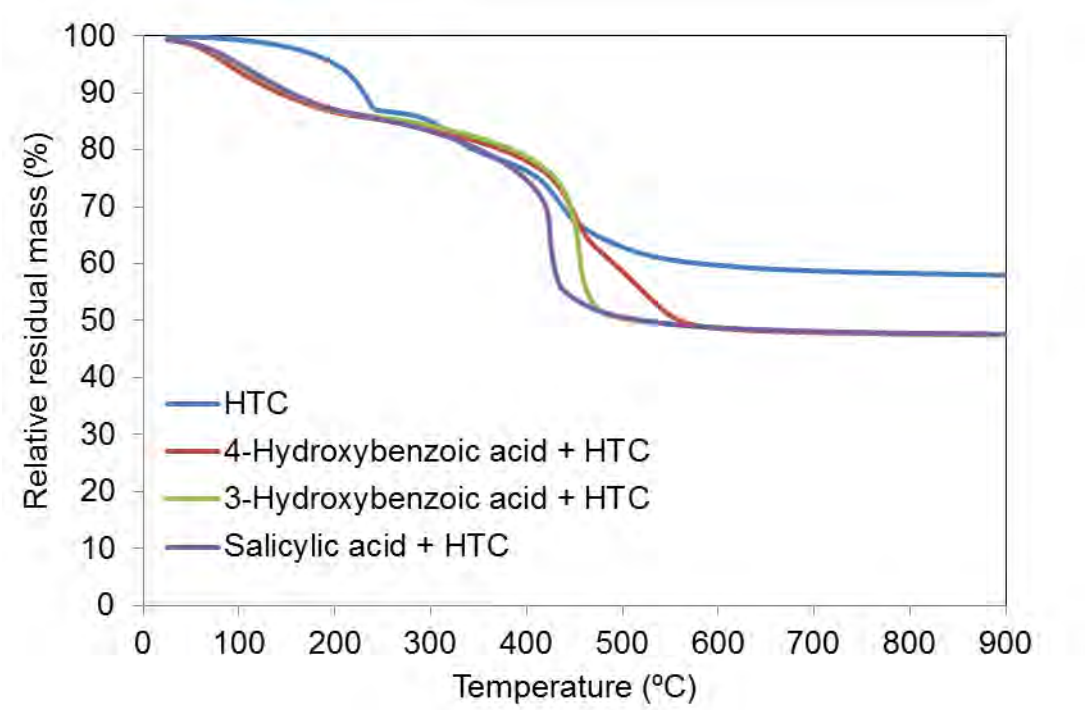

Figure 4.1.8: TGA curves for reconstruction stabilisers intercalated with ortho, meta and para hydroxybenzoic acids.

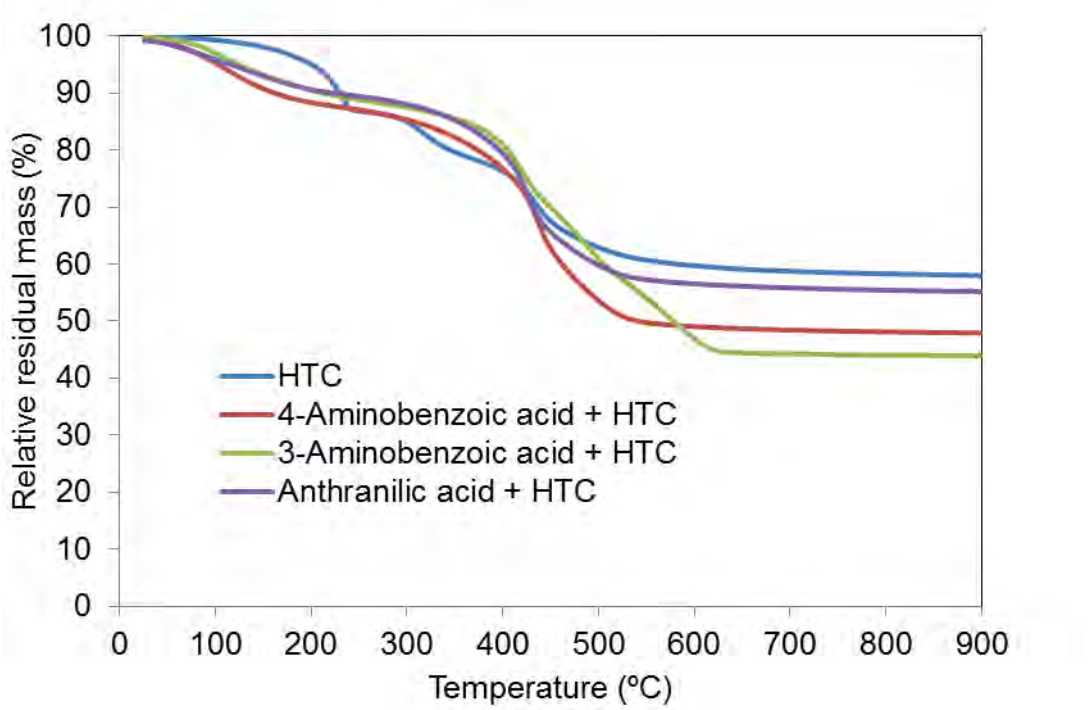

Figure 4.1.9: TGA curves for reconstruction stabilisers intercalated with ortho, meta and para aminobenzoic acids.

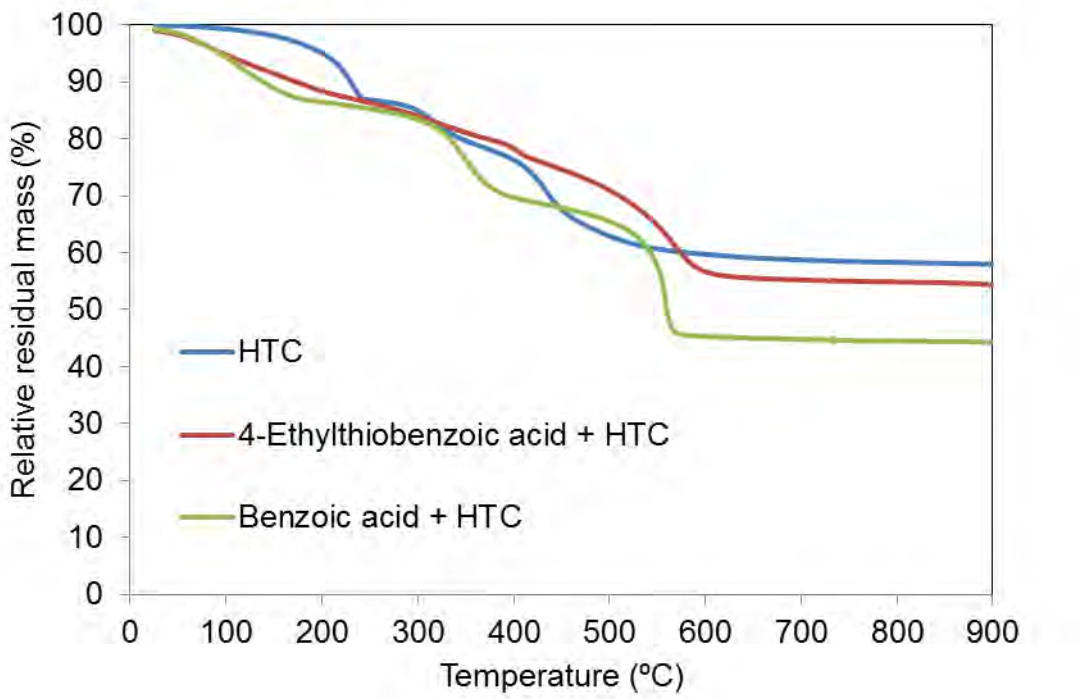

Figure 4.1.10: TGA curves for reconstruction stabilisers intercalated with 4-ethylthiobenzoic acid and benzoic acid.

According to Costa *et al* (2008), when hydrotalcite and hydrotalcite-like clays undergo TGA, a two-stage decomposition process occurs: a low temperature decomposition from ambient temperature to about 225 °C and a higher temperature decomposition from 225 °C to 500 °C. The lower temperature decomposition is characterised by losses of the LDH surface water and the interlayer water molecules. The higher temperature decomposition is characterised by losses of the interlayer carbonate anions as well as dehydroxylation of the metallic layers. In all of the tested samples, the organic intercalants evolved as volatiles during the higher temperature decomposition. This fact was used to determine the organic loading of the LDH.

All the TGA curves were analysed in the same manner: the mass loss percentage that occurred due to the loss of the surface and interlayer water was recorded for each stabiliser. Each curve was adjusted to neglect the surface and interlayer water loss in order to normalise all the curves.

This was done because the amount of interlayer water and surface water absorbed during each compound synthesis is different.

The mass loss percentage of the organic intercalant was then calculated by subtracting the mass percentage of a particular LDH at 900 °C from the mass percentage of neat hydrotalcite at 900 °C. In other words, it was assumed that the difference in mass loss between the neat material and the intercalated material could only be due to the organic material present in the latter.

Theoretical organic mass loss percentages were calculated. An example follows below.

Given the following decomposition reaction of hydrotalcite that takes place during TGA:

$$Mg_4Al_2CO_3(OH)_{12} \longrightarrow 4MgO{\cdot}Al_2O_3 + \text{volatiles}$$

Where the volatiles in this case are H_2O and CO_2. Note that the crystal water that would normally be a part of the hydrotalcite has been neglected (driven off in the first TGA step) in order to be consistent with the analysis method. The $MgO{\cdot}Al_2O_3$ compound is the residual compound remaining at the end of the TGA. The residual mass percentage is calculated by dividing the molar mass of the residual compound by the molar mass of LDH. The hydrotalcite had a theoretical residual mass percentage of 68.13 % and an actual residual mass percentage of 69.43 %. The slight difference in these values is possibly due to contamination during the synthesis process which would result in a higher mass percentage for the actual value. This also indicates a well synthesised and good starting hydrotalcite used for the reconstruction synthesis.

The same method can be applied to an intercalated LDH for example, hydrotalcite intercalated with an aminobenzoic acid:

$$Mg_4Al_2(C_7H_6NO_2)_2(OH)_{12} \longrightarrow 4MgO{\cdot}Al_2O_3 + \text{volatiles}$$

The residual mass loss percentage is calculated in the same way as the neat material; however, the mass loss percentage due to organics is calculated by subtracting the intercalated compound's residual mass loss from the neat compound's residual mass loss.

Table 4.1.2 depicts the theoretical organic mass loss percentages and the actual organic mass loss percentages calculated from the TGA data for the reconstruction synthesised stabilisers.

Table 4.1.2: Theoretical and actual organic mass loss percentages for the reconstruction synthesised stabilisers.

Stabiliser	Theoretical organic mass loss %	Actual organic mass loss %
4-Hydroxybenzoic acid + HTC	24.77	17.02
3-Hydroxybenzoic acid + HTC	24.77	10.53
Salicylic acid + HTC	24.77	15.53
4-Aminobenzoic acid + HTC	24.66	15.83
3-Aminobenzoic acid + HTC	24.66	21.94
Anthranilic acid + HTC	24.66	0.83
4-Ethylthiobenzoic acid + HTC	29.15	4.74
Benzoic acid + HTC	22.89	18.29
Thiosalicylic acid + HTC	26.49	9.39
4-Mercaptobenzoic acid + HTC	26.49	6.16

From the values above it may be seen that none of the organic acids intercalated completely into hydrotalcite *via* the reconstruction method. The actual organic mass loss percentages give an indication of the organic loading of the hydrotalcite be it either by intercalation of the organic anion or surface adsorption of the intercalant.

Figures 4.1.11 to 4.1.14 depict TGA graphs for the co-precipitation synthesised stabilisers. The hydrotalcite mass loss curve is posted on all the TGA graphs for comparison.

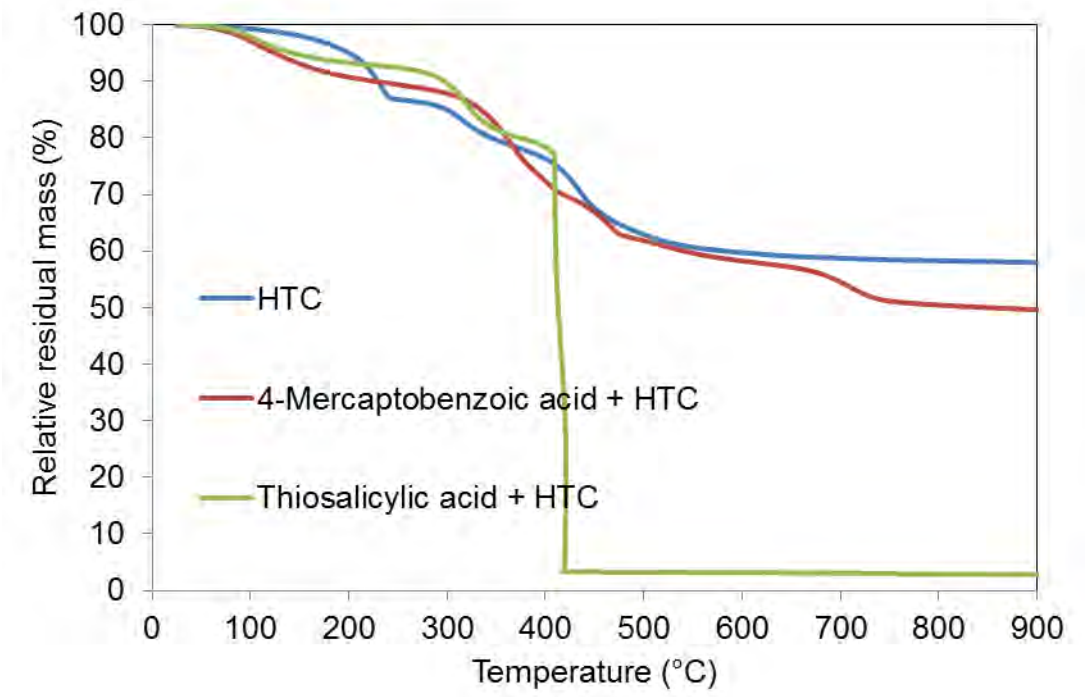

Figure 4.1.11: TGA curves for co-precipitation stabilisers intercalated with ortho and para mercaptobenzoic acids.

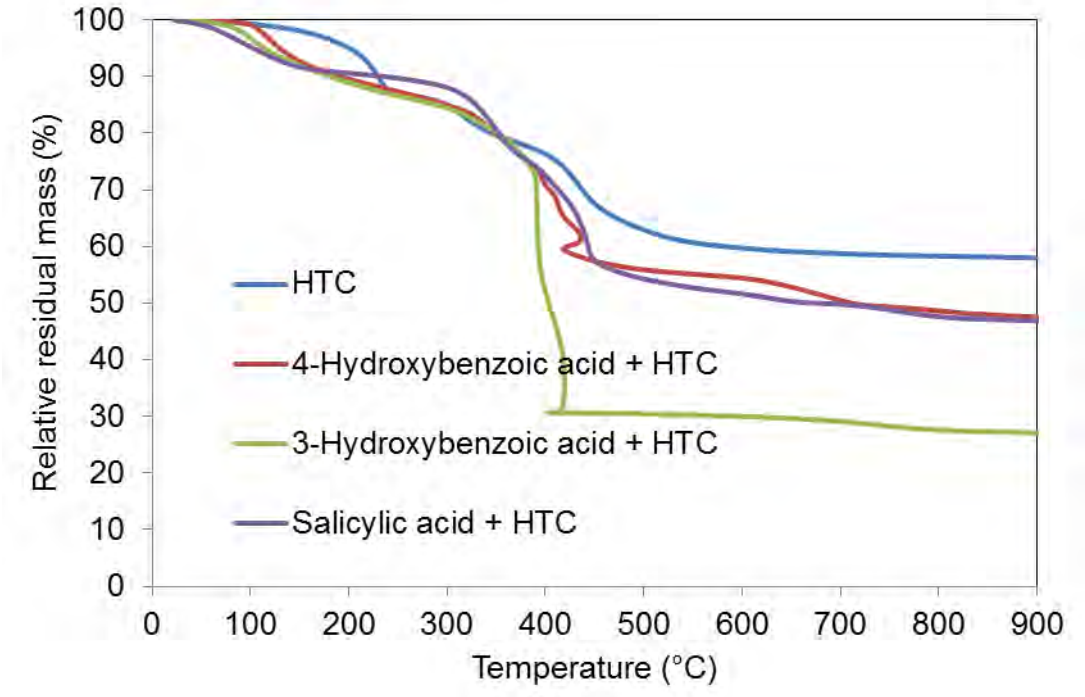

Figure 4.1.12: TGA curves for co-precipitation stabilisers intercalated with ortho, meta and para hydroxybenzoic acids.

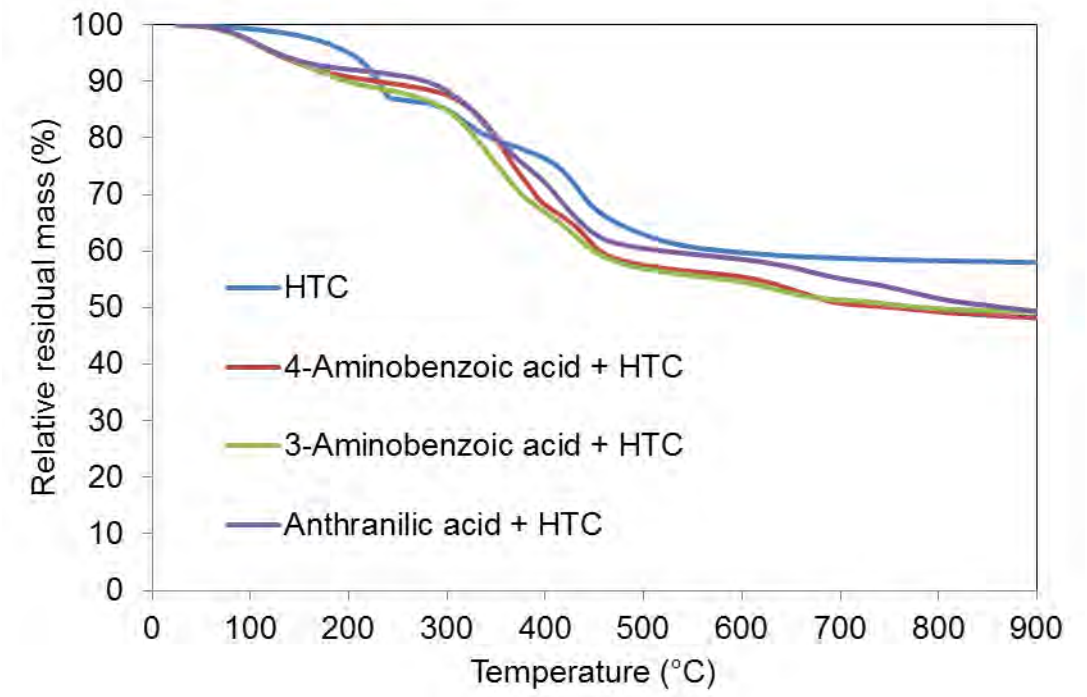

Figure 4.1.13: TGA curves for co-precipitation stabilisers intercalated with ortho, meta and para aminobenzoic acids.

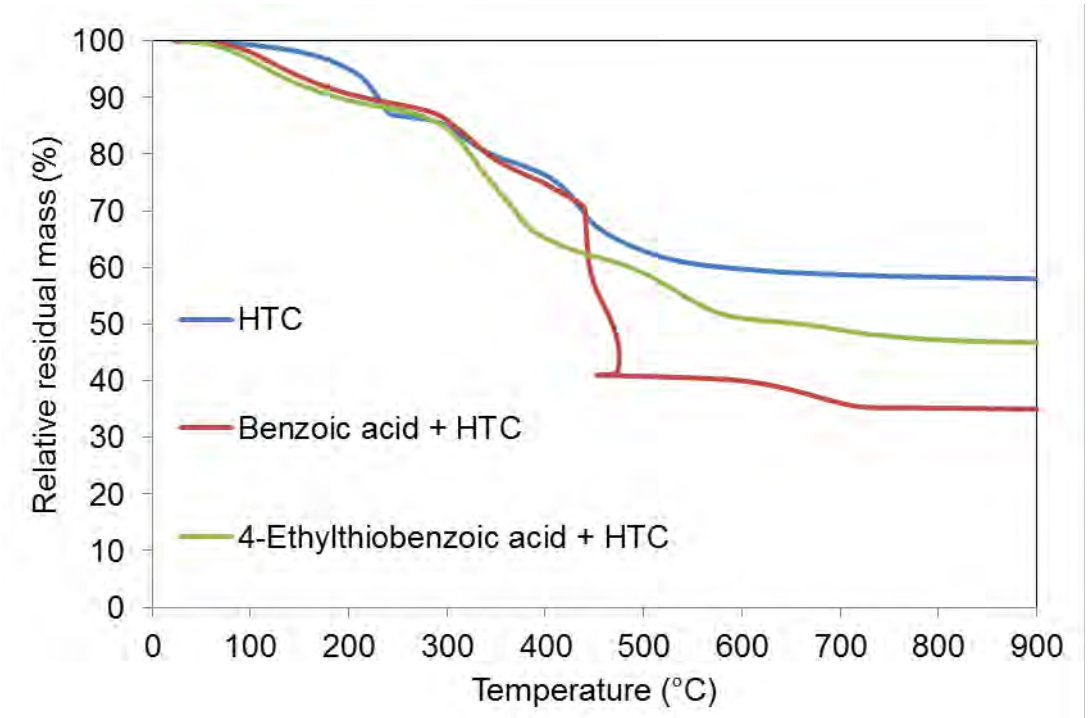

Figure 4.1.14: TGA curves for co-precipitation stabilisers intercalated with 4-ethylthiobenzoic acid and benzoic acid.

The theoretical and organic mass loss percentages for these stabilisers can be found in the Table 4.1.3.

Table 4.1.3: Theoretical and actual organic mass loss percentages for the co-precipitation synthesised stabilisers.

Stabiliser	Theoretical organic mass loss %	Actual organic mass loss %
4-Hydroxybenzoic acid + HTC	24.77	12.92
3-Hydroxybenzoic acid + HTC	24.77	32.87
Salicylic acid + HTC	24.77	13.75
4-Aminobenzoic acid + HTC	24.66	12.94
3-Aminobenzoic acid + HTC	24.66	10.85
Anthranilic acid + HTC	24.66	13.19
4-Ethylthiobenzoic acid + HTC	29.15	13.34
Benzoic acid + HTC	22.89	26.63
Thiosalicylic acid + HTC	26.49	60.51
4-Mercaptobenzoic acid + HTC	26.49	12.17

The actual organic mass loss percentage for thiosalicylic acid + HTC was calculated to be 60.51 %. This outlier was rejected and believed to be due to equipment or experimental error, although this may be possible in theory. The sample was not reanalysed due to time constraints. From the results in Table 4.1.3 it may also be seen that 3-hydroxybenzoic acid + HTC and benzoic acid + HTC have actual organic mass loss percentages above their theoretical values. In all cases this may be caused by unreacted intercalant still present in the stabiliser as free acid or attached to the surface of the compound.

4.1.3 Fourier transform infrared spectroscopy

FTIR analysis was performed on both the reconstruction synthesised stabilisers and the co-precipitation synthesised stabilisers to further investigate the chemical make-up of the stabilisers. All the FTIR spectra for the synthesised samples are shown in Appendix B.

The FTIR results were used in conjunction with the XRD results to determine whether intercalation of the hydrotalcite or surface adsorption of the intercalated compound had occurred. The FTIR analysis was qualitative in nature and was not used to determine the loading of the intercalated compound.

Table 4.1.4 contains the absorption peak and frequency ranges of vibrational transitions of stable and transient molecules used to interpret the FTIR results obtained.

Table 4.1.4: Infrared absorption frequencies found in the analysed samples

Component	Wavenumber (cm^{-1})	Reference
Bonded OH	3250 – 3600	Nicolet, sa
Amine Bend	1550-1640	Nicolet, sa
OH from Carboxylic Acid	2550 – 3200	Nicolet, sa
COO^-	1560 – 1610	Nicolet, sa
Benzene Ring	1480 – 1525 1610 – 1620	Nicolet, sa
COOH	920 – 970 1400 – 1440 1650 – 1700	Nicolet, sa
CO_3^-	1350-1380	Cavani *et al* 1991
Phenolic C-O	1100-1350	Beauchamp, sa
Monosubstituted Benzene	670 – 690 715 – 760	Nicolet, sa
1:2 - Substituted Benzene	740 – 760	Nicolet, sa
1:3 - Substituted Benzene	700 – 715 770 – 795	Nicolet, sa
1:4 - Substituted Benzene	800 – 835	Nicolet, sa

Figure 4.1.15 depicts the FTIR spectra for neat hydrotalcite and Figure 4.1.16 for calcined hydrotalcite.

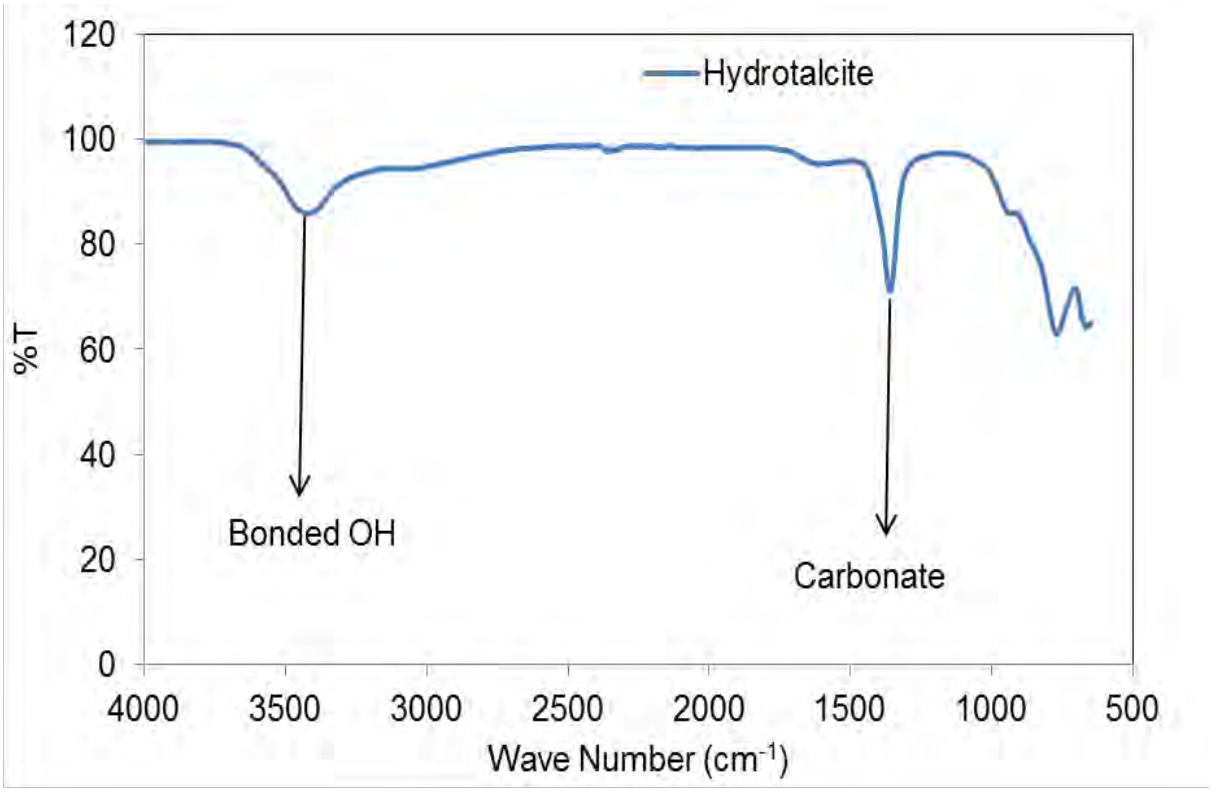

Figure 4.1.15: FTIR spectra for neat hydrotalcite

The main peaks of interest in Figure 4.1.15 above have been annotated. The bonded OH peak is indicative of OH^- anions within the brucite like layer of the hydrotalcite. The carbonate peak is indicative of the carbonate anion in the interlayer of the LDH.

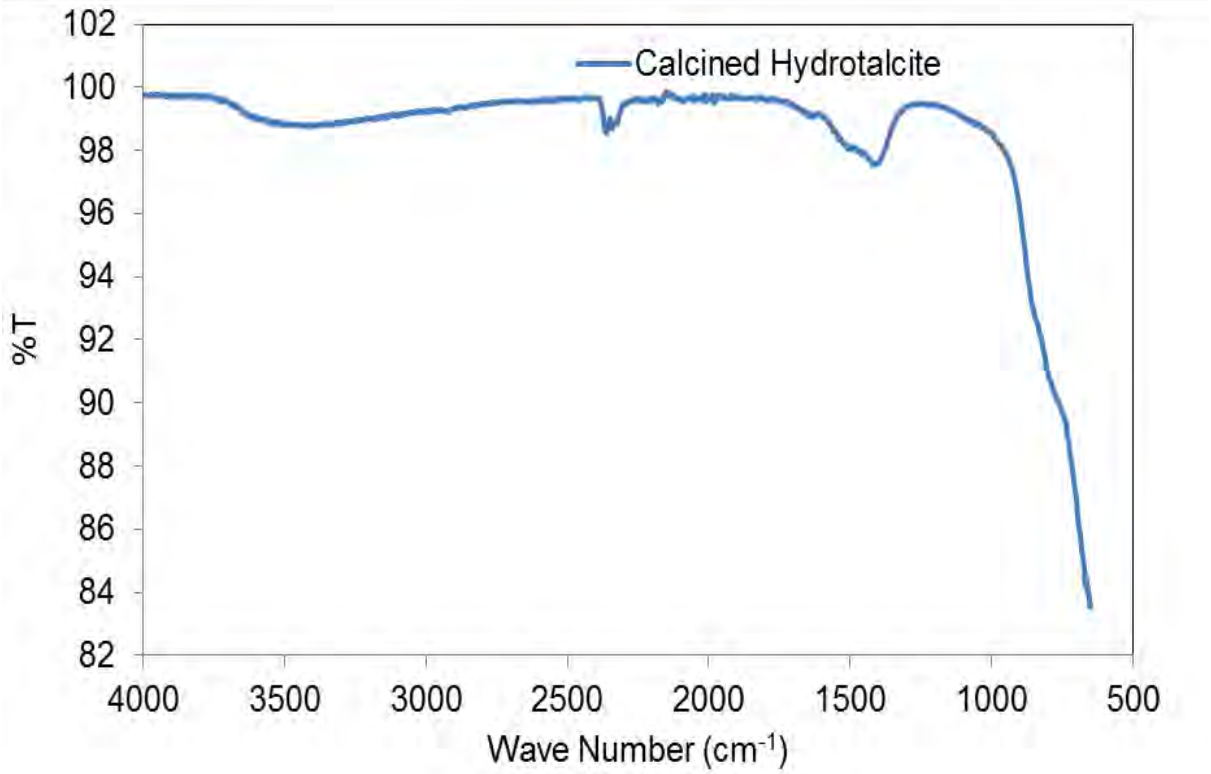

Figure 4.1.16: FTIR spectra for calcined hydrotalcite

The lack of the bonded OH and carbonate peaks on figure 4.1.16 indicates that the calcination process completely removed carbonate from the hydrotalcite.

Figure 4.1.17 depicts the FTIR spectra for 4-aminobenzoic acid + HTC (reconstruction):

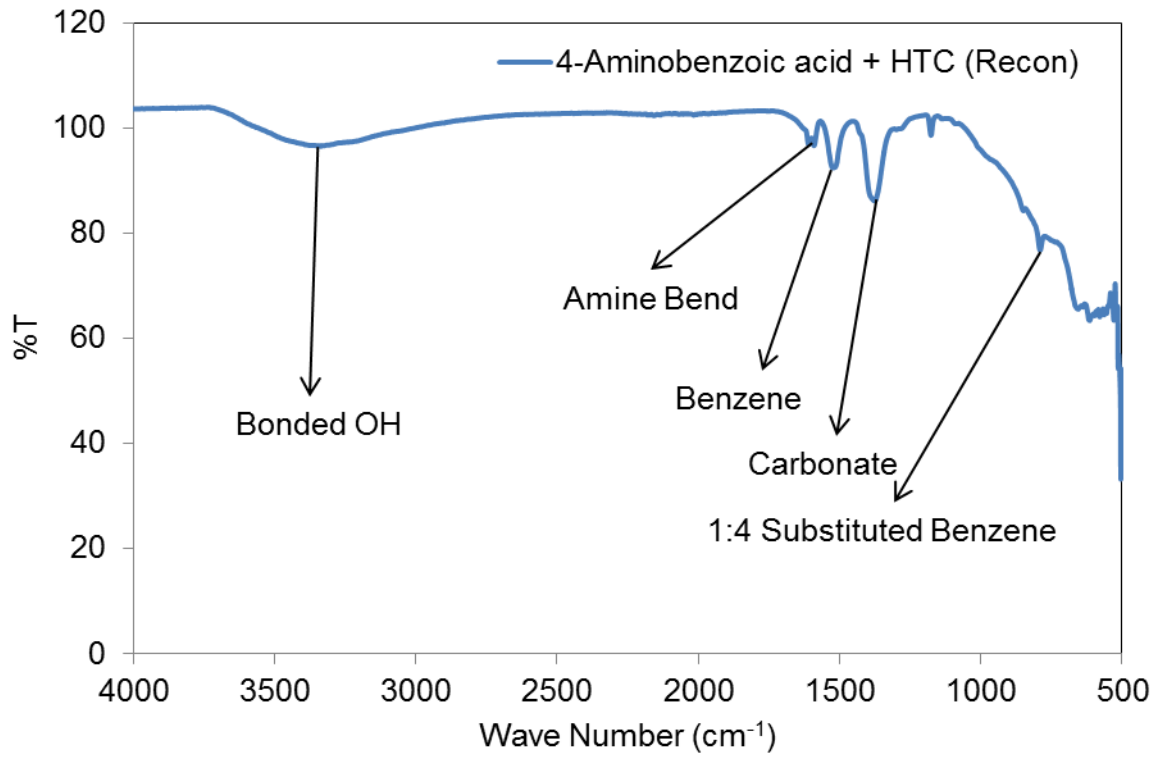

Figure 4.1.17: FTIR spectra for 4-Aminobenzoic acid + HTC (reconstruction)

The amine bend peak, the benzene peak and the 1:4 Substituted benzene peak indicate the presence of the intercalated anion either between the layers of the hydrotalcite or adsorbed onto the surface of the clay. It is interesting to note the presence of carbonate within the stabiliser.

The presence of carbonate should indicate that the intercalation of the organic acid has been unsuccessful; however, the XRD result for this stabiliser confirmed intercalation. The presence of carbonate could thus be indicative of partial intercalation occurring.

Figure 4.1.18 depicts the FTIR spectra for benzoic acid + HTC (reconstruction):

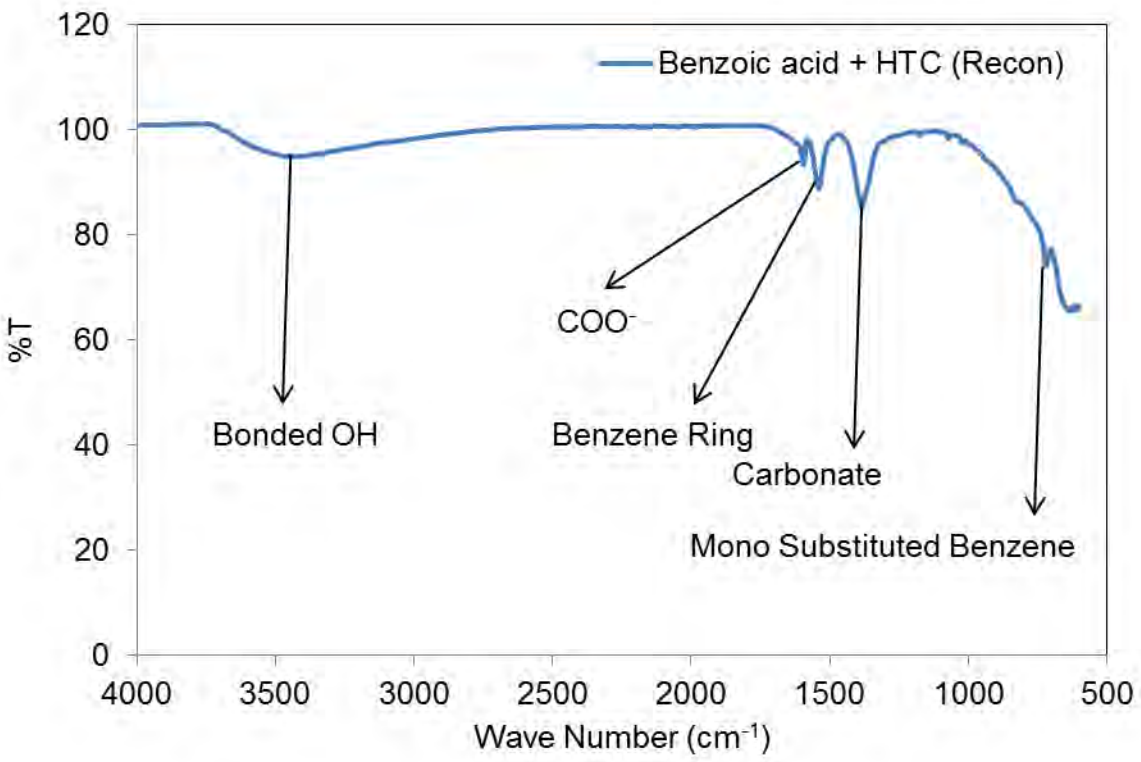

Figure 4.1.18: FTIR spectra for benzoic acid + HTC (reconstruction)

The XRD data for this stabiliser showed that no organic acid intercalation took place; however a LDH did form. This is evident from the presence of the bonded OH peak and the carbonate peak in figure 4.1.16. The presence of the benzene ring peak and the mono substituted benzene peak indicate that the organic acid (benzoic acid) is present in the stabiliser.

It is interesting to take note of the presence of a COO^- peak on the FTIR spectra. During the anion exchange reaction that takes place during the intercalation process, a proton is removed from the carboxylic acid functional group of the organic acid to be intercalated. This organic anion then exchanges places with the carbonate anion within the interlayer of the hydrotalcite.

The presence of this COO^- peak as well as the carbonate peak on the spectra could be evidence of partial intercalation of the organic acid.

Table 4.1.5 shows a summary of the FTIR results for the reconstruction synthesised stabilisers.

From Table 4.1.5 it may be seen that all the organic acids that were to be intercalated are present in their respective stabilisers. This is indicated by the presence of the 1:2, 1:3 and 1:4 substituted benzene peaks on the FTIR spectra which indicate the presence of an ortho, meta or para substituted stabiliser respectively. In the case of the benzoic acid stabiliser, the presence of the monosubstituted benzene peak indicates the presence of benzoic acid in the stabiliser. All the organic acids have either partially intercalated into the hydrotalcite or have been adsorbed onto the surface of the clay.

Table 4.1.5: FTIR result summary for reconstruction synthesised stabilisers

	Peaks Identified										
Stabiliser	Bonded OH	Amine Bend	OH from Carboxylic Acid	COO^-	Benzene Ring	COOH	CO_3^-	Phenolic C-O	Monosubstituted Benzene	1:2 - Substituted Benzene	1:3 - Substituted Benzene	1:4 - Substituted Benzene
Benzoic acid + HTC	Yes			Yes	Yes		Yes		Yes			
Anthranilic acid + HTC	Yes	Yes		Yes	Yes		Yes			Yes		
3-Aminobenzoic acid + HTC	Yes	Yes					Yes				Yes	
4-Aminobenzoic acid + HTC	Yes	Yes			Yes		Yes					Yes
Salicylic acid + HTC	Yes			Yes	Yes		Yes			Yes		
3-Hydroxybenzoic acid + HTC	Yes				Yes		Yes				Yes	
4-Hydroxybenzoic acid + HTC	Yes				Yes		Yes	Yes				Yes
Thiosalicylic acid + HTC	Yes			Yes			Yes			Yes		
4-Mercaptobenzoic acid + HTC	Yes			Yes	Yes		Yes					Yes
4-Ethylthiobenzoic acid + HTC	Yes		Yes	Yes	Yes	Yes						Yes

Table 4.1.6 shows a summary of the FTIR results for the co-precipitation synthesised stabilisers.

According to the XRD results for the co-precipitation stabilisers in section 4.1.1.2, none of the organic acids intercalated into hydrotalcite; however from the results in table 4.1.6, all the stabilisers save 3-hydroxybenzoic acid + HTC, displayed the COO^- peak on their FTIR spectra. This could be an indication of partial intercalation as mentioned above.

All of the co-precipitation synthesised stabilisers displayed carbonate peaks. These carbonate peaks reinforce the results in the XRD results section which say that all of the co-precipitation synthesised stabilisers formed carbonate intercalated LDHs.

From the table it is evident that all the organic acids that were to be intercalated into hydrotalcite are present in their stabilisers. The monosubstituted benzene peak provides evidence that benzoic acid is present with its LDH. All the other stabilisers save 3-aminobenzoic acid + HTC are present with their respective LDHs due to the appearance of the 1:2, 1:3 and 1:4 Substituted Benzene peaks on the FTIR spectra. The amine bend peak on the 3-aminobenzoic acid + HTC spectra shows that the organic acid is present with its LDH.

Table 4.1.6: FTIR result summary for co-precipitation synthesised stabilisers

	Peaks Identified											
Stabiliser	Bonded OH	Amine Bend	OH from Carboxylic Acid	COO^-	Benzene Ring	COOH	CO_3^-	Phenolic C-O	Monosubstituted Benzene	1:2 - Substituted Benzene	1:3 - Substituted Benzene	1:4 - Substituted Benzene
Benzoic acid + HTC				Yes		Yes	Yes		Yes			
Anthranilic acid + HTC				Yes	Yes		Yes			Yes		
3-Aminobenzoic acid + HTC	Yes	Yes		Yes			Yes					
4-Aminobenzoic acid + HTC	Yes	Yes		Yes			Yes					Yes
Salicylic acid + HTC	Yes			Yes			Yes	Yes		Yes		
3-Hydroxybenzoic acid + HTC	Yes						Yes				Yes	
4-Hydroxybenzoic acid + HTC	Yes			Yes	Yes		Yes					Yes
Thiosalicylic acid + HTC				Yes			Yes			Yes		
4-Mercaptobenzoic acid + HTC	Yes			Yes			Yes					Yes
4-Ethylthiobenzoic acid + HTC	Yes		Yes	Yes	Yes		Yes					Yes

4.1.4 Particle size analysis

Particle size analysis was done on both the stabilisers synthesised by the reconstruction method and the co-precipitation method. For the reconstruction method some of the stabilisers had particle size distributions of a bimodal nature. An example of this can be found in figure 4.1.18 below.

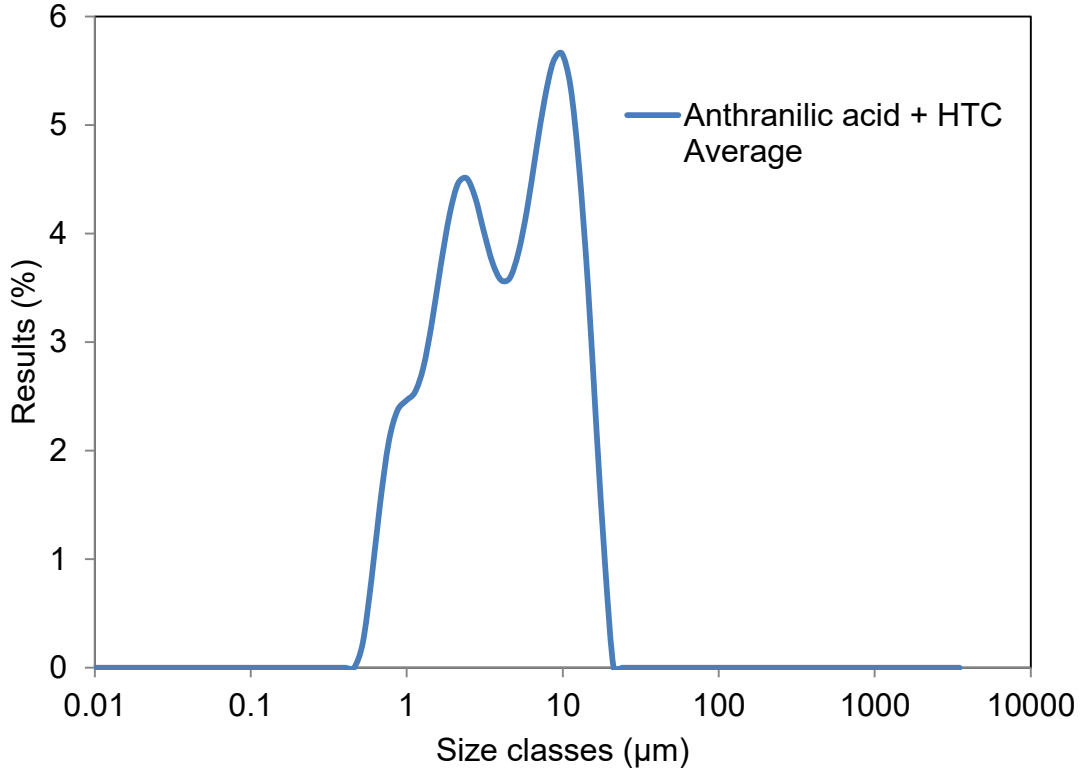

Figure 4.1.19: Average particle size distribution for anthranilic acid intercalated into hydrotalcite using the reconstruction method.

The bimodal distribution may be seen from the two large peaks in the figure. This type of distribution is a result of the way the LDH particles pass the Mastersizer's laser detector. Due to the fact that LDH particles are platelets, one peak gives a measurement of the width of the platelets while the other peak gives an indication of the thickness of the stacked platelets.

Although measures were taken to prevent particle agglomeration within the Mastersizer, ultrasound, agglomeration did occur for some of the stabilisers. Figure 4.1.20 below depicts this particle agglomeration.

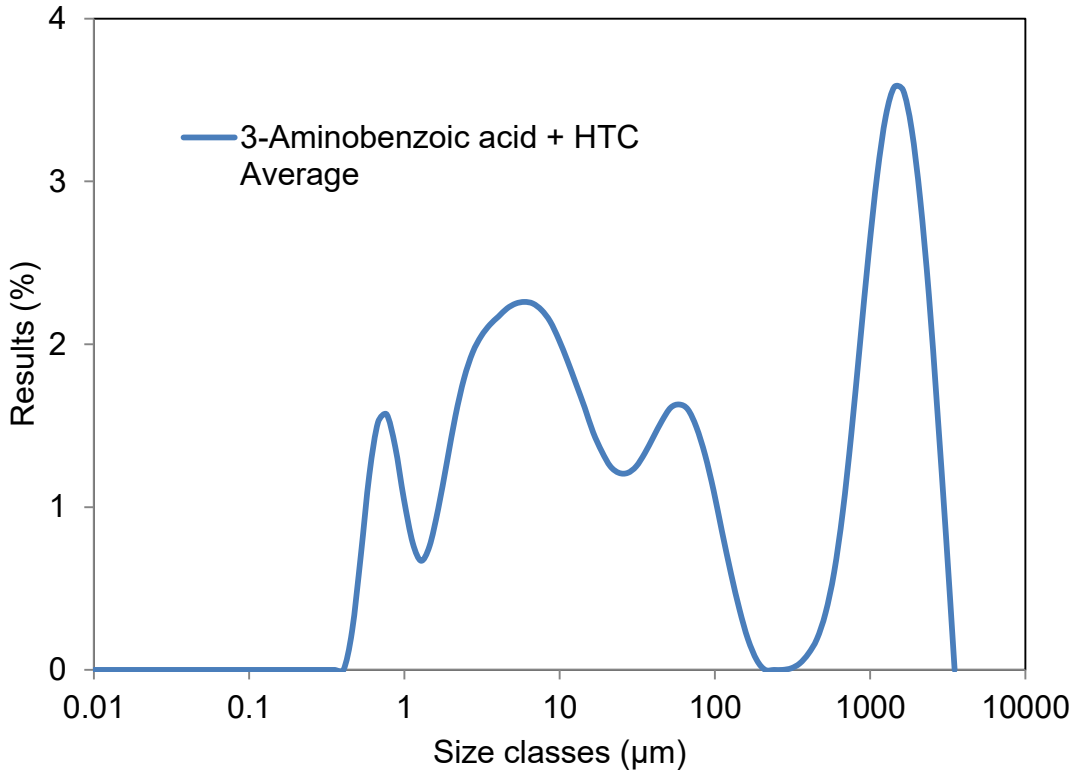

Figure 4.1.20: Average particle size distribution for 3-aminobenzoic acid intercalated into hydrotalcite using the reconstruction method.

The large peak above the 1 000 µm size class is an indication of agglomeration.

The remaining particle size distribution figures are located in Appendix C.

The tables below depict the average d_{10}, d_{50} and d_{90} measurements for the reconstruction stabilisers and the co-precipitation stabilisers. The particle sizes of hydrotalcite are included in both tables for comparison.

From tables 4.1.7 and 4.1.8 it may be seen which stabilisers showed signs of agglomeration within the Mastersizer. These stabilisers have d_{90} measurements of over 1 500 µm.

The particle sizes for the co-precipitation stabilisers are generally larger than their reconstruction method synthesis counterparts. This is probably due to the materials having different crystal structures due to different syntheses methods.

Table 4.1.7: Reconstruction stabiliser average particle sizes

Stabiliser	d_{10} (µm)	d_{50} (µm)	d_{90} (µm)
Hydrotalcite	0.75	3.38	26.60
Benzoic acid + HTC	0.90	4.03	19.30
Anthranilic acid + HTC	1.16	4.51	13.20
3-Aminobenzoic acid + HTC	1.68	28.30	1910
4-Aminobenzoic acid + HTC	1.08	4.32	14.20
Thiosalicylic acid + HTC	0.89	2.31	7.29
4-Mercaptobenzoic acid + HTC	1.29	4.46	15.00
Salicylic acid + HTC	0.82	3.64	19.80
3-Hydroxybenzoic acid + HTC	1.93	6.47	20.90
4-Hydroxybenzoic acid + HTC	0.67	2.80	19.50
4-Ethylthiobenzoic acid + HTC	0.93	2.30	5.38

Table 4.1.8: Co-precipitation average particle sizes

Stabiliser	d_{10} (µm)	d_{50} (µm)	d_{90} (µm)
Hydrotalcite	0.75	3.38	26.60
Benzoic acid + HTC	3.32	13.60	75.80
Anthranilic acid + HTC	3.54	21.90	1150
3-Aminobenzoic acid + HTC	2.94	11.80	49.50
4-Aminobenzoic acid + HTC	2.86	13.20	1690
Thiosalicylic acid + HTC	3.58	12.10	42.40
4-Mercaptobenzoic acid + HTC	2.33	14.10	1780
Salicylic acid + HTC	3.14	10.60	33.90
3-Hydroxybenzoic acid + HTC	4.07	25.40	73.30
4-Hydroxybenzoic acid + HTC	3.19	29.10	1930
4-Ethylthiobenzoic acid + HTC	57.0	275	585

4.2 Heat stability results

4.2.1 Co-precipitation synthesis vs reconstruction synthesis

Figure 4.2.1 compares the early stability of the stabilisers synthesised with the co-precipitation method to the early stability of the stabilisers synthesised with the reconstruction method. The stability values for the reconstruction synthesis data are average values. The data for every torque rheometer run can be found in Appendix D.

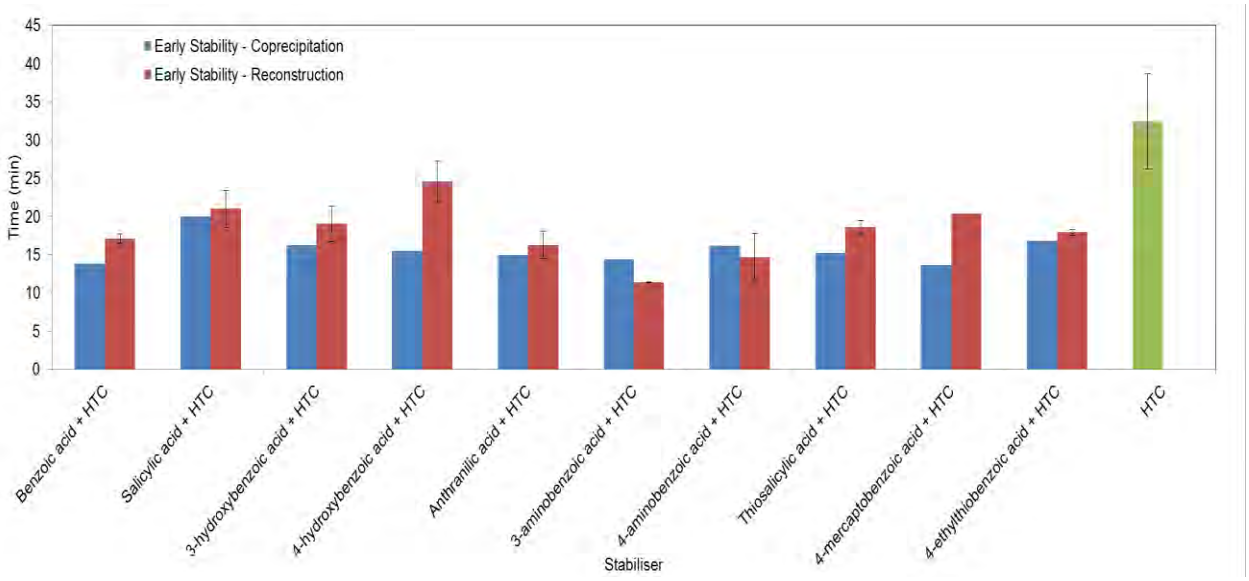

Figure 4.2.1: Comparison of the effect of synthesis method on early stability.

It should be noted that only error bars were generated for the stabilisers that had undergone three runs each in the Rheomix.

Each error bar is an indication of the standard deviation for a set of runs. The stabiliser with the largest standard deviation is hydrotalcite with a value of 6.21 min.

From figure 4.2.1 it may be seen that the majority of stabilisers synthesised with the reconstruction method outperformed their co-precipitation counterparts in terms of early stability.

From figure 4.2.1 it may be seen that the neat, unmodified hydrotalcite is the best early stabiliser with an early stability time of 32.40 min. This result is somewhat unsurprising considering that hydrotalcite has a proven track record of enhancing

PVC thermal stability. This may also be due to the fact that a “constant mass” of stabiliser were added to each formulation. Due to the higher molar masses of the organic acids vs the interlayer carbonate, the same mass of organic modified stabilisers will absorb less of the released HCl. Only under synergistic conditions should an enhancement of stability be expected. In other words the organic acids reduce the material’s ion exchange capacity based on mass.

The best performing modified stabiliser in terms of early stability is 4-hydroxybenzoic acid + HTC synthesised with the reconstruction method. This stabiliser had an early stability time of 24.54 min.

The best organic acids that were intercalated into hydrotalcite were the hydroxybenzoic acids. With reference to the literature in section 2.4.5 hydroxyl groups on substituted benzoic acids are highly activating. This fact implies that the hydroxybenzoic acids are more capable of free radical stabilisation than the other intercalated compounds i.e. the hydroxybenzoic acids are more willing to substitute the attached –OH group for free radical groups from the degrading PVC chain. The hydroxybenzoic acids outperform the aminobenzoic acids, even though the amino group is more activating than the hydroxyl group.

With early stability, it is especially important to take note of how much intercalant was loaded into hydrotalcite and whether this loading has any bearing on the early stability provided by a stabiliser.

Figure 4.2.2 depicts early stability time as a function of organic loading mass percentage for the reconstruction synthesised stabilisers.

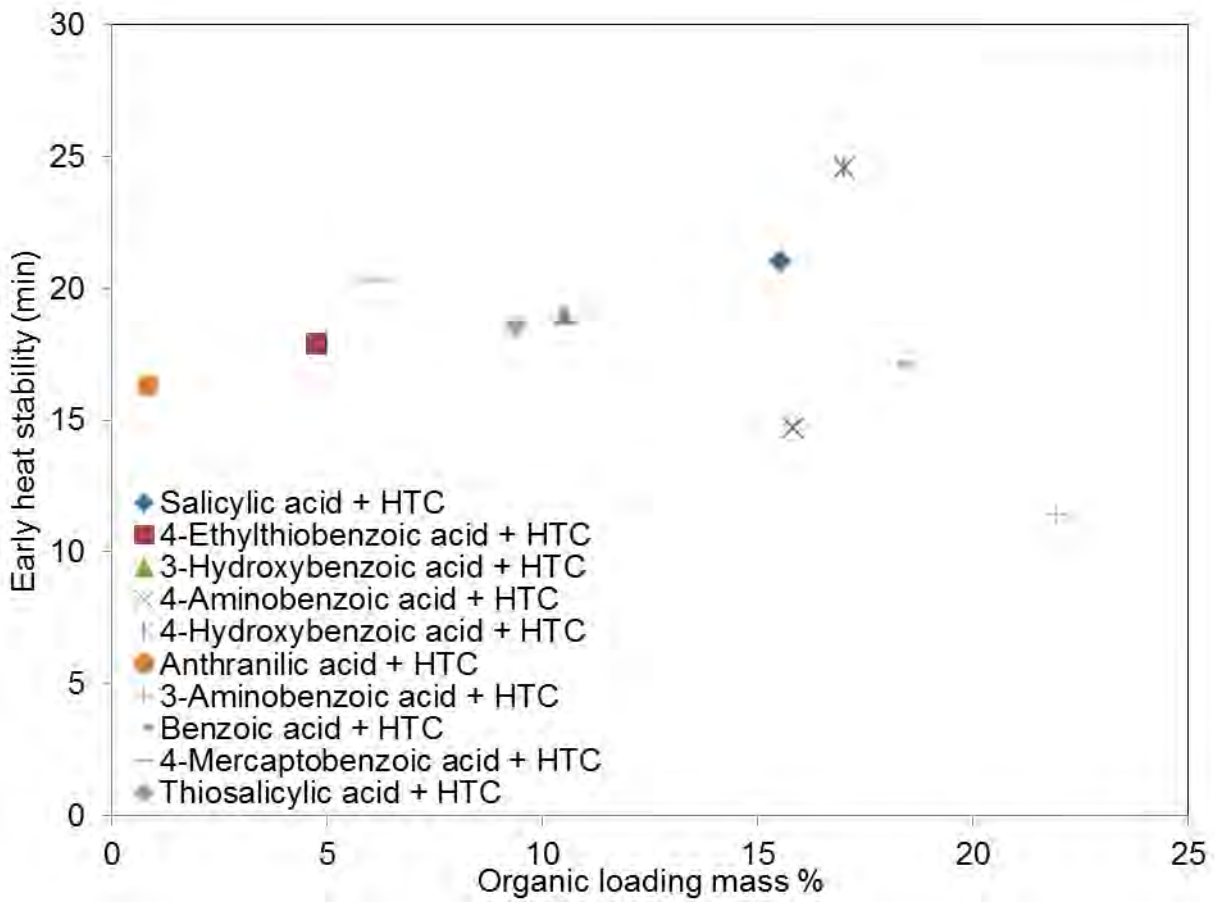

Figure 4.2.2: Reconstruction stabiliser early heat stability as a function of organic loading mass percentage

From figure 4.2.2 it can be seen that there is a relationship between the early heat stability provided by a stabiliser and the loading of the organic compound. The early heat stability increases as the organic loading mass percentage increases until around 17 %. At mass percentages above 17 % the heat stability time decreases. This indicates that an optimal loading point exists at 17 % for the reconstruction synthesised stabilisers. If the stabiliser loading is too high, as is the case with 3-aminobenzoic acid + HTC, degradation of PVC may be increased. This occurs due to the increased presence of Lewis acid compounds in the system. As stated in section 2.2, these Lewis acids act as catalysts for the dehydrochlorination reaction.

These results are somewhat distorted by the fact that the loading was not a controlled variable in the experiment.

Figure 4.2.3 depicts early stability time as a function of organic loading mass percentage for the co-precipitation synthesised stabilisers.

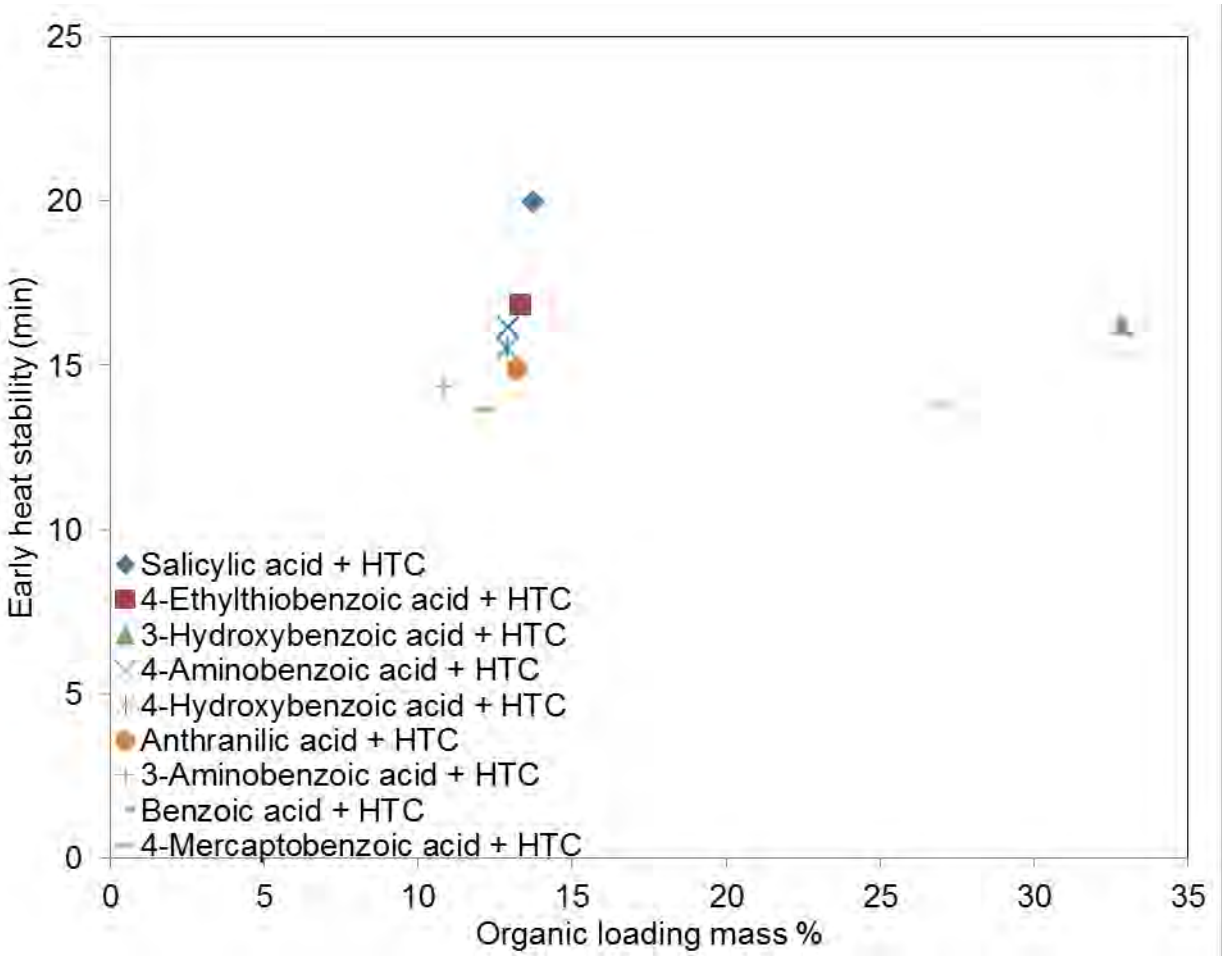

Figure 4.2.3: Co-precipitation stabiliser early heat stability as a function of organic loading mass percentage

From figure 4.2.3 above it can be seen that the co-precipitation method synthesised stabilisers had much more consistent loading values than that of the reconstruction stabilisers.

Looking at the range of organic loading mass percentages from 10.85 % to 13.75 %, early heat stability does indeed increase with organic loading.

This trend is much less pronounced than that of the reconstruction stabilisers.

From figure 4.2.3 it can be seen that the optimal loading for stabilisers synthesised with the co-precipitation is around 14 %.

Much like the reconstruction stabilisers, it can be seen that very high organic loadings are capable of causing a decrease in early stability time.

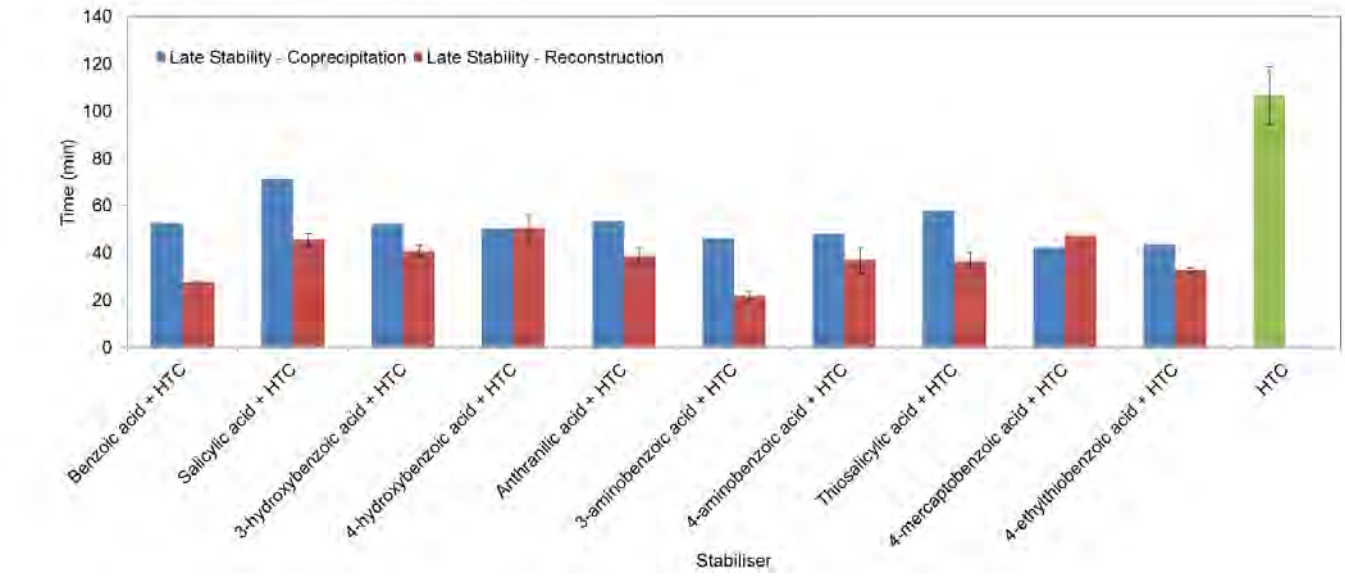

Figure 4.2.4: Comparison of the effect of synthesis method on late stability.

Figure 4.2.4 compares the late stability of the stabilisers synthesised with the co-precipitation method to the late stability of the stabilisers synthesised with the reconstruction method.

From figure 4.2.4 it can be seen that the majority of the co-precipitation stabilisers outperform the reconstruction stabilisers in terms of late stability. None of the modified stabilisers outperformed neat hydrotalcite which had a late stability time of 106.51 min. The best performing modified stabiliser in terms of late stability was salicylic acid + HTC synthesised with the co-precipitation method. This stabiliser had a late stability time of 71.32 min. High late stability time values indicate that the stabiliser had good HCl scavenging properties i.e. chloride anions are able to displace either the interstitial salicylic acid anion within the interlayer of clay structure or the salicylic acid molecules that have adhered to the outer surface of the clay.

4.2.2 The effect of substituent group type

The following substituent groups were tested: amino, hydroxyl, mercapto and ethylthio. Figure 4.2.5 below shows the effect of stabilisers with ortho position substituent groups on both the early and late stability of PVC. These stabilisers were synthesised using the reconstruction method.

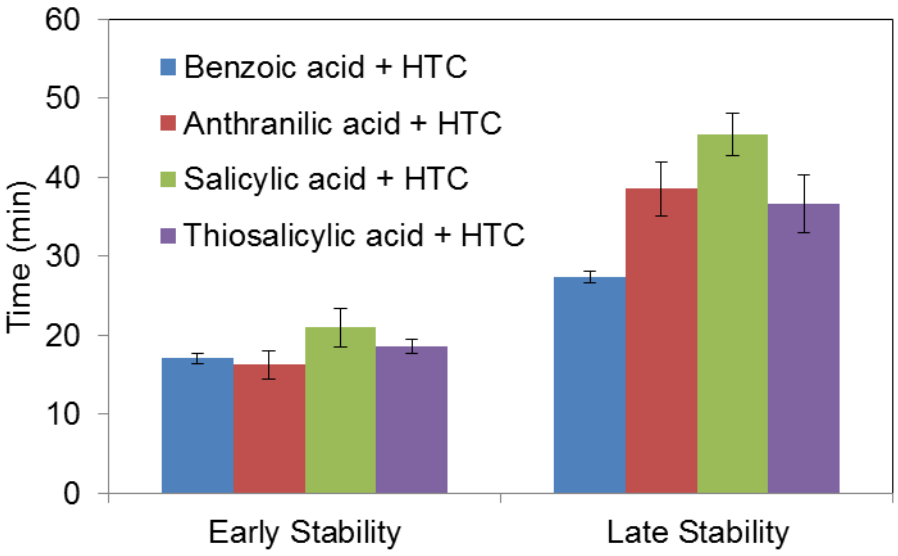

Figure 4.2.5: Comparison of the effect of substituent group type for ortho position reconstruction stabilisers.

Using benzoic acid + HTC as a baseline for this experiment i.e. an organic acid with no substituent group; one can clearly see that the type of substituent group does indeed play an effect on PVC heat stability. From the figure it can be seen that the presence of a substituent group on the intercalated organic acid has a greater effect on the late stability than the early stability of PVC. All three of the stabilisers with ortho position substituent groups outperformed benzoic acid + HTC in terms of late stability. In terms of early stability, only anthranilic acid + HTC performed worse than benzoic acid.

The early stability times of the stabilisers with substituent groups are much closer to that of the early stability time of benzoic acid whereas with the late stability times there is a much larger difference between benzoic acid HTC's late stability and that of the ortho substituent group stabilisers.

It can be seen that the stabiliser with the hydroxyl substituent group, salicylic acid, provides the best early and late stability out of these ortho position reconstruction stabilisers. Salicylic acid + HTC had an early stability time of 21.00 min and a late stability time of 45.41 min.

Figure 4.2.6 depicts the effect of co-precipitation synthesised stabilisers with substituent groups in the ortho position on the early and late stability of PVC.

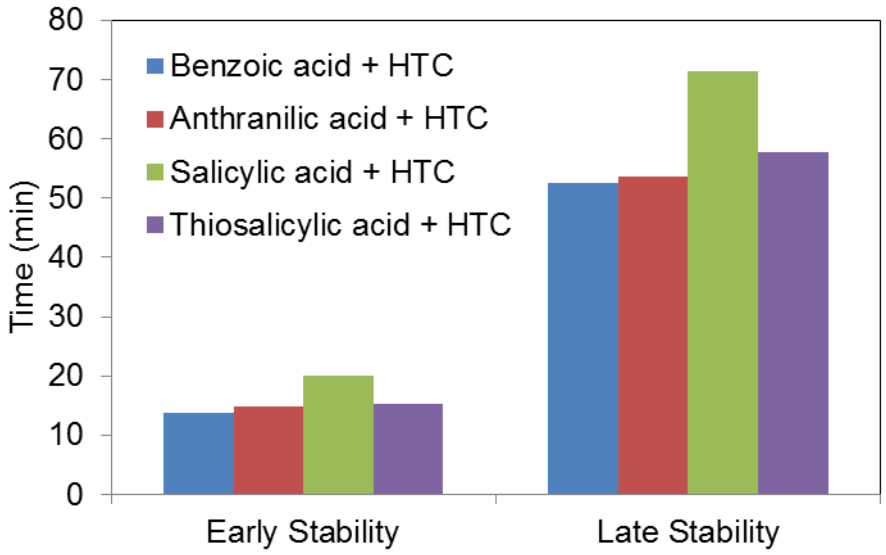

Figure 4.2.6: Comparison of the effect of substituent group type for ortho position co-precipitation stabilisers.

The ortho position co-precipitation stabilisers show a similar trend to that of the reconstruction stabilisers, with salicylic acid having both the best early and late stability times of 19.98 min and 71.32 min respectively.

Figure 4.2.7 depicts the effect of reconstruction synthesised stabilisers with substituent groups in the meta position on the early and late stability of PVC.

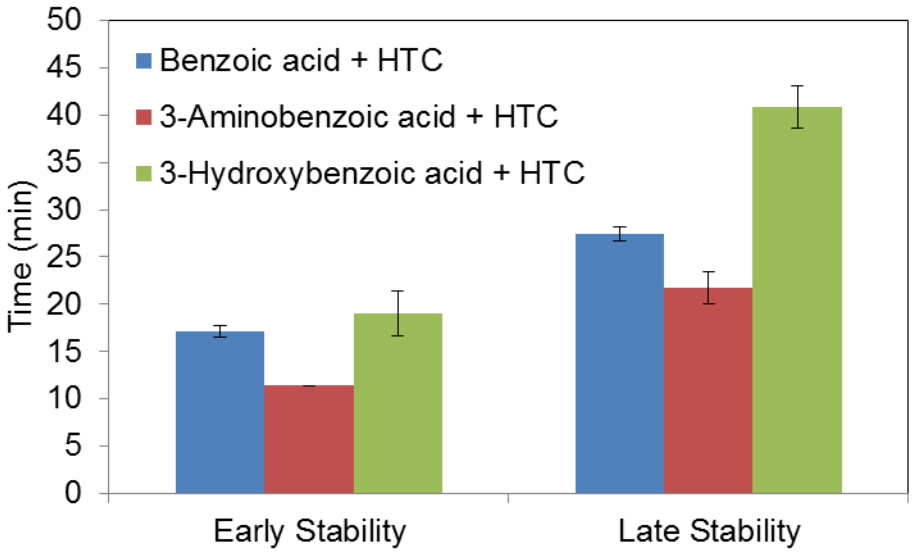

Figure 4.2.7: Comparison of the effect of substituent group type for meta position reconstruction stabilisers.

Much like the ortho position reconstruction stabilisers, the stabiliser with the hydroxyl substituent group has the best early and late stability; 3-hydroxybenzoic acid + HTC has an early stability time of 19.02 min and a late stability time of 40.83 min.

Figure 4.2.8 depicts the effect of co-precipitation synthesised stabilisers with substituent groups in the meta position on PVC heat stability.

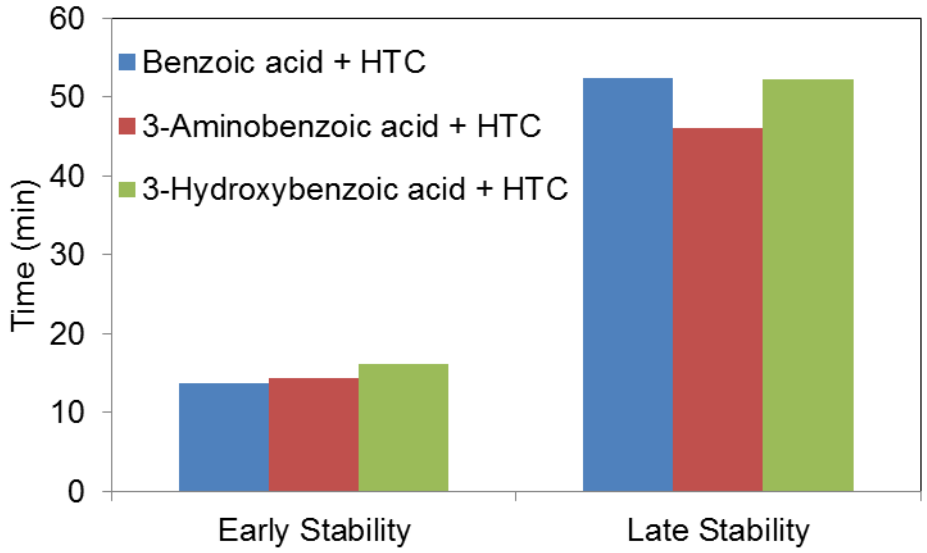

Figure 4.2.8: Comparison of the effect of substituent group type for meta position co-precipitation stabilisers.

From figure 4.2.8 it may be seen that 3-hydroxybenzoic acid + HTC is the best performing early stabiliser with an early stability time of 16.21 min. It is interesting to note that for the late stability, benzoic acid + HTC performed slightly better than 3-hydroxybenzoic acid + HTC with a late stability time of 52.49 min. 3-hydroxybenzoic acid + HTC has a late stability time of 52.34 min.

Figure 4.2.9 depicts the effect of reconstruction synthesised stabilisers with substituent groups in the para position on PVC heat stability.

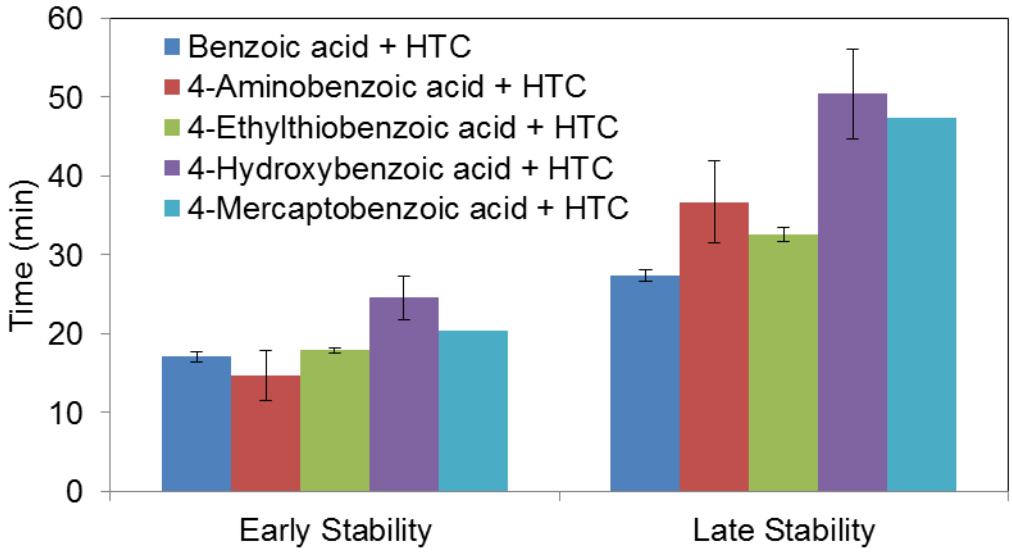

Figure 4.2.9: Comparison of the effect of substituent group type for para position reconstruction stabilisers.

In terms of early stability, the para position reconstruction stabilisers show a similar trend to that of the ortho and meta position reconstruction stabilisers with all the para position substituent stabilisers, save anthranilic outperforming benzoic acid + HTC. Similarly, all the para position substituent stabilisers have better late stability then benzoic acid + HTC. Once again, the best performing substituent group is the hydroxyl group with 4-hydroxybenzoic acid + HTC having an early stability time of 24.54 min and a late stability time of 50.39 min.

Figure 4.2.10 depicts the effect of co-precipitation synthesised stabilisers with substituent groups in the para position on PVC heat stability.

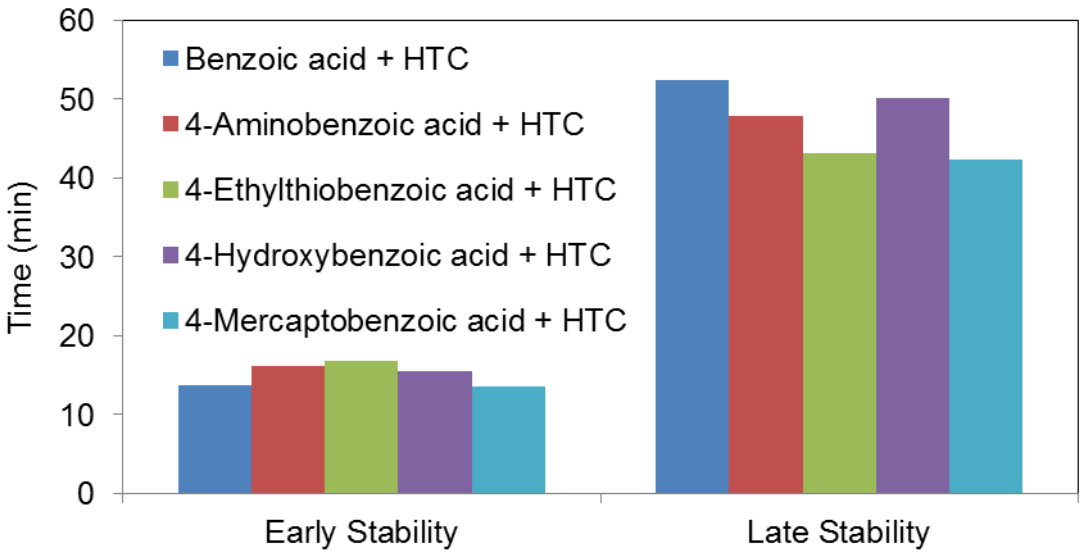

Figure 4.2.10: Comparison of the effect of substituent group type for para position co-precipitation stabilisers.

From figure 4.2.10 it may be seen that the best performing early stabiliser is 4-ethylthiobenzoic acid + HTC with an early stability time of 16.84 min. The best performing late stabiliser is benzoic acid + HTC with a late stability time of 52.49 min slightly edging ahead of 4-hydroxybenzoic acid which had a late stability time of 50.16 min.

Comparing all of the results presented above, it may be seen that the best performing substituent group from both the reconstruction and co-precipitation based stabilisers is the hydroxyl group. This is true for both early and late stability.

Table 4.2.1 the ranks of the various substituents of the aromatic acids intercalated into hydrotalcite *via* the reconstruction method. The first pKa value and second pKa value (if available) are also shown for each aromatic acid substituent. The first pKa value is the acid disassociation constant for the first ionisation of the aromatic acid. The second pKa value is the acid disassociation constant for the second ionisation of the aromatic acid. The ranks in this table are based on the early stability values in figure 4.2.1.

The pKa values were taken from the Chemicalize website (Marvin 16.9.26, 2016). This website uses software created by ChemAxon to calculate properties for different chemical compounds.

Table 4.2.1: Substituent rankings of the aromatic acids intercalated into hydrotalcite.

	Ortho			Meta			Para		
Rank	Substituent	pKa	pKa 2	Substituent	pKa	pKa 2	Substituent	pKa	pKa 2
1	OH	2.79	13.23	OH	3.84	9.55	OH	4.38	9.67
2	SH	3.34	6.19	None	4.08	-	SH	4.12	6.21
3	None	4.08	-	NH_2	4.81	3.27	C_2H_5S	4.10	-
4	NH_2	4.89	1.95				None	4.08	-
							NH_2	4.77	2.69

As stated in section 2.5.4 electron withdrawal decreases reactivity toward electrophilic aromatic substitution and increases acidity. Electron donation increases reactivity toward electrophilic aromatic substitution and decreases acidity. This infers that the pKa values for a particular aromatic acid may be used as a measure of its reactivity. The implication of this fact is that the selection of an aromatic acid for stabilisation can be based solely on its pKa value, if the value is in a certain range.

The pKa 2 values in table 4.2.1 seem to support this notion with the first ranked stabilisers having the highest pKa 2 values. As one proceeds down the rankings, the pKa 2 values decrease. This implies that if an organic acid has a high pKa 2 value i.e. above 9.5, it will impart good stabilisation properties when intercalated into hydrotalcite. The pKa 2 values of the amino substituents are very low when compared to the other substituents. This is due to the fact that as further ionisation of the molecules occurs the NH_2 groups become more acidic NH_3^+ groups thus increasing the acidity of the compound. This also increases the Lewis acid character of the compound which in turn will lead to increased PVC degradation as mentioned previously.

4.2.3 The effect of substituent group position

Figure 4.2.11 shows the early and late heat stability afforded to PVC by the amino and hydroxyl stabilisers synthesised with the reconstruction method.

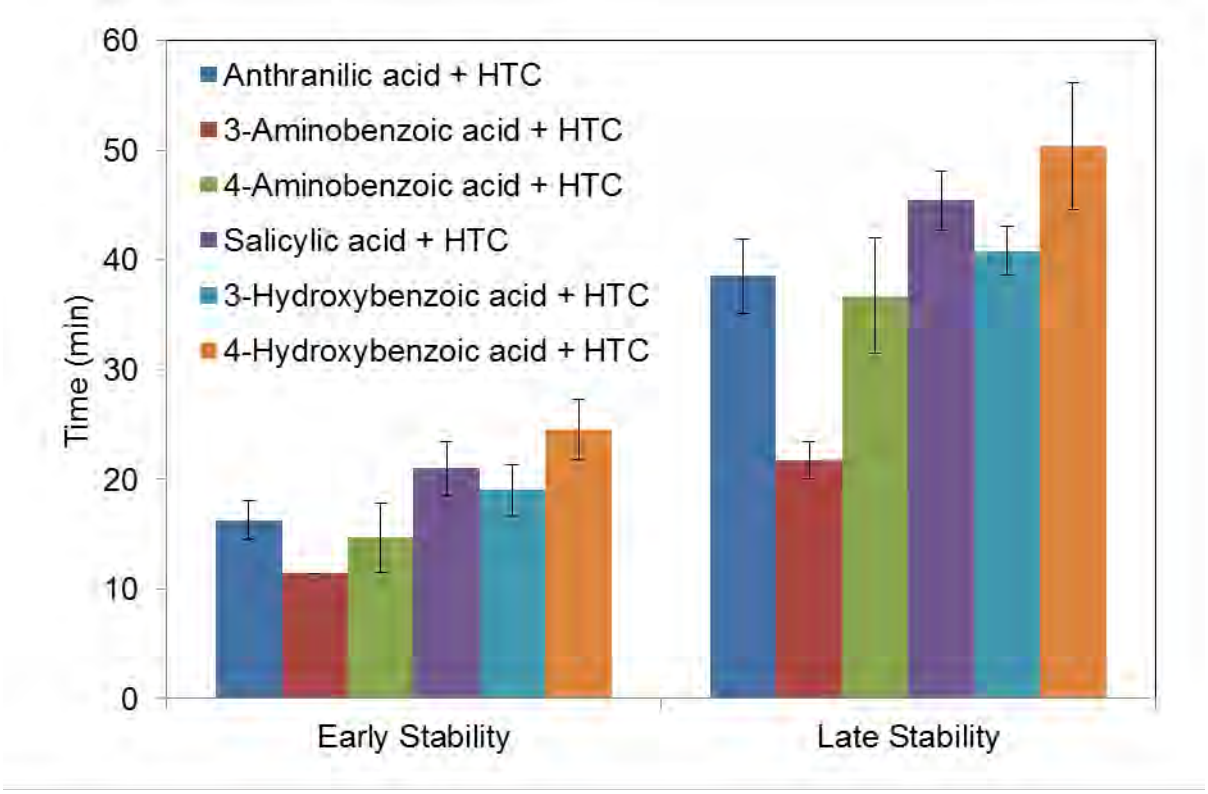

Figure 4.2.11: Early and late stability of amino and hydroxyl stabilisers (reconstruction) comparing the effect of substituent group position.

From figure 4.2.11 it can be seen that stabilisers with the substituent group in the meta position perform poorly when compared to their ortho and para counterparts. The ortho and para substituent groups outperform the meta groups, due to the fact that they are more activating i.e. they are better electron donators and are therefore more capable of free radical scavenging and stabilising the PVC chain.

Figure 4.2.12 depicts the early and late heat stability afforded to PVC by the amino and hydroxyl stabilisers synthesised with the co-precipitation method.

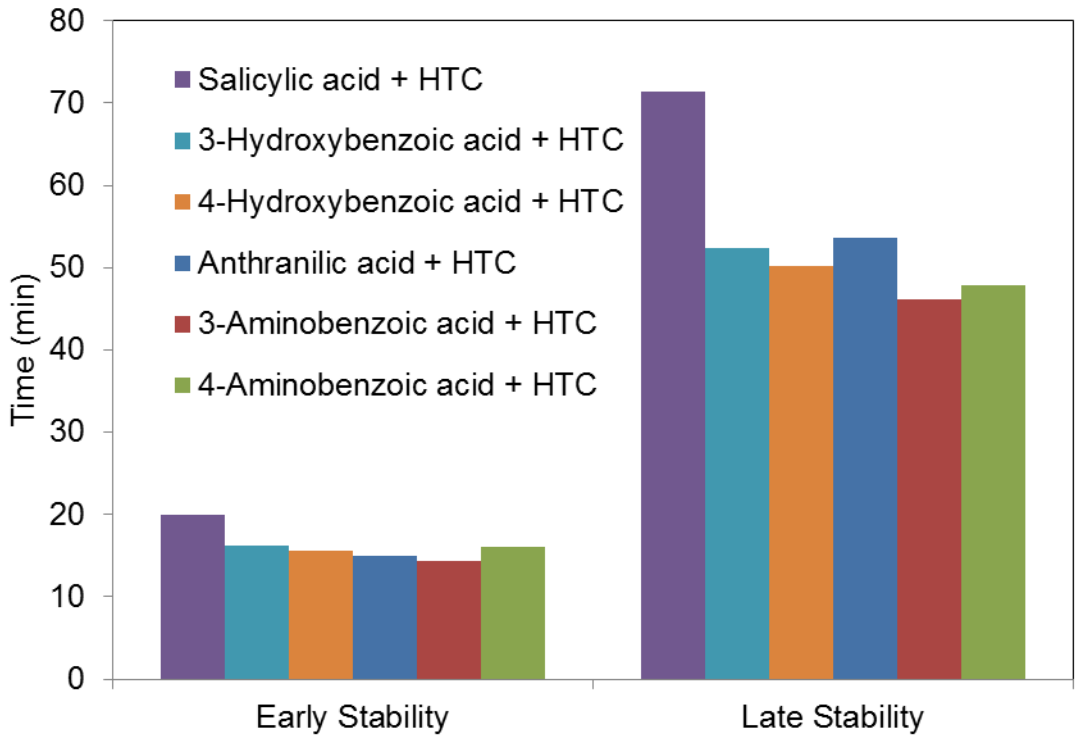

Figure 4.2.12: Early and late stability of amino and hydroxyl stabilisers (co-precipitation) comparing the effect of substituent group position.

The co-precipitation stabilisers show a similar trend to their reconstruction stabiliser counterparts, with the ortho and para stabilisers outperforming the meta stabilisers in the case of the aminobenzoic acid stabilisers. However, with the hydroybenzoic acid stabilisers, the meta position 3-hydroxybenzoic acid + HTC slightly outperforms the para position 4-hydroxbenzoic acid + HTC. Neither of these two stabilisers performed better than their ortho counterpart, salicylic acid + HTC.

4.2.4 The effect of substituent group length

4-mercaptobenzoic acid + HTC and 4-ethylthiobenzoic acid + HTC were compared to benzoic acid + HTC to see whether the length of the aromatic substituent had any influence on the heat stability of PVC.

Figure 4.2.13 depicts this comparison for the reconstruction synthesised stabilisers.

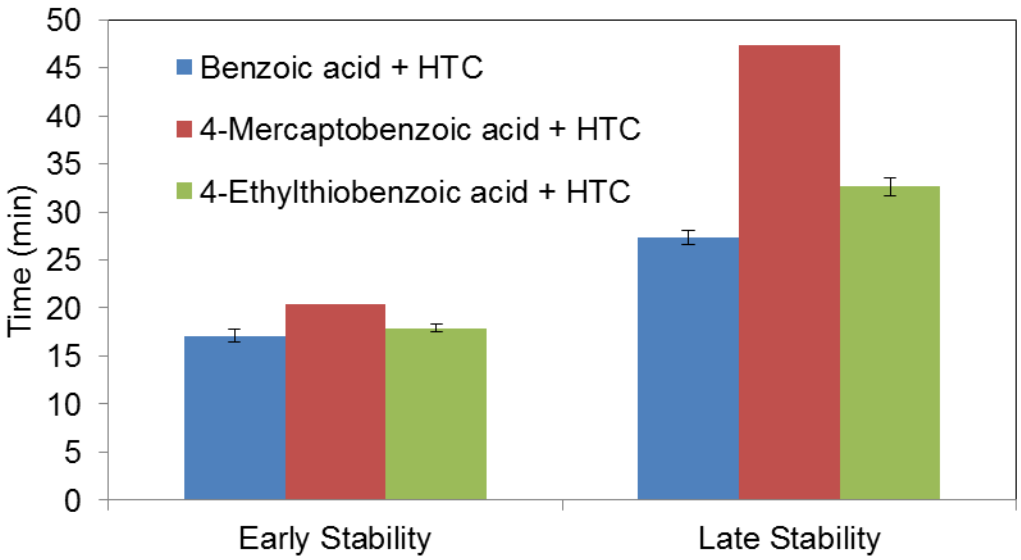

Figure 4.2.13: The effect of substituent group length on PVC heat stability for reconstruction synthesised stabilisers.

From figure 4.2.13 may be seen that the substituent length does play a positive effect on the heat stability of PVC. 4-mercaptobenzoic acid + HTC and 4-ethylthiobenzoic acid + HTC have better early and late stability times then benzoic acid + HTC. 4-mercaptobenzoic acid + HTC has an early stability time of 20.33 min and a late stability time of 47.41 min. 4-ethylthiobenzoic acid has an early stability time of 17.89 min and a late stability time of 32.64 min.

Figure 4.2.14 below depicts the effect of substituent group length on PVC heat stability for the co-precipitation synthesised stabilisers.

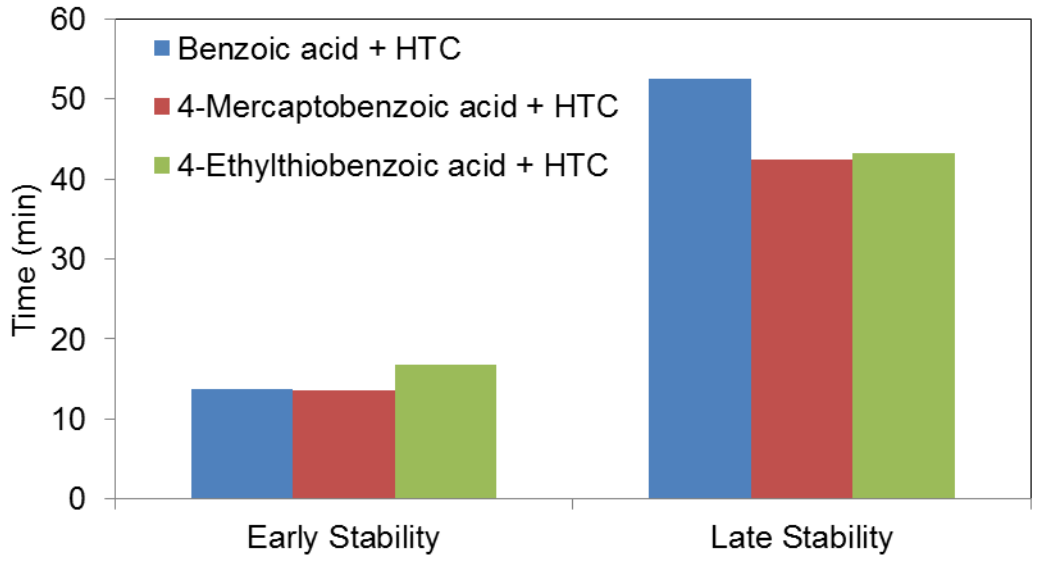

Figure 4.2.14: The effect of substituent group length on PVC heat stability for co-precipitation synthesised stabilisers.

It can be seen that a longer substituent group for co-precipitation synthesised stabilisers will lead to better early stability for PVC. 4-ethylbenzoic acid + HTC has an early stability time of 16.84 min. The same cannot be said for long term stabilisation where it can be seen that 4-mercaptobenzoic acid + HTC and 4-ethylthiobenzoic acid + HTC have worse long term stability than benzoic acid + HTC.

When comparing the substituent group length results for the two synthesis methods, there is no defined trend that determines whether the substituent group length has an overall positive effect on PVC heat stability. It can be determined that these results are somewhat inconclusive as a whole.

5. Conclusions and recommendations

According to the XRD data, only 4-aminobenzoic acid and thiosalicylic acid were successfully intercalated into hydrotalcite with the reconstruction method. For the co-precipitation method, no successful intercalations occurred; however layered double hydroxides formed for every synthesis.

The FTIR and the TGA results confirm the presence of the organic aromatic acids in all the synthesised stabilisers. This implies that either partial intercalation or surface adsorption of these molecules occurred for both synthesis methods.

It is recommended that synthesis conditions be better controlled in order to avoid contamination and to promote better intercalation.

The stabilisers synthesised with the reconstruction method outperformed their co-precipitation counterparts in terms of early stability. In terms of late stability, it was proven that the co-precipitation method formed better secondary stabilisers than the reconstruction method. None of the stabilisers synthesised in this investigation outperformed neat hydrotalcite.

The best performing modified stabiliser in terms of early stability is 4-hydroxybenzoic acid + HTC synthesised with the reconstruction method. The best performing modified stabiliser in terms of late stability was salicylic acid + HTC synthesised with the co-precipitation method.

A relationship does exist between the organic intercalant loading and heat stability for both the reconstruction and the co-precipitation synthesised stabilisers. As the intercalant loading increases to about 17 % on a mass basis so too does the early stability of PVC given by the reconstruction synthesised stabilisers. Past 17 % mass loading, the stability of PVC decreases due to enhanced Lewis acid concentration in the system which catalyses the degradation reaction. For the co-precipitation synthesised stabilisers this optimal loading point is from 10.85 % to 13.75 %.

The hydroxybenzoic acids were the best performing organic acids intercalated into hydrotalcite. The highly activating nature of the hydroxyl substituent group gives a higher capability of free-radical scavenging for the hydrotalcites intercalated with hydroxybenzoic acids.

The substituent group positions that give the best PVC heat stability are the ortho and para positions. The groups in these positions are more activating than the meta substituent groups and are therefore more capable of free radical scavenging and stabilising the PVC chain.

It may be assumed that for aromatic acids intercalated into hydrotalcite, the pKa 2 value of the acid may be used as a means of selecting an acid for stabilisation purposes. If an organic acid with a high pKa 2 value is intercalated into hydrotalcite, the resulting compound will give good heat stabilisation properties to PVC.

No definite conclusion could be made about the effect of substituent group length on the heat stability of PVC. It is recommended that further investigation be done to see if there is any definitive relationship that exists. In order for this experiment to yield viable results, the intercalant loading needs to be controlled in order to reduce experimental variability.

By combining the properties of the stabilisers mentioned above, it is possible to synthesise a stabiliser that has all these desirable traits. A suitable organic acid may be chosen and subsequently intercalated into hydrotalcite. For example, the proposed organic acid for intercalation should have a substituent group in either the ortho or the para position. This substituent group should also contain the hydroxyl group as this group has been proven to give good stabilisation properties. Optimal loadings of this acid into the LDH should also be found so as to save on material costs and to prevent potentially negative reactions with the PVC chain during stabilisation.

6. References

Acton, QA (2013) *Cyclic Hydrocarbons – Advances in Research and Application*, Scholarly Editions, Atlanta.

American Society for Testing and Materials, (2002). *ASTM D 2538-02- Standard Practice for Fusion of Poly(Vinyl Chloride) (PVC) Compounds Using a Torque Rheometer,* United States of America: ASTM.

American Society for Testing and Materials, (2004). *ASTM D 2115-04- Standard Practice for Oven Heat Stability of Poly(Vinyl Chloride) Compositions,* United States of America: ASTM.

Arkis, E and Balköse, D (2005), "Thermal stabilisation of poly(vinyl chloride) by organotin compounds", *Polymer Degradation and Stability,* 88, (1), 46-51.

Auerbach, SM, Carrado, KA and Dutta, PK (2004) *Handbook of Layered Materials,* Marcel Dekker, New York.

Bacalogulu, R and Fisch, MH (2000) *Thermal Degradation and Stabilisation of PVC,* Hanser, Munich.

Beauchamp, P "Spectroscopy Data Tables", http://www.cpp.edu/~psbeauchamp/pdf/424_spectra_tables.pdf [2015, December 27]

Bergaya, F, Theng, BKG and Lagaly, G (2011) *Handbook of Clay Science,* Elsevier Science, Amsterdam.

Bruice, PY (2014) *Organic Chemistry*, Pearson, New York

Cavani, F, Trifiro, F and Vaccari, A (1991) "Hydrotalcite-type anionic clays: Preparation, Properties and Applications", *Catalysis Today*, 11, 173-301.

Chemicalize (2016) “Chemical property web viewer”, Marvin 16.9.26, https://chemicalize.com/#/calculation

Chemsketch (2016) “Chemical structure drawing tool”, ACDLabs 14.01

Costa, FR, Leuteritz, A, Wagenknecht, U, Jehnichen, D, Häußler, L and Heinrich, G (2008) "Intercalation of Mg-Al layered double hydroxide by anionic surfactants: Preparation and characterisation" *Applied Clay Science*, 38, 153-164.

Cygan, RT, Liang, JJ and Kalinichev, AG (2004), “Molecular models of hydroxide, oxyhydroxide and clay phases and the development of a general force field”, *Journal of Physical Chemistry*, 108, (4), 1255-1266.

Giles, HF, Mount, EM and Wagner, JR (2007) Extrusion: *The definitive process guide and handbook*, William Andrew, New York.

Gökçel, HI, Balköse, D and Köktürk, U (1998) "Effects of mixed metal stearates on thermal stability of rigid PVC", *European Polymer Journal*, 35, 1501-1508.

Gupta, S, Agarwal, DD and Banerjee, S (2009), "Thermal stabilization of poly(vinyl chloride) by hydrotalcites, zeolites, and conventional stabilizers", *Journal of Vinyl and Additive Technology,* 15, (3), 164-170.

International Standards Office, (1990a). *ISO 182-1 Plastic- Determination of the tendency of compounds and products based on vinyl chloride homopolymers and copolymers to evolve hydrogen chloride and any other acidic products at elevated temperatures – Part 1: Congo red method*, Switzerland: ISO.

International Standards Office, (1990b). *ISO 182-2 Plastic- Determination of the tendency of compounds and products based on vinyl chloride homopolymers and copolymers to evolve hydrogen chloride and any other acidic products at elevated temperatures – Part 2: pH method*, Switzerland: ISO.

International Standards Office, (1993). *ISO 182-3 Plastic- Determination of the tendency of compounds and products based on vinyl chloride homopolymers and copolymers to evolve hydrogen chloride and any other acidic products at elevated temperatures – Part 3: Conductometric method*, Switzerland: ISO.

Jahrling, M (2009) “Examining the Fusion and Degradation Behaviour of PVC Dry Blends with the Haake Polylab QC”, http://www.thermoscientific.com/content/dam/tfs/ATG/CAD/CAD%20Documents/App

lication%20&%20Technical%20Notes/Material%20Characterization%20and%20Testing/Modular%20Lab%20Extruders%20and%20Mixers/D10351~.pdf [2014, September 19].

Jan, C and Bart, J (2006) *Polymer additive analytics: Industrial Practice and Case Studies*, Firenze University Press, Florence.

Kohno, Y, Tosuka, K, Ikoma, S, Yoda, K, Shibata, M, Matsushima,R, Tomita, Y, Maeda, Y and Kobayashi, K (2009) “Photostability enhancement of anionic natural dye by intercalation into hydrotalcite”, *Journal of Colloid and Interface Science*, 337, 117-121.

Laguna, H, Loera, S, Ibarra IA, Lima, E, Vera, MA and Lara, V (2007) “Azoic dyes hosted on hydrotalcite-like compounds: Non-toxic hybrid pigments” *Microporous and Mesoporous Materials*, 98(1), 234-241.

Lin, Y, Wang, J, Evans, DG and Li, D (2006), "Layered and intercalated hydrotalcite-like materials as thermal stabilizers in PVC resin", *Journal of Physics and Chemistry of Solids,* 67, (5–6), 998-1001.

Manzi-Nshuti, C, Chen, D, Su, S and Wilkie, CA (2009) "The effects of intralayer metal composition of layered double hydroxides on glass transition, dispersion, thermal and fire properties of their PMMA nanocomposites", *Thermochimica Acta*, 495, (1-2), 63-71.

Markarian, J (2007), “PVC additives – What lies ahead?”, *Plastic additives and compounding,* November-December 2007, 22-25.

Markland, C, Williams, GR and O’Hare, D (2011) “The intercalation of flavouring compounds into layered double hydroxides”, *Journal of Material Chemistry*, 21, 17896-17903.

McNeill, IC, Memetea, L and Cole, WJ (1995), "A study of the products of PVC thermal degradation", *Polymer Degradation and Stability,* 49, (1), 181-191.

Nicolet “Infrared Correlation Chart” http://ftirsearch.com/ [2015, December 27].

Othman, MR, Helwani, Z, Martunus and Fernando, WJN (2009), “Synthetic hydrotalcites from different routes and their application as catalysts and gas adsorbents: a review”, *Applied Organometallic Chemistry*, 23, 335-346.

Rossi, C, Schoubben, A, Ricci, M, Perioli, L, Ambrogi, V, Latterini, L, Aloisi, GG and Rossi, A (2005) “Intercalation of the radical scavenger ferulic acid in hydrotalcite-like anionic clays” *International Journal of Pharmaceutics*, 295, 47-55.

Schmidt, M (2013) “pH Effects on Intercalation of Layered Double Hydroxides using Katoite as a Precursor”, CSC 411 Report, Dept Chem Eng, University of Pretoria

Vieille, L, Rousselot, I, Leroux, F, Besse, JP and Taviot-Gueho, C (2003), “Hydrocalumite and its Polymer Derivatives. 1. Reversible Thermal Behaviour of Friedel’s Salt: A Direct Observation by means of High-Temperature in Situ Powder X-ray Diffraction”, *Chemistry of Materials*, 15, (23), 4361-4368.

Wilkes, CE, Summers, JW, Daniels, CA and Berard, MT (2005) *PVC Handbook,* Hanser, Munich.

Wypych, G (2008) *PVC Degradation & Stabilization,* ChemTec Publishing, Toronto.

Appendix A: XRD results

A.1 Reconstruction method synthesis

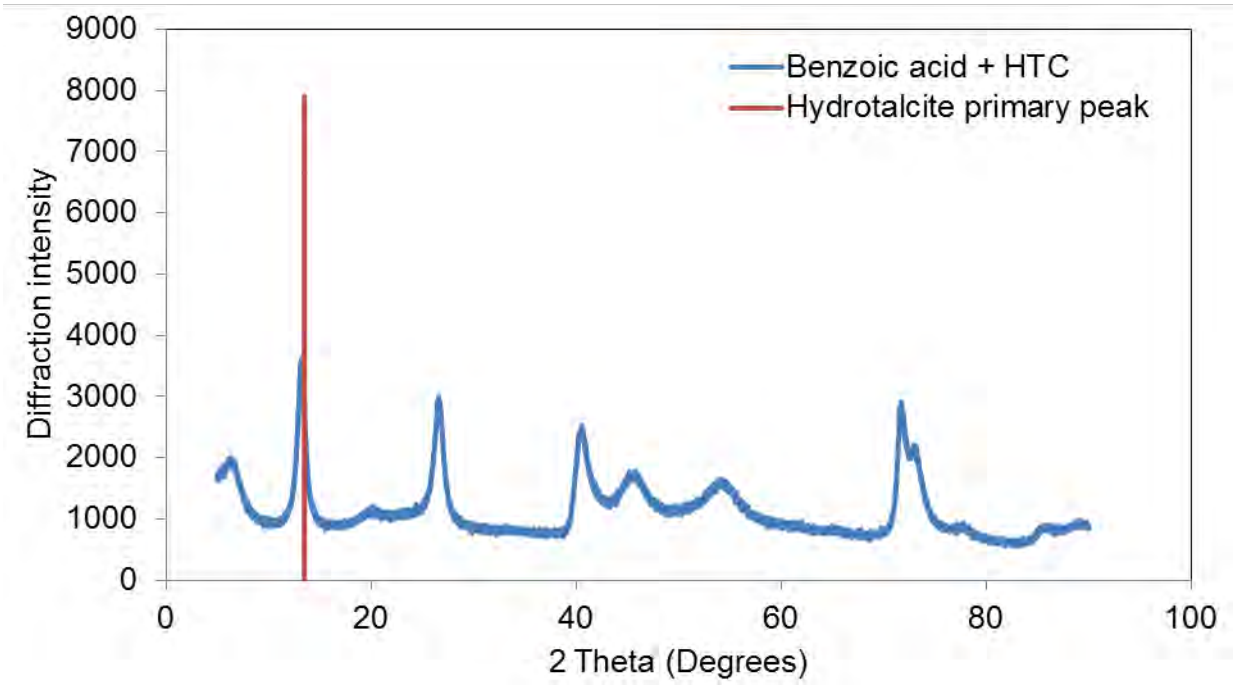

Figure A.1.1: XRD pattern for benzoic acid + HTC.

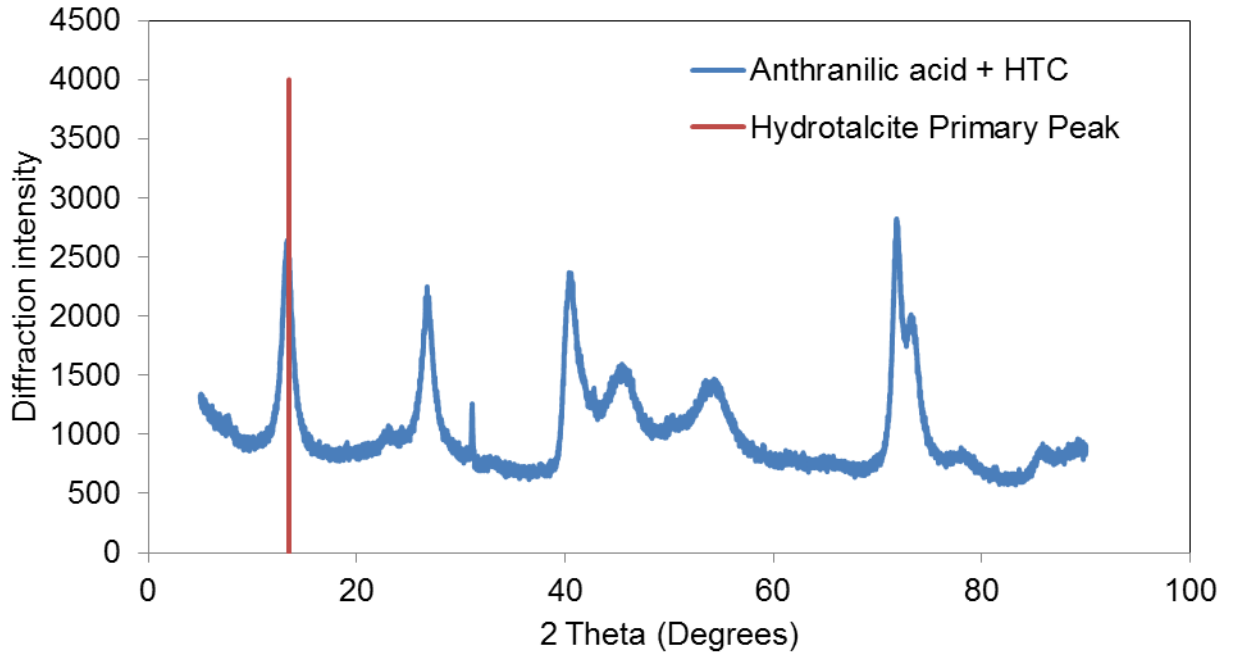

Figure A.1.2: XRD pattern for anthranilic acid + HTC.

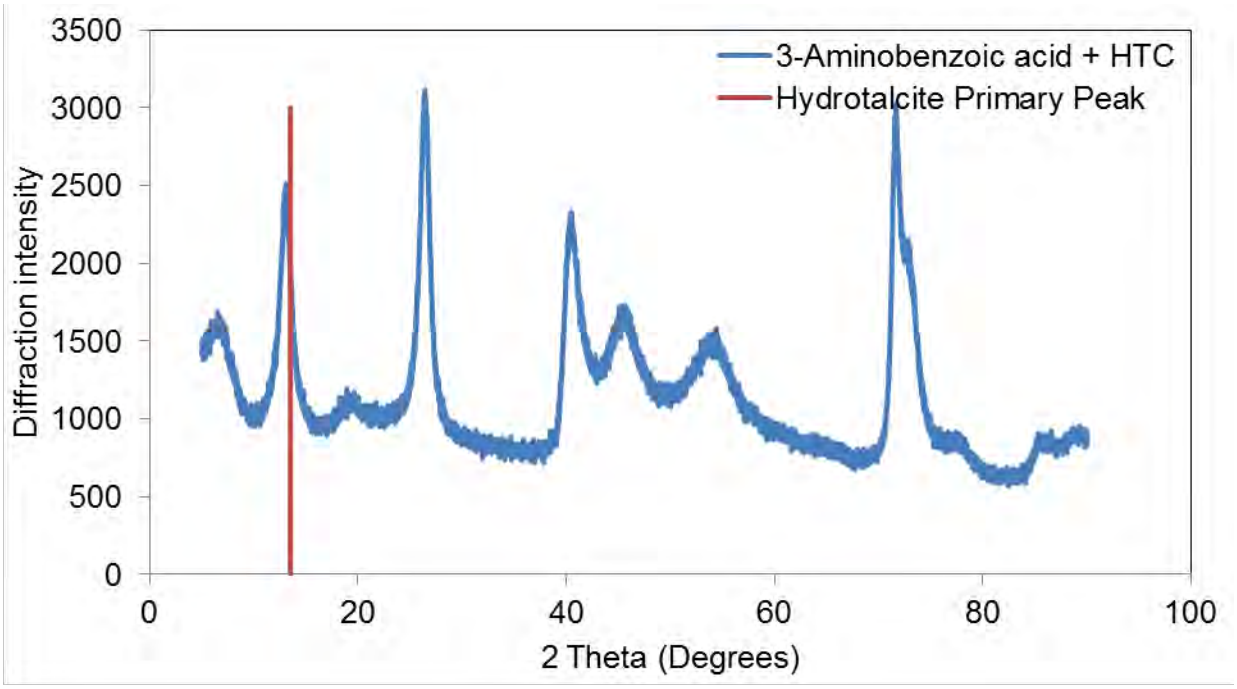

Figure A.1.3: XRD pattern for 3-aminobenzoic acid + HTC.

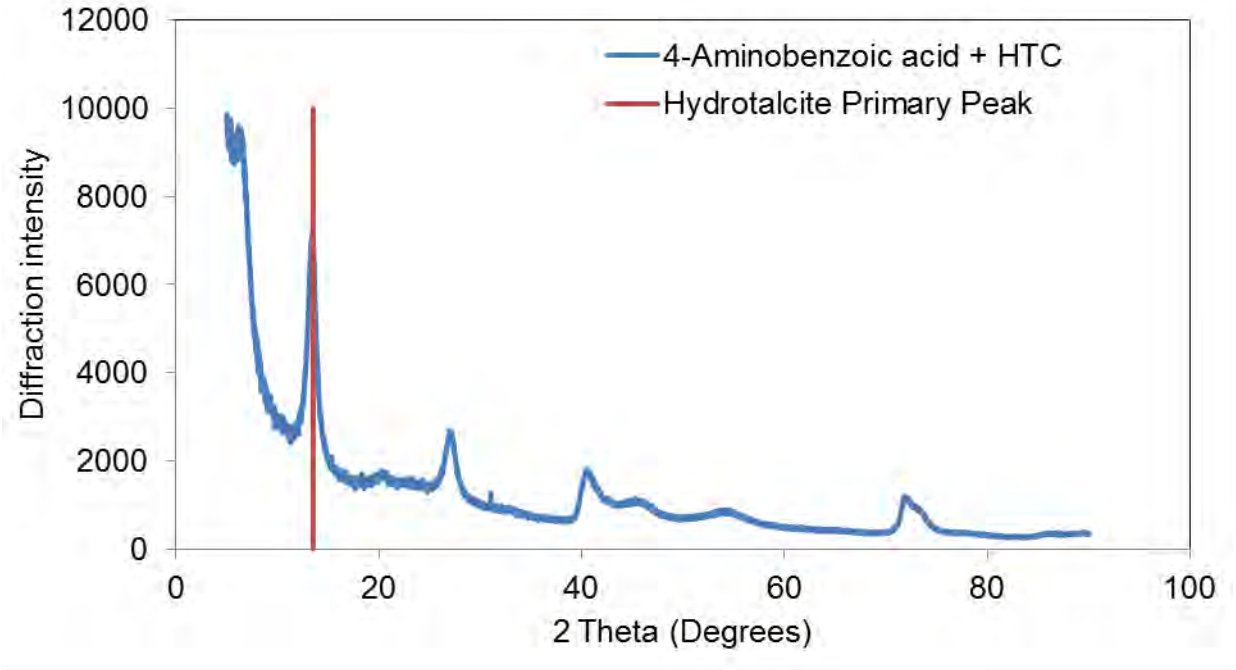

Figure A.1.4: XRD pattern for 4-aminobenzoic acid + HTC.

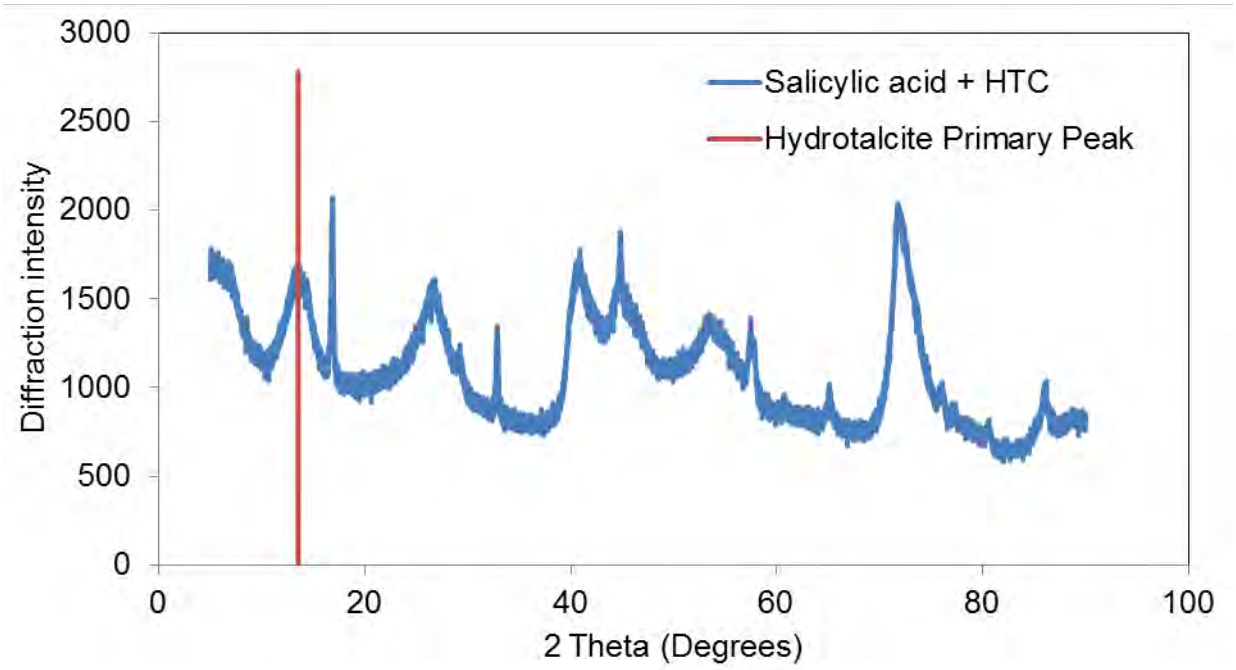

Figure A.1.5: XRD pattern for salicylic acid + HTC.

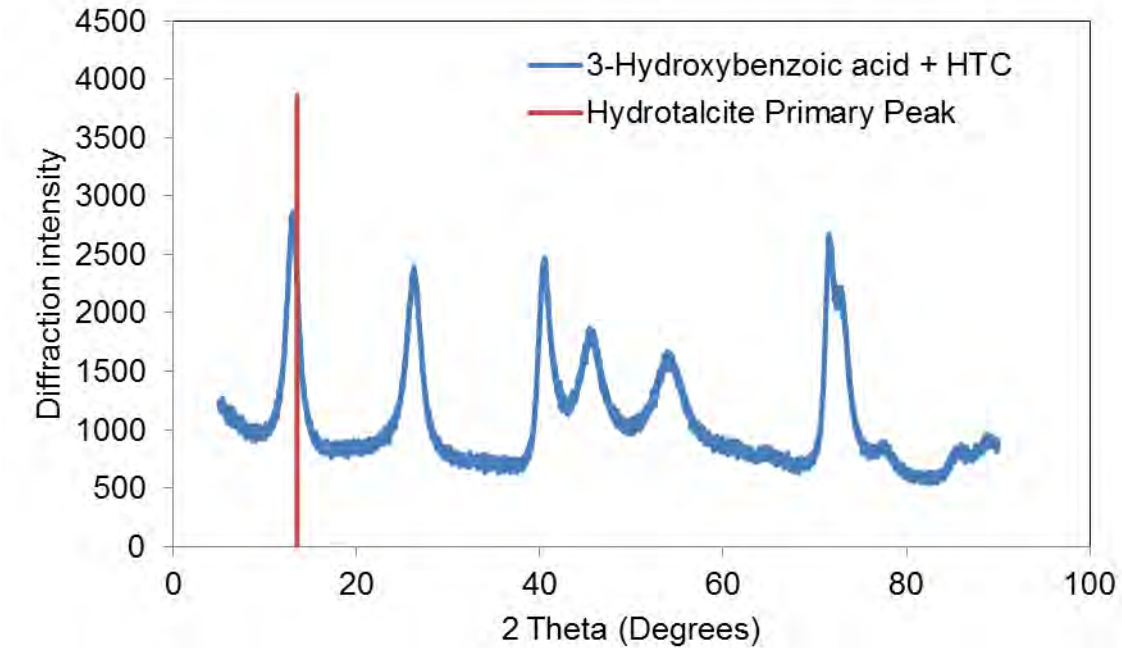

Figure A.1.6: XRD pattern for 3-hydroxybenzoic acid + HTC

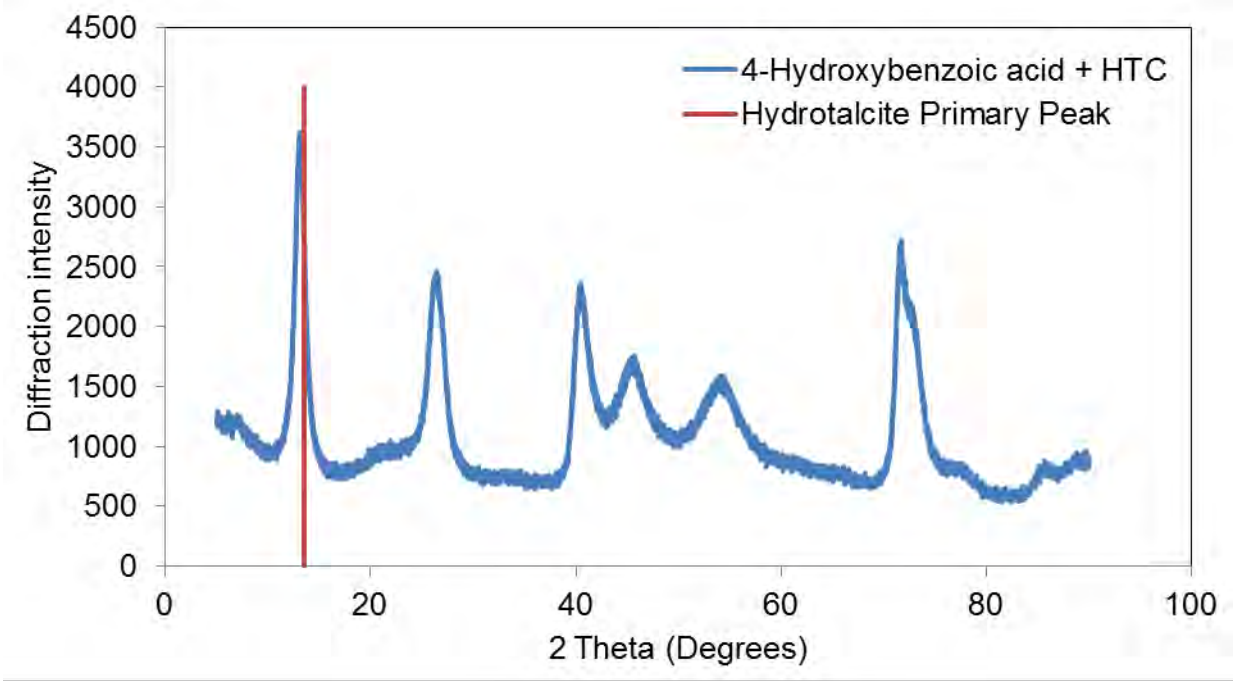

Figure A.1.7: XRD pattern for 4-hydroxybenzoic acid + HTC

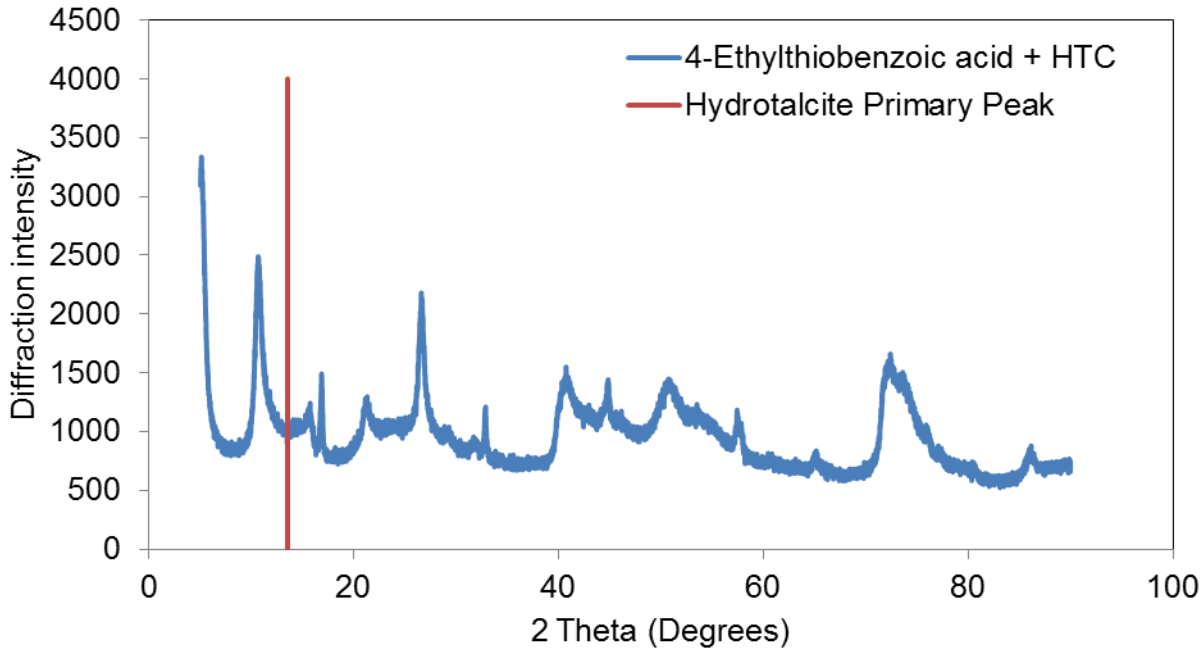

Figure A.1.8: XRD pattern for 4-ethylthiobenzoic acid + HTC

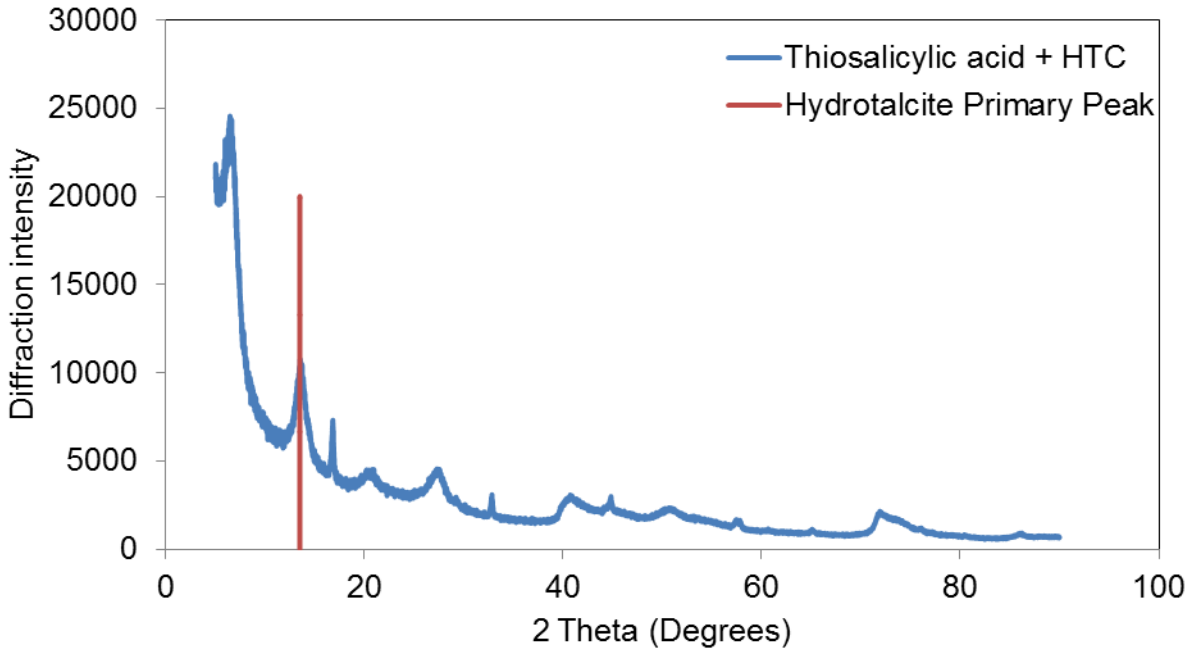

Figure A.1.9: XRD pattern for thiosalicylic acid + HTC

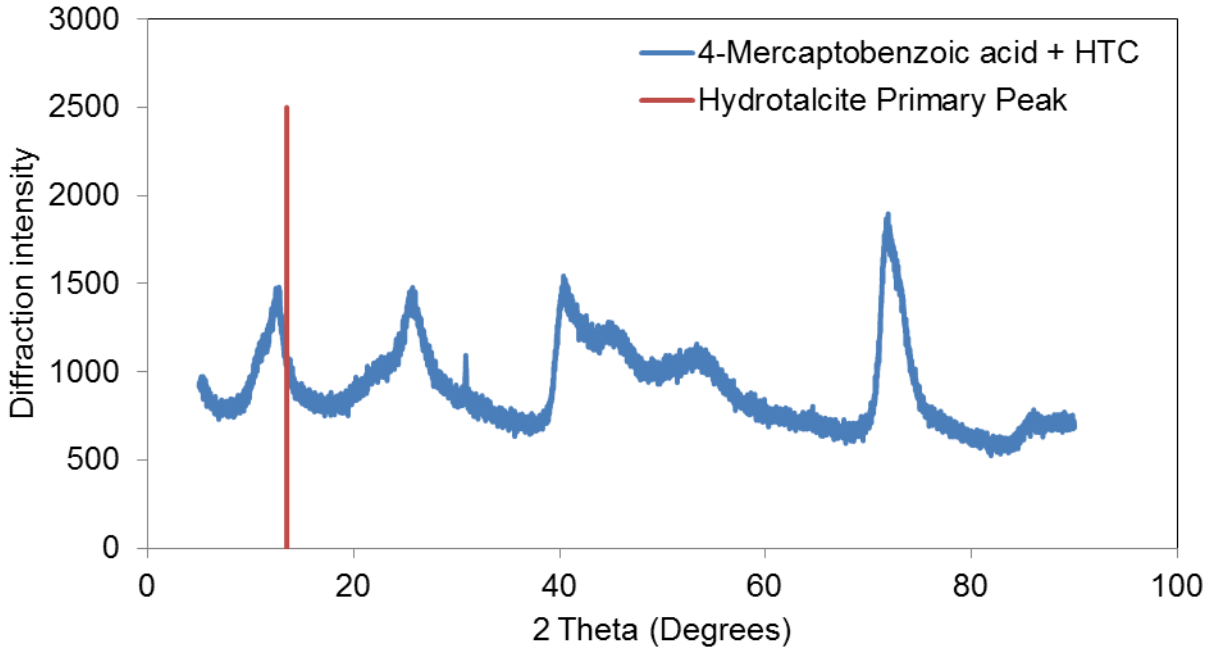

Figure A.1.10: XRD pattern for 4-mercaptobenzoic acid + HTC

A.2 Co-precipitation method synthesis

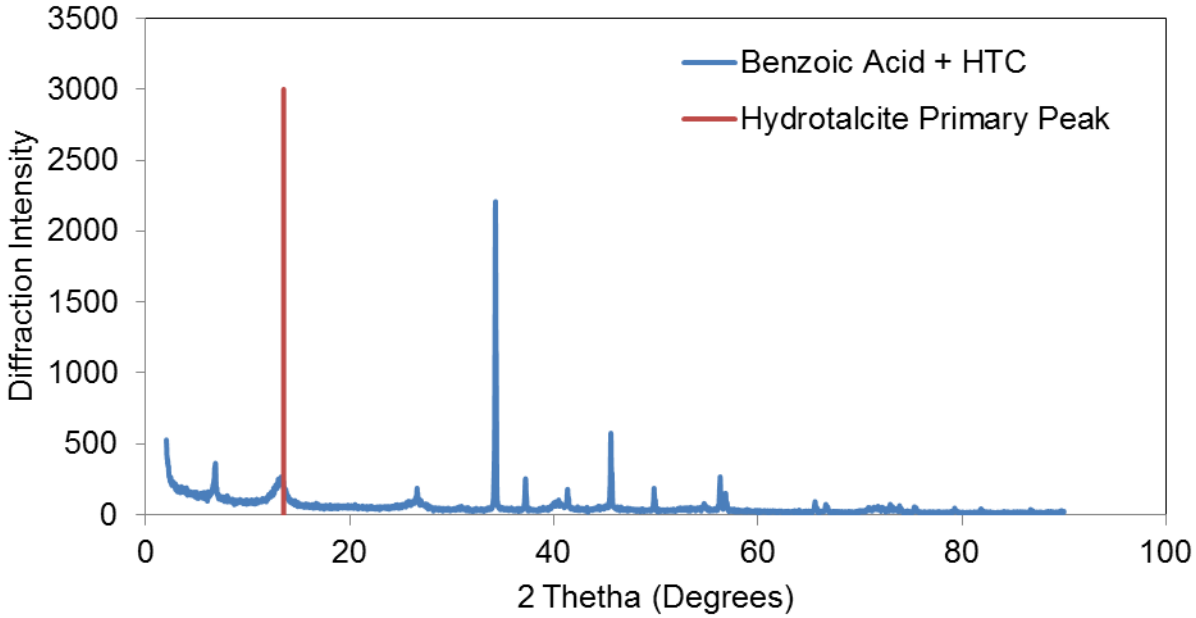

Figure A.2.1: XRD pattern for benzoic acid + HTC.

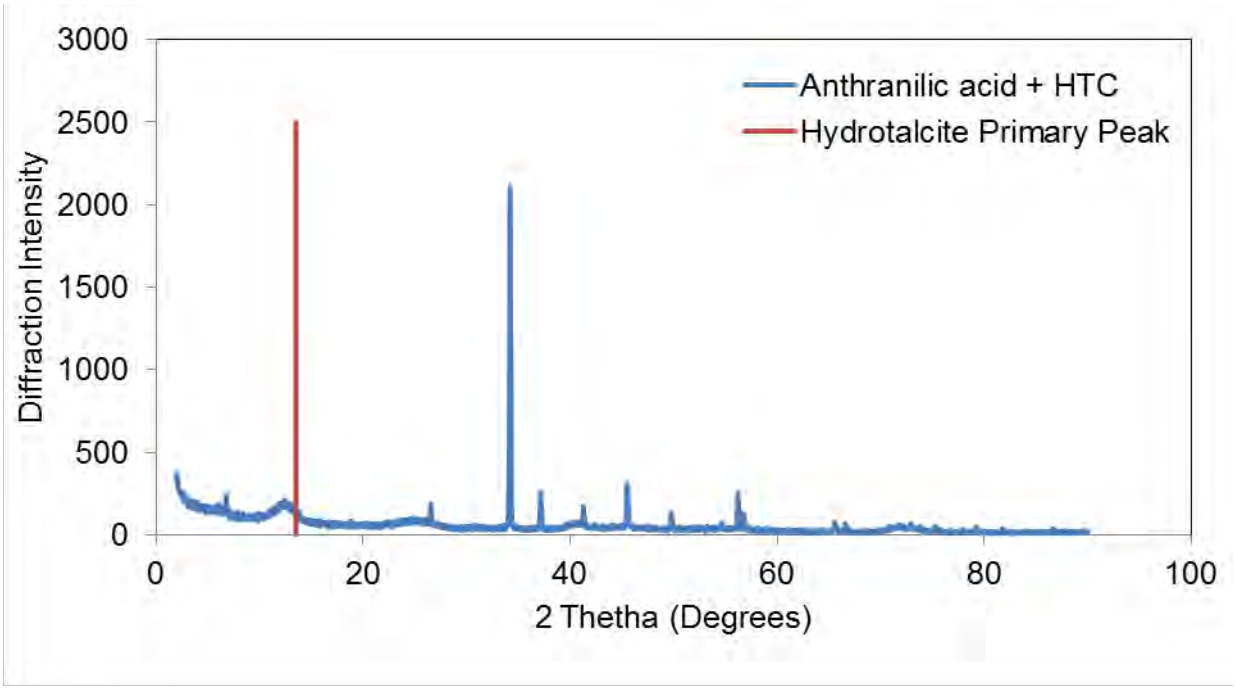

Figure A.2.2: XRD pattern for anthranilic acid + HTC.

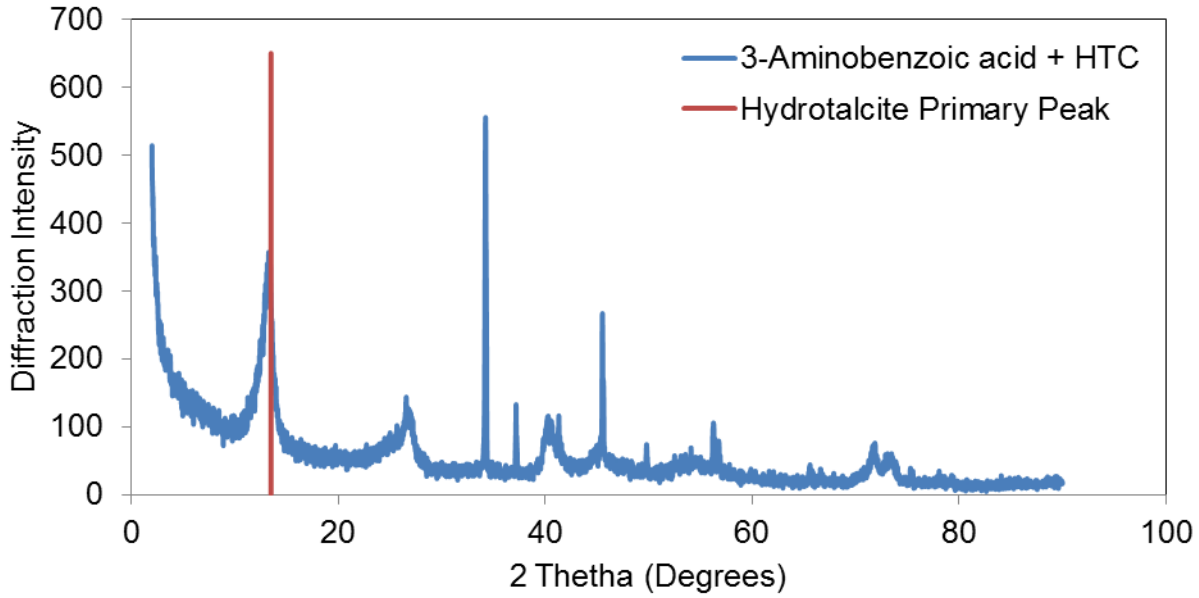

Figure A.2.3: XRD pattern for 3-aminobenzoic acid + HTC.

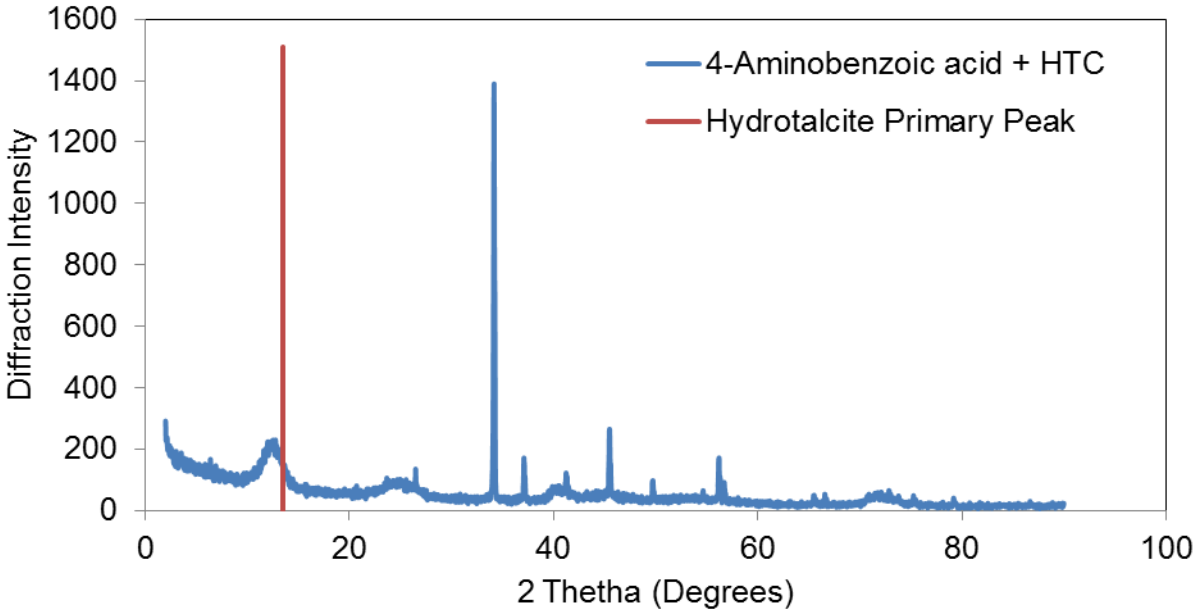

Figure A.2.4: XRD pattern for 4-aminobenzoic acid + HTC.

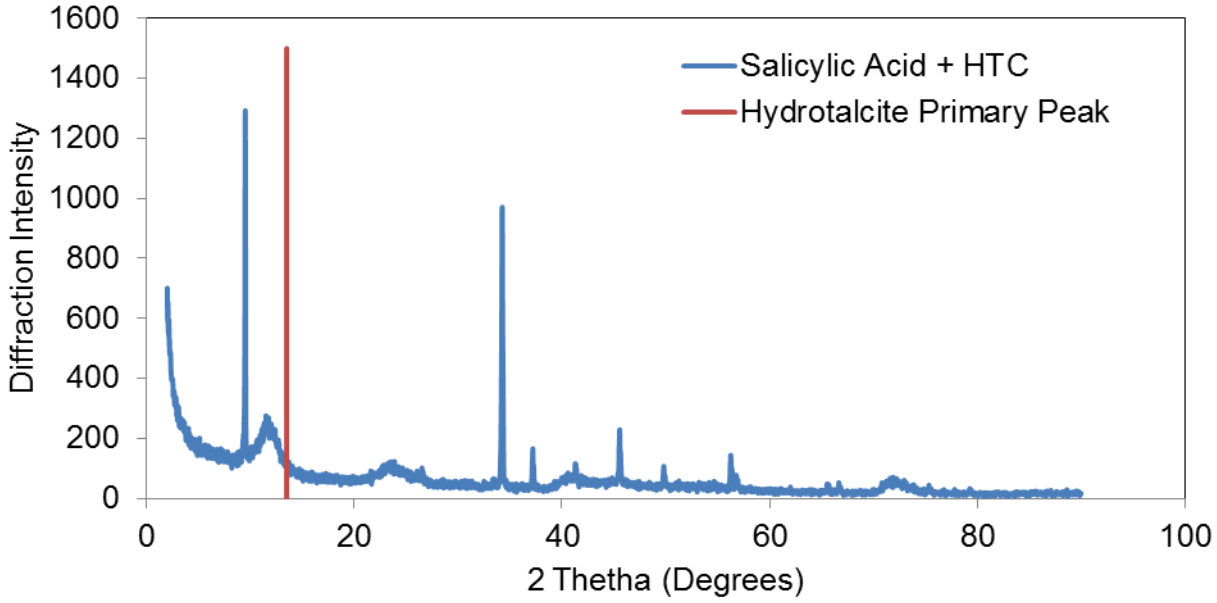

Figure A.2.5: XRD pattern for salicylic acid + HTC.

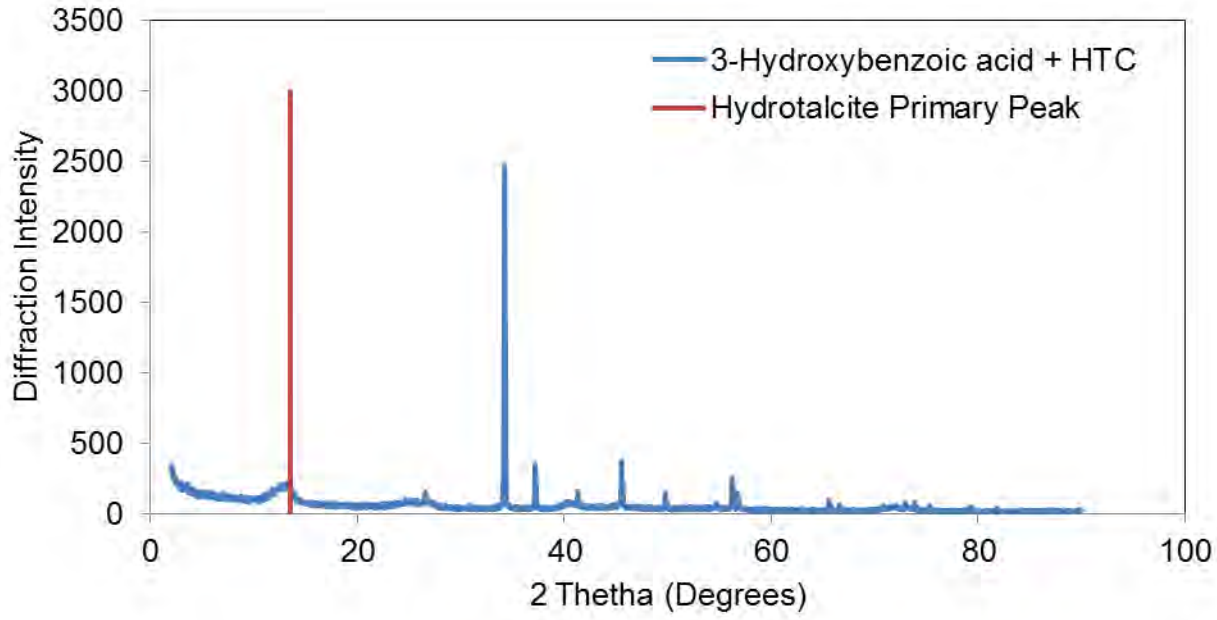

Figure A.2.6: XRD pattern for 3-hydroxybenzoic acid + HTC

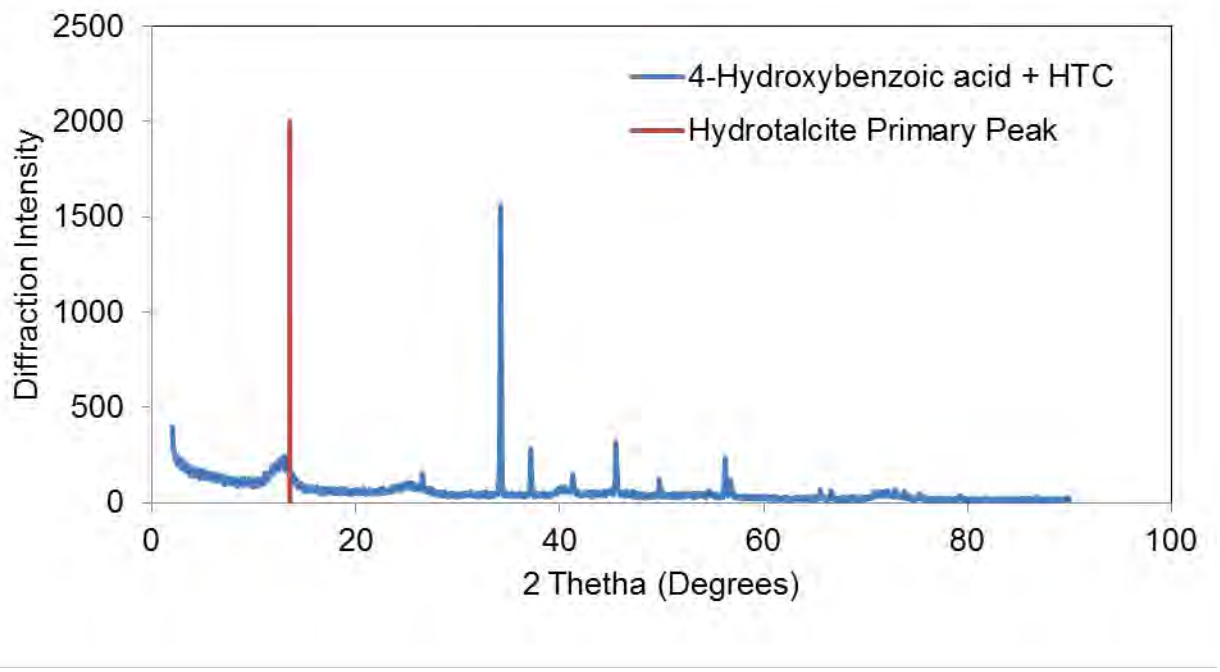

Figure A.2.7: XRD pattern for 4-hydroxybenzoic acid + HTC

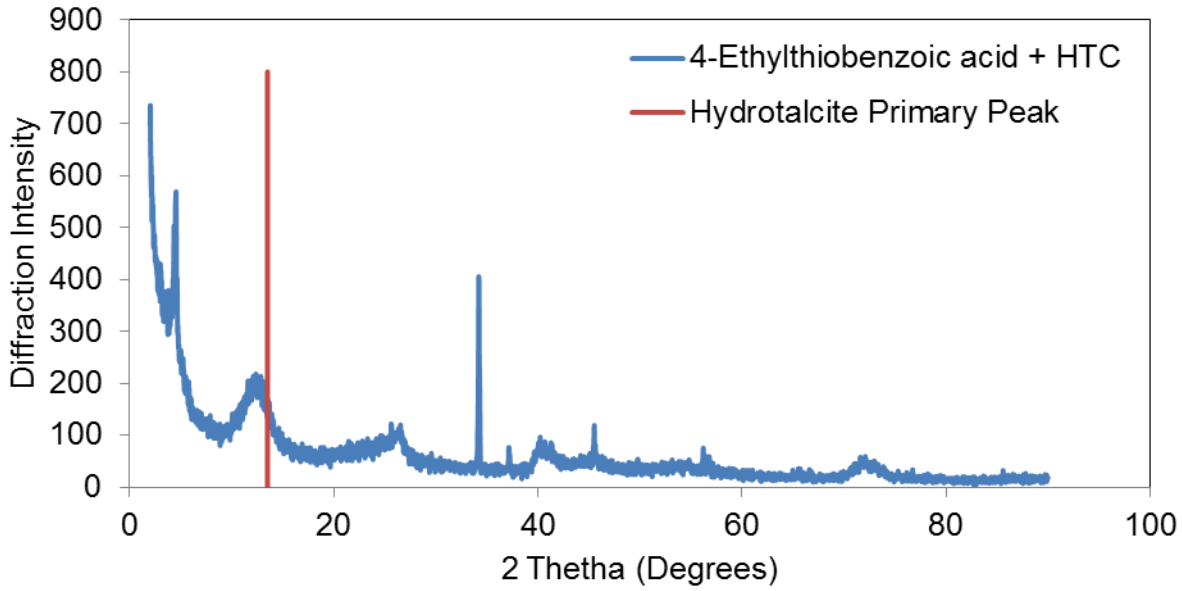

Figure A.2.8: XRD pattern for 4-ethylthiobenzoic acid + HTC

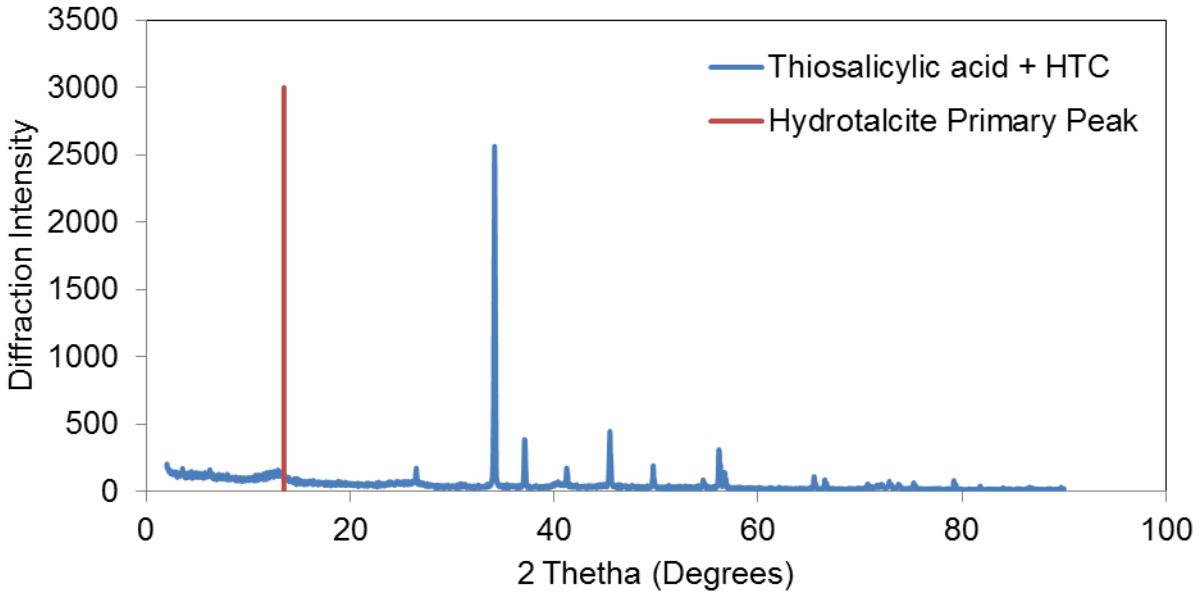

Figure A.2.9: XRD pattern for thiosalicylic acid + HTC

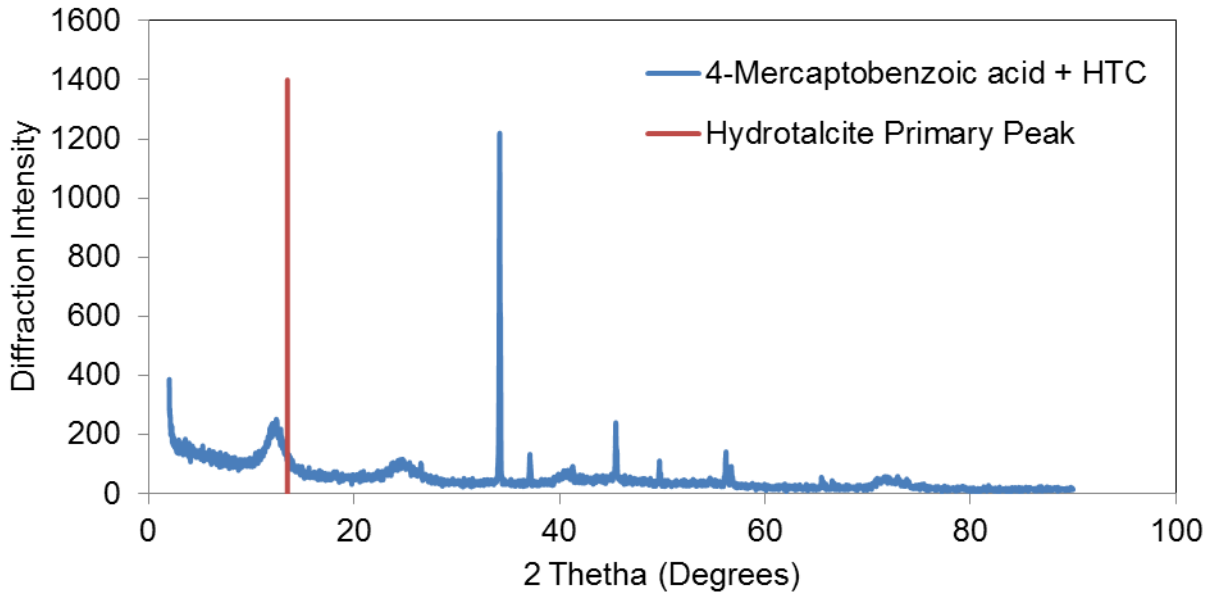

Figure A.2.10: XRD pattern for 4-mercaptobenzoic acid + HTC

Appendix B – FTIR results

B.1 Reconstruction method synthesis

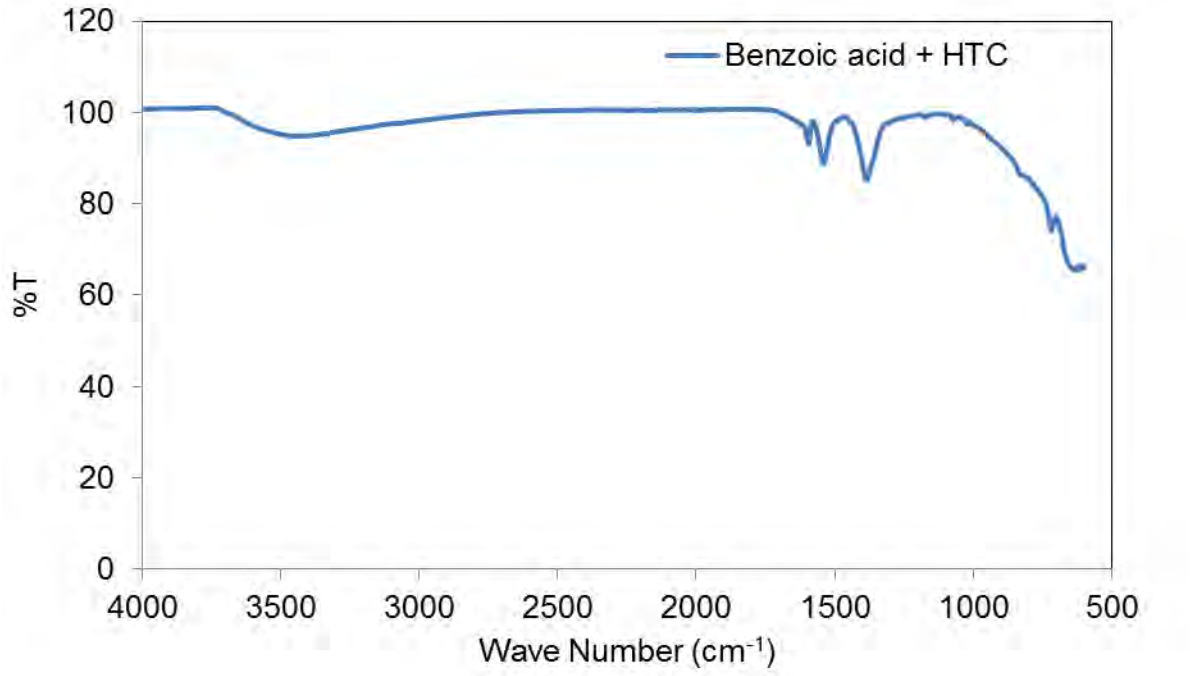

Figure B.1.1: FTIR spectra for benzoic acid + HTC.

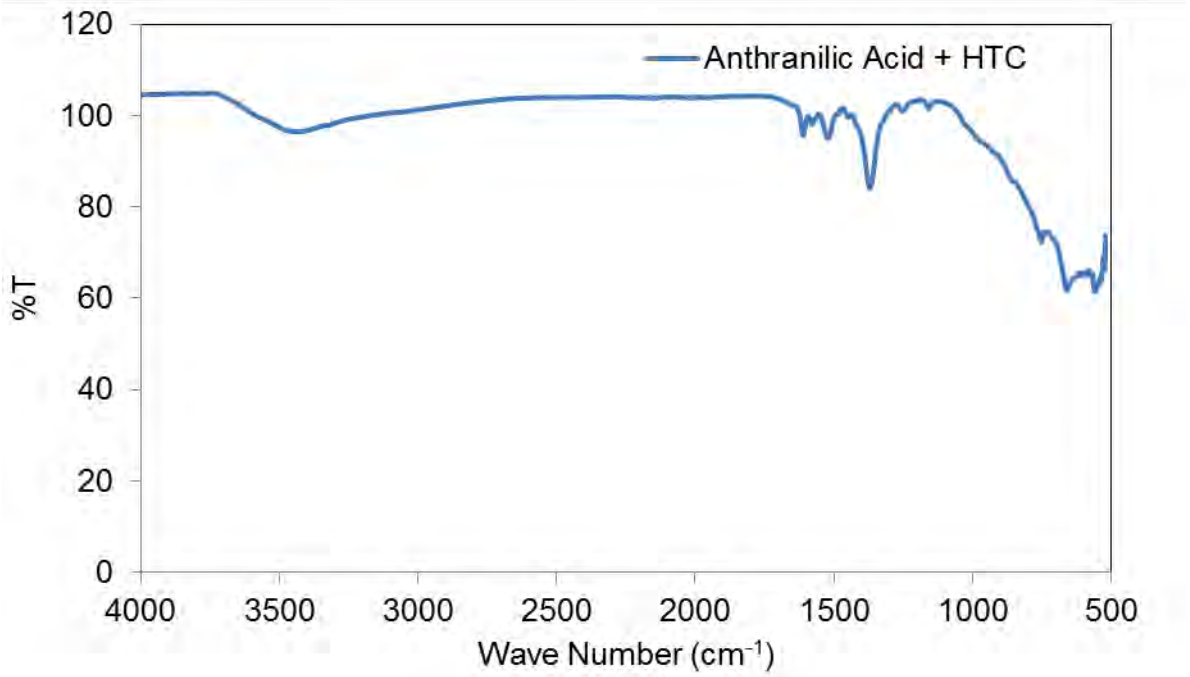

Figure B.1.2: FTIR spectra for anthranilic acid + HTC.

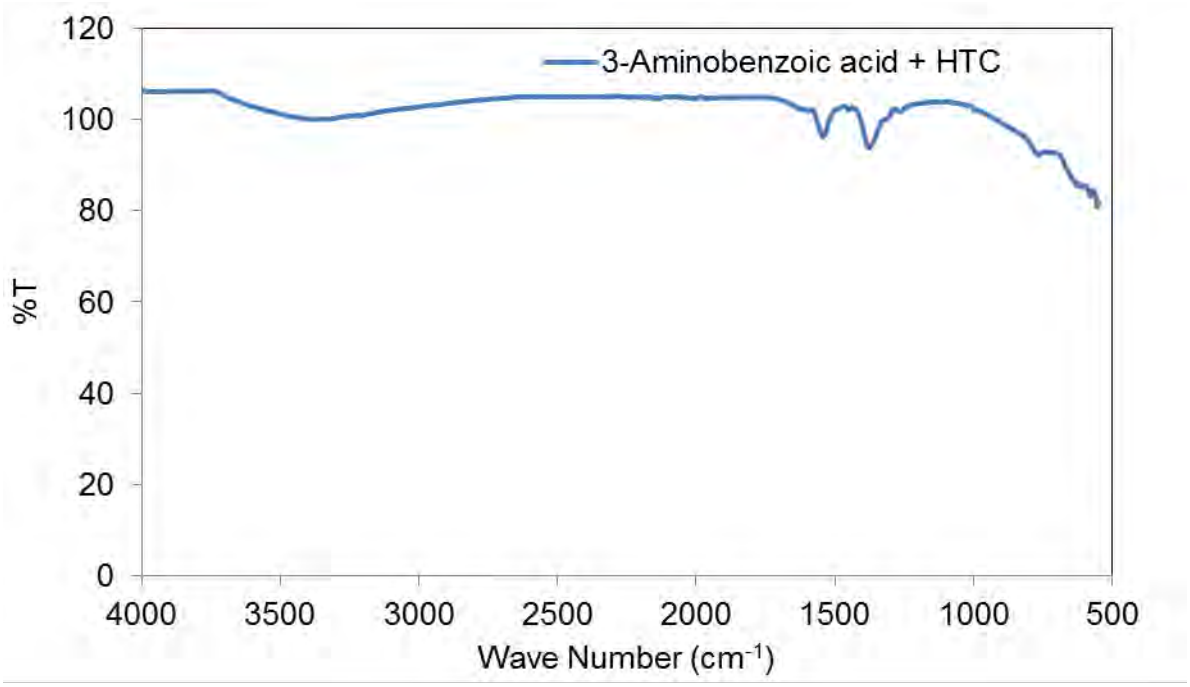

Figure B.1.3: FTIR spectra for 3-aminobenzoic acid + HTC.

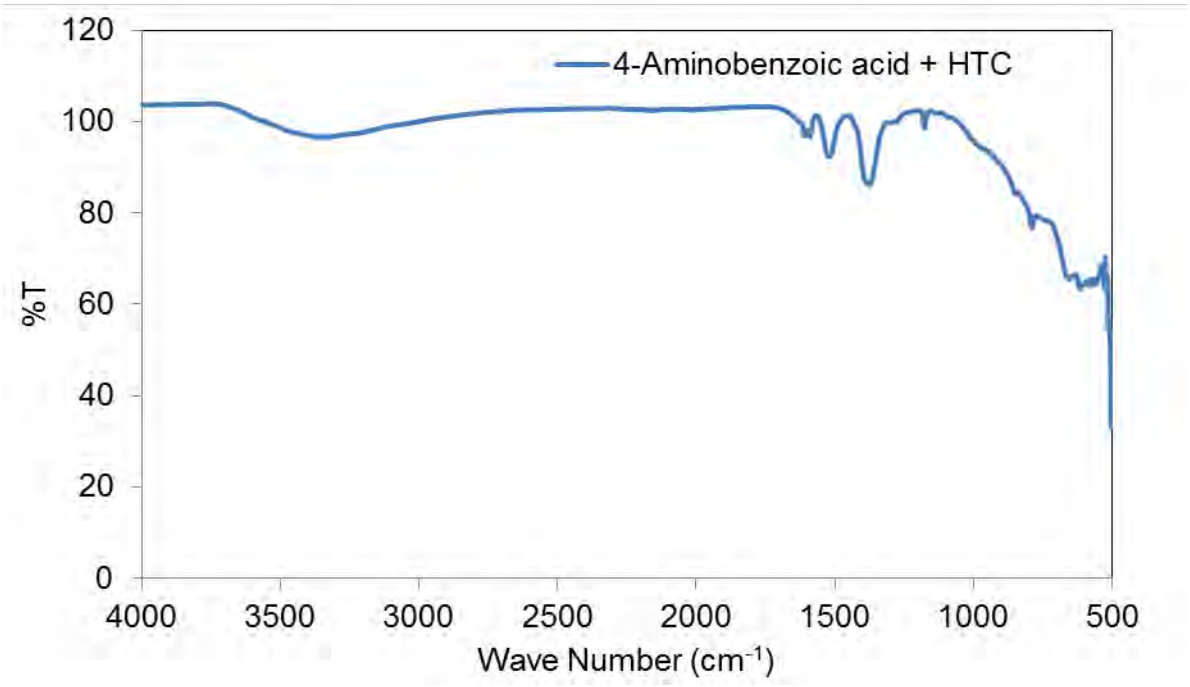

Figure B.1.4: FTIR spectra for 4-aminobenzoic acid + HTC.

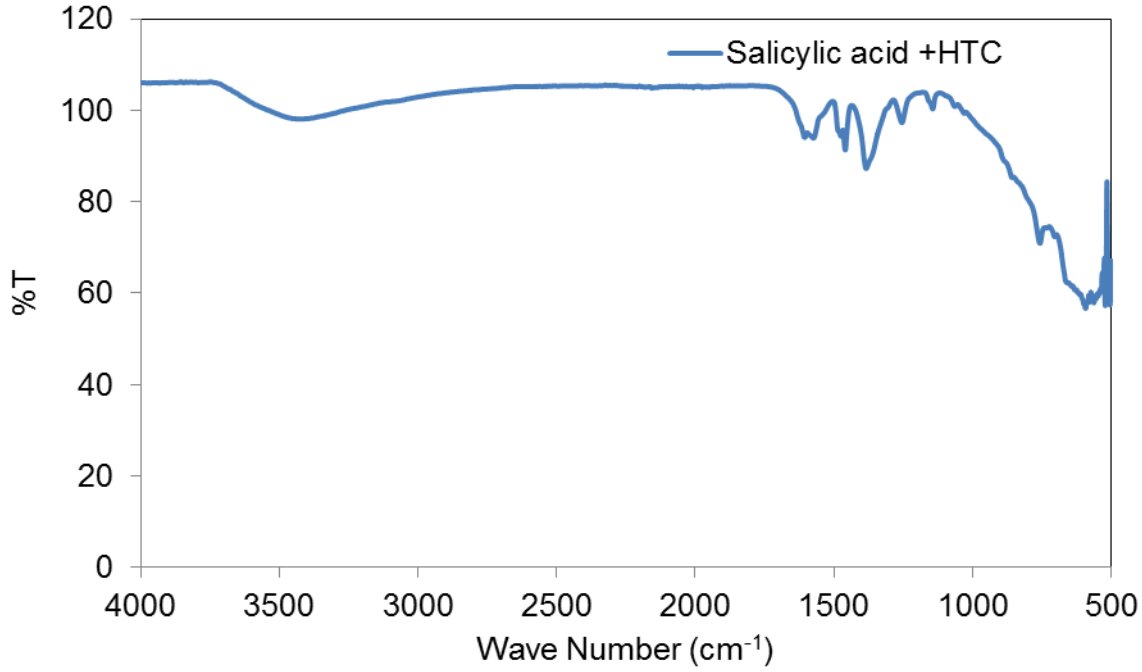

Figure B.1.5: FTIR spectra for salicylic acid + HTC.

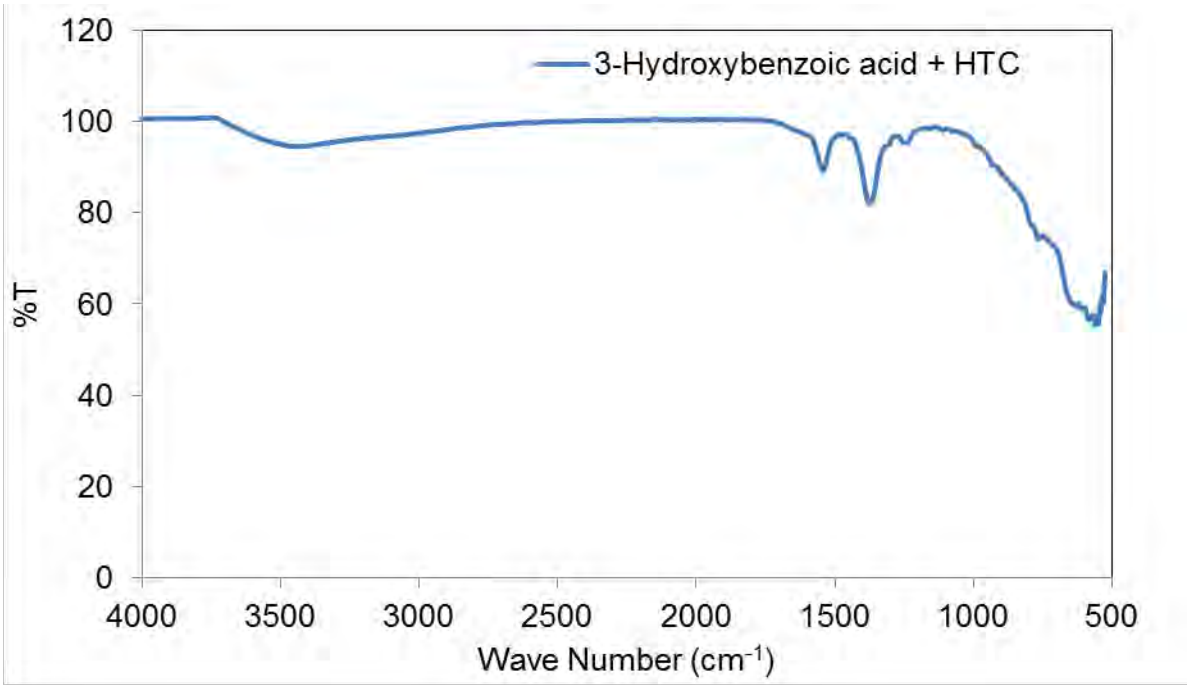

Figure B.1.6: FTIR spectra for 3-hydroxybenzoic acid + HTC.

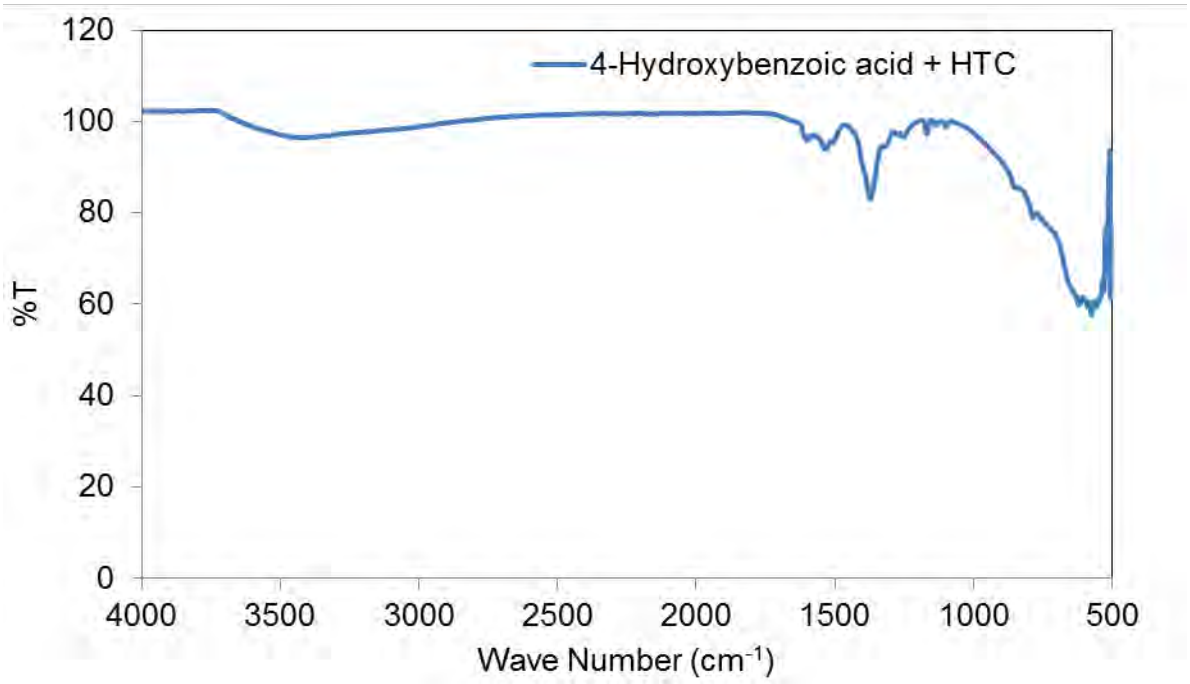

Figure B.1.7: FTIR spectra for 4-hydroxybenzoic acid + HTC.

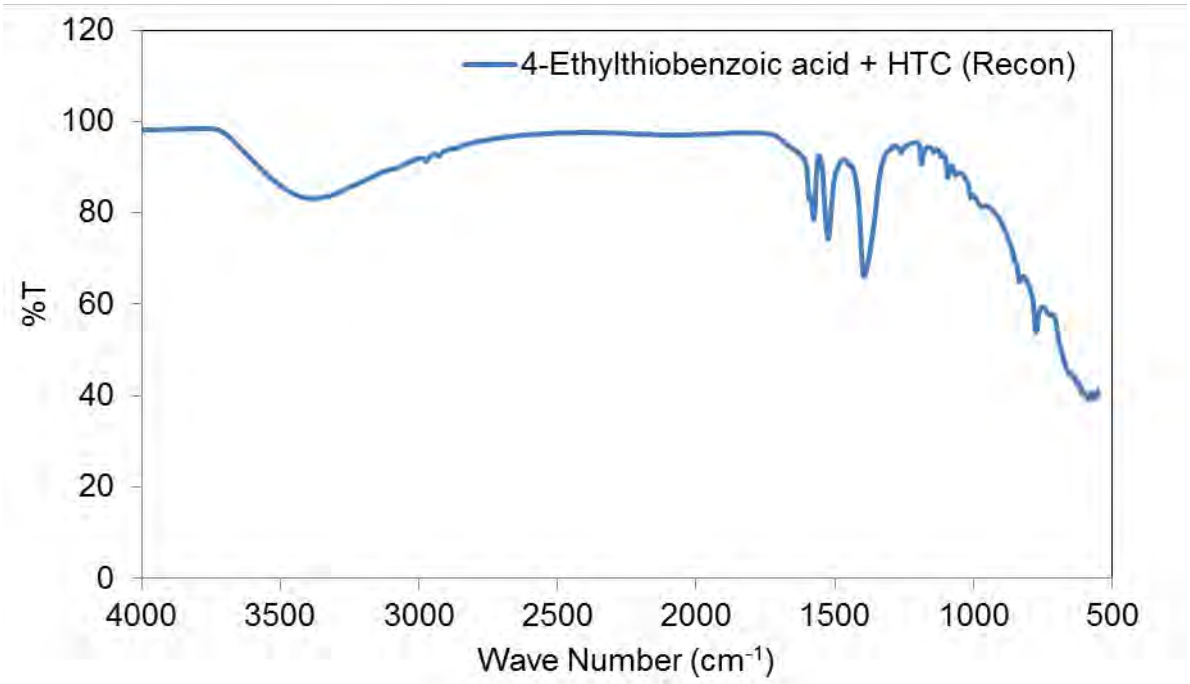

Figure B.1.8: FTIR spectra for 4-ethylthiobenzoic acid + HTC.

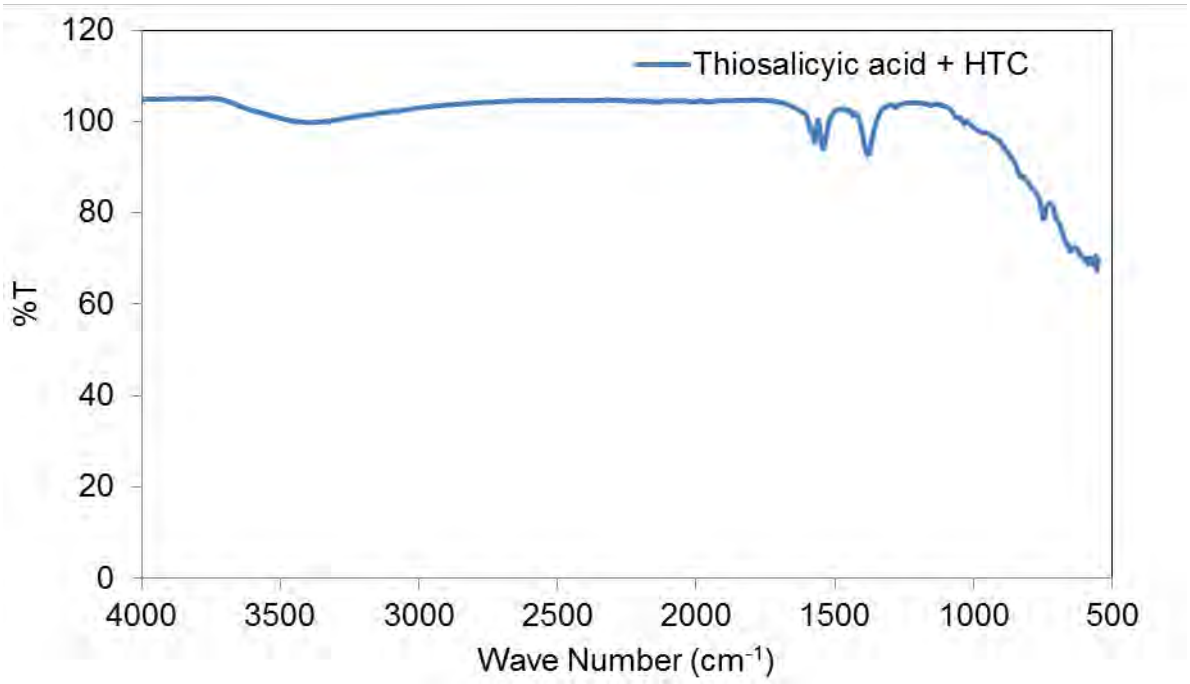

Figure B.1.9: FTIR spectra for thiosalicylic acid + HTC.

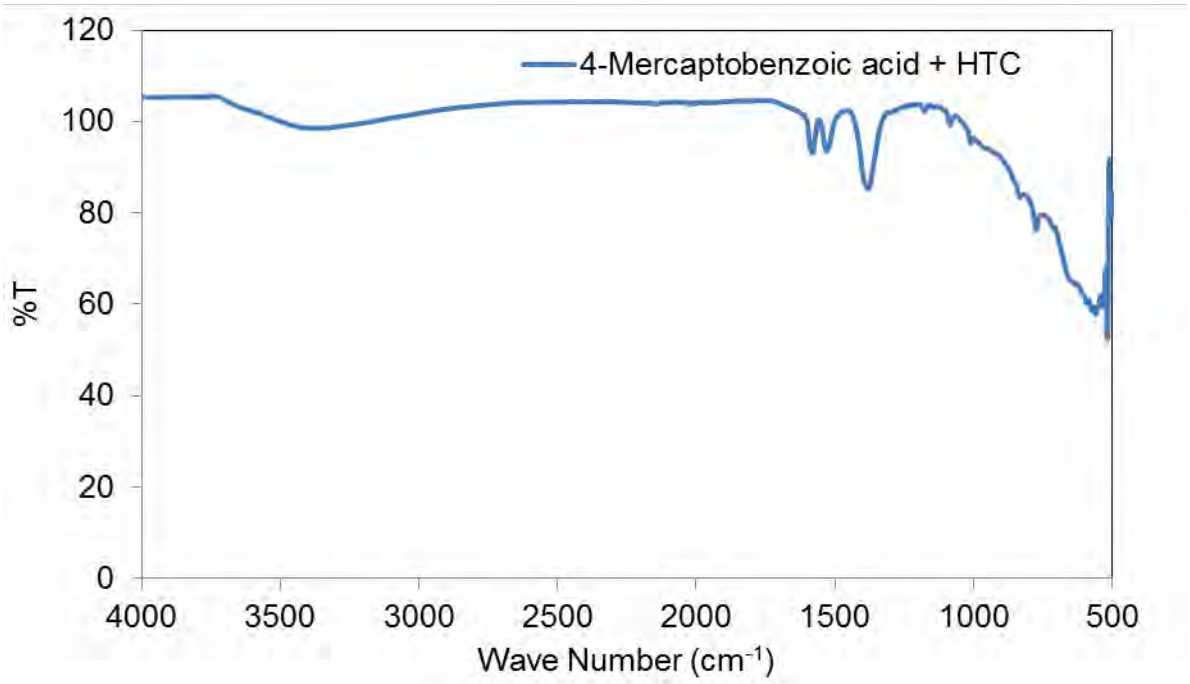

Figure B.1.10: FTIR spectra for 4-mercaptobenzoic acid + HTC.

B.2 - Co-precipitation method synthesis

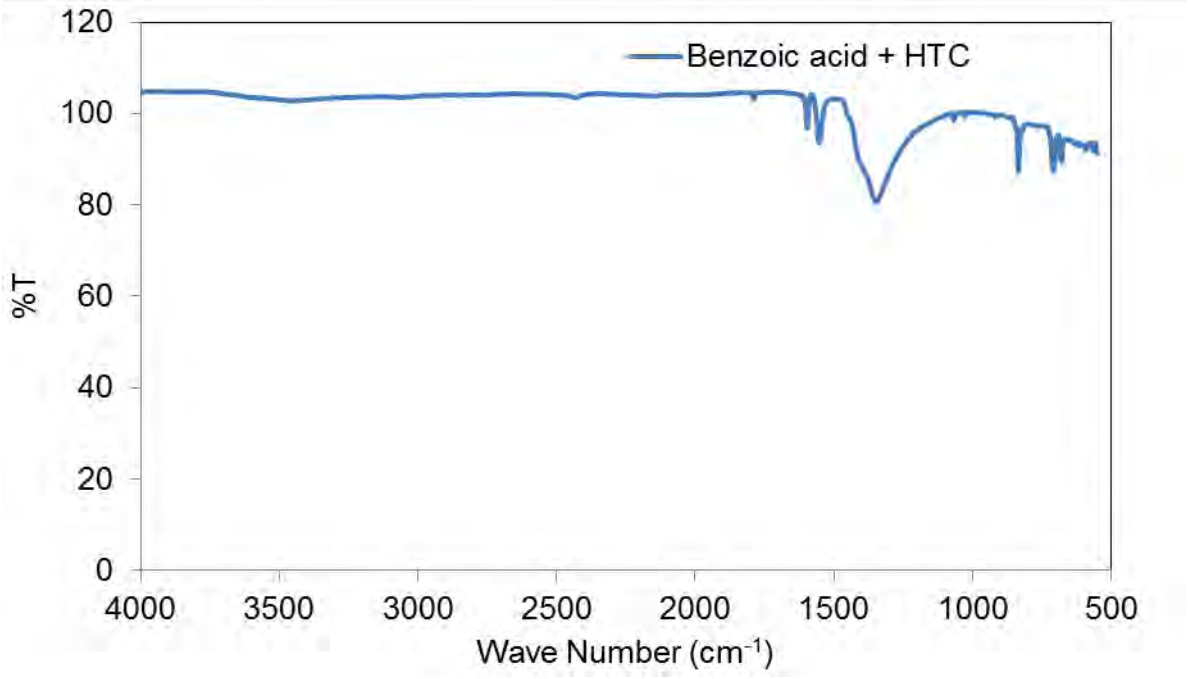

Figure B.2.1: FTIR spectra for benzoic acid + HTC.

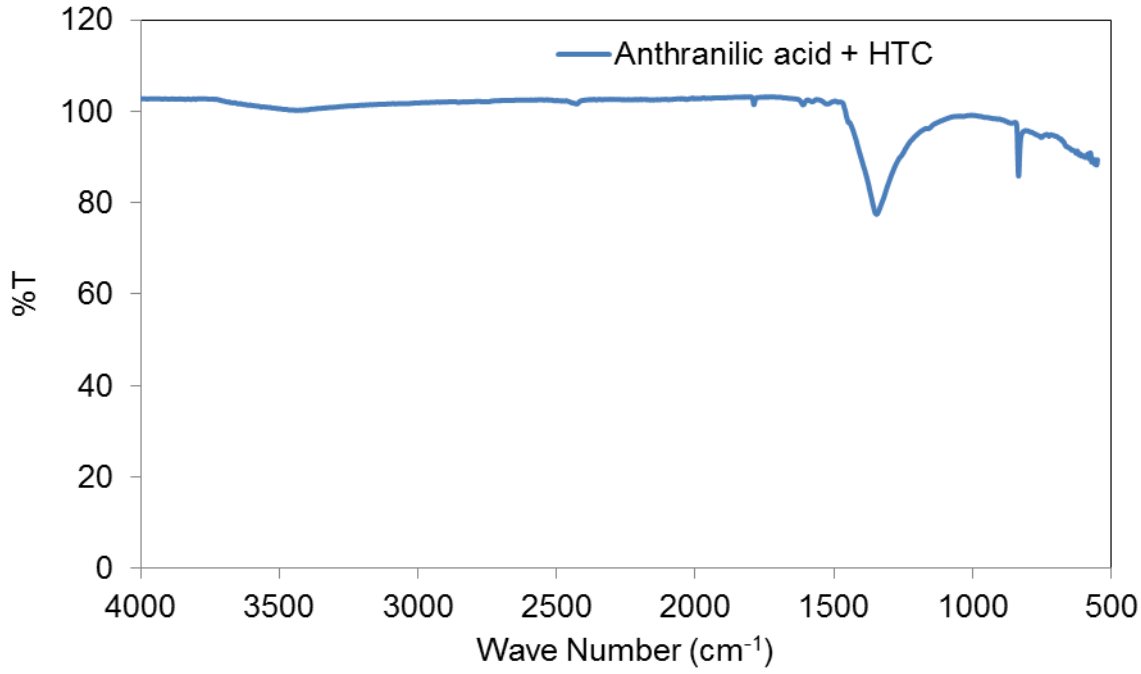

Figure B.2.2: FTIR spectra for anthranilic acid + HTC.

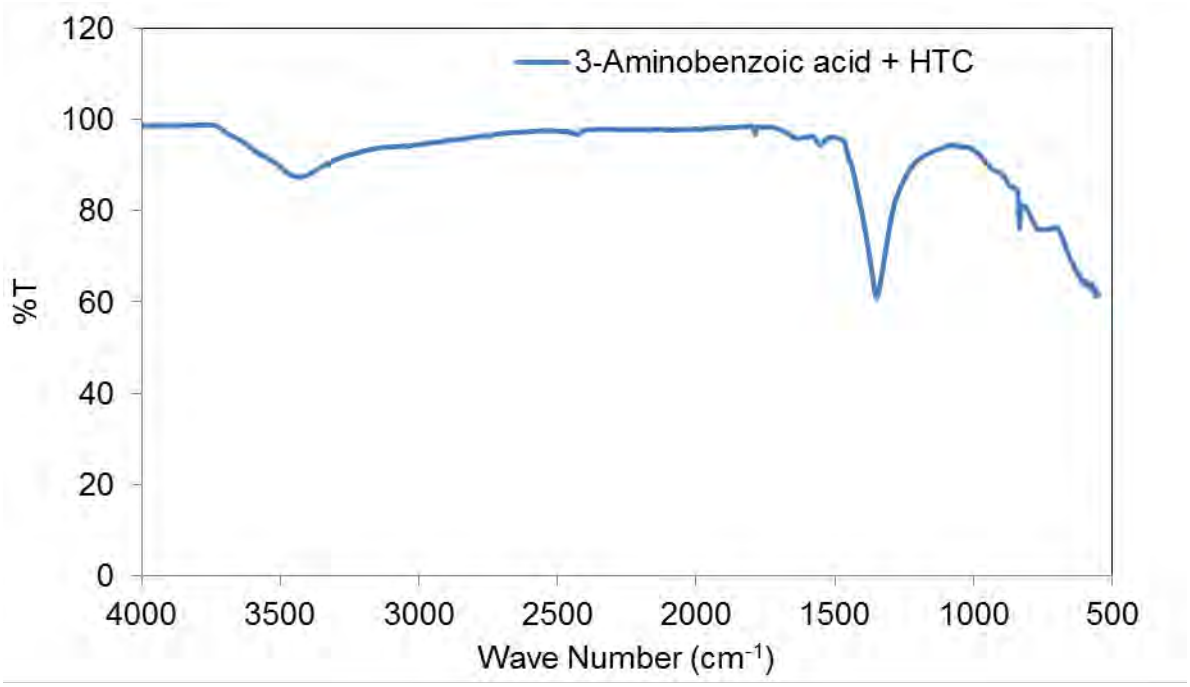

Figure B.2.3: FTIR spectra for 3-aminobenzoic acid + HTC.

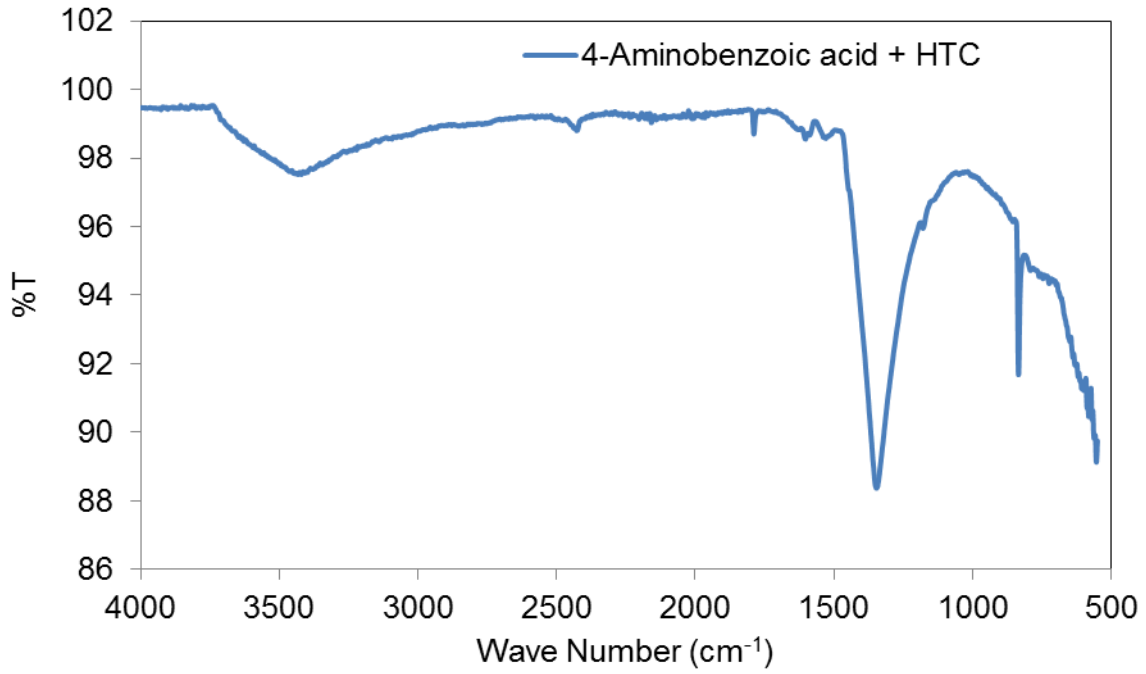

Figure B.2.4: FTIR spectra for 4-aminobenzoic acid + HTC.

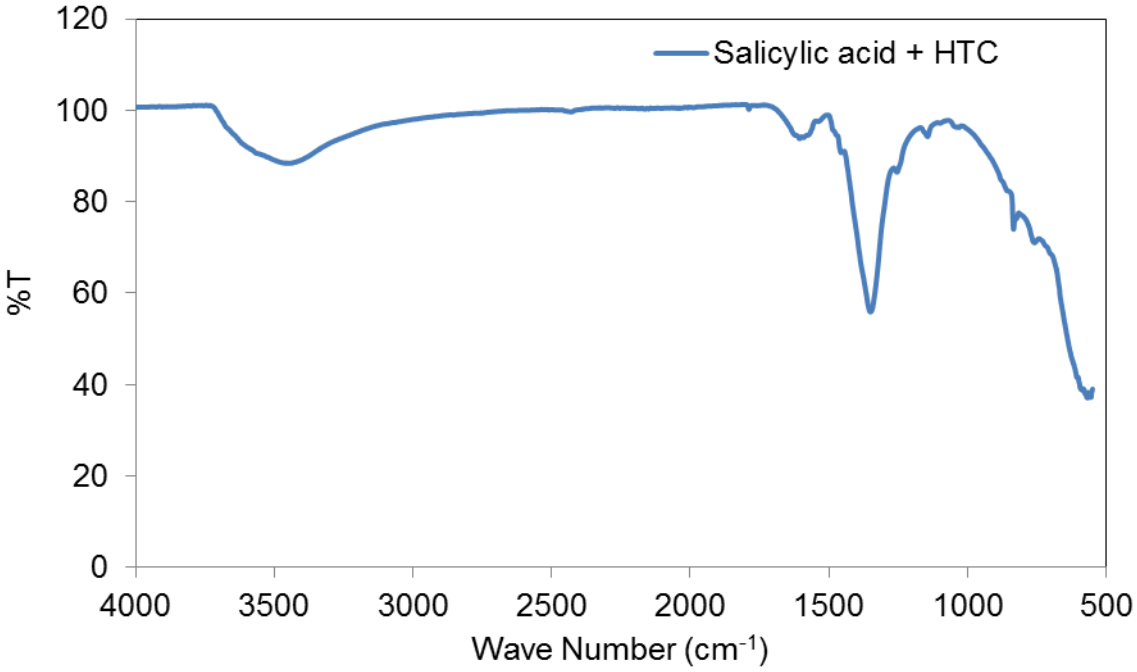

Figure B.2.5: FTIR spectra for salicylic acid + HTC.

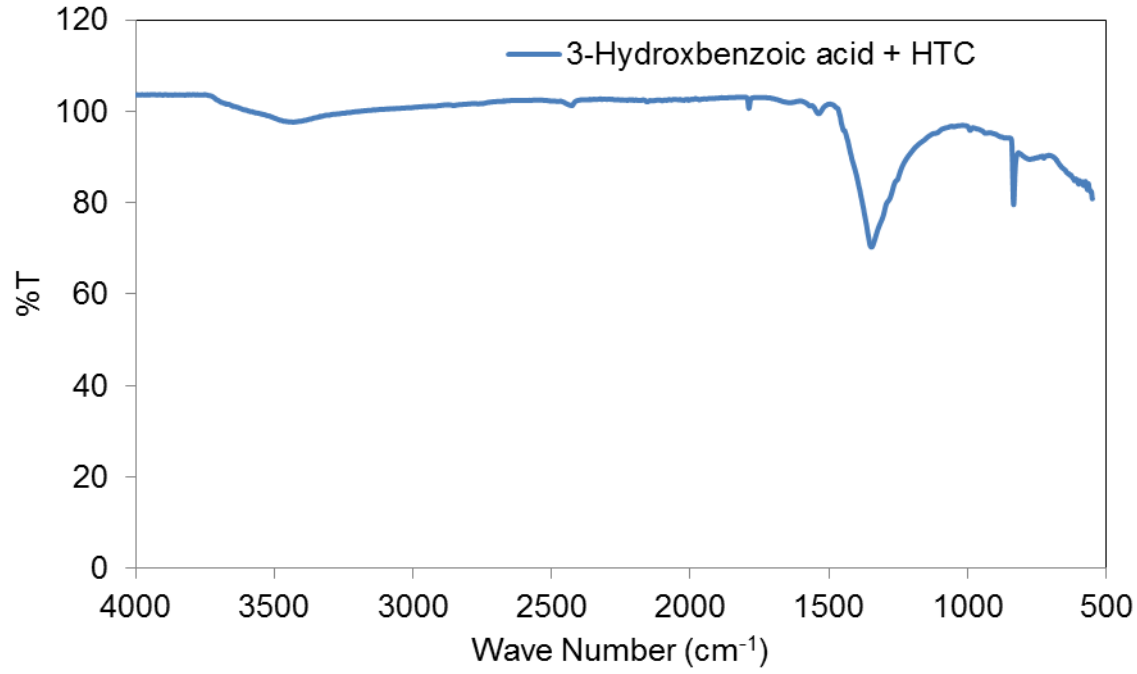

Figure B.2.6: FTIR spectra for 3-hydroxybenzoic acid + HTC.

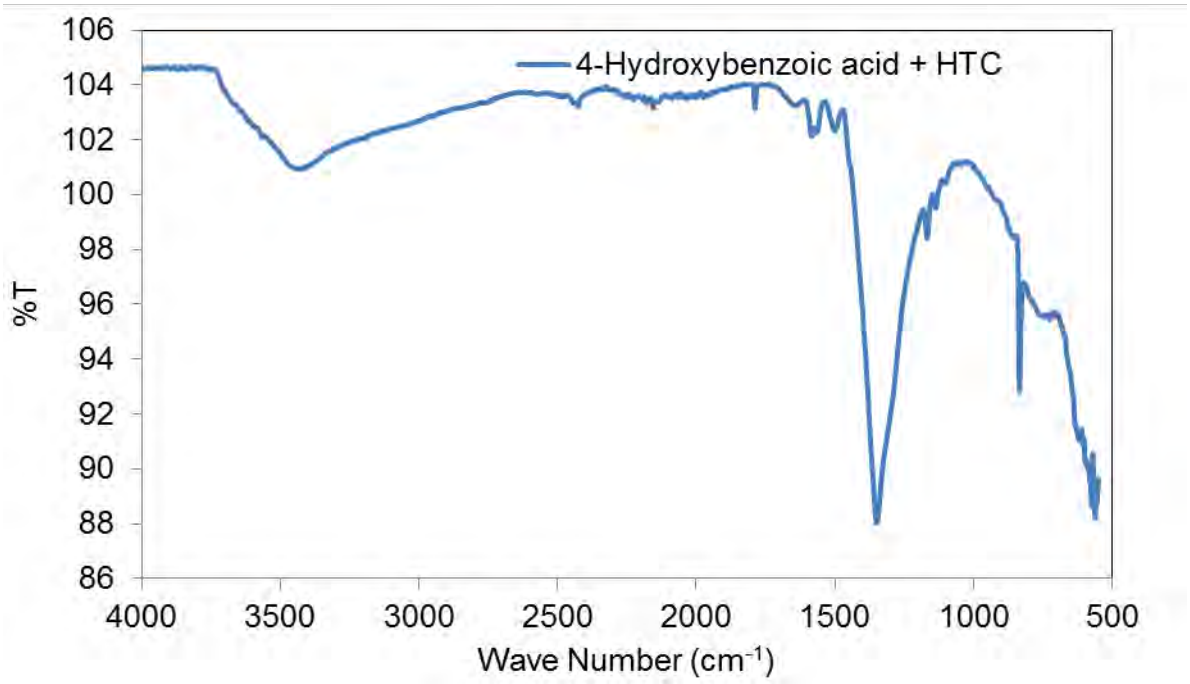

Figure B.2.7: FTIR spectra for 4-hydroxybenzoic acid + HTC.

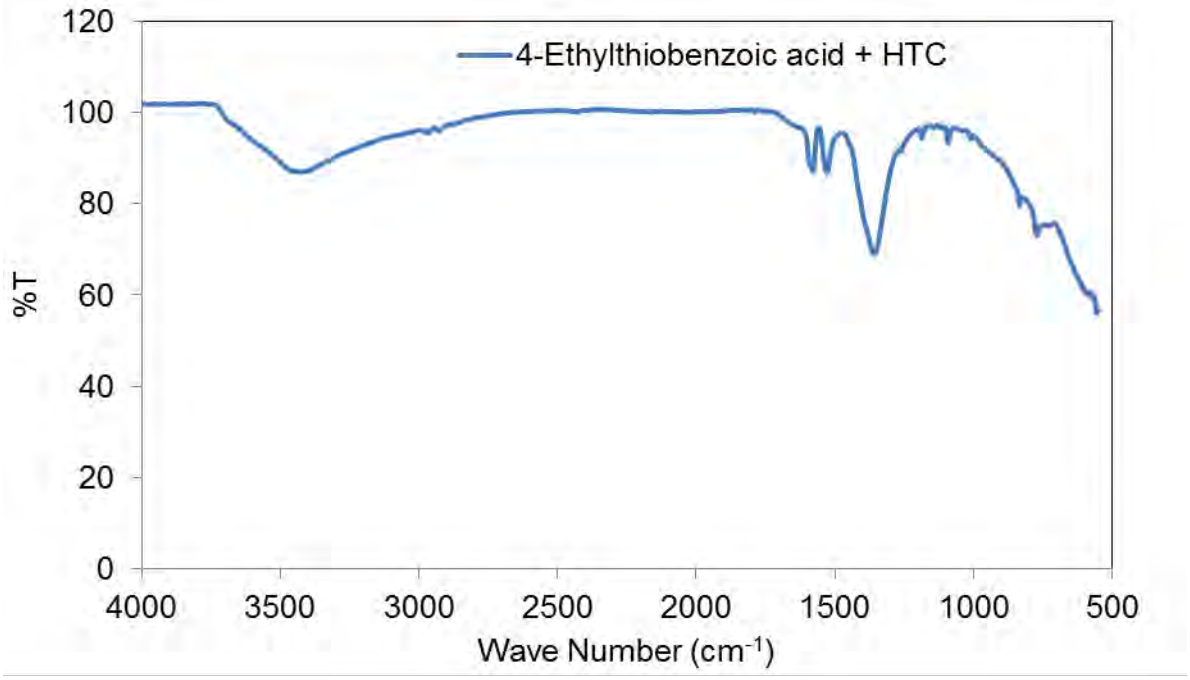

Figure B.2.8: FTIR spectra for 4-ethylthiobenzoic acid + HTC.

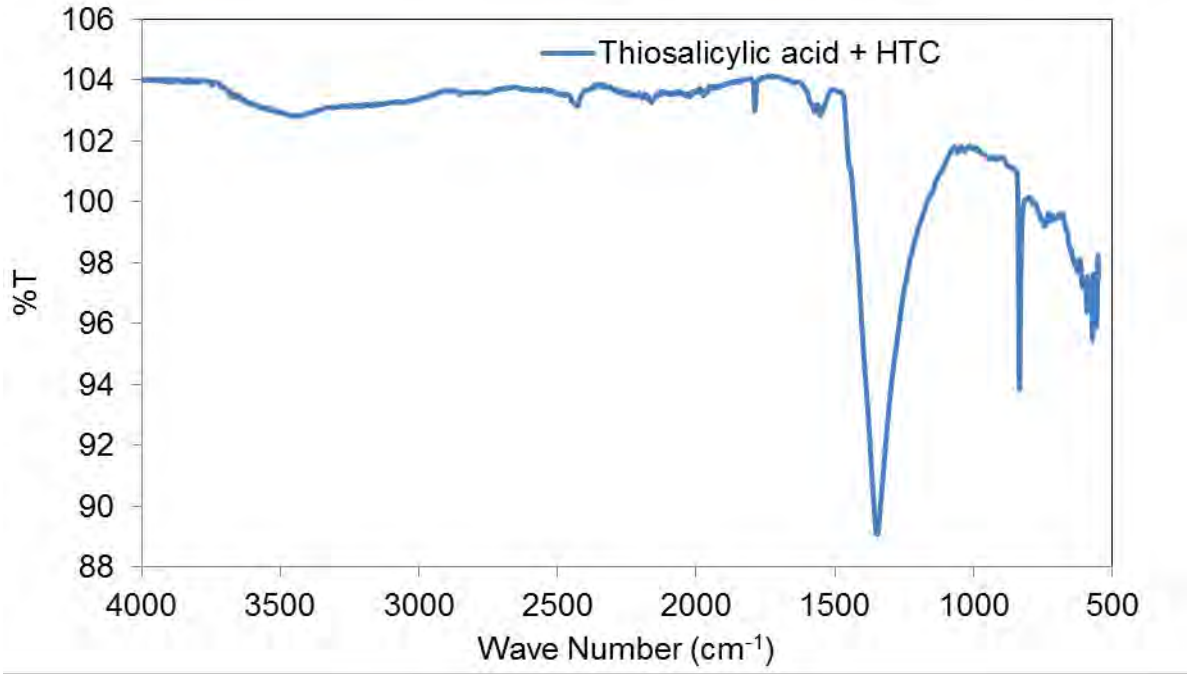

Figure B.2.9: FTIR spectra for thiosalicylic acid + HTC.

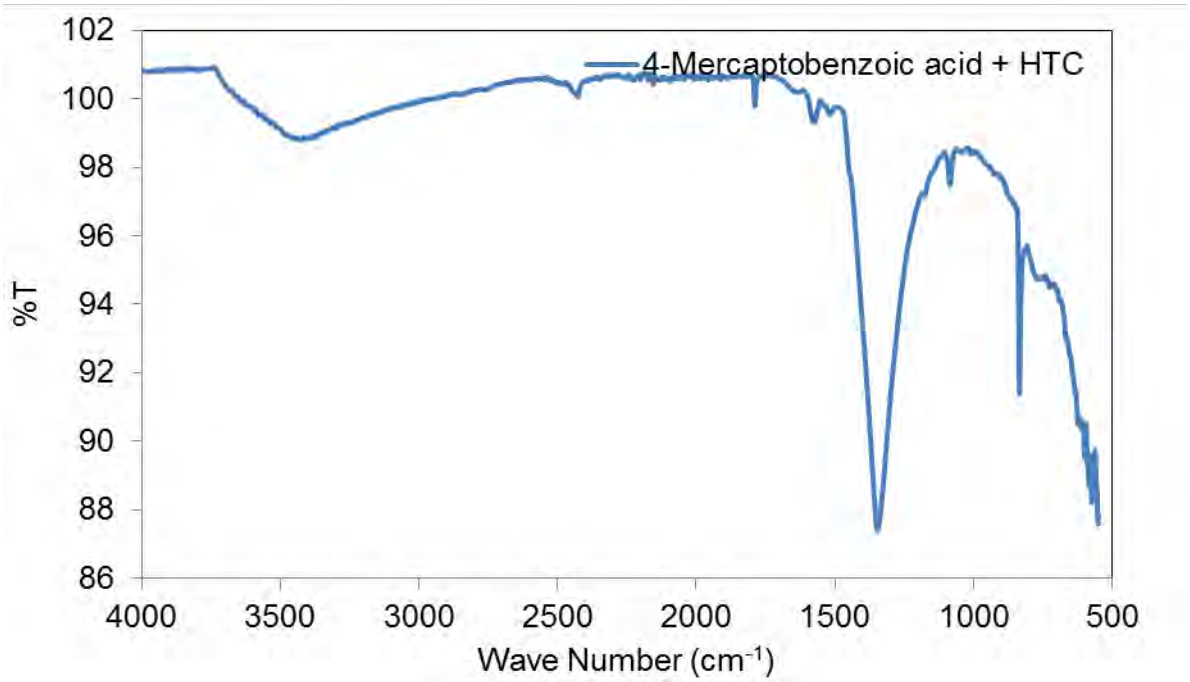

Figure B.2.10: FTIR spectra for 4-mercaptobenzoic acid + HTC.

Appendix C: Particle size distributions

C.1 - Reconstruction method synthesis

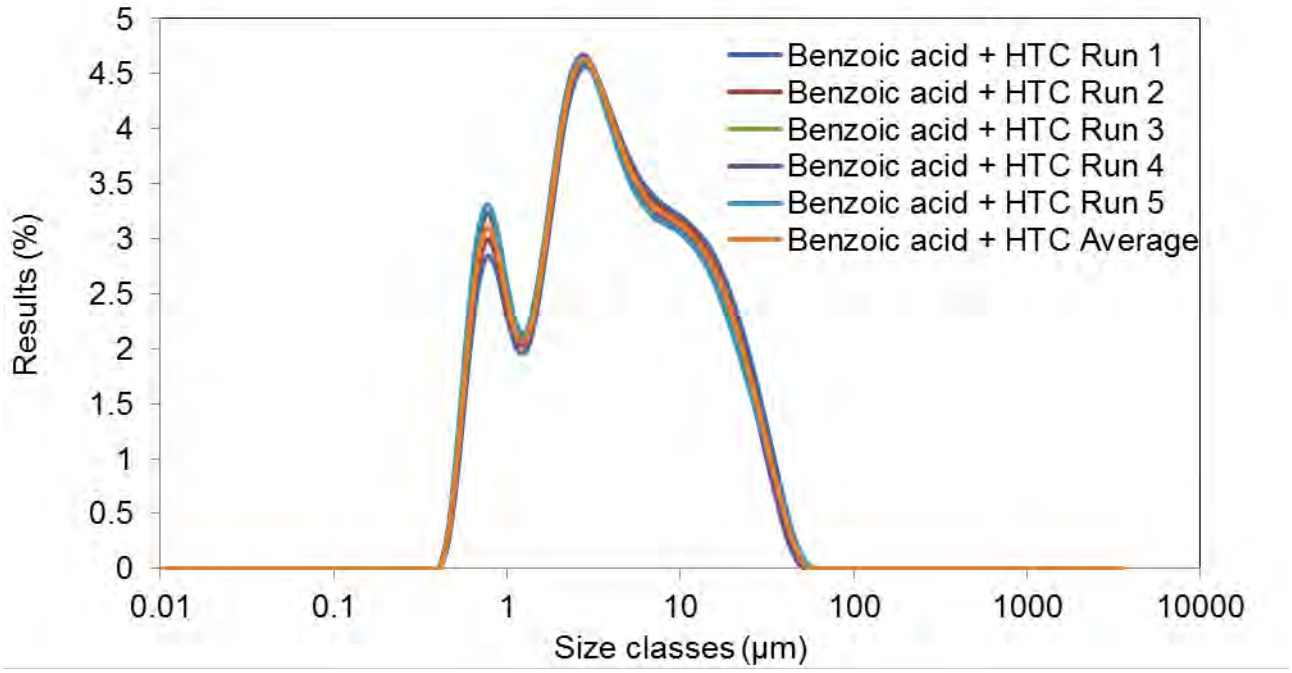

Figure C.1.1: Particle size distribution for benzoic acid + HTC.

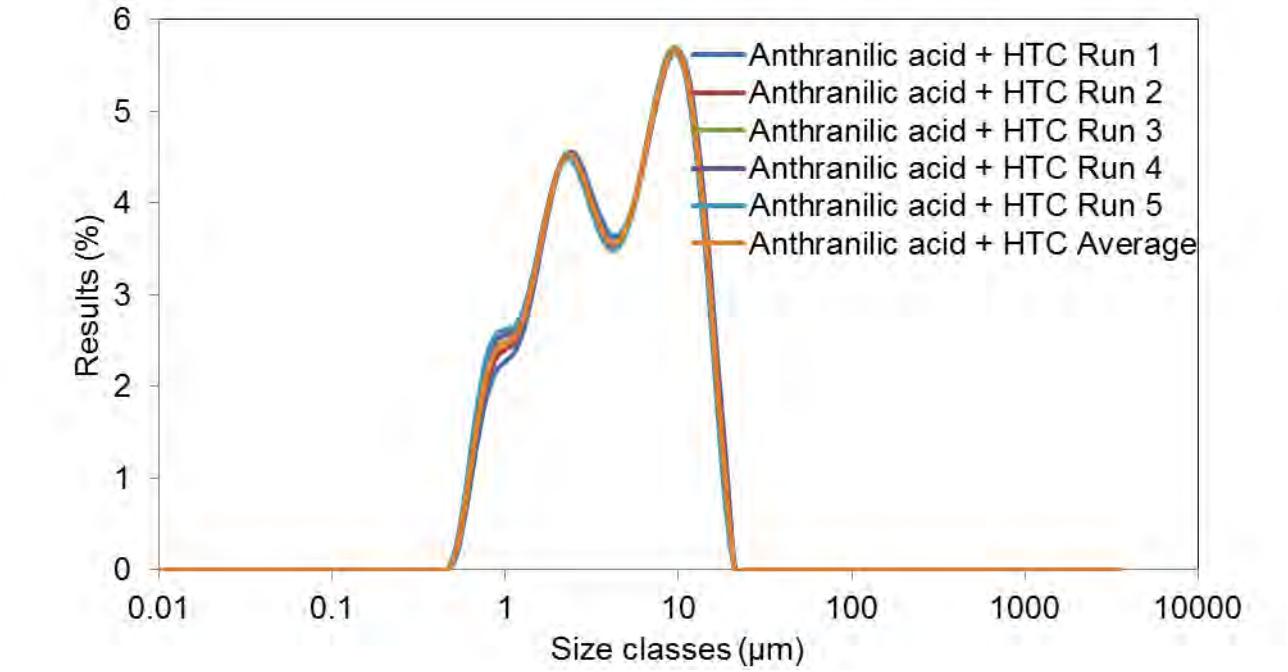

Figure C.1.2: Particle size distribution for anthranilic acid + HTC.

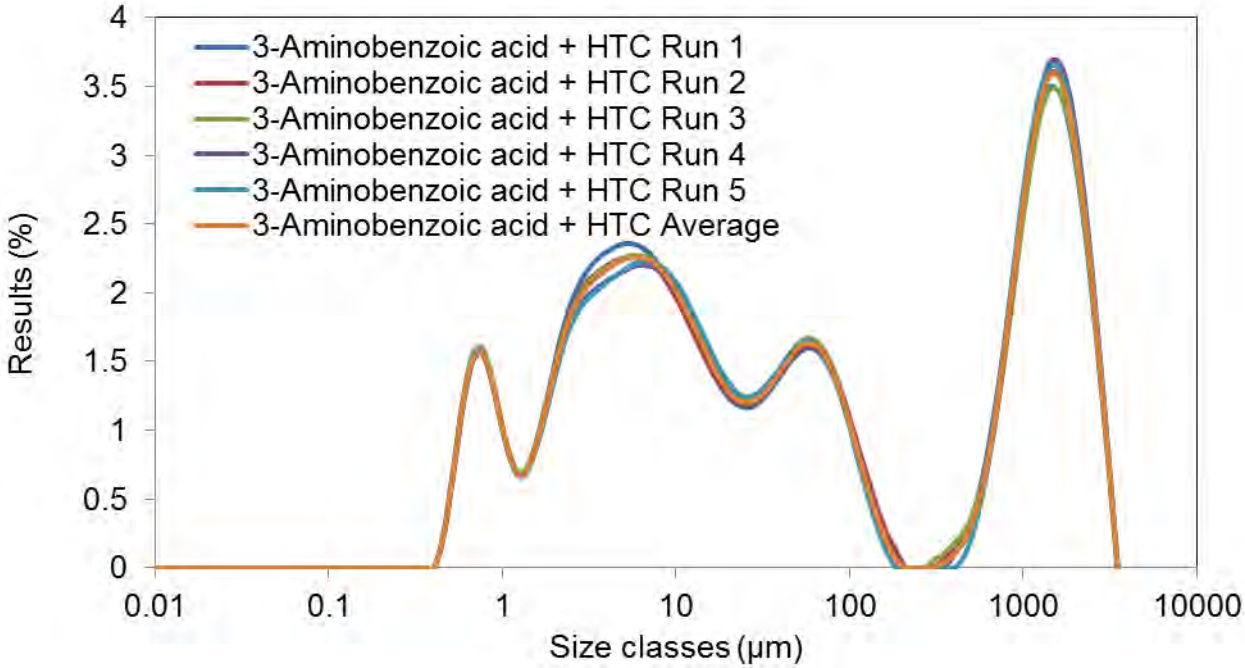

Figure C.1.3: Particle size distribution for 3-aminobenzoic acid + HTC.

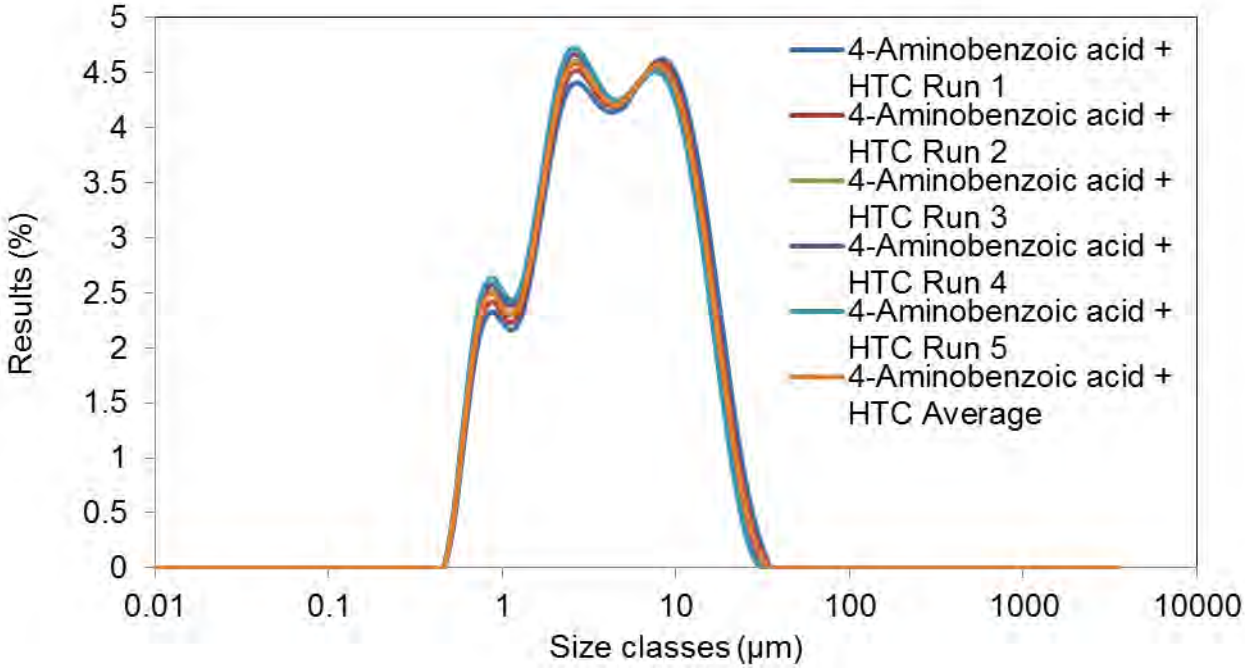

Figure C.1.4: Particle size distribution for 4-aminobenzoic acid + HTC.

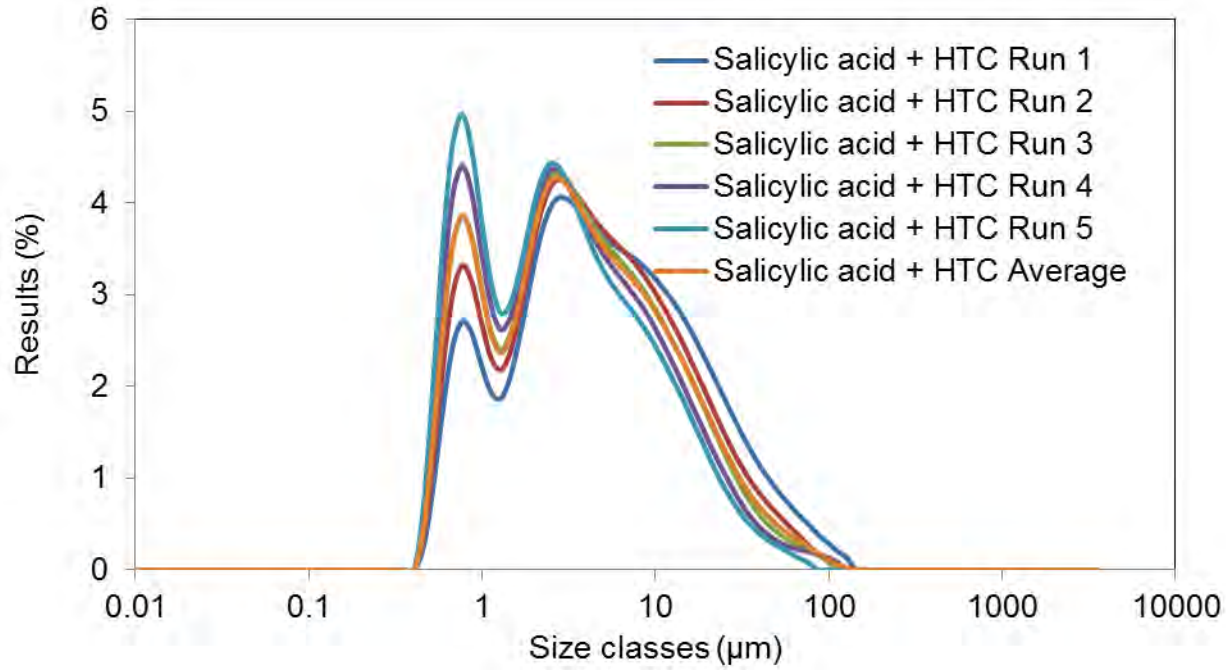

Figure C.1.5: Particle size distribution for salicylic acid + HTC.

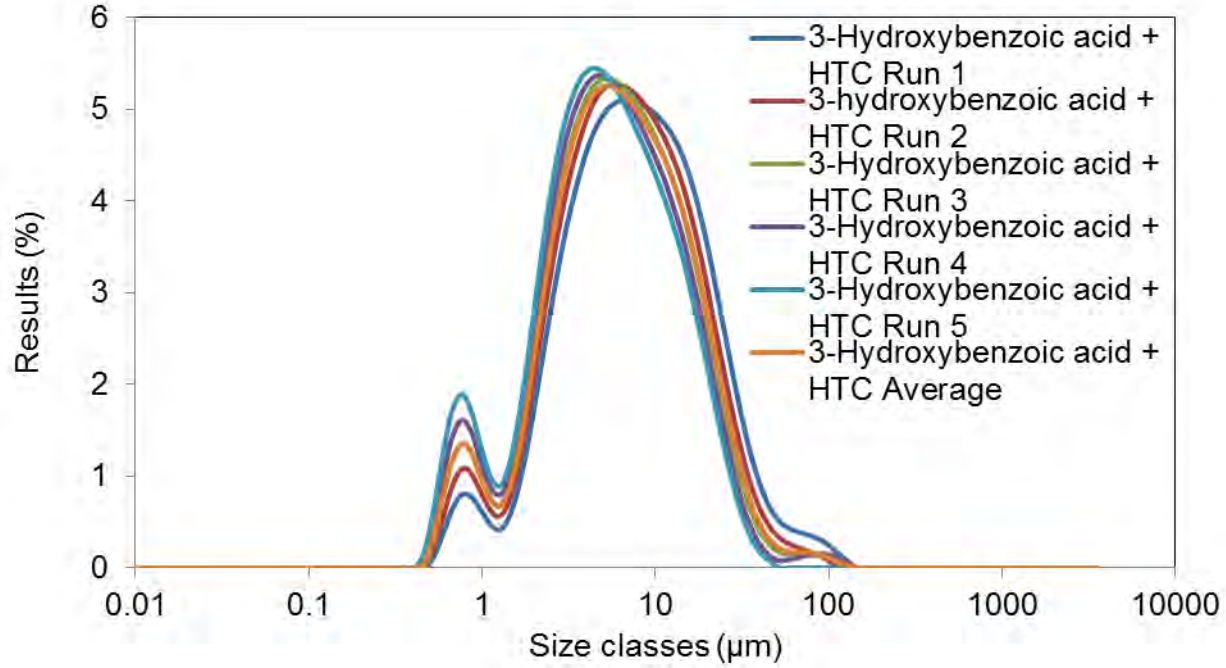

Figure C.1.6: Particle size distribution for 3-hydroxybenzoic acid + HTC.

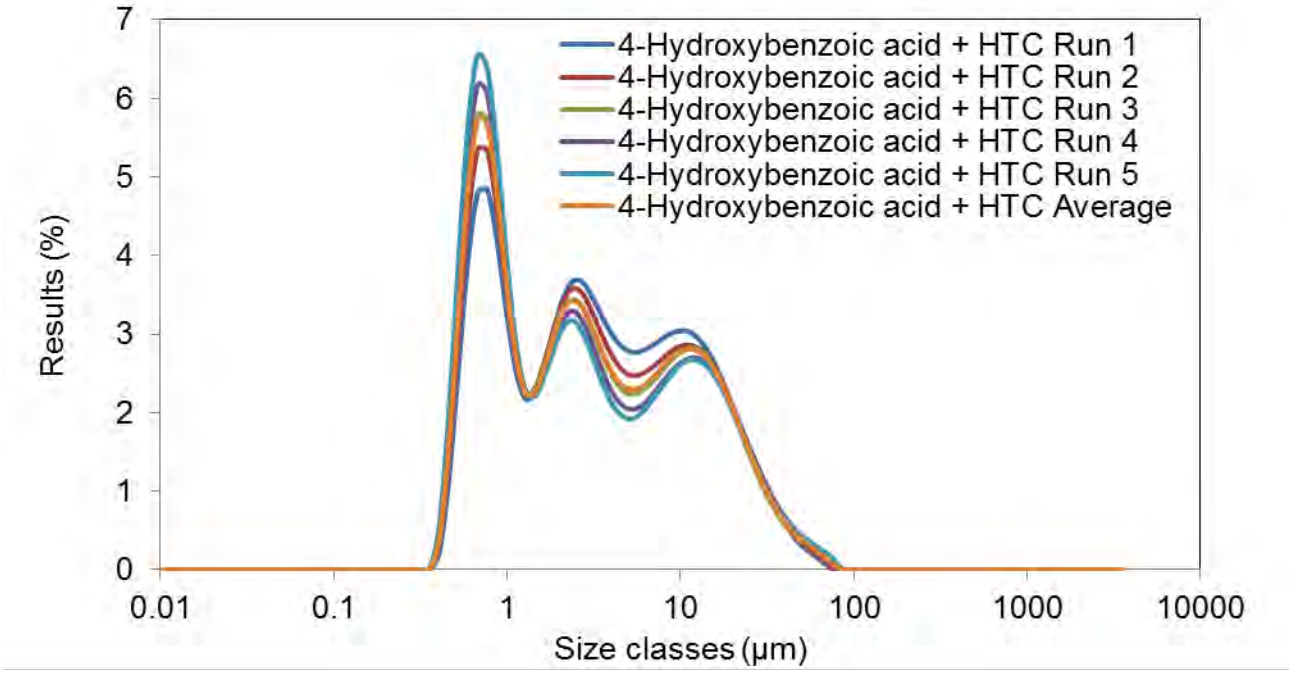

Figure C.1.7: Particle size distribution for 4-hydroxybenzoic acid + HTC.

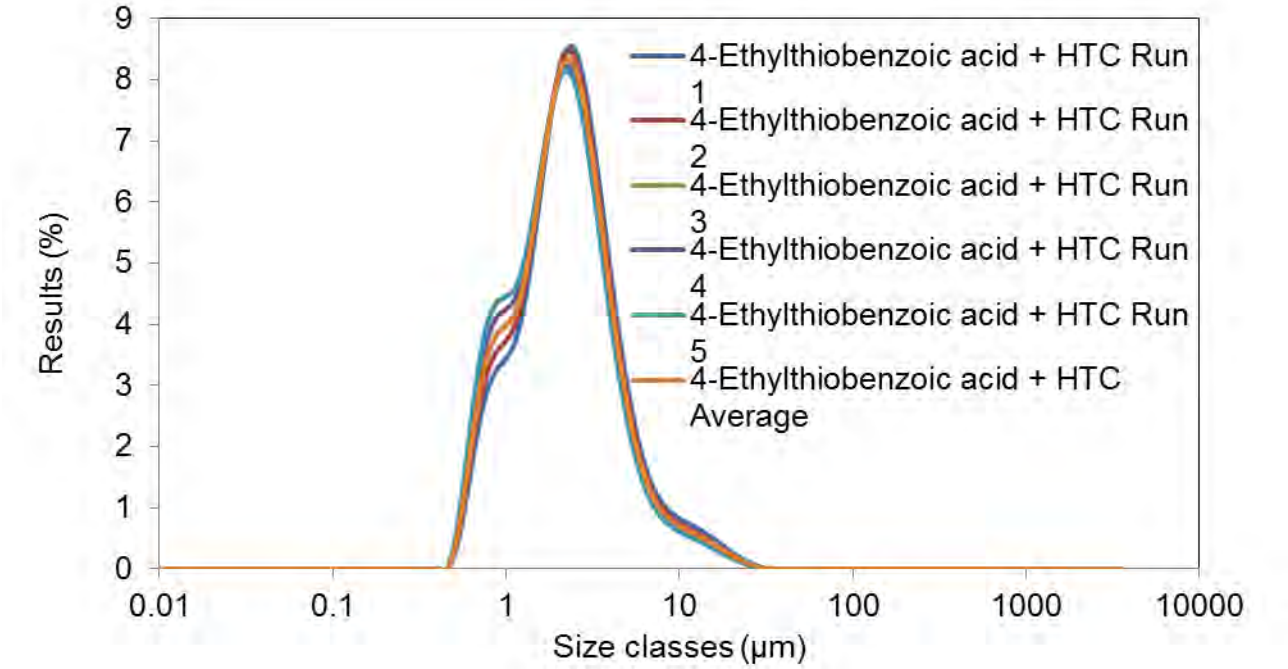

Figure C.1.8: Particle size distribution for 4-ethylthiobenzoic acid + HTC.

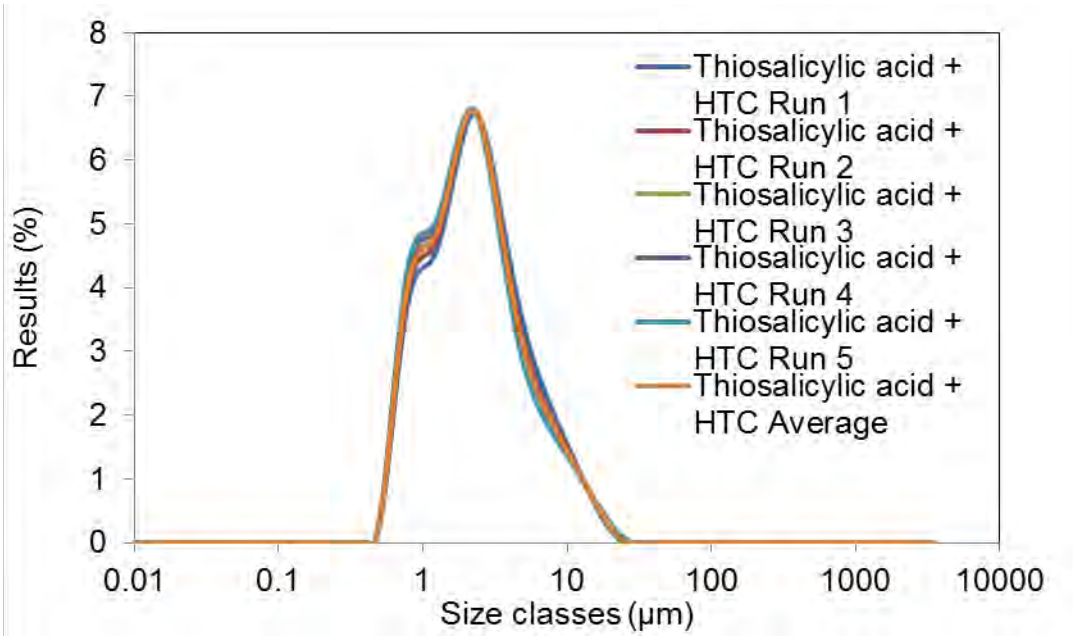

Figure C.1.9: Particle size distribution for thiosalicylic acid + HTC.

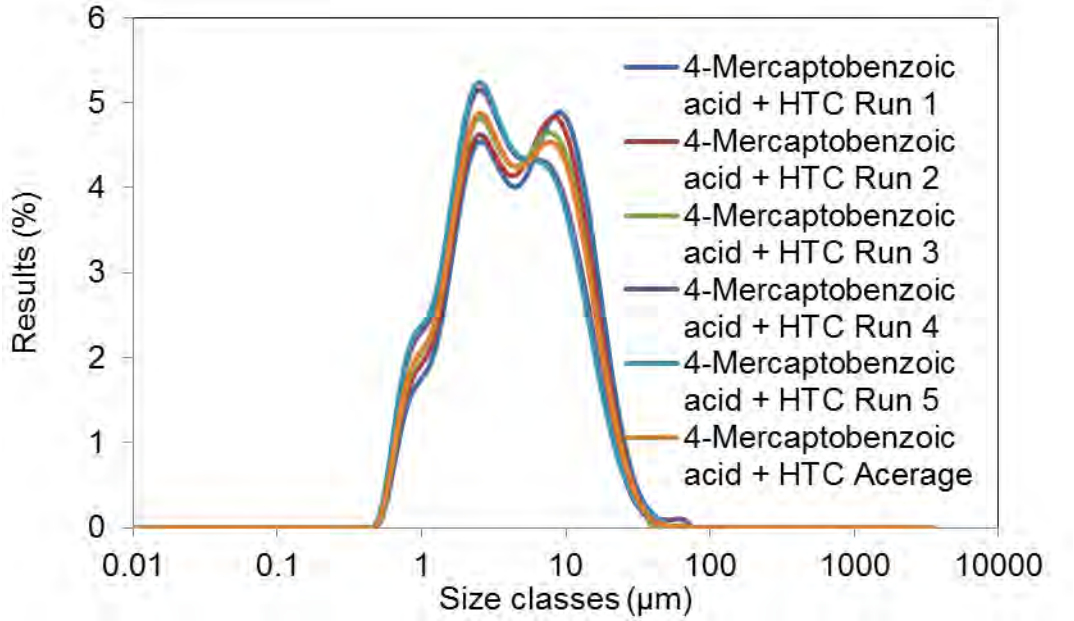

Figure C.1.10: Particle size distribution for 4-mercaptobenzoic acid + HTC.

C.2 – Co-precipitation method synthesis

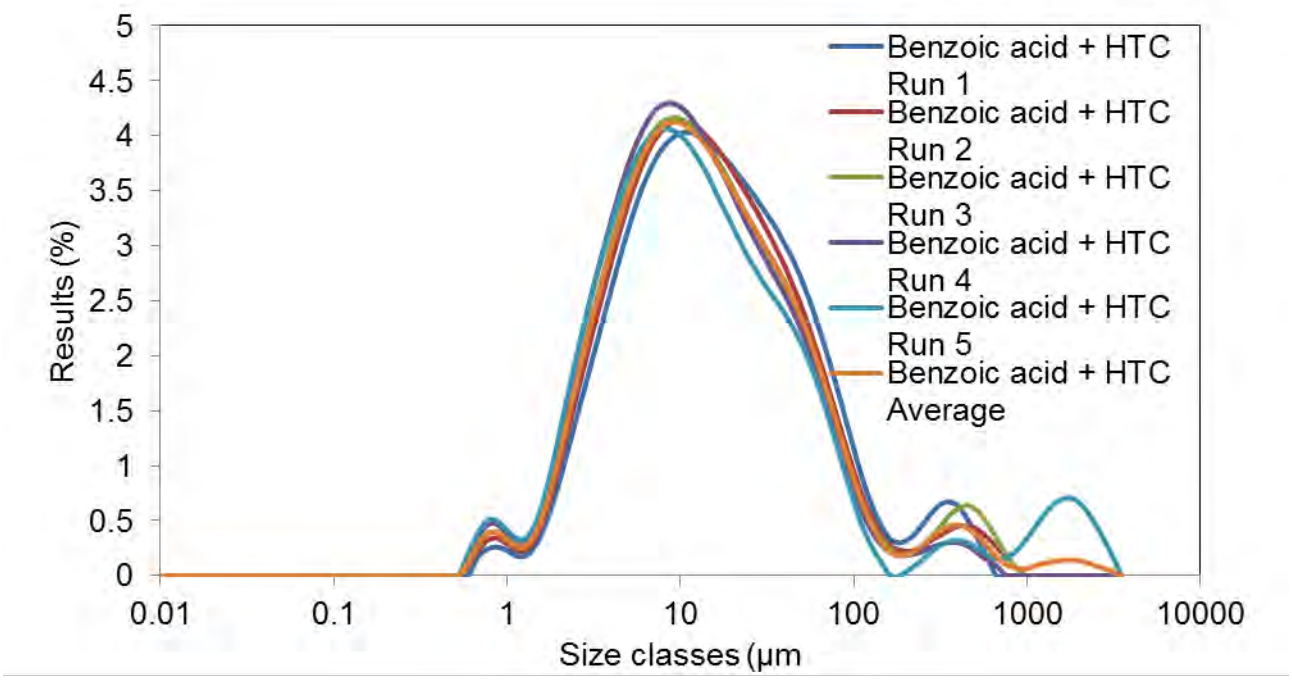

Figure C.2.1: Particle size distribution for benzoic acid + HTC.

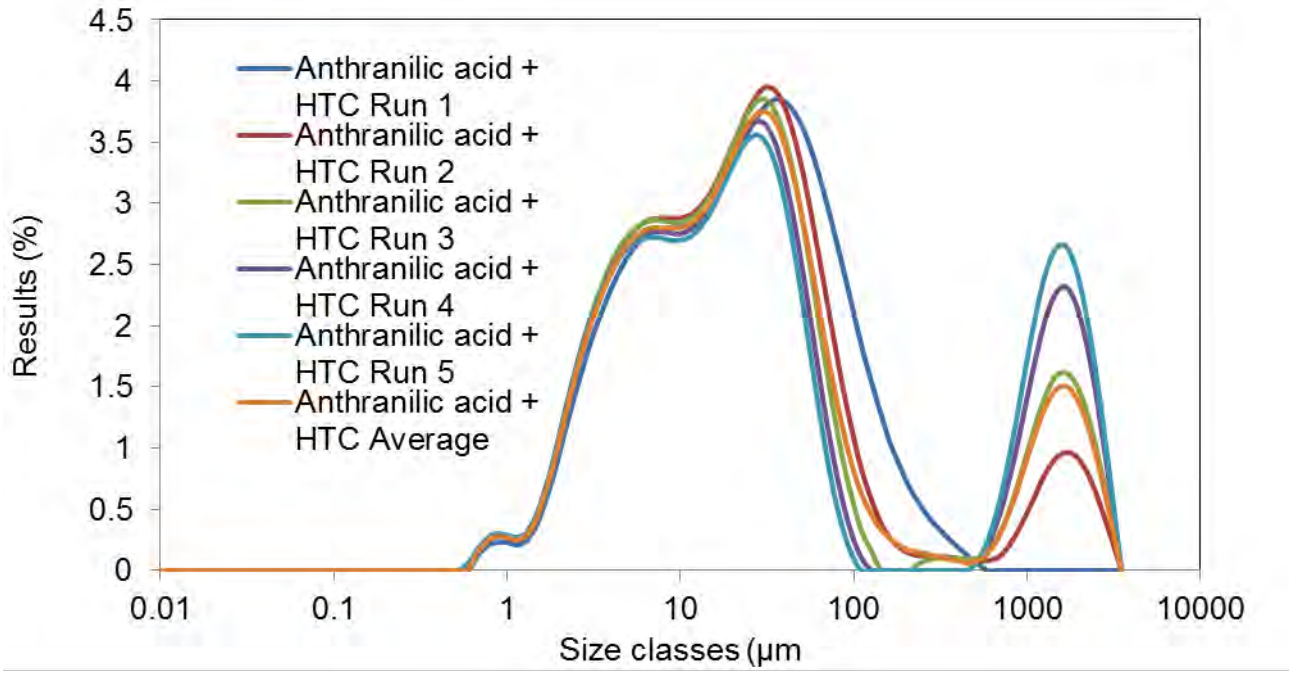

Figure C.2.2: Particle size distribution for anthranilic acid + HTC.

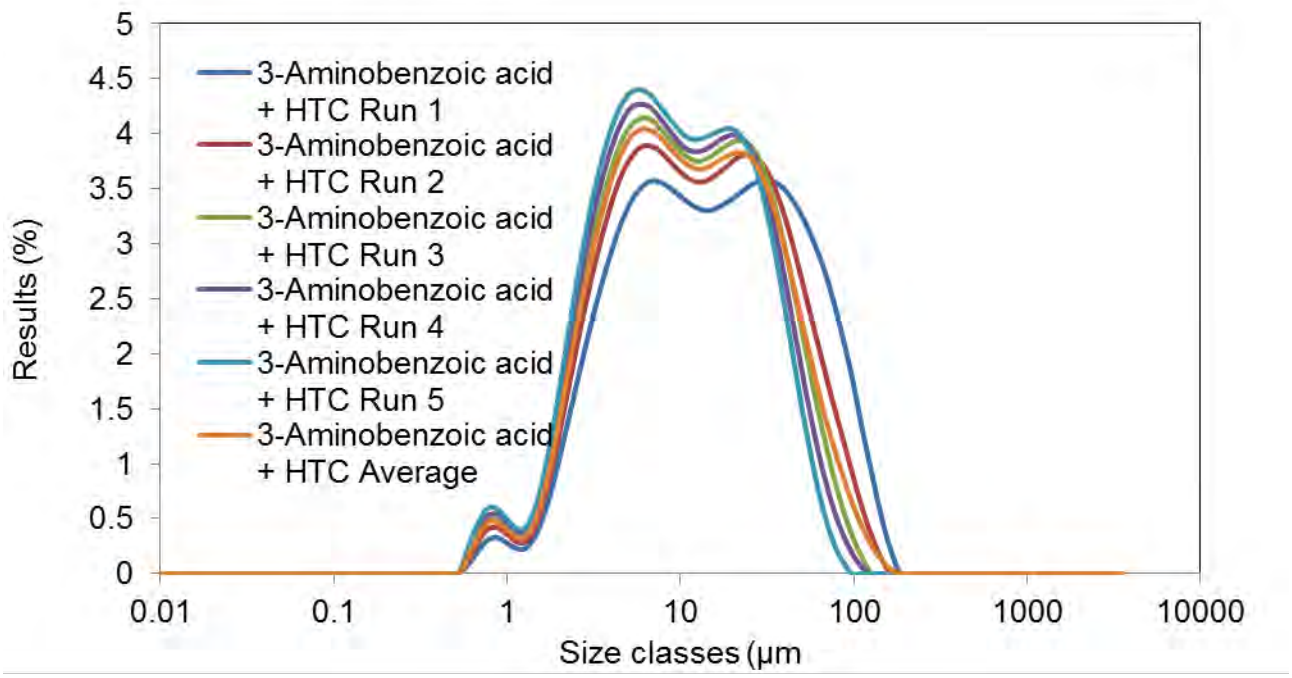

Figure C.2.3: Particle size distribution for 3-aminobenzoic acid + HTC.

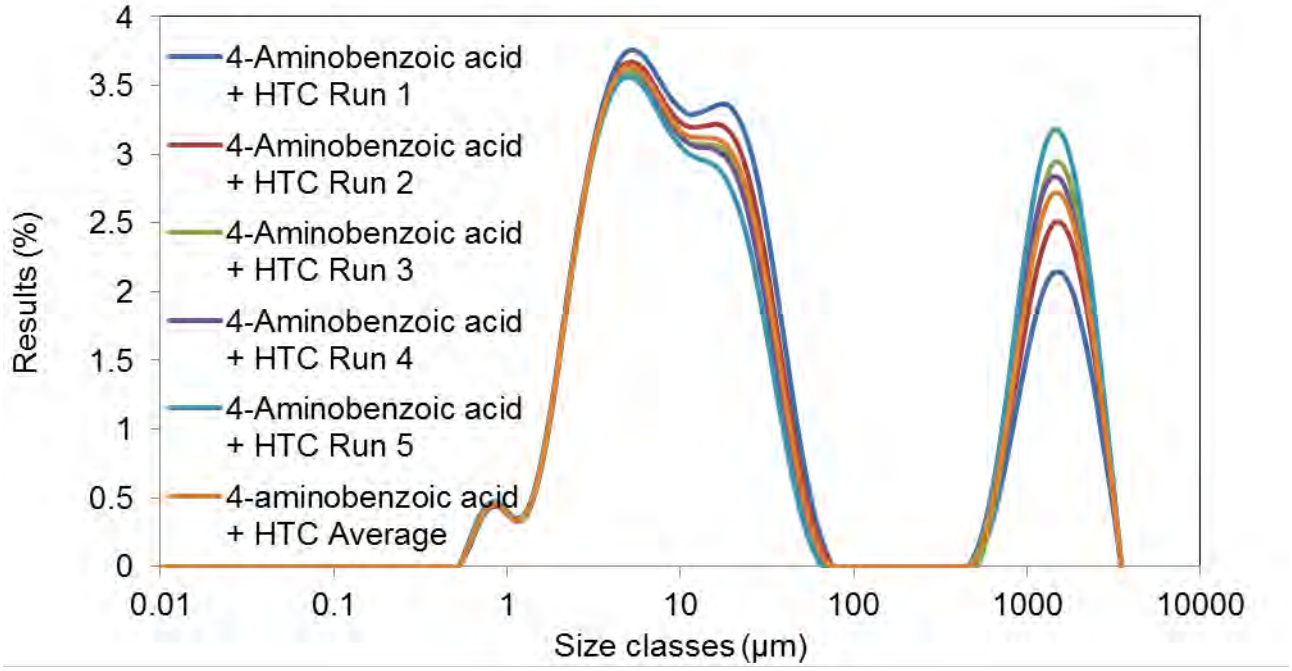

Figure C.2.4: Particle size distribution for 4-aminobenzoic acid + HTC.

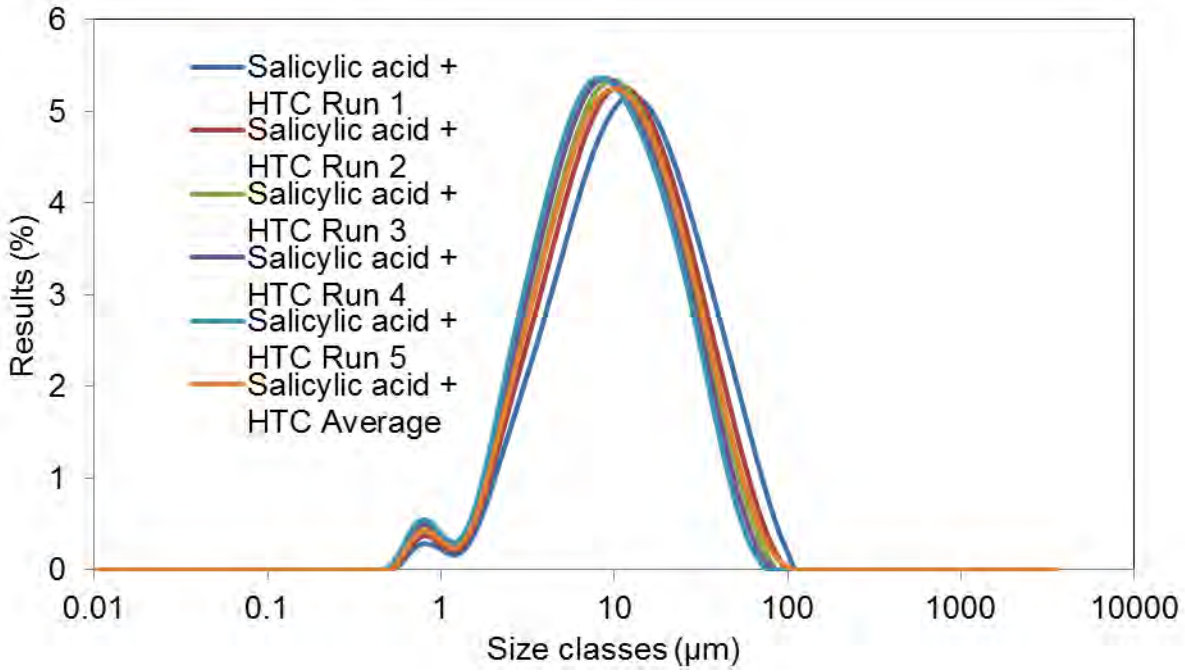

Figure C.2.5: Particle size distribution for salicylic acid + HTC.

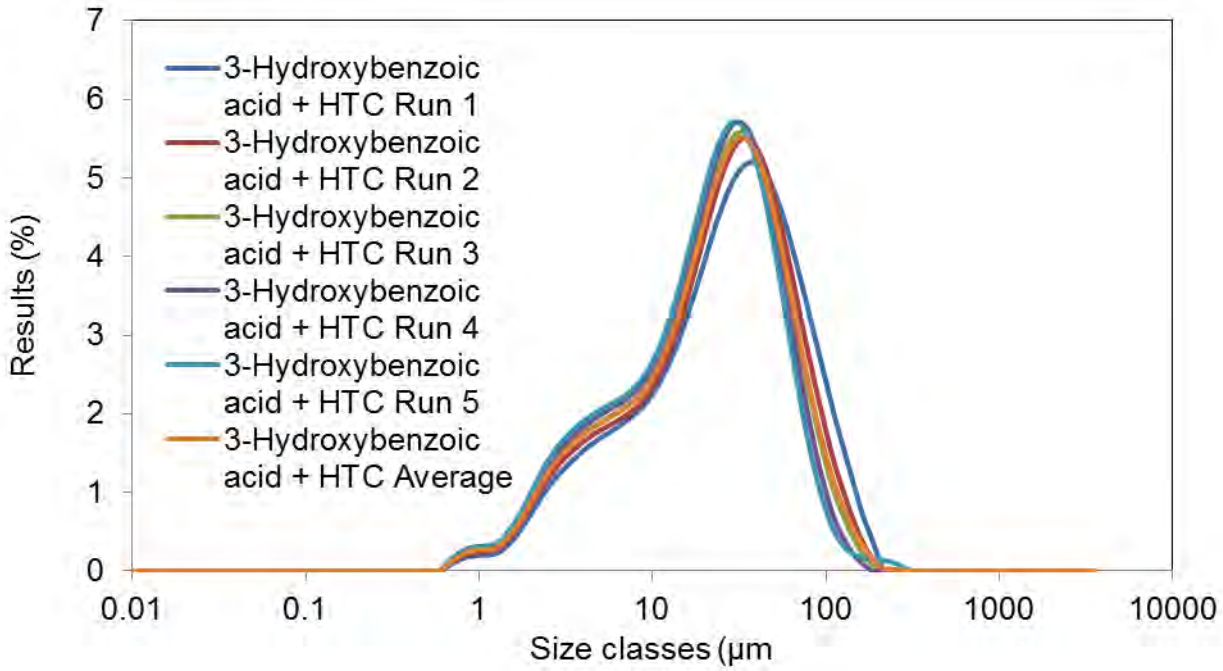

Figure C.2.6: Particle size distribution for 3-hydroxybenzoic acid + HTC.

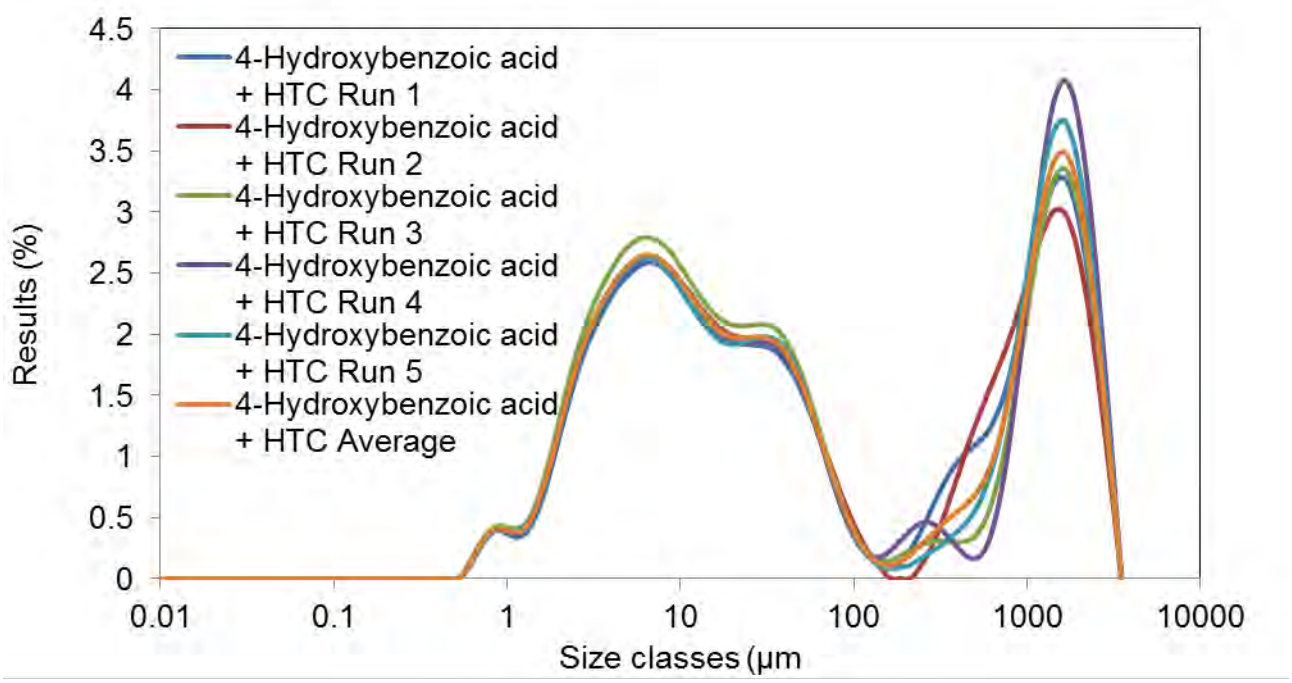

Figure C.2.7: Particle size distribution for 4-hydroxybenzoic acid + HTC.

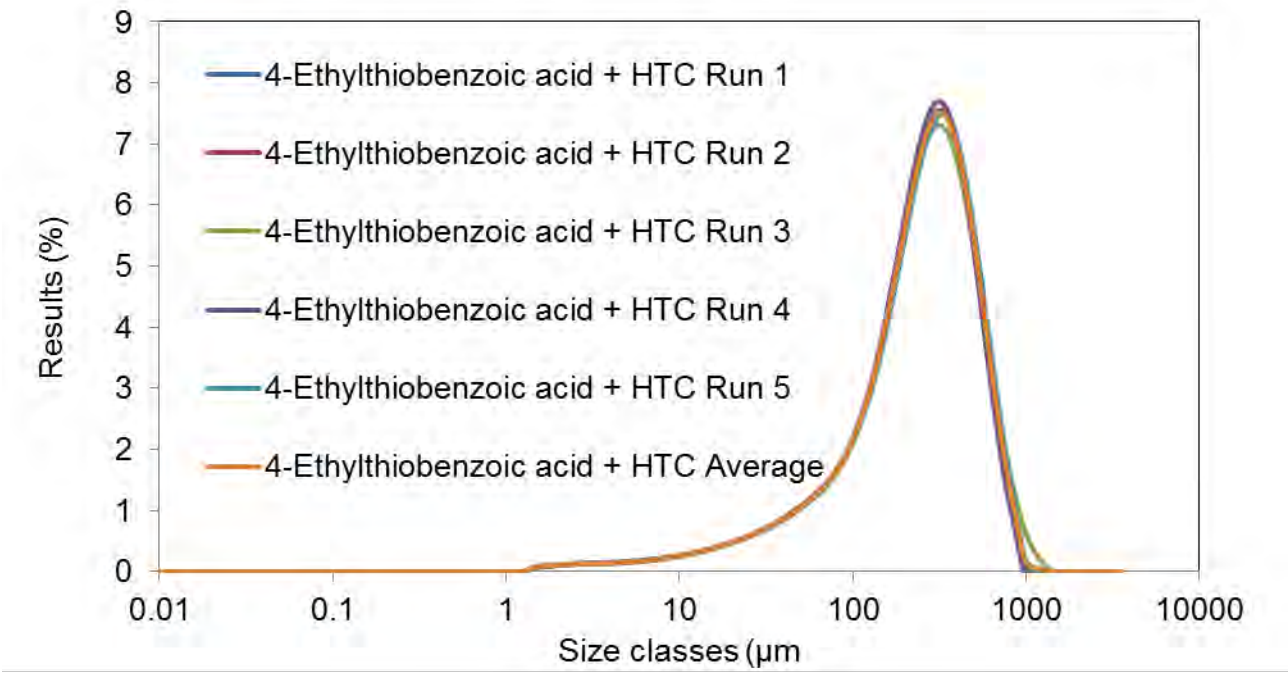

Figure C.2.8: Particle size distribution for 4-ethylthiobenzoic acid + HTC.

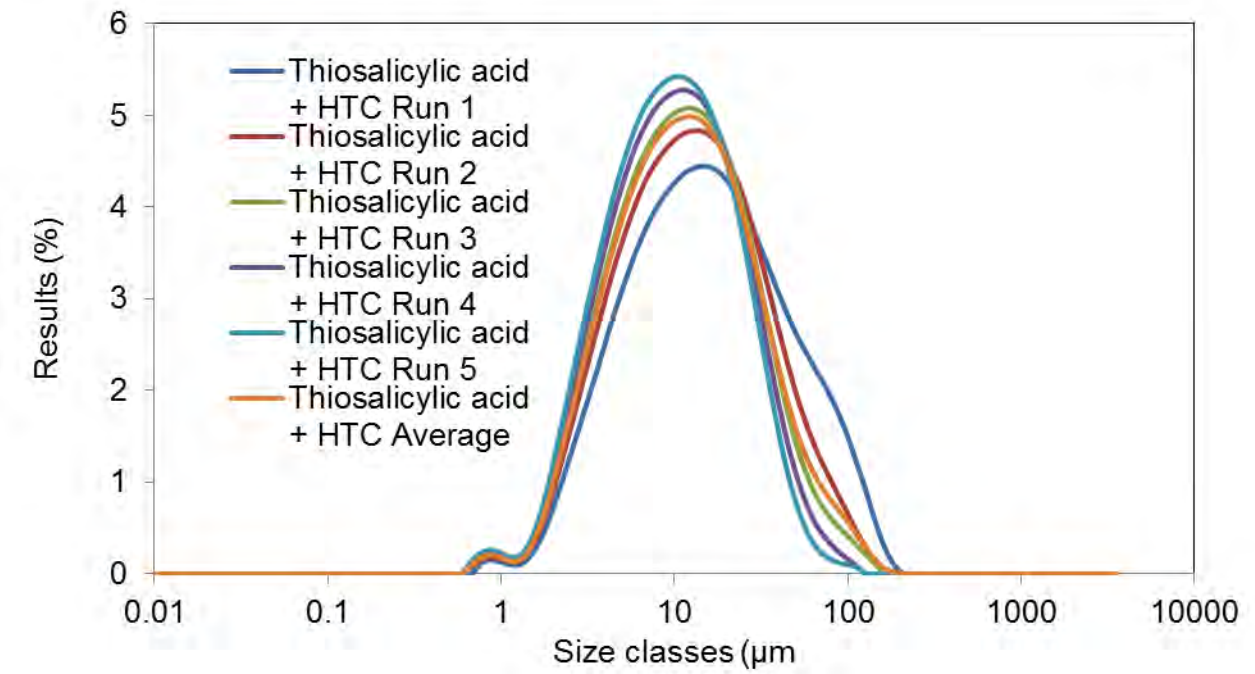

Figure C.2.9: Particle size distribution for thiosalicylic acid + HTC.

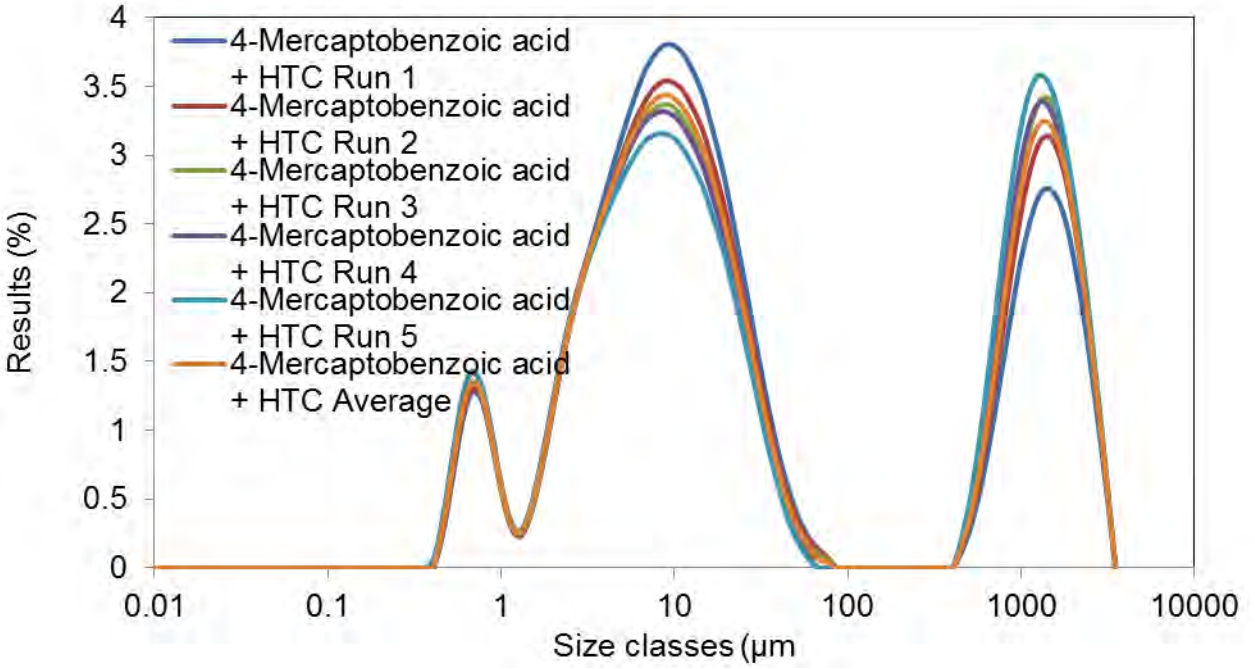

Figure C.2.10: Particle size distribution for 4-mercaptobenzoic acid + HTC.

Appendix D – Torque curves

D.1 Reconstruction method synthesis

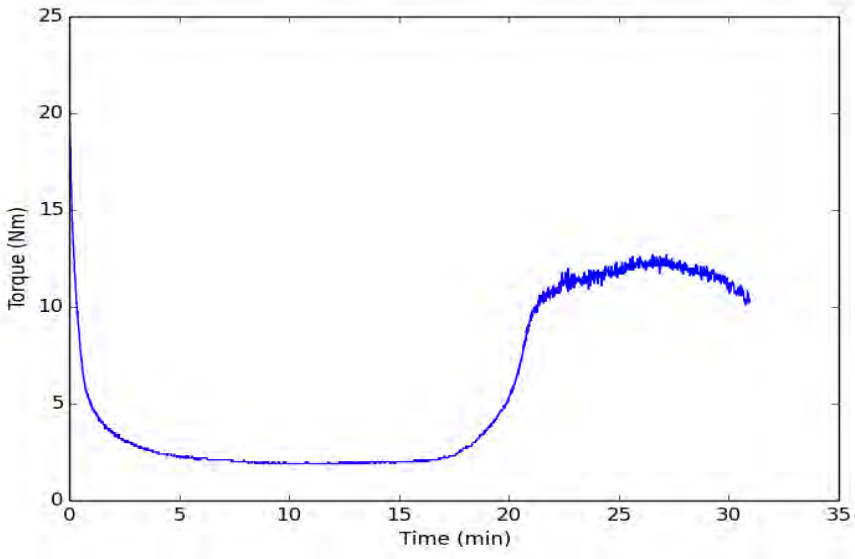

Figure D.1.1: Torque curve for benzoic acid + HTC run 1.

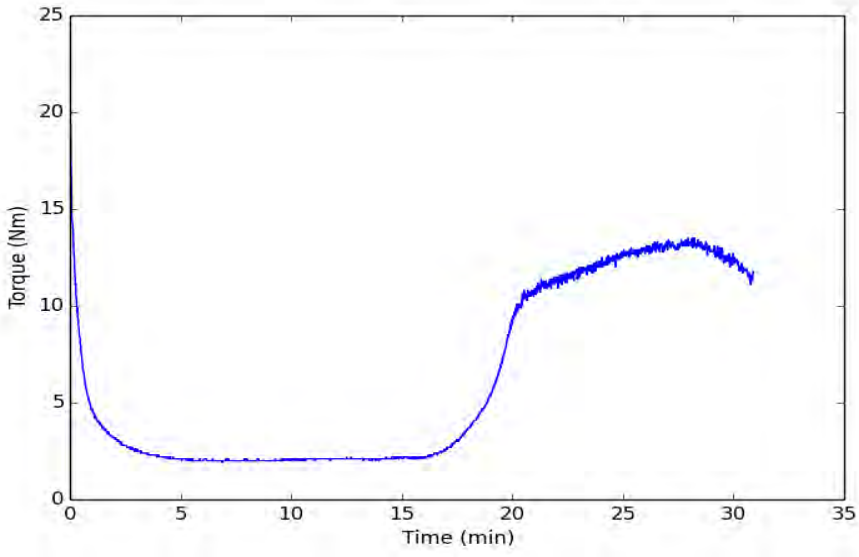

Figure D.1.2: Torque curve for benzoic acid + HTC run 2.

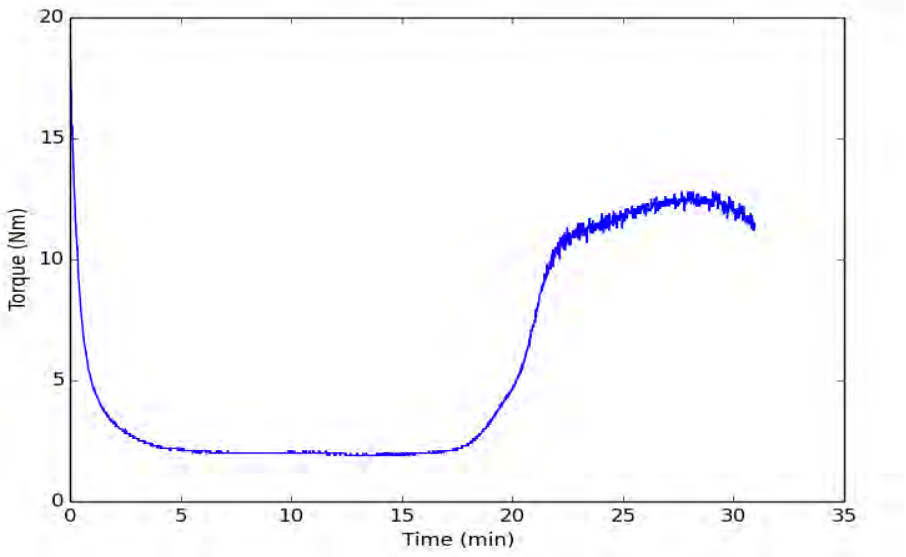

Figure D.1.3: Torque curve for benzoic acid + HTC run 3.

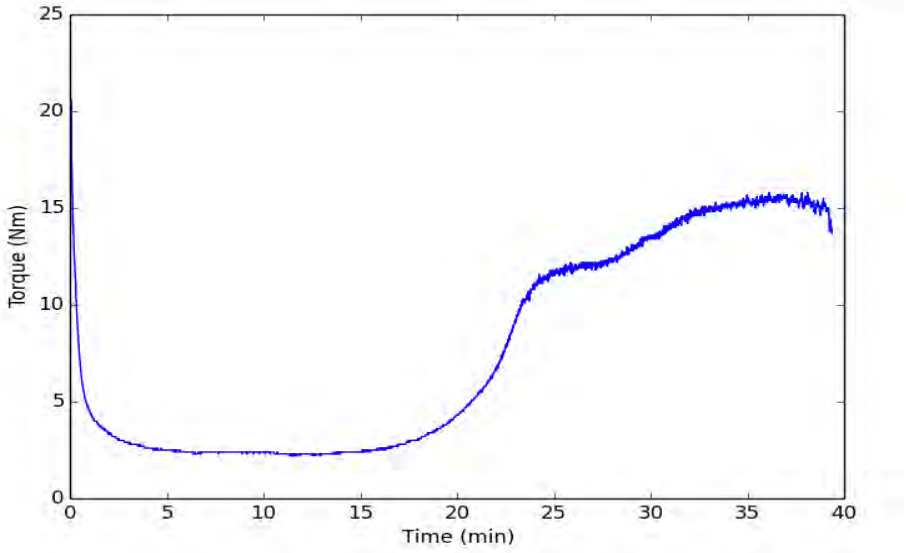

Figure D.1.4: Torque curve for anthranilic acid + HTC run 1.

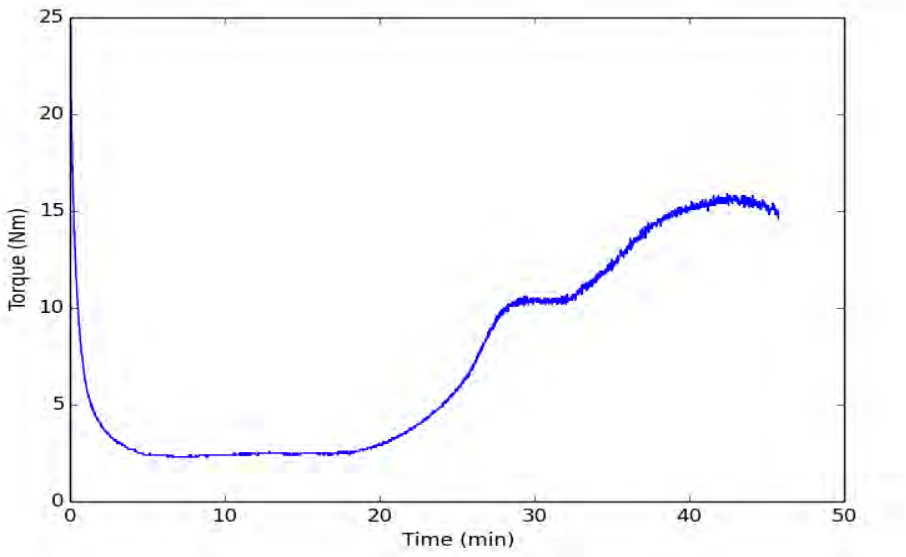

Figure D.1.5: Torque curve for anthranilic acid + HTC run 2.

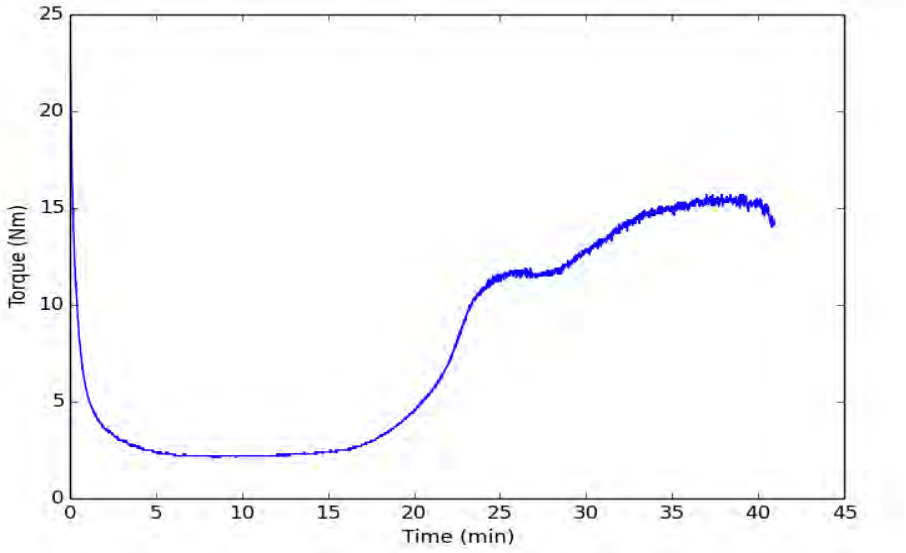

Figure D.1.6: Torque curve for anthranilic acid + HTC run 3.

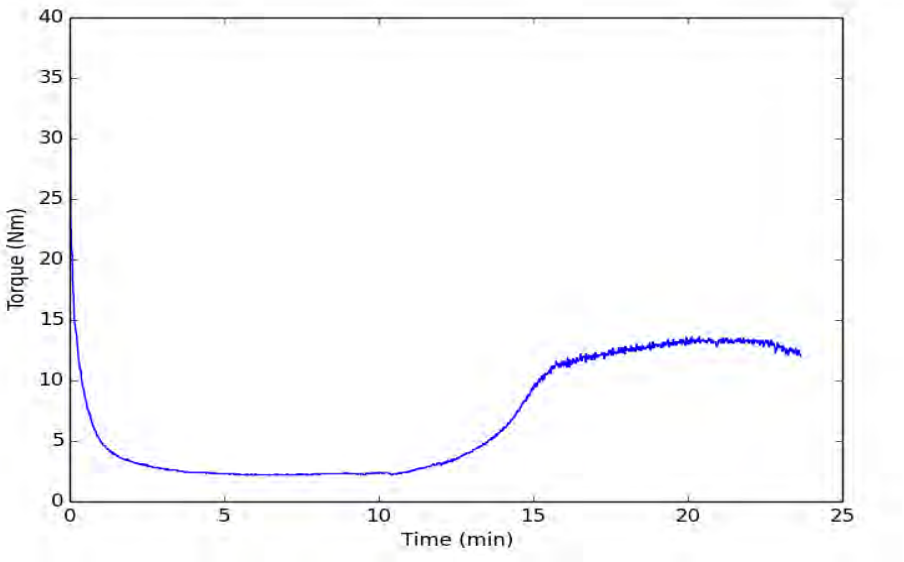

Figure D.1.7: Torque curve for 3-aminobenzoic acid + HTC run 1.

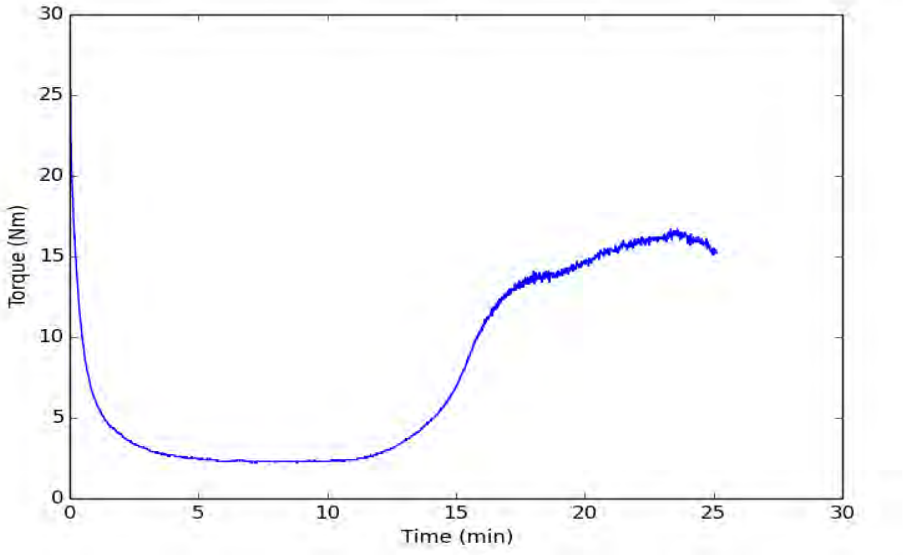

Figure D.1.8: Torque curve for 3-aminobenzoic acid + HTC run 2.

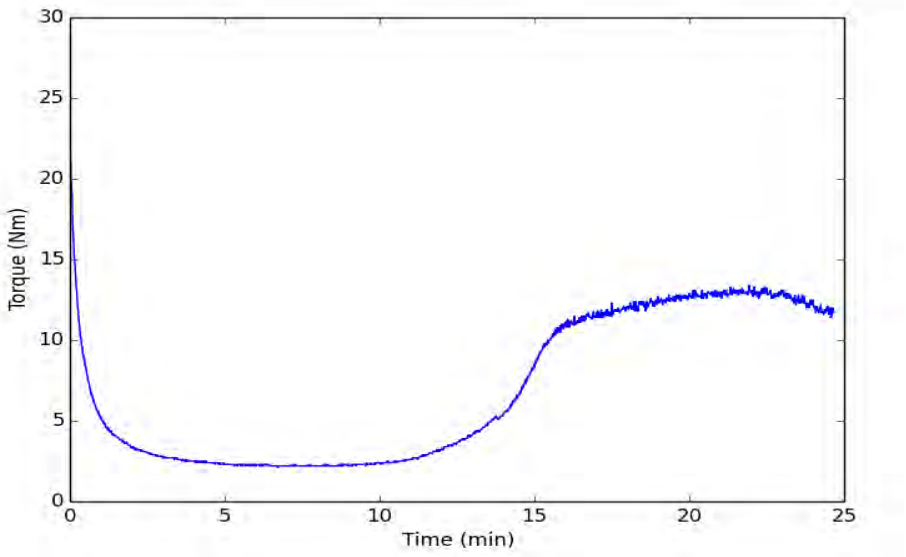

Figure D.1.9: Torque curve for 3-aminobenzoic acid + HTC run 3.

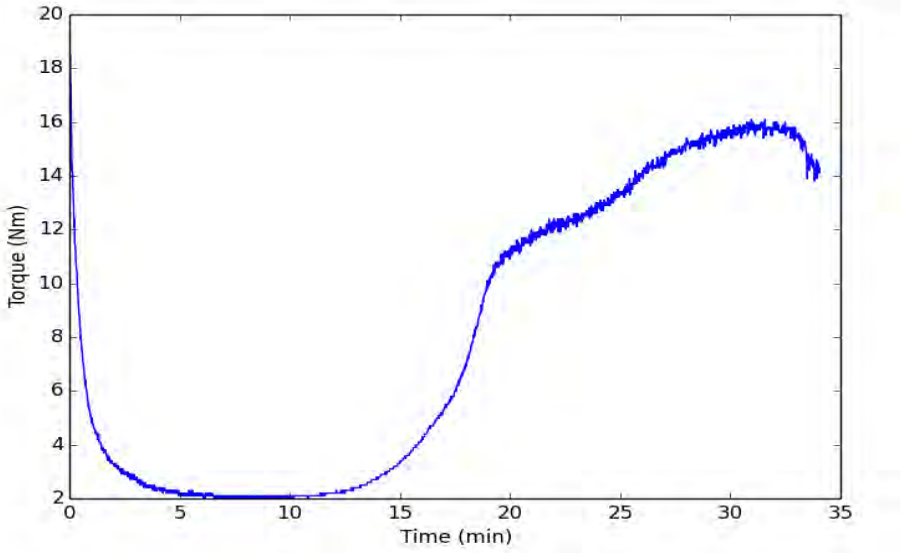

Figure D.1.10: Torque curve for 4-aminobenzoic acid + HTC run 1.

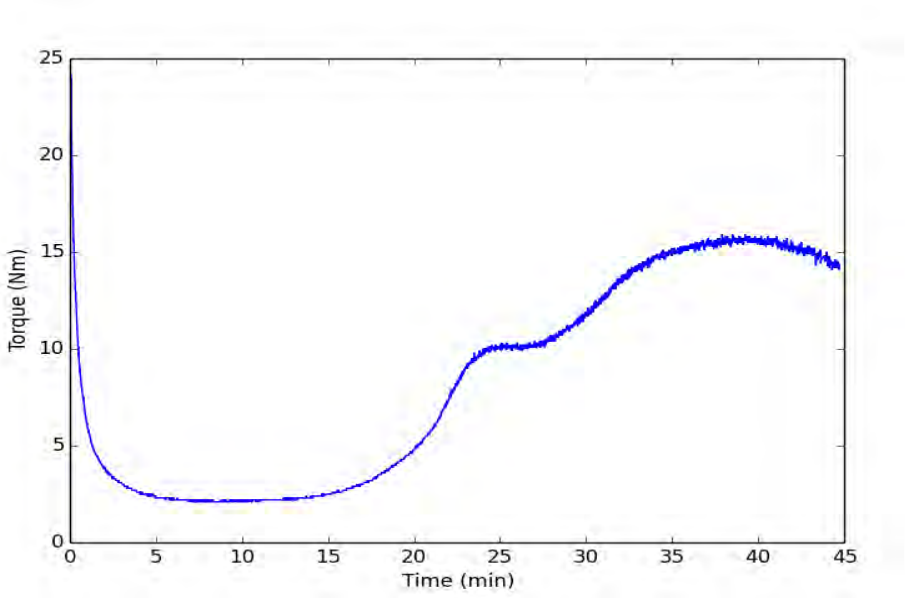

Figure D.1.11: Torque curve for 4-aminobenzoic acid + HTC run 2.

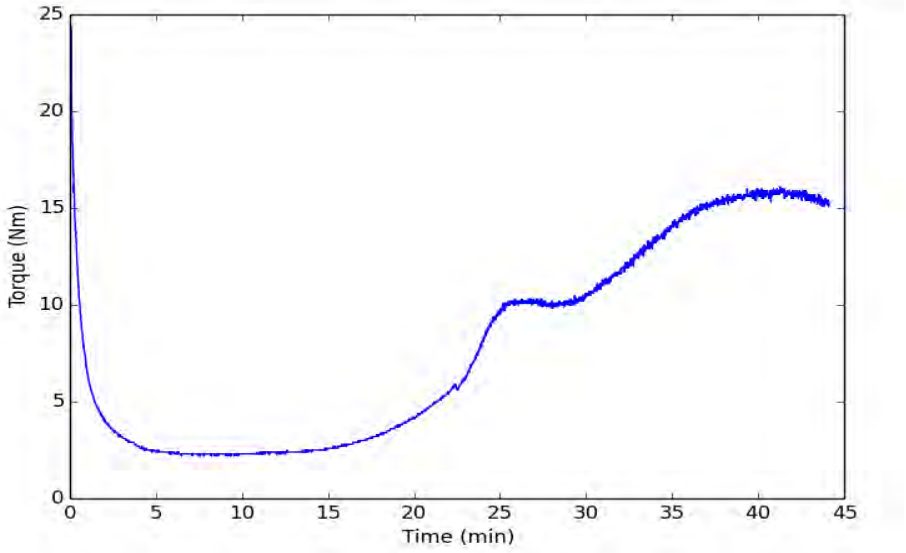

Figure D.1.12: Torque curve for 4-aminobenzoic acid + HTC run 3.

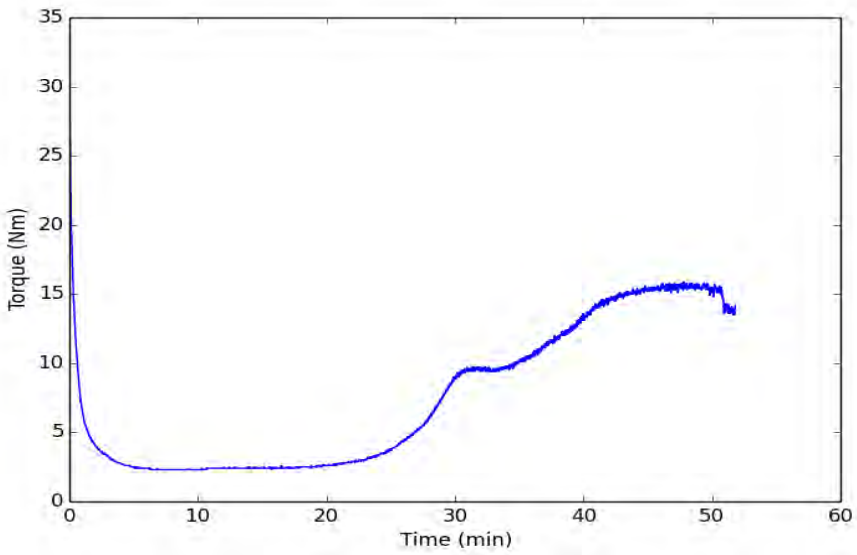

Figure D.1.13: Torque curve for salicylic acid + HTC run 1.

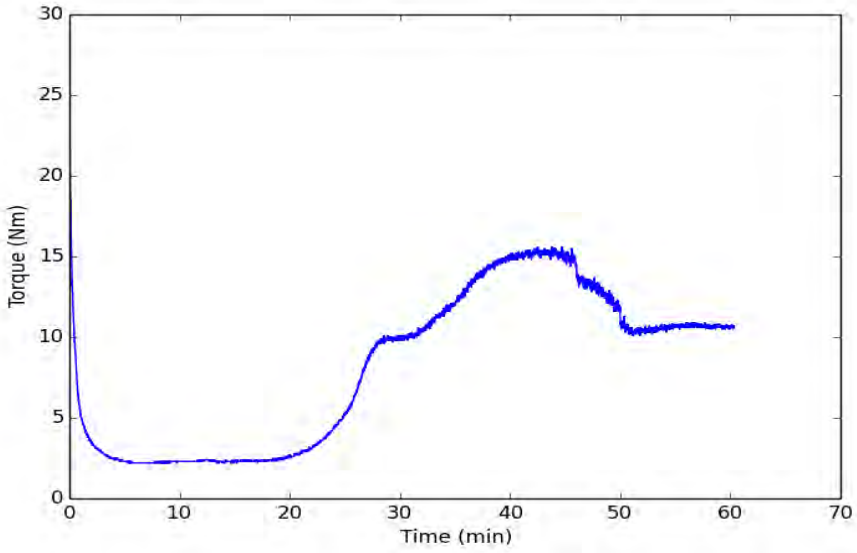

Figure D.1.14: Torque curve for salicylic acid + HTC run 2.

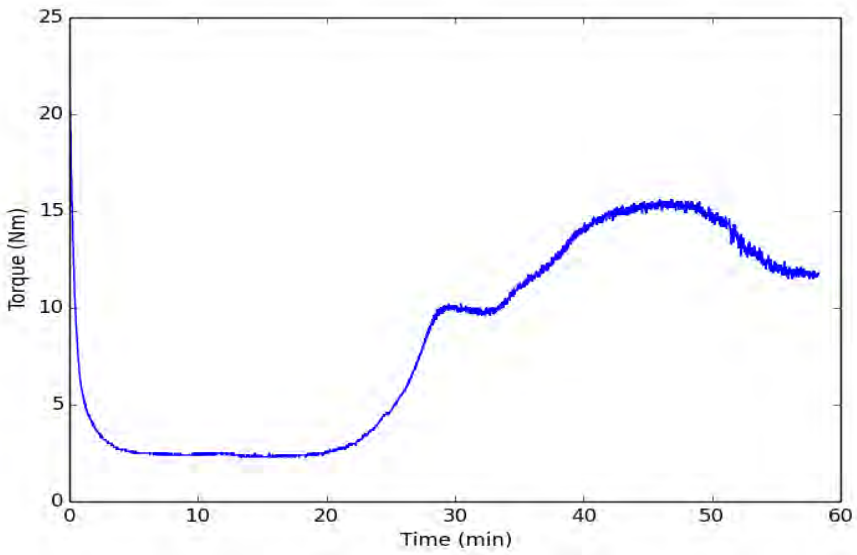

Figure D.1.15: Torque curve for salicylic acid + HTC run 3.

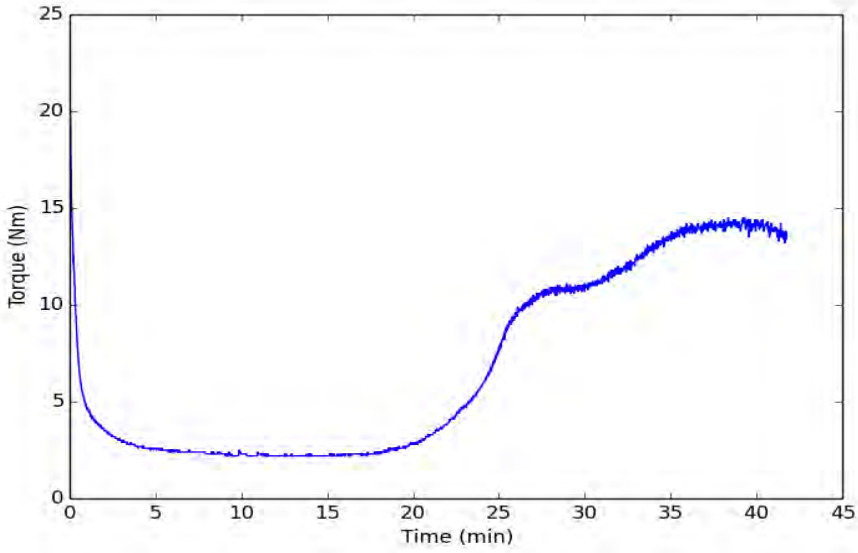

Figure D.1.16: Torque curve for 3-hydroxybenzoic acid + HTC run 1.

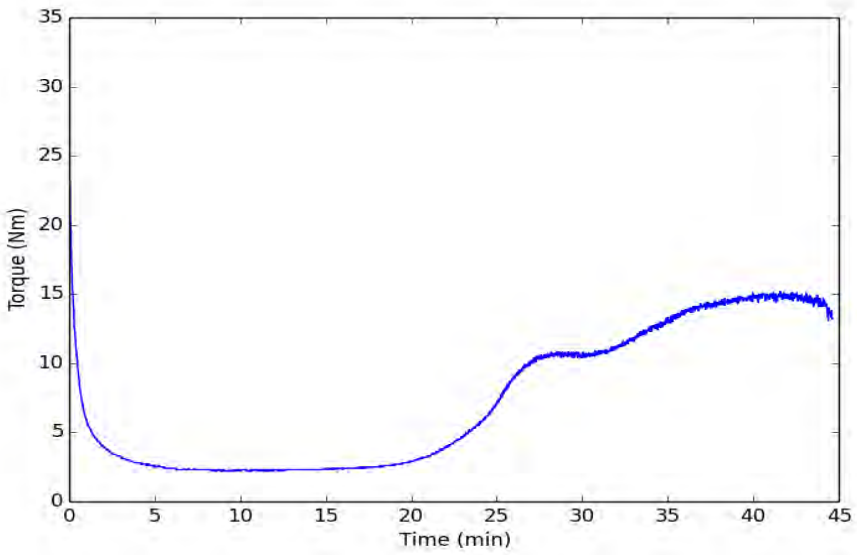

Figure D.1.17: Torque curve for 3-hydroxybenzoic acid + HTC run 2.

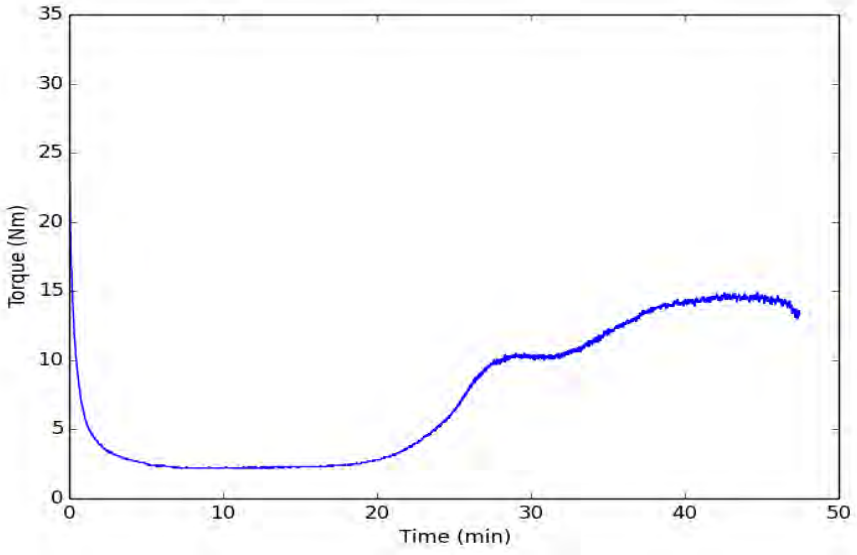

Figure D.1.18: Torque curve for 3-hydroxybenzoic acid + HTC run 3.

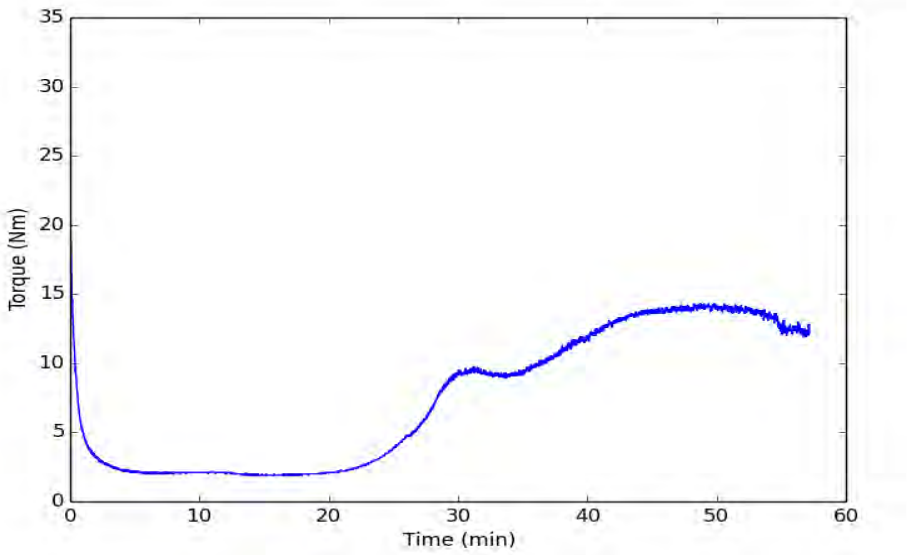

Figure D.1.19: Torque curve for 4-hydroxybenzoic acid + HTC run 1.

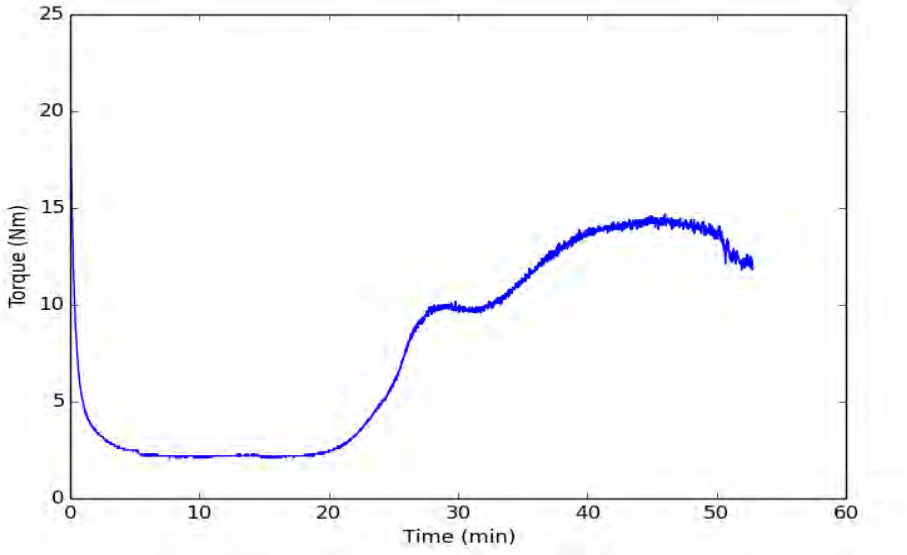

Figure D.1.20: Torque curve for 4-hydroxybenzoic acid + HTC run 2.

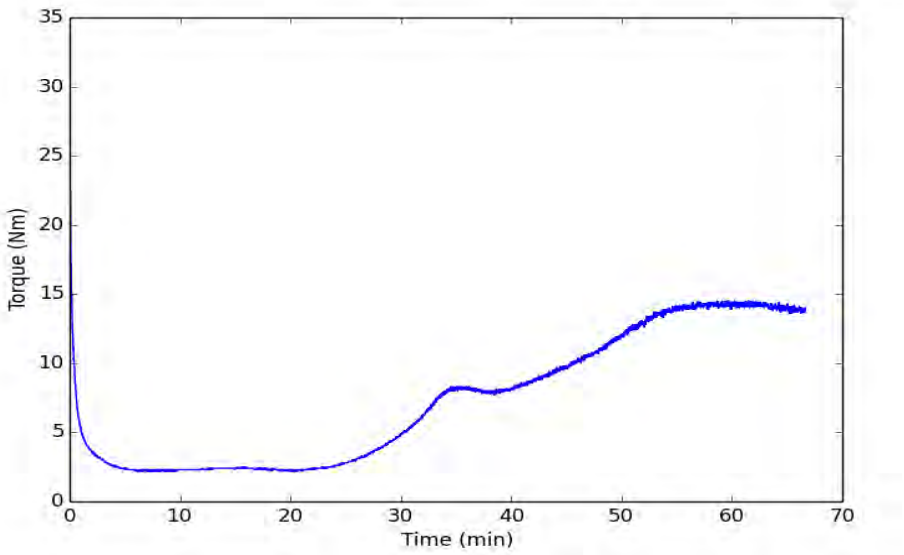

Figure D.1.21: Torque curve for 4-hydroxybenzoic acid + HTC run 3.

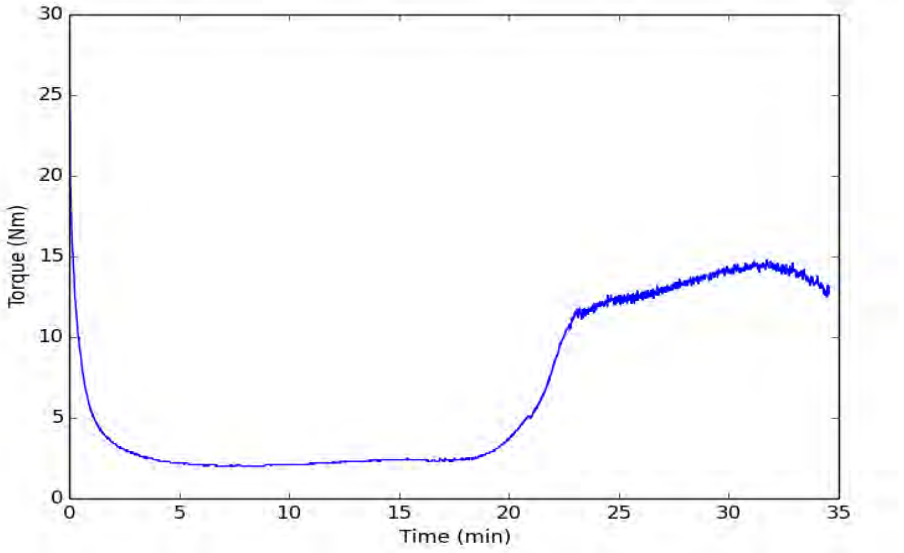

Figure D.1.22: Torque curve for 4-ethylthiobenzoic acid + HTC run 1.

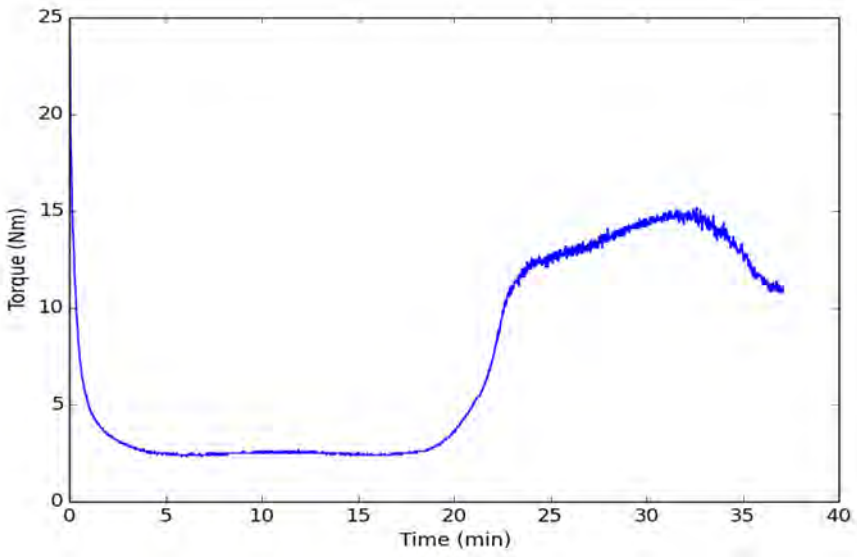

Figure D.1.23: Torque curve for 4-ethylthiobenzoic acid + HTC run 2.

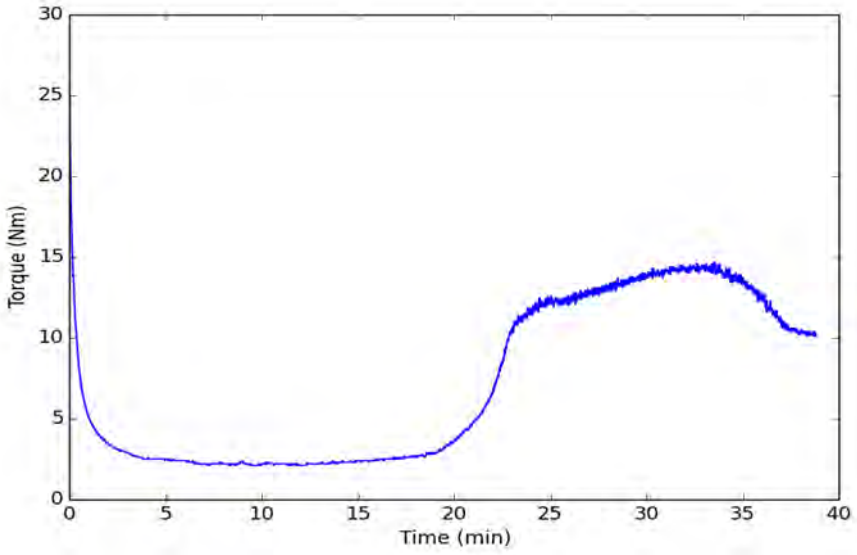

Figure D.1.24: Torque curve for 4-ethylthiobenzoic acid + HTC run 3.

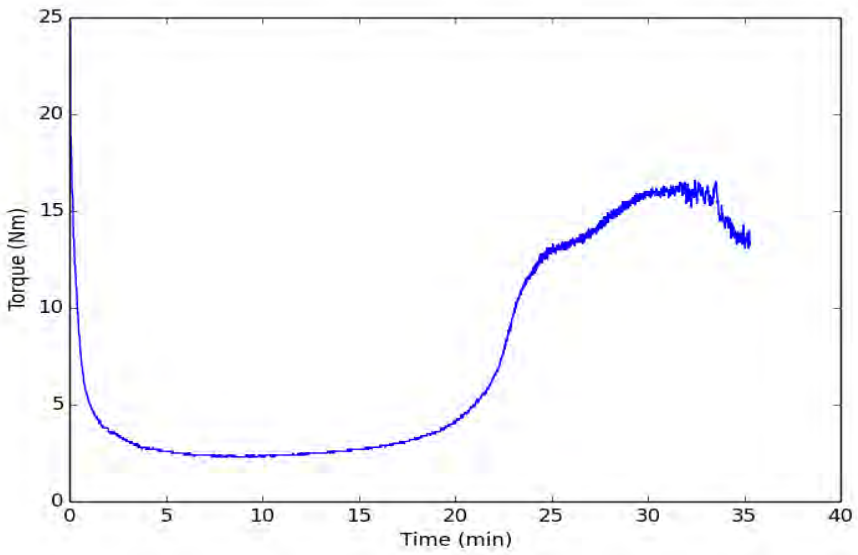

Figure D.1.25: Torque curve for thiosalicylic acid + HTC run 1.

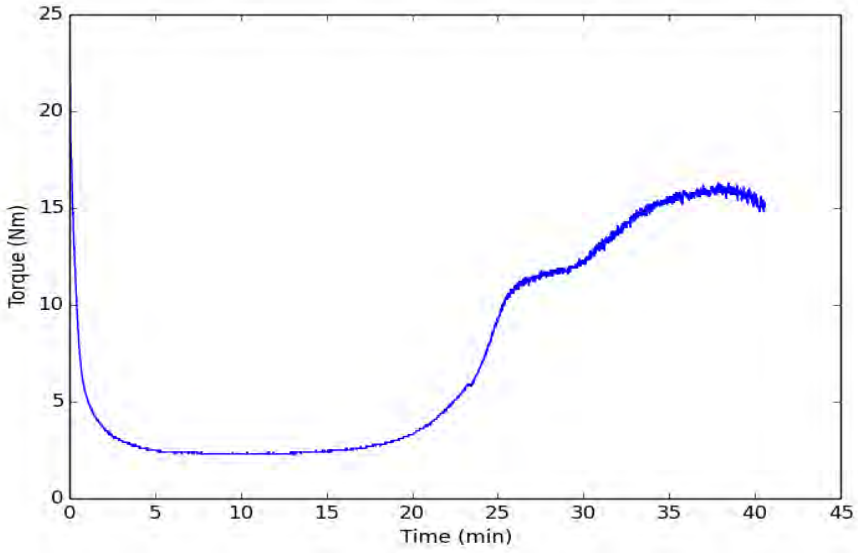

Figure D.1.26: Torque curve for thiosalicylic acid + HTC run 2.

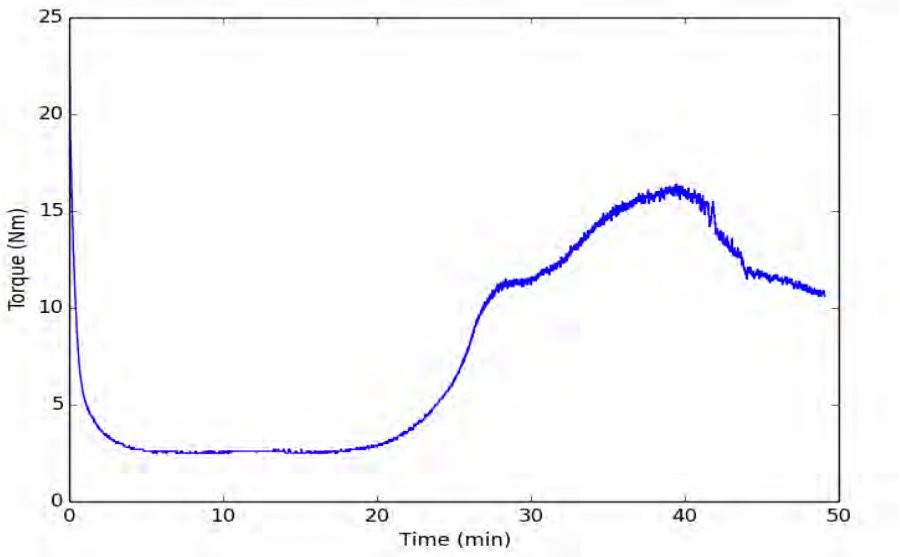

Figure D.1.27: Torque curve for thiosalicylic acid + HTC run 3.

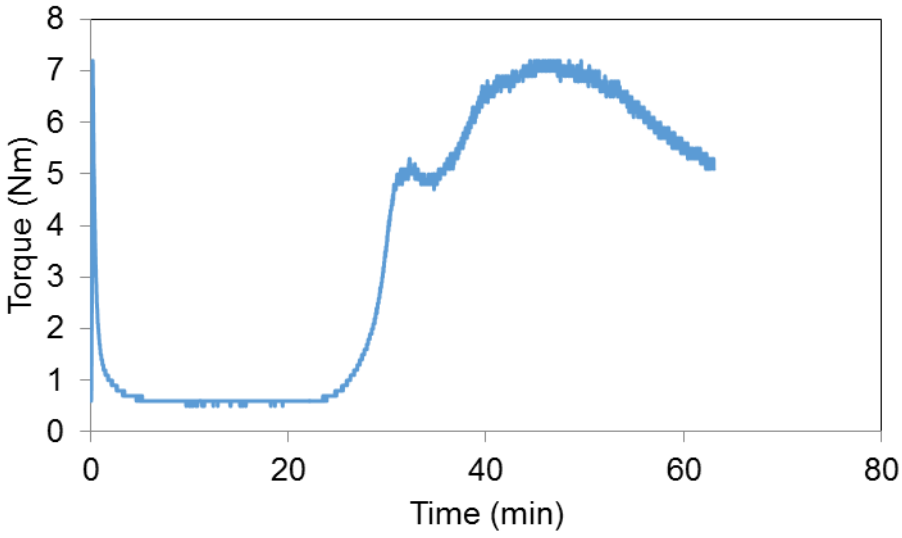

Figure D.1.28: Torque curve for 4-mercaptobenzoic acid + HTC.

D.2 – Co-precipitation method synthesis

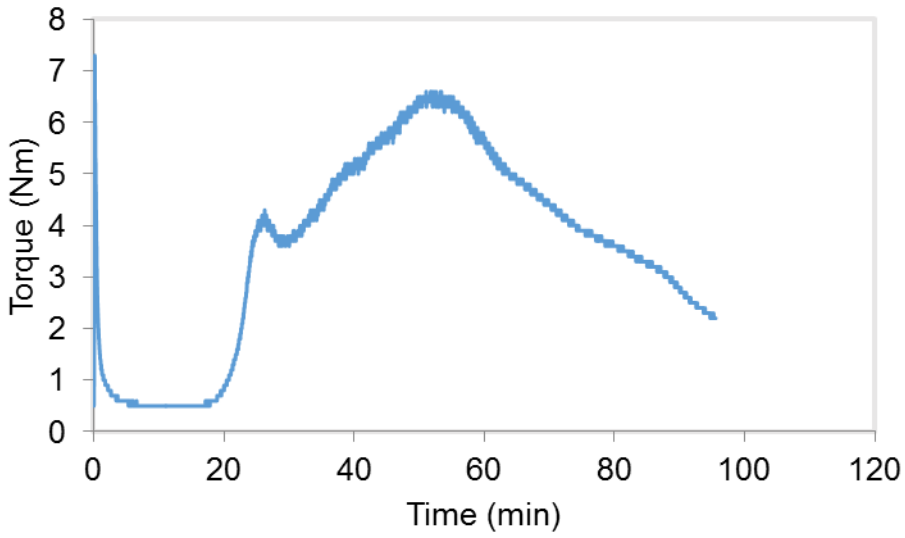

Figure D.2.1: Torque curve for benzoic acid + HTC.

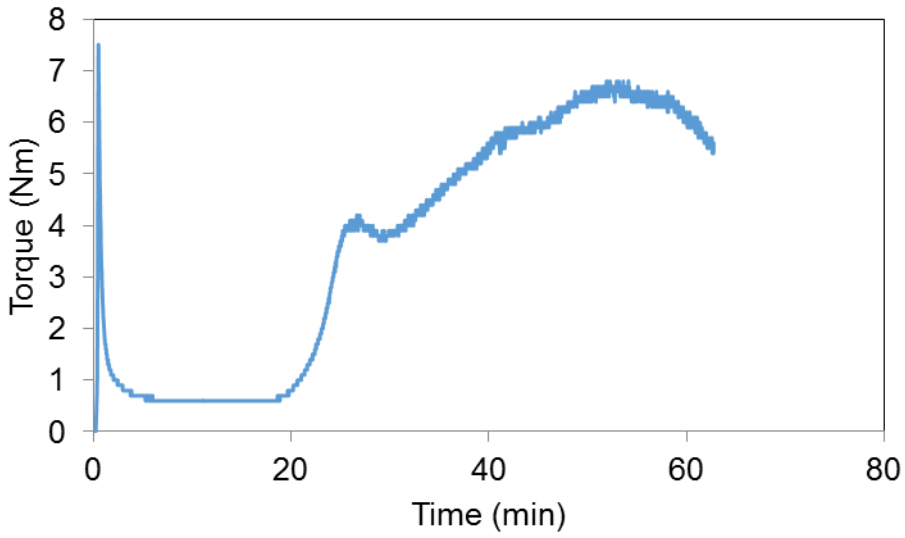

Figure D.2.2: Torque curve for anthranilic acid + HTC.

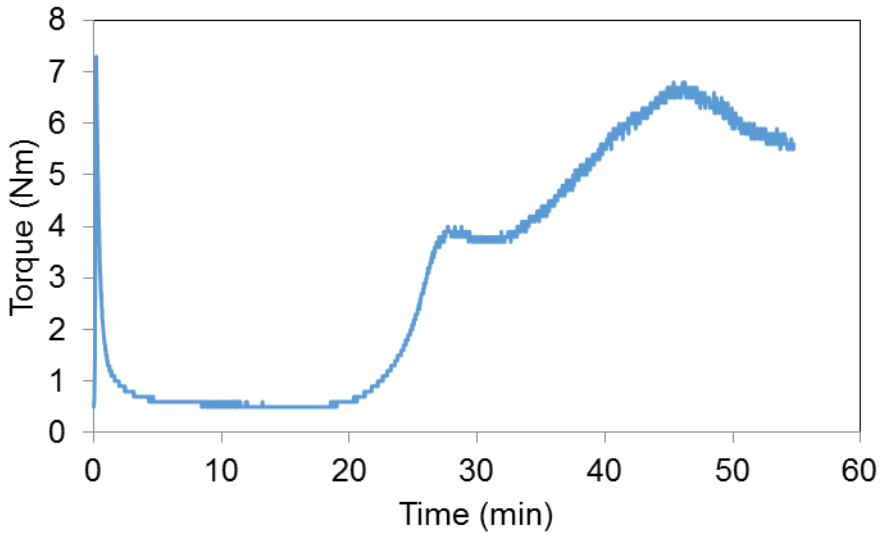

Figure D.2.3: Torque curve for 3-aminobenzoic acid + HTC.

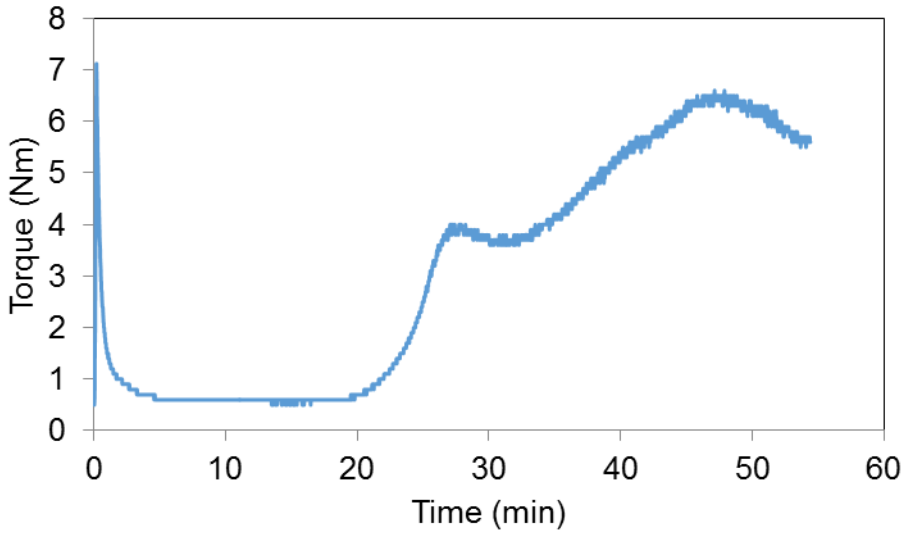

Figure D.2.4: Torque curve for 4-aminobenzoic acid + HTC.

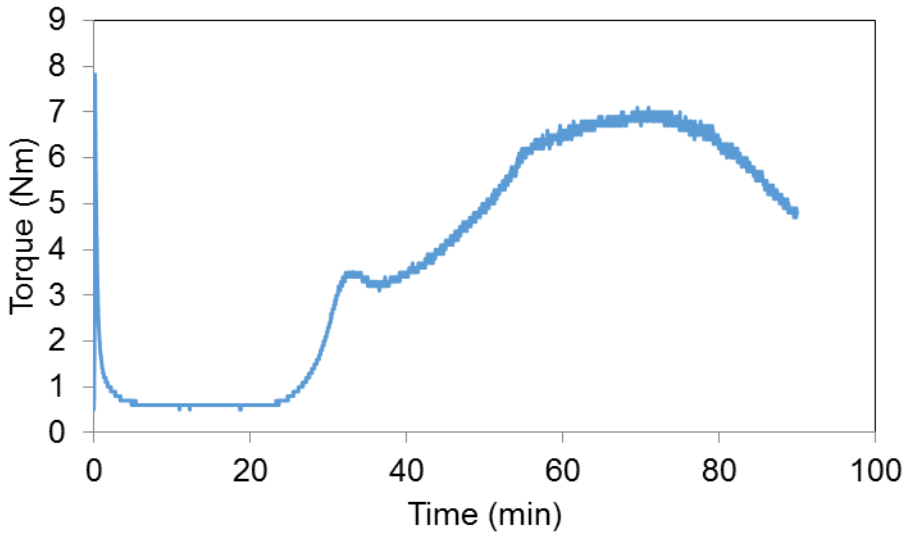

Figure D.2.5: Torque curve for salicylic acid + HTC.

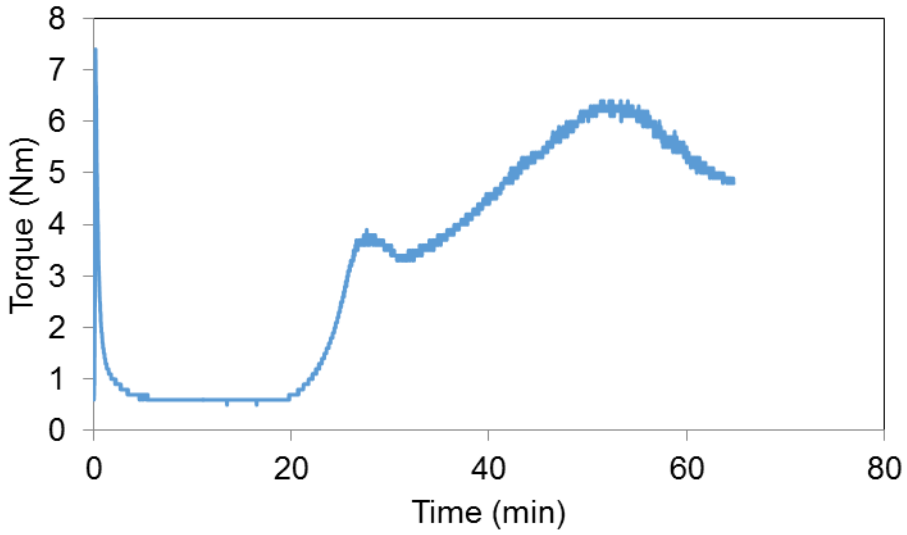

Figure D.2.6: Torque curve for 3-hydroxybenzoic acid + HTC.

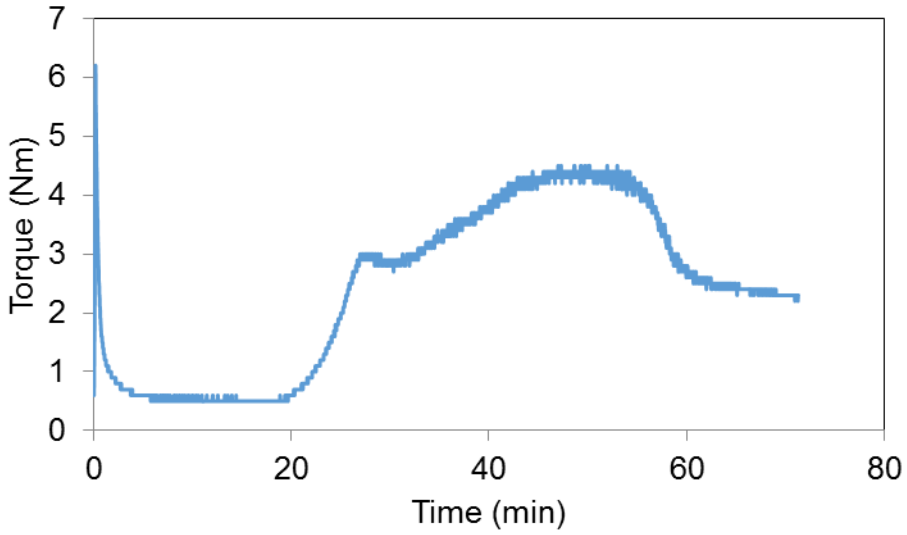

Figure D.2.7: Torque curve for 4-hydroxybenzoic acid + HTC.

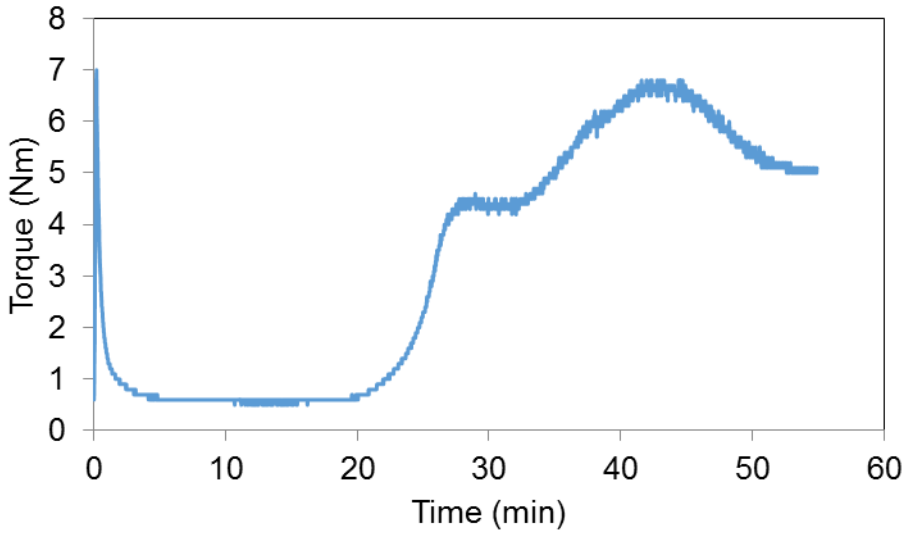

Figure D.2.8: Torque curve for 4-ethylthiobenzoic acid + HTC.

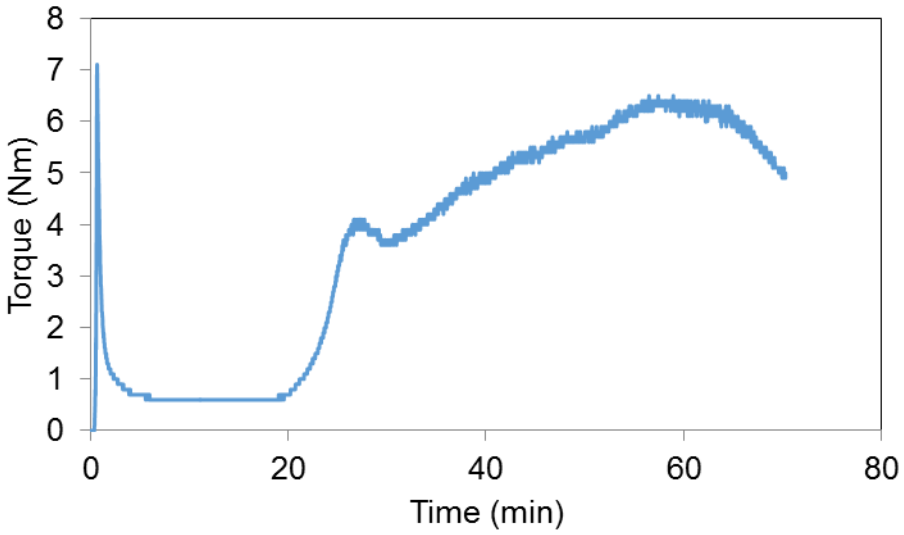

Figure D.2.9: Torque curve for thiosalicylic acid + HTC.

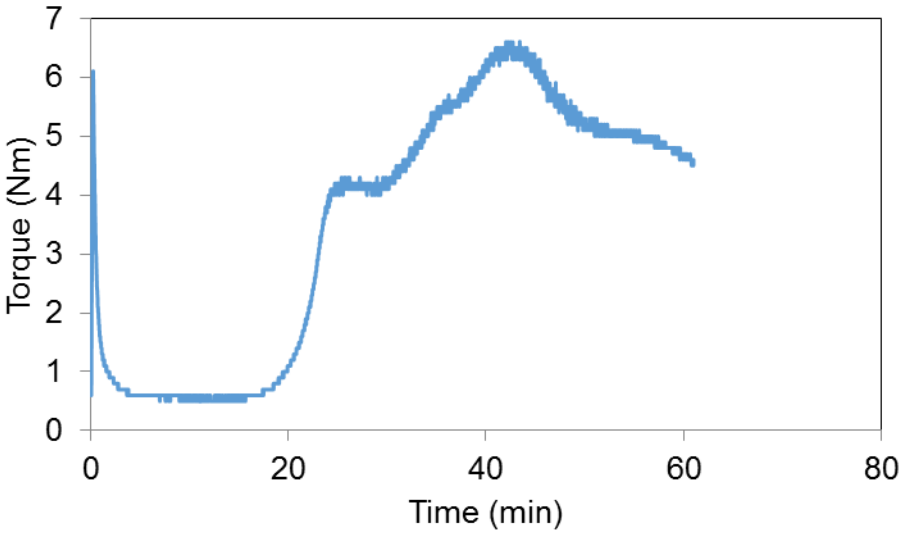

Figure D.2.10: Torque curve for 4-mercaptobenzoic acid + HTC.

D.3 – Neat hydrotalcite torque curves

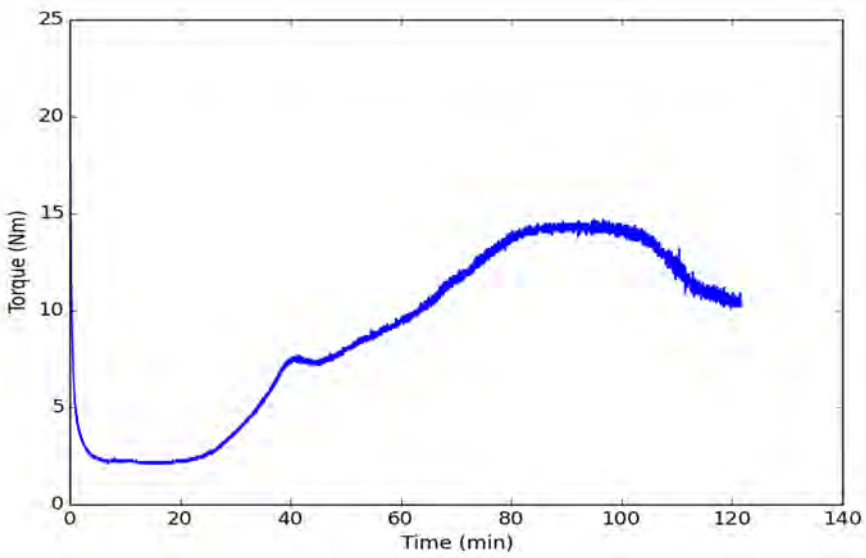

Figure D.3.1: Torque curve for HTC run 1.

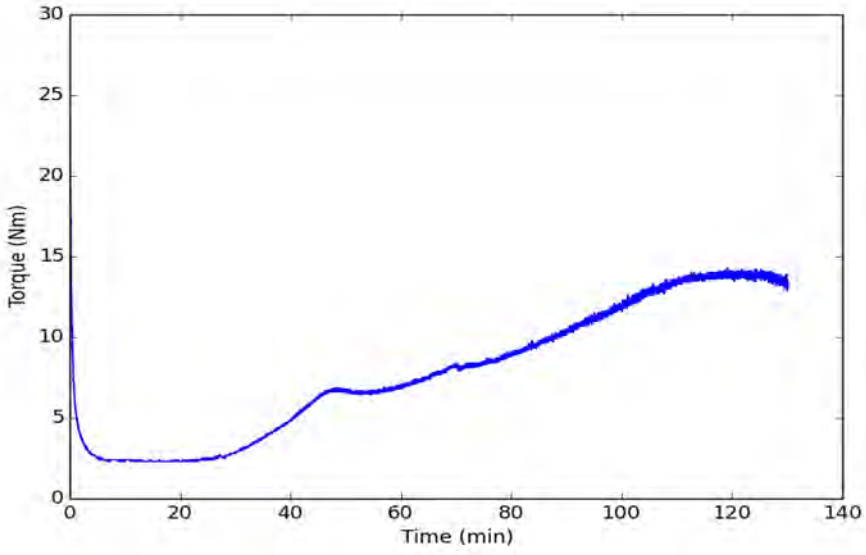

Figure D.3.2: Torque curve for HTC run 2.

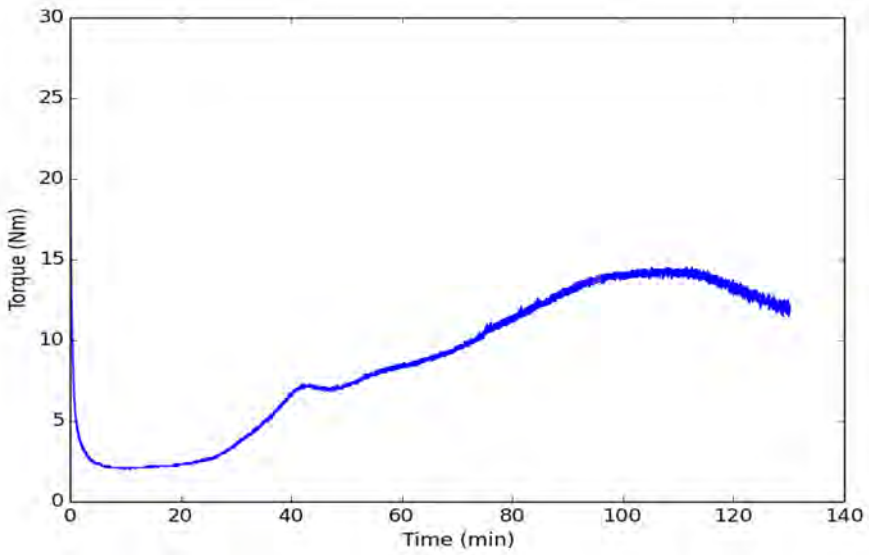

Figure D.3.3: Torque curve for HTC run 3.